2013-12

Sources of wind variability at a single station in complex terrain during tropical cyclone passage

Feldmeier, Joel W.

Monterey, California: Naval Postgraduate School

NAVAL POSTGRADUATE SCHOOL

MONTEREY, CALIFORNIA

DISSERTATION

SOURCES OF WIND VARIABILITY AT A SINGLE STATION IN COMPLEX TERRAIN DURING TROPICAL CYCLONE PASSAGE

by

Joel W. Feldmeier

December 2013

Dissertation Supervisor: Wendell A. Nuss

THIS PAGE INTENTIONALLY LEFT BLANK

REPORT DOCUMENTATION PAGE			*Form Approved OMB No. 0704-0188*
Public reporting burden for this collection of information is estimated to average 1 hour per response, including the time for reviewing instruction, searching existing data sources, gathering and maintaining the data needed, and completing and reviewing the collection of information. Send comments regarding this burden estimate or any other aspect of this collection of information, including suggestions for reducing this burden, to Washington headquarters Services, Directorate for Information Operations and Reports, 1215 Jefferson Davis Highway, Suite 1204, Arlington, VA 22202-4302, and to the Office of Management and Budget, Paperwork Reduction Project (0704-0188) Washington DC 20503.			
1. AGENCY USE ONLY ***(Leave blank)***	**2. REPORT DATE** December 2013	**3. REPORT TYPE AND DATES COVERED** Dissertation	
4. TITLE AND SUBTITLE SOURCES OF WIND VARIABILITY AT A SINGLE STATION IN COMPLEX TERRAIN DURING TROPICAL CYCLONE PASSAGE		**5. FUNDING NUMBERS**	
6. AUTHOR(S) Joel W. Feldmeier			
7. PERFORMING ORGANIZATION NAME(S) AND ADDRESS(ES) Naval Postgraduate School Monterey, CA 93943-5000		**8. PERFORMING ORGANIZATION REPORT NUMBER**	
9. SPONSORING /MONITORING AGENCY NAME(S) AND ADDRESS(ES) N/A		**10. SPONSORING/MONITORING AGENCY REPORT NUMBER**	
11. SUPPLEMENTARY NOTES The views expressed in this thesis are those of the author and do not reflect the official policy or position of the Department of Defense or the U.S. Government. IRB protocol number ____NA_____			
12a. DISTRIBUTION / AVAILABILITY STATEMENT Approved for public release; distribution is unlimited		**12b. DISTRIBUTION CODE** A	

13. ABSTRACT (maximum 200 words)

Although Sasebo, Japan's, harbor is usually a "typhoon haven" from tropical cyclone winds, due to terrain-blocking effects, in rare cases damaging winds occur that may be attributed to terrain channeling. Prediction techniques are developed and tested to improve forecast capability of maximum sustained winds and wind gusts that are the basis for tropical cyclone conditions of readiness. Verification observations from a site that was available during 1990–1998 were found to provide a false sense of security due to its urban location and 13 m anemometer height. Representing the Sasebo terrain effects with a large database of reanalysis winds had limited success unless the top 1000 wind speeds from each cardinal wind direction were used. A parametric wind model that utilized the JTWC wind radii to represent the wind profile shape resulted in better local wind prediction at Sasebo and a small, flat island, but demonstrated the requirement for a wind-reduction factor to represent frictional effects. This parametric wind model, which is multiplied by directionally-dependent acceleration factors to represent Sasebo terrain effects, was most successful for an independent sample of tropical cyclones passing within 200 nautical miles of Sasebo from 2011–2012 and for selected forecast case studies.

14. SUBJECT TERMS Single station forecasting, Sasebo, tropical cyclones, terrain effects, probabilistic forecasting.			**15. NUMBER OF PAGES** 239
			16. PRICE CODE
17. SECURITY CLASSIFICATION OF REPORT Unclassified	**18. SECURITY CLASSIFICATION OF THIS PAGE** Unclassified	**19. SECURITY CLASSIFICATION OF ABSTRACT** Unclassified	**20. LIMITATION OF ABSTRACT** UU

NSN 7540-01-280-5500 Standard Form 298 (Rev. 2-89)
Prescribed by ANSI Std. 239-18

THIS PAGE INTENTIONALLY LEFT BLANK

Approved for public release; distribution is unlimited

SOURCES OF WIND VARIABILITY AT A SINGLE STATION IN COMPLEX TERRAIN DURING TROPICAL CYCLONE PASSAGE

Joel W. Feldmeier
Commander, United States Navy
B.S., Carnegie Mellon University, 1996
M.S., University of Idaho, 2003
M.S., Naval Postgraduate School, 2005

Submitted in partial fulfillment of the
requirements for the degree of

DOCTOR OF PHILOSOPHY IN METEOROLOGY

from the

NAVAL POSTGRADUATE SCHOOL
December 2013

Author: _____
Joel W. Feldmeier

Approved by:

_____
Wendell A. Nuss
Professor of Meteorology, Dissertation Supervisor

_____	_____
Russell L. Elsberry Emeritus Professor of Meteorology	Patrick A. Harr Professor of Meteorology
_____	_____
Charles R. Sampson Naval Research Lab, Monterey, CA	Robin T. Tokmakian Professor of Oceanography

Approved by: _____
Wendell A. Nuss, Chair, Department of Meteorology

Approved by: _____
Douglas Moses, Vice Provost for Academic Affairs

THIS PAGE INTENTIONALLY LEFT BLANK

ABSTRACT

Although Sasebo, Japan's, harbor is usually a "typhoon haven" from tropical cyclone winds, due to terrain-blocking effects, in rare cases damaging winds occur that may be attributed to terrain channeling. Prediction techniques are developed and tested to improve forecast capability of maximum sustained winds and wind gusts that are the basis for tropical cyclone conditions of readiness. Verification observations from a site that was available during 1990–1998 were found to provide a false sense of security due to its urban location and 13 m anemometer height. Representing the Sasebo terrain effects with a large database of reanalysis winds had limited success unless the top 1000 wind speeds from each cardinal wind direction were used. A parametric wind model that utilized the JTWC wind radii to represent the wind profile shape resulted in better local wind prediction at Sasebo and a small, flat island, but demonstrated the requirement for a wind-reduction factor to represent frictional effects. This parametric wind model, which is multiplied by directionally-dependent acceleration factors to represent Sasebo terrain effects, was most successful for an independent sample of tropical cyclones passing within 200 nautical miles of Sasebo from 2011–2012 and for selected forecast case studies.

THIS PAGE INTENTIONALLY LEFT BLANK

TABLE OF CONTENTS

LIST OF FIGURES

LIST OF TABLES

LIST OF ACRONYMS AND ABBREVIATIONS

AEROS	Atmospheric Environmental Regional Observing System
AMEDAS	Automated Meteorological Data Acquisition System
ARG	Amphibious Ready Group
ASOS	Automated Surface Observing Station
CFAS	Commander Fleet Activities Sasebo
CFSR	Climate Forecast System Reanalysis
COAMPS	Coupled Ocean/Atmosphere Mesoscale Prediction System
CPA	Closest point of approach
ET	Extratropical transition
FNMOC	Fleet Numerical Meteorology and Oceanography Center
GFS	Global Forecast System
JMA	Japanese Meteorological Agency
JMSDF	Japanese Maritime Self Defense Force
JTWC	Joint Typhoon Warning Center
MCMRON	Mine Countermeasures Squadron
METOC	Meteorology and oceanography
NCDC	National Climatic Data Center
NeWMeK	Network for Wind Measurement in Kyushu
NHC	National Hurricane Center
NRL	Naval Research Lab
NWS	National Weather Service
PAW	Parametric adjusted winds
PUW	Parametric unadjusted winds
RTRR	Range-to-radius ratio
SST	Sea-surface temperature
TC	Tropical cyclone
TCCOR	Tropical Cyclone Condition of Readiness
TPU	Tropical Prediction Utility
WESTPAC	Western Pacific
WFO	Weather forecast office

THIS PAGE INTENTIONALLY LEFT BLANK

ACKNOWLEDGMENTS

It is impossible to adequately thank all of the people who have helped me in my life and my career, especially in striving for this longtime personal and professional goal.

My special thanks go to all of the members of my committee. Wendell Nuss offered me both guidance and independence in seeing where this research would take me. Patrick Harr provided valuable guidance throughout my time as a PhD student. Professor Russell Elsberry provided extensive editorial and scientific guidance for this dissertation. Robin Tokmakian offered needed perspective on my research and I am especially grateful she agreed to be on my committee after already having been a co-advisor on my master's thesis. Buck Sampson provided much assistance and encouragement, as well as being an inspiration for transitioning research to forecaster-usable products.

Tom Murphree, thank you for your science mentorship over the years. Like many students before me, I am indebted to Bob Creasey who downloaded, sorted, and packaged decades of reanalysis data for my use. Dick Lind provided extensive assistance in preparing for a trip to Sasebo where I was able to take observations during a typhoon passage. Mary Jordan, thank you for your perspective and encouragement. Many, many shipmates over the years have helped me begin to learn about the Navy and meteorology. I especially want to thank my colleagues from the center in Yokosuka, the OA division on *USS Essex* (LHD 2), and all of my fellow PhD students.

Thank you also to Eriko Tomokiyo at Kyushu University for sharing your research and helping me with NeWMeK data. Thank you to Yumi Sato of the Sasebo Fire Department for your assistance with data as well.

I was very fortunate to be born into a scientifically minded family. I can and have called on my brother, mother, and father for scientific and mathematical advice. Thanks for the help and, of course, your love and support.

Last, but never least, to Hiromi, Reese, and Hana. Thank you for putting up with me. I love you.

THIS PAGE INTENTIONALLY LEFT BLANK

I. INTRODUCTION

A. MOTIVATIONS

Tough decisions must be made when a tropical cyclone (TC) approaches land. Should a facility, town, or city be evacuated? Should airplanes, boats, and ships remain in port, or seek safety elsewhere? What precautions can and should be undertaken, and what level of risk is acceptable? Although TCs cause damage in a variety of ways, a decision for a specific location largely depends on the answer to "what will the winds be here?" To answer that, it is necessary, but not sufficient, to correctly forecast TC track and intensity at the synoptic scale or mesoscale. Rather, the relative impacts of a variety of other factors, including but not limited to terrain interaction, must also be considered.

1. Operational Requirements for TC-Related Winds

Existing probabilistic forecast tools that are based on ensembles of many variations of the TC track and structure provide percent likelihood of a 34 and 50 kt wind occurrence in the area surrounding a TC. However, these tools do not take into account the peculiarities of any individual shore station. An appealing idea is to find simple station-specific modifications to the TC wind field, apply those to each member of the existing ensemble, and use the results to create probabilistic forecasts tailored to the station. This is a computationally inexpensive alternative to setting up a conventional high resolution numerical model centered on a station, and running that 1,000 times. If this technique shows any skill for a test case, it should be easily adaptable to different stations and would complement ongoing work at the Naval Research Lab (NRL) in Monterey, California, to improve wind probability products for U.S. military bases in the Western Pacific (WESTPAC) (C.R. Sampson 2013, personal communication).

Tropical cyclones pose an interesting operational forecast challenge where local forecasters are often legally and procedurally bound to start their forecast from the products of a separate forecast office. Centralized offices such as the National Hurricane Center (NHC) and Joint Typhoon Warning Center (JTWC) have impressive institutional knowledge and records of fairly continuous improvement in their forecasts. However,

the TC forecast tracks and warnings they issue necessarily focus on the large-scale structure of the storm, and are not intended as local scale forecasts. In fact, JTWC warning messages include caution statements that their provided wind radii forecasts are valid over water only. Additionally, JTWC analyzes the environment and the strengths and weaknesses of various numerical prediction models to create their own unique track and intensity forecasts. While overall beneficial, this creates a practical problem for a local forecaster in that the JTWC track likely matches none of the synoptic-scale models he or she has access to. It is therefore also likely that none of the mesoscale models that have initial conditions from those synoptic-scale models will have a TC vortex in the JTWC forecast location. That can make extrapolating down to a local forecast from numerical output very challenging, particularly if the TC vortex interacts with land.

None of these issues are new in the sense that forecasters routinely interpret and adjust numerical output for the positioning and timing of various weather features. However, that the local forecast must always be consistent with the provided NHC or JTWC warning adds a level of constraint. This constraint is being addressed in part by the development of mesoscale models such as Coupled Ocean Atmosphere Mesoscale Prediction System-TC (COAMPS-TC), which uses a relocation method to place a tropical cyclone vortex at the official warning position in the initializing synoptic-scale model analysis (Naval Research Lab 2012a). However, the resulting output will still be heavily dependent on the synoptic-scale model, and the horizontal resolution may be insufficient to adequately resolve the winds at one station. Also, this technique is a storm-centered forecast and even if the grid spacing is on order of one kilometer, it is unlikely to capture sub-kilometer sub-grid scale effects that could be critical to a local forecast. Therefore, this study will explore whether or not statistical-deterministic modifications to a larger scale TC forecast may provide a more practical result.

These ideas about local effects on TC-induced winds will be examined at Sasebo, Japan. Because this location has extensive fuel and ammunition depots, a 4-ship Amphibious Ready Group (ARG) and associated landing craft and support units, and a 4-ship Mine Countermeasures Squadron (MCMRON), it has high operational relevance to the U.S. Navy. Sasebo is located in the northwest corner of Kyushu Island (Figure 1).

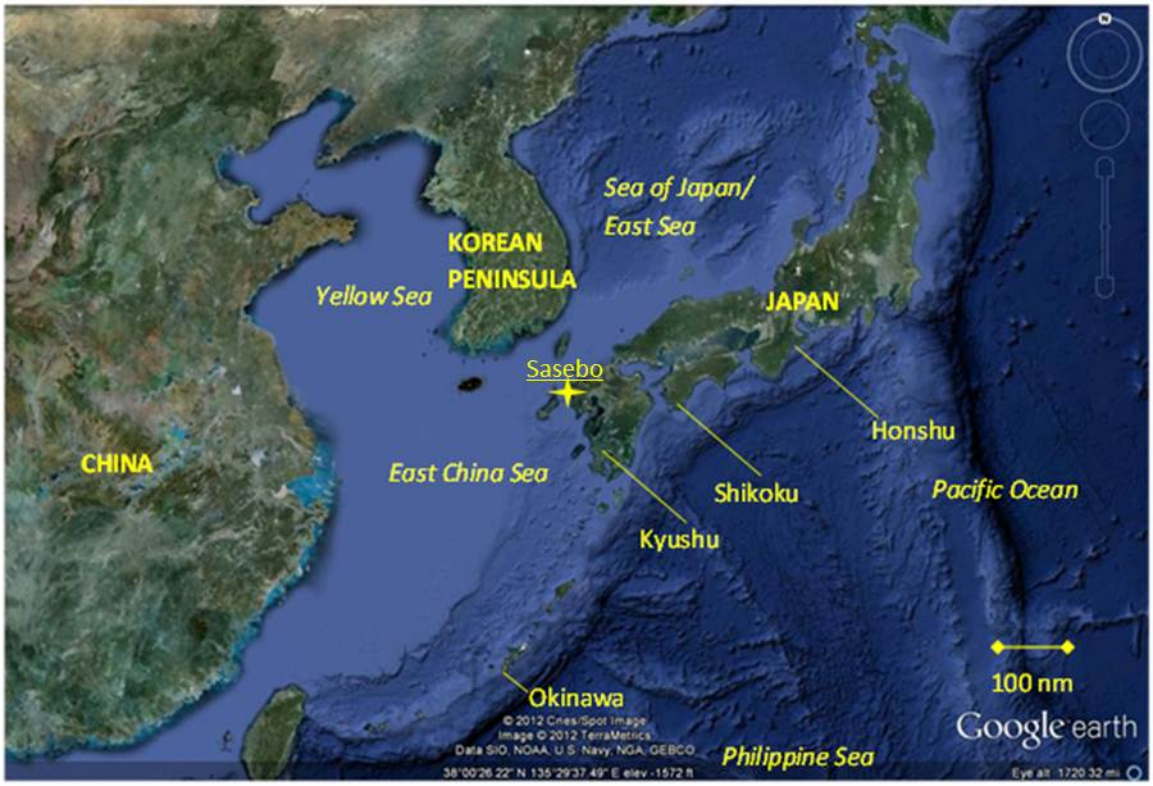

Figure 1. Key geographic features in the area around Sasebo, Japan (yellow star) (after Google Inc. 2013).

The Sasebo harbor is surrounded by relatively complex terrain (Figure 2), particularly when compared to continental U.S. Navy installations such as Norfolk, VA or Mayport, FL. Of particular note is an approximately 5 km long, roughly north-south oriented gap of low elevation located immediately north of the U.S. Naval facilities in Sasebo. The boundaries of the gap are primarily delineated by Mt. Yumihari on the west, and Mt. Eboshi on the east. A less defined east-west gap also encompasses the U.S. base. As in many ports, very large cranes are often in operation and are quite sensitive to winds even below typical small-craft warning criteria (25–30 kt). In addition, many logistic evolutions are done with cranes on floating barges to ships at anchor, so that winds and seas in the harbor well below TC strength can have serious impacts.

Figure 2. Primary topographical features in the area surrounding the Sasebo port and main base area. Note the north-south oriented gap between Mt. Yumihari and Mt. Eboshi (after Google Inc. 2013).

Although generally deemed a Typhoon Haven, several incidents of wind-related damage in Sasebo have been recorded in the last 30 years during TCs. Of particular note, USS *Saint Louis* (LKA 116) drifted off the pier and nearly broke her mooring lines even though two tugs were attempting to hold her against the wind. USS *Dubuque* (LPD 8) and USS *Fort McHenry* (LSD 43) damaged or pulled several ton bollards off the pier. A seawall adjacent to port operations on base was destroyed, and five ships dragged or had other issues while trying to ride out TCs at anchor in Sasebo harbor (Naval Research Lab 2012b). Although infrequent events, these examples demonstrate significant impacts from TCs can occur in Sasebo. It should also be noted that most of these incidents were not direct TC "hits" on Sasebo (i.e., the eyewall passing over or near to the base), but when the closest point of approach (CPA) was tens to hundreds of nautical miles (n mi) away.

One particular case deserves special mention. Typhoon Tokage in October 2004 passed well to the east of Sasebo, off the east coast of Kyushu. Although Sasebo was at all times well outside the analyzed 34 kt wind radius of Tokage, sustained winds were

recorded at over 35 kt for several hourly observations with periods of greater than 40 kt. Additionally, the strongest gust wind recorded in Sasebo by the Japanese Meteorological Agency (JMA) over the last 50 years occurred as Tokage passed, with gusts of 49.3 m/s or approximately 96 kt (Japanese Meteorological Agency 2013a). The base in Sasebo avoided major damage, but did receive moderate damage to the roofs of several buildings (Stars and Stripes 2013).

When it comes to ship sortie choices or decisions for setting Tropical Cyclone Conditions of Readiness (TCCOR), the timing of high wind onset is arguably as crucial as wind strength during the passage. U.S. ships in Sasebo have somewhat limited sortie options when a TC approaches. China, to the west, is the lee shore of any approaching tropical cyclone. The Yellow Sea (Figure 1) to the northwest is very shallow, relatively narrow, and does not offer good sea room for riding out heavy weather conditions. The Sea of Japan/East Sea is sometimes an option, but has limited sea room and maneuvering options should a TC track shift there and is inconvenient unless the ships were already planning to operate in those waters. Ships strive to avoid both high winds and seas, and sea states in the East China Sea can quickly build to untenable levels well before a tropical cyclone even reaches Okinawa (approximately 400 n mi to the south of Sasebo). The safest option, should a sortie be considered necessary, would be to head east of Kyushu where ships can likely find calm conditions associated with the persistent Western Pacific High, and have plenty of sea room should TC tracks shift. However, to get to a safe position the ships must leave port, proceed down the west coast of Kyushu (approximately 150 n mi) and head out several hundred miles into the Philippine Sea/North Pacific. Ideally, they would do that before a TC reaches the latitude of Okinawa. For the best sortie decision a decision-maker would therefore want to know that conditions in Sasebo caused by an approaching TC would be dangerous on order of 100 hours ahead of time. If terrain-based or other local wind enhancements occur, for example, as the TC approaches that could cause dangerous winds earlier and/or stronger than suggested by TC track and TC scale wind forecasts. On the other hand, terrain

blocking of the high winds may become more significant if the TC approaches from a certain direction, which could then increase confidence that a sortie will not be necessary, even if the TC scale forecast suggests otherwise.

The TCCOR system is designed to provide warnings to U.S. bases of damaging or destructive conditions, ideally at least 72 hours ahead of time. What wind speeds are considered destructive can vary based on criteria determined at different levels in the chain of command. Typical criteria includes sustained winds of 50 kt or greater or gusts of 60 kt or greater (Commander U.S. Naval Forces Japan 2010). Although continuing efforts are being made to reduce TC track and intensity errors, little has been done operationally to improve gust forecasts, which is troubling as significant damage can occur from even short gusts that are superposed on sustained winds below the TCCOR criteria. A decision maker would ideally be given time of onset and offset, severity, and frequency for both sustained winds and gusts, and all within a probabilistic framework so that levels of acceptable risk can be determined.

2. Current Methodologies for TC-Related Wind Specifications

A variety of approaches to create local-scale forecasts during the approach of a TC have been used. The U.S. National Weather Service (NWS) weather forecast offices (WFOs), who are responsible for such local forecasts, are provided with a tool (TCMWindTool) that interpolates between the NHC-provided TC forecast wind radii to a 5 km x 5 km grid. Then land friction is taken into account (forecaster-adjustable) to give a local wind prediction (National Weather Service 2010; Tyner 2012). Although WFO forecasters are directed to apply knowledge of local mesoscale features to modify the TCMWindTool output, they are expressly prohibited from exceeding the maximum TC sustained wind forecast provided by the NHC (National Weather Service 2012). Therefore, factors such as terrain-enhancement of the local winds are discounted. No requirements, restrictions or particular guidance as to gust forecasts are provided by the NWS to WFOs.

For the United States Department of Defense (DoD), forecast aids used vary by station. The Automated Destructive Wind Forecast System (ADWF) used at most Navy

continental U.S. stations (H.W. Wilson 2012, personal communication) also uses interpolation between NHC wind radii. However, the Typhoon Determination (TYDET) program used at Kadena Air Force Base on Okinawa (Fenlason 2006) uses a nomogram approach that will be described below.

During the 1980s, a series of forecast aids called nomograms were developed by Jarrell and Englebretson (1982) and Jarrell (1988) specifically for U.S. Navy use during TCs at several stations in WESTPAC. These are still operationally used for Yokosuka, Iwakuni, and Sasebo. Nomograms consist of percentage contours overlaid on a chart centered on the station. The forecaster overlays the TC track forecast from JTWC onto the nomogram and then multiplies the TC intensity forecast by the contour percentage on which the TC position lies to obtain a gust prediction. Sustained winds (i.e., one-minute average) are taken as 2/3 of the gust strength. As an example, consider the case in Figure 3 in which JTWC has forecast the TC to be just south of Korea with maximum sustained winds of 105 kt and gusts to 130 kt. Since the TC position is within the nomogram 70th percentile contour, the Sasebo gust forecast would be 0.7 times 105 kt or 73.5 kt. Then the Sasebo sustained wind forecast is 2/3 of 73.5 kt or 49 kt. Note that this particular nomogram is intended to provide maximum value forecasts.

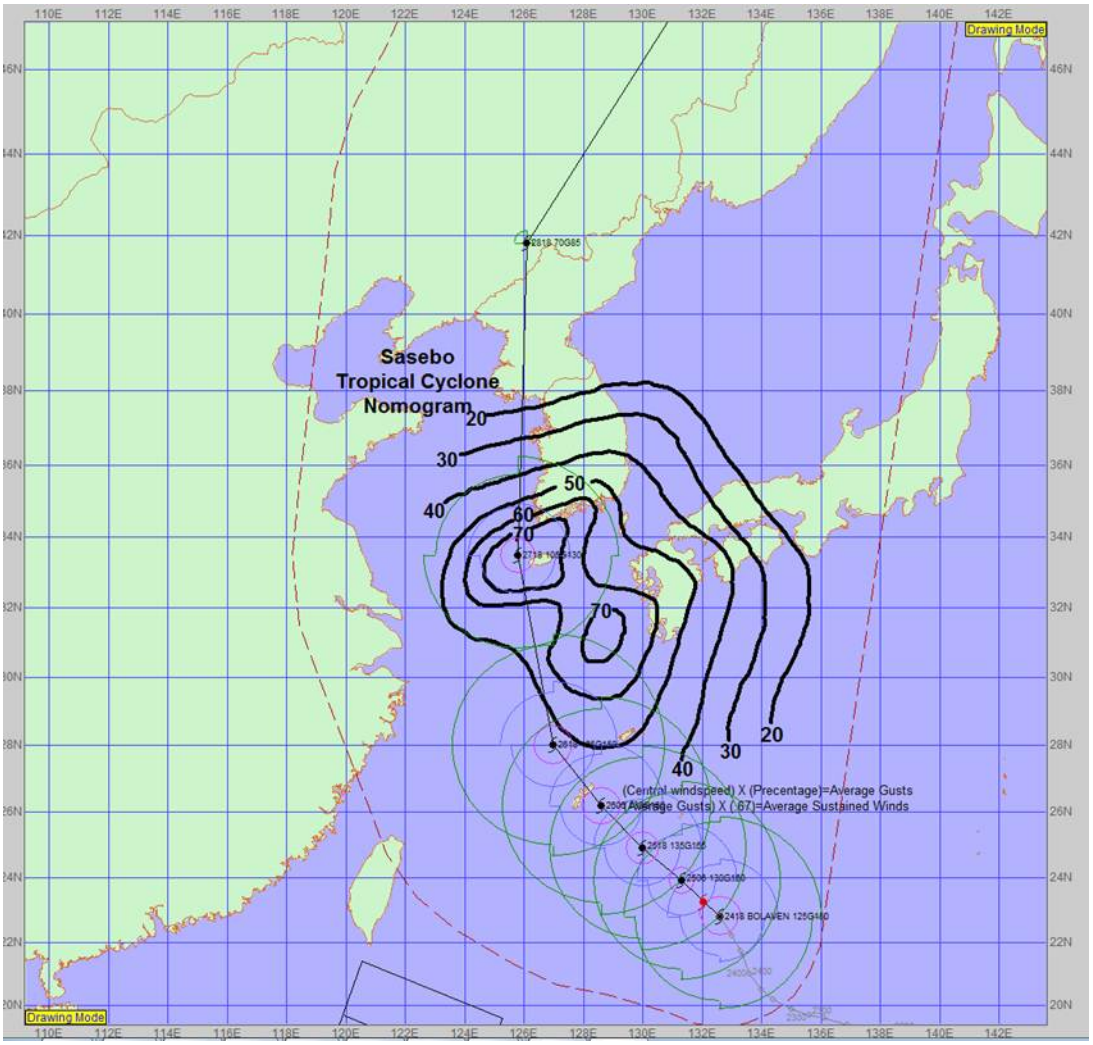

Figure 3. An example of the application of the Sasebo TC nomogram for a case in which the TC is forecast to be just southwest of the Korea peninsula. Since this position is within the 70% contour, the gust forecast for Sasebo is 0.7 times the JTWC intensity forecast (105 kt, not shown) (after FNMOC 2013).

As these nomograms were created from on-station historical observations during TCs, they indirectly include some terrain impacts. Different nomograms were developed for maximum and mean winds, and for TCs of typhoon strength (intensity of 64 kts or greater) or of tropical storm strength. Anecdotal experience when the author was stationed in Yokosuka, Japan and Sasebo, Japan from 2005–2010, as well as a previous tour in Sasebo from 1999–2001, indicates that the nomograms have performed well enough to retain forecaster trust. However, it is also recognized that these nomograms do not account for differences between small storms vs. large storms, eyewall replacement

cycles, storm translation speed, or extratropical transition structures. Since the nomograms only rely on the forecast intensity and not on the analyzed TC wind radii, a modified nomogram that also takes the TC structure into account would be beneficial.

Local wind forecasts can be extracted from numerical model outputs (e.g., COAMPS-TC). As noted above, the timing of a forecast is directly tied to its usefulness. Although 72 hours may be sufficient time for a base to prepare its infrastructure, ship sortie decisions often require longer lead time for varying states of engineering readiness. Additionally, ships will need to clear the immediate geographic vicinity of a station before the arrival of heavy seas, which can precede a storm center by hundreds of miles. In the ideal scenario, accurate TC impact forecasts would be available much longer than 72 hours ahead of time, which is why JTWC issues TC forecasts out to 120 hours. Conventional COAMPS output is typically available at 18-km resolution up to an 84-hour forecast, which may or may not give enough lead time (depending on accuracy). However, such a model resolution may not be adequate as the main base at Sasebo is on order of 1 km wide, and the terrain gaps surrounding the base are on order of 1 km wide and several km in length (Figure 2). Any impacts from the terrain immediately around base are likely unresolvable unless grid-spacing is reduced to sub-kilometer. While possible, setting up and maintaining such a high resolution model represents a significant investment of time and computing resources for low frequency events.

Rather than provide a specific forecast of conditions on station, the Tropical Prediction Utility (TPU) is a tool that grew out of the need to support Tropical Cyclone Condition of Readiness (TCCOR) recommendations to Commander Naval Forces Japan. JTWC warning messages are input to the TPU to create a graphic that takes into account recent JTWC forecast error trends and depicts the level of TCCOR for the geographic areas near the TC track. TCCOR criteria winds are expected to occur at TCCOR I. Therefore the TCCOR I area is basically the 50 kt wind radii from the JTWC warning (Figure 4). This TPU provides an objective guidance for recommendations: when a TCCOR line/area touches a station, recommend that TCCOR (Wallace 2008). It should be noted again that no actual on-station forecast wind speed is available from the TPU.

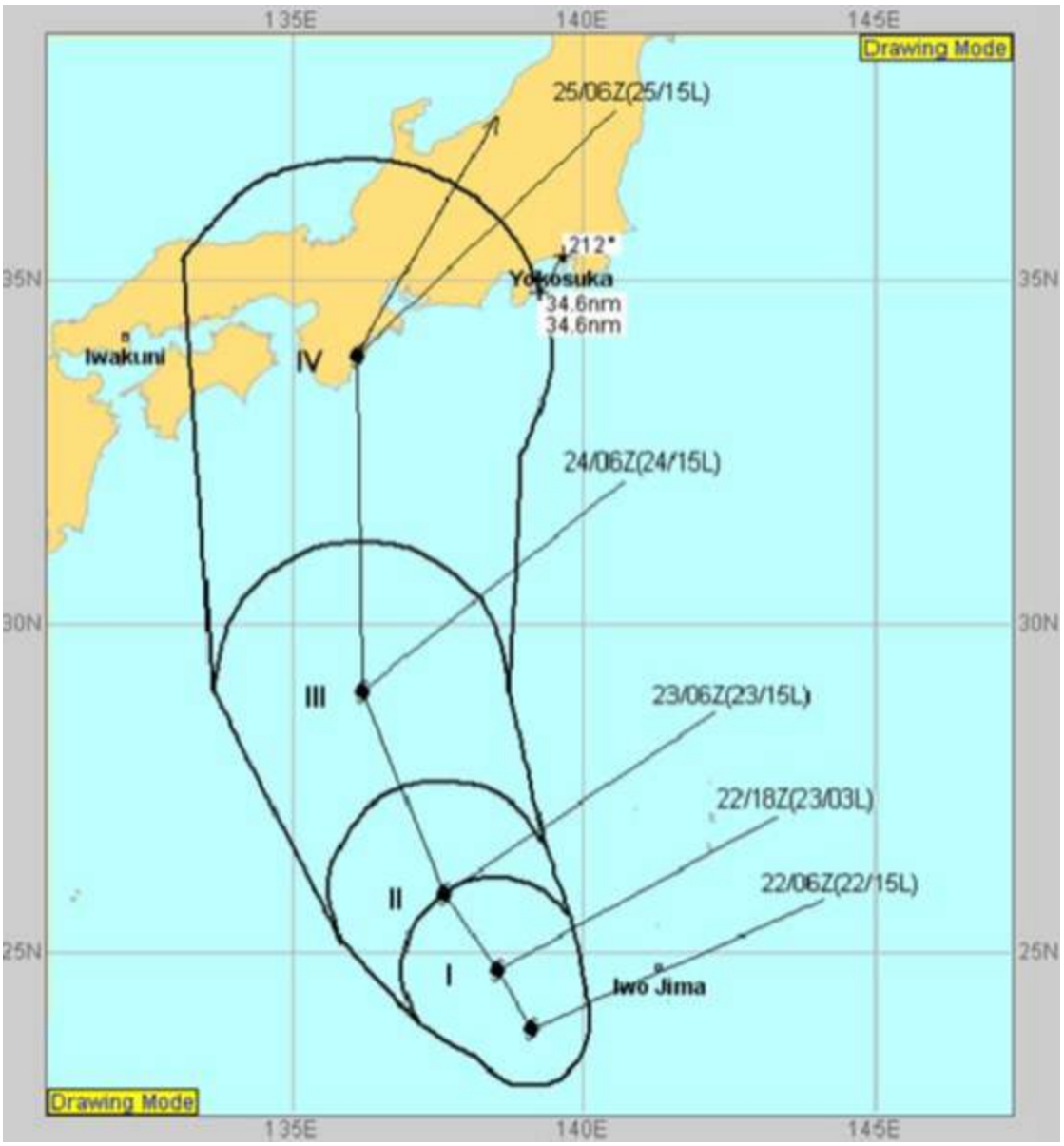

Figure 4. Example of the Tropical Prediction Utility (TPU) used for TCCOR recommendations I, II, III, and IV at U.S. bases in Japan. Multiple TC forecast locations are shown, but the graphic depicts current recommendations based on the most recent warning (from Wallace 2008, Figure 9).

Local terrain effects are not directly taken into account by TPU, and human factors play into the forecasts, recommendations, and final decision. For example, a forecaster will examine numerical weather prediction (NWP) guidance, other resources, and the TPU output when creating a forecast. Providing the forecaster more information on specific terrain impacts at an individual station would certainly help in that analysis.

Additionally, Commanders have to take into account factors such as weekends, holidays, and overtime (which deal with costs, workforce availability for preparations, and general awareness) when deciding when to set TCCORs. Note that the decision process on whether or not to sortie ships or aircraft from U.S. bases is separate from the TCCOR process, although they impact each other.

Ensemble forecasting techniques for TC impacts on the U.S. Navy are being developed. Chances of destructive/damaging conditions occurring at a given location can be calculated and compared with thresholds (adjustable with experience) for the setting of TCCOR or making sortie decisions (e.g., Sampson et al. 2012). The greatest strength of this technique is the use of ensembles better captures the multiple possible scenarios inherent in track uncertainty. The greatest limitation is that as currently used for TC forecasting, only a synoptic-scale model is perturbed and used to provide an ensemble of tracks and intensities, from which wind radii are parametrically calculated. That calculation does not account for terrain interaction, only landfall (i.e., the TC eye touches land).

3. Scientific Considerations in Estimating TC-Related Winds

Single station wind observations include variability such as lulls, periods of high sustained winds, extreme gusts, and shifting directions. Some of that variability is stochastic and will never be readily predictable. However, when a TC is impacting a local area (range criteria discussed later), some predictable variability is expected from the storm's movement, structure, and dynamics. Combinations of changes in bearing or range from a station and intensity (intensity here referring to maximum sustained winds as forecast or analyzed by a TC warning center) of the TC are sources of synoptic scale or mesoscale variability. A station may be covered by an area of enhanced convection, such as rain-band structures, and temporarily experience higher winds. Events like TC eyewall replacement, expansion or contraction, or track wobble could perturb the TC wind field, and by extension the wind observations at a station.

Additional sources of wind variability at a single station are expected in the mesoscale to microscale range. A key question is: can this "local" variability be separated

from TC scale variability? Although boundary layer meteorology techniques provide one way of exploring this question, forecasters have long relied on “rules of thumb” to adjust their local scale forecasts from larger scale forcing. The best rules of thumb are empirically derived representations of real physical processes that have sensible impacts on local weather. Therefore, it is interesting to consider if dynamical-statistical methods or statistical-empirical techniques can characterize some fraction of this observed wind variability at a single station. This approach seems particularly well suited for persistent features such as the terrain surrounding a station.

Terrain interactions may explain much of the difference between TC scale wind fields and what is observed locally, but other factors, such as local and synoptic pressure gradients or extratropical synoptic features, are also important. The TC vortex cannot be considered in isolation. As indicated above, extremely high-resolution numerical models may provide estimates of the relative importance of different factors. The alternative explored here is to first create a simple predictive system that reasonably captures terrain effects on the TC wind field. If persistent patterns in prediction errors emerge from a comparison of these predictions to single station observations, these patterns might represent important identifiable and predictable influences on the wind variability.

Another way to consider this issue is as a “representation problem.” Namely, are trends in TC intensity representative of winds experienced at a single station? Conversely, are single station observations useful to verify TC intensity? An initial forecast for a single station can be derived from the TC scale wind field. Even after adjusting for frictional effects, this may be inadequate. Does local terrain blocking make local wind speeds much lower than otherwise expected? Are there periods of much higher than expected winds that may be caused by some local acceleration factor? Additionally, is there some radius around a single station at which the winds are roughly the same? That is, over what characteristic scale do terrain and other factors become important?

Terrain impacts on wind are not always well understood. For a single station surrounded by complex terrain (e.g., a “sheltered” harbor), the assumption is generally that wind blocking will occur, but when and how much? Is there an effectively isotropic response or is there a clear directional variability? How much do kilometer-scale and

smaller features matter? Can terrain be the cause of accelerations, and what specific mechanisms would cause that? Are terrain effects evident for sustained winds only, gusts only, or for both?

As to other factors, they can be examined in isolation or how they might interact with terrain. For example, a synoptic-scale pressure gradient can cause wind acceleration, or that acceleration might be enhanced via alignment with a mountain gap in local terrain. The background synoptic flow into which a TC approaches may contain stationary boundaries, or transiting high and low pressure systems that will impact the overall winds on station. Whether or not TC landfall (the eyewall touching land) occurs, the fraction of storm over land and water, angle of approach to land, and type of land surface can all matter. In addition, poleward-moving TCs may undergo extratropical transition and have highly modified wind fields. All of the above questions and issues return to the main theme of determining what the wind will be at a specific location. This is deterministically impractical depending on time scales of interest, but perhaps a reasonable probabilistic prediction can be made.

B. PROPOSED PARAMETRIC MODEL APPROACH TO TC-RELATED WINDS

A variety of approaches to understand wind variability on multiple scales have been undertaken by meteorologists, civil engineers, and those interested in wind power. For TC-related wind variability, some simplified parametric models (equations) have been proposed that use a variety of inputs to provide a wind speed at a specified radius and bearing from the TC center. A commonly cited and recently revised version by Holland et al. (2010) uses outer wind and surface pressure, sea-surface temperature (SST), radius of maximum winds, and central pressure. Individual parametric models have advantages and disadvantages. For example, the modified Rankine vortex approach requires very few inputs and can have wavenumber-1 asymmetry but basically has a continuous falloff of winds with radius (MacAfee et al. 2006). Efforts continue to include such features as secondary eyewalls. Of particular interest, in 2007 the Sixth International Workshop on Tropical Cyclones recommended “development, testing, and documentation of a public domain parametric wind field model that includes asymmetries

to aid in the diagnosis of TC wind structure" as well as "improved understanding of the effects of variability of surface land roughness and topography on forecast wind speed" (World Meteorological Organization 2012). These relatively simple models are of particular interest because they provide a common standard for comparisons with observations and to make comparisons between individual storms. For example, two TCs may be of similar size, intensity, and have similar tracks past a station but vary from each other and the simplistic vortex representation in different and important ways.

It is relatively easy to do a coordinate transform on a parametric model so that it is centered on a station of interest. That is, one would input the bearing, range, and intensity of a TC to get a predicted on-station wind value. Since the equation is already a function of bearing, it is a simple matter to add new bearing-dependent terms that represent different terrain features or other directionally-dependent factors unique to the station. Put another way, the winds from the direct TC vortex circulation interact with the local area around a station and are therefore modified prior to being recorded. Although this approach cannot hope to capture all of the wind variability at a station, it should capture the TC-scale variability caused by TC intensity changes and track (range and bearing). If the additional bearing-dependent terms prove at all useful, the technique should also capture persistent terrain or other directionally-dependent effects. This procedure also has the added advantage that any future TC track and intensity forecasts improvements would also lead to improvements with this technique.

A key input variable in the modified Rankine vortex parametric technique that is used in the TC wind probability products mentioned above is the radius of maximum winds. JTWC (and other TC warning centers) analyzes/forecasts radius of maximum winds, as well as eyewall radius and wind radii (e.g., radius of 34 kt or 50 kt wind from TC center). This information can be used to modify the basic parametric equation prior to any additional directionally-based effects being considered. This may lead to a useful forecast improvement in and of itself, or in combination with terrain/other effects considered. Again, it should be emphasized that parametric models are quite simplistic so that a desktop computer can run applicable code for an individual TC in a matter of seconds. Running the code for even a 1000 member ensemble of possible TC tracks is

much less involved than running more conventional weather models or ensembles. Taking all of these factors into account, an in-depth look at parametric models for local forecasting during TC approach seems in order.

C. HYPOTHESES

- **Hypothesis 1:** A substantial fraction of the wind variability experienced in Sasebo, Japan, during the passage of a TC is caused by persistent and identifiable station-specific factors.
- **Hypothesis 2:** Station-specific factors such as terrain features and/or surface roughness lead to wind direction-based variability around Sasebo that can be empirically/statistically determined.
- **Hypothesis 3:** Directional factors are an important factor to be considered in forecasting both sustained wind and wind gusts at Sasebo.
- **Hypothesis 4:** Nomograms provide one approach to understanding directional variability, but as currently used do not include variations in storm structure. Modifications to the Sasebo nomograms are possible that take into account the station's position relative to the TC circulation, instead of just range to TC center, and thus better account for wind variability.
- **Hypothesis 5:** Parametric models modified with analyzed or forecast parameters from typhoon warning centers, and further modified with wind direction-dependent variables, will explain a substantial fraction of Sasebo wind variability during TC passage and thus are an alternative to nomogram-based predictions.
- **Hypothesis 6:** Persistent errors in these modified nomogram predictions and/or modified parametric model predictions from winds actually experienced in Sasebo can be used to infer other important persistent factors contributing to the wind variability.

THIS PAGE INTENTIONALLY LEFT BLANK

II. STATION CHARACTERISTICS, DATA, AND METHODS

Sasebo, Japan has been a significant naval base for over 100 years, and has had a U.S. base since 1946 (Commander Fleet Activities Sasebo 2013). Various Japanese and American weather observing locations and forecast offices have been established, moved, and disestablished over the decades. Given the complex terrain of the Sasebo area, and the attendant impacts on the observed wind, due care is required when examining historical observations or using those observations to develop empirical rules for any particular location.

A. LOCAL TERRAIN AND PAST AND PRESENT WEATHER SENSORS

To reach the port of Sasebo, ships enter a narrow (approximately 1 km) inlet on the west coast of Kyushu, travel approximately 5 km east with hills ranging from 50 to 150 m on both sides, as the bay opens to its widest extent of about 3 km between points of land. Then ships turn north to travel another 5 km through a 1–2 km wide passage, also ranged on both sides with hills (some locally termed mountains) up to 240 m. Flat areas of elevation near sea level are very small, with noticeable changes in elevation within tens of meters of the shoreline. Naval and shipbuilding facilities dominate the port, with smaller areas for commercial piers, ferries, and recreational craft. As noted above, the U.S. base, known as Commander Fleet Activities Sasebo (CFAS), sits approximately due south of a gap between Mt. Yumihari (364 m elevation, with a nearby 385 m peak 500 m to the north) and Mt. Eboshi (568 m elevation) (Geospatial Information Authority of Japan 2013). Pictures of the area are provided in Figures 5–10:

Figure 5. Southeastward view from near the peak of Mt. Yumihari.

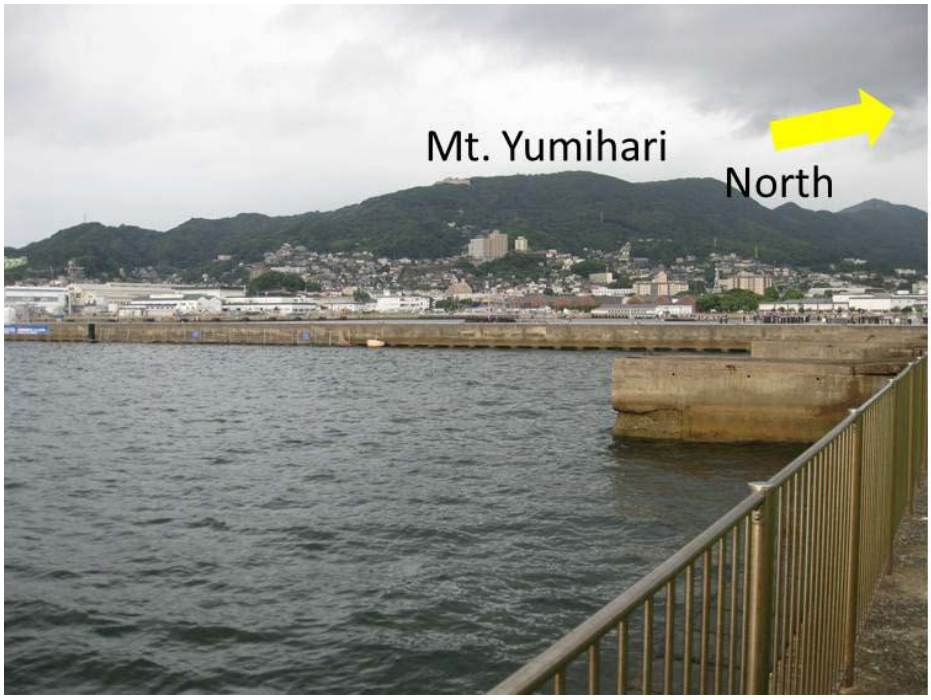

Figure 6. View of Mt. Yumihari from southeast corner of main CFAS area. All buildings shown here on flat terrain are part of CFAS. Note this is approximately the reverse view of Figure 5. Large deck amphibious ships berth in this basin.

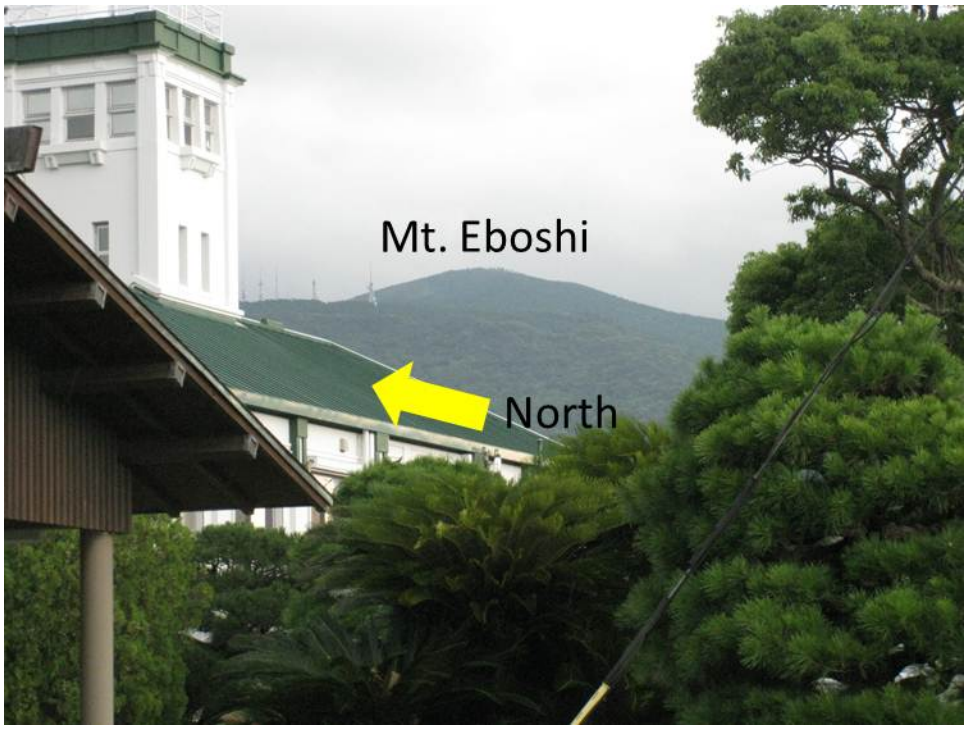

Figure 7. View of Mt. Eboshi from same approximate position as in Figure 6. Note that the guide-wire in the foreground supports a mast with an on-base weather sensor (Vaisala). The green-roofed building is CFAS headquarters.

Figure 8. Southeast view from same vantage as Figure 7.

Figure 9. South to south-southwest view from CFAS. Buildings/tanks in distance are part of the U.S. Navy Akasaki fuel depot area. Photo from same approximate location as in Figures 6–8.

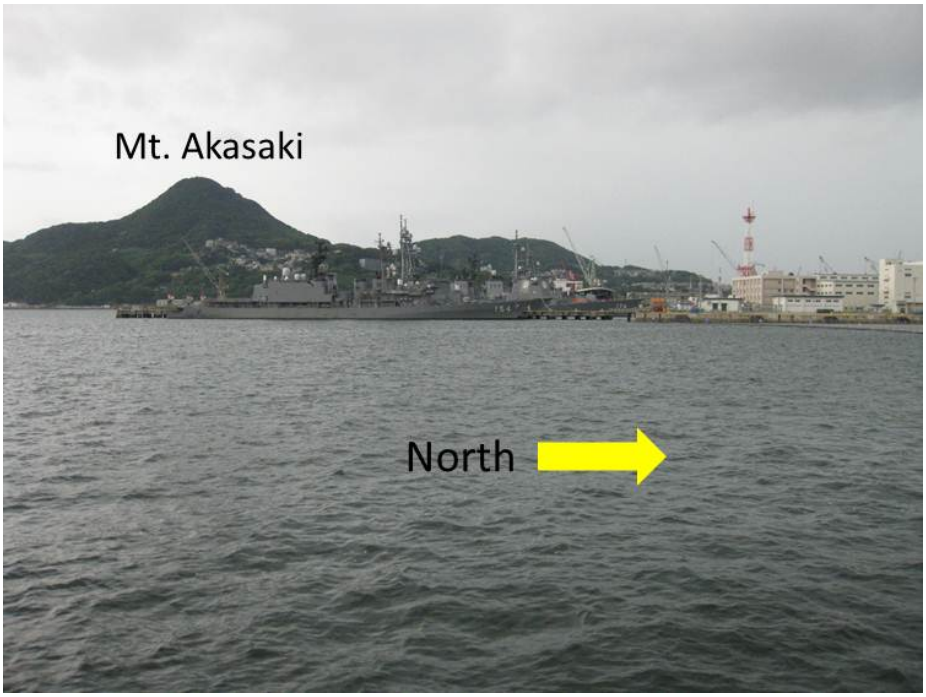

Figure 10. West view from same location in CFAS as in Figures 6–9. The pier for the large deck amphibious ship stationed in Sasebo is to the immediate right of the picture.

Historically, JMA sensors have been placed in the northeast corner of the port area. U.S. Navy sensors have been placed in at least four locations in the main CFAS area. For several years an Automated Surface Observing Station (ASOS) was placed at the U.S. Navy helicopter pad in Akasaki (west side of harbor). An additional U.S. sensor was placed at the Iorizaki fuel depot area in 2009, which is approximately where inbound ships turn from an eastward heading to a northward heading. The Japanese Maritime Self Defense Force (JMSDF) maintains a small weather detachment and sensor in a compound immediately across the street from the CFAS main gate and adjacent to the U.S. Department of Defense main base housing and elementary school. Kyushu Denki, which is the local power company, maintains anemometers on transmission towers throughout Kyushu, including one sensor on the southwest slope of Mt. Eboshi. That network is known as the Network for Wind Measurement in Kyushu (NeWMeK). An additional weather station is maintained by the Sasebo City Fire Department, and the Japanese Ministry of Environment places anemometers on some of their pollution sensors in a network referred to as the Atmospheric Environmental Regional Observing System (AEROS, sometimes referred to as SORAMAME). An overview of important sensor locations is provided in Figure 11. Figure 12 depicts the CFAS Vaisala sensor in more detail:

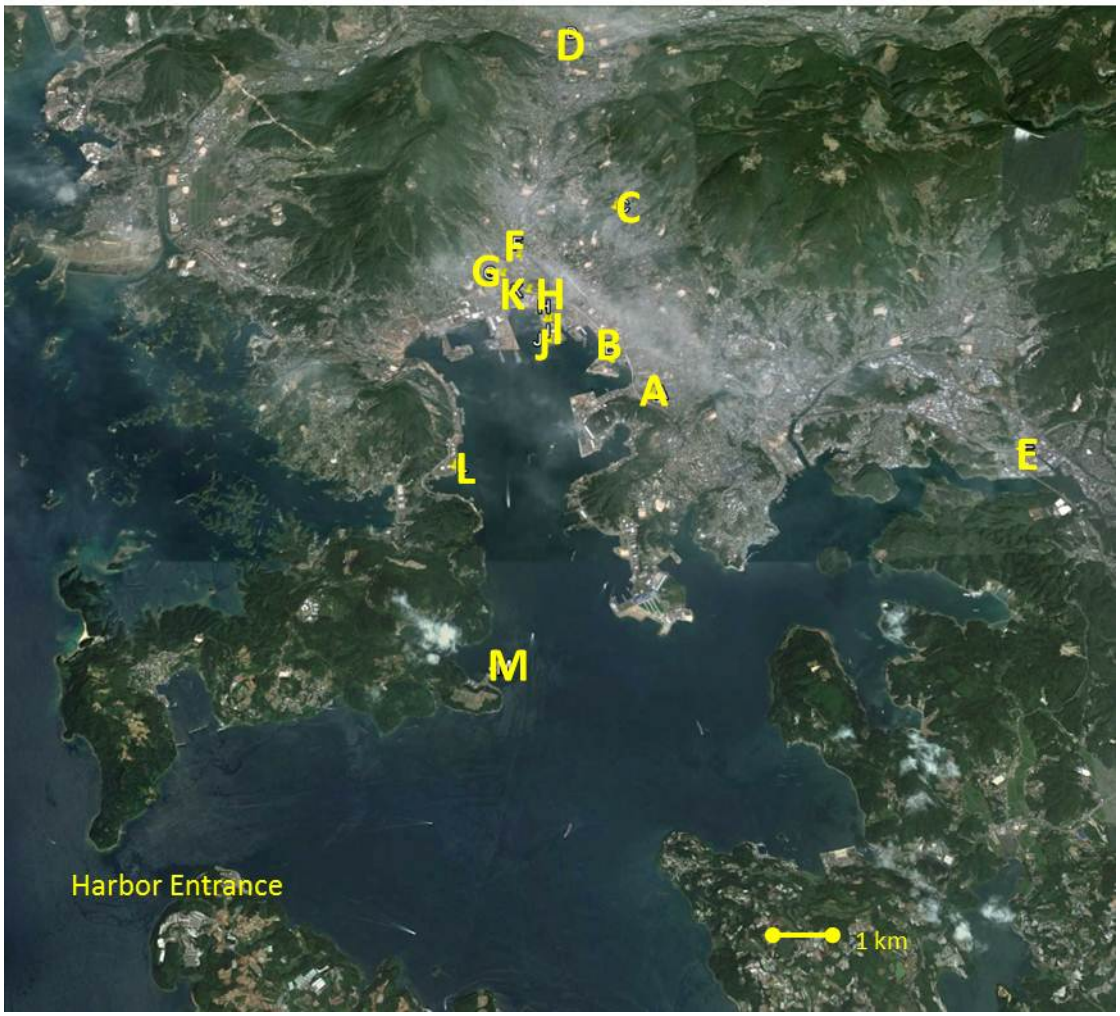

Figure 11. Principle weather observation stations—A: JMA Station until March 2002; B: Current JMA Station; C: NeWMeK Station 44; D: Oono AEROS Station; E: Daitou AEROS Station; F: Sasebo Central Fire Station; G: JMSDF Observation Station (METAR identification S-RH); H: CFAS Port Operations Building Davis Weather Sensor (in operation circa 2001 to 2007); I: CFAS Building 98 Davis Weather Sensor (in operation circa 2007 to present); J: CFAS Vaisala Weather Sensor (in operation circa 2008 to present); K: Additional CFAS Davis Weather Sensor (in operation circa 2003 to 2007); L: CFAS Heliport ASOS (removed circa 2004); M: CFAS Iorizaki Davis Weather Sensor (2009 to present) (after Google Inc., 2013).

Figure 12. CFAS Vaisala installation with the top of mast indicated in the inset. View is toward the S from the approximate same location as Figures 6–10. Note that the sensor has the least obstructions from SE to the NNW. A small picnic structure is immediately to the N with low buildings and trees within ~50 m from NNE to SSE.

B. UTILITY OF VARIOUS DATA SETS

1. Automated Meteorological Data Acquisition System

The Automated Meteorological Data Acquisition System (AMEDAS) is a nationwide network of sensors run by the JMA. The AMEDAS record for Sasebo is the most comprehensive of all data sets available and will be used as the standard against which all others are compared. However, several facts must be immediately highlighted:

- The sensor position was moved in January 2002
- The current anemometer height is 35 m, vice the widely used 10 m standard (Digital Typhoon 2013)
- With minor exceptions, publicly available observations were recorded every 3 hours or at synoptic times (i.e., 0000 UTC, 0600 UTC, 1200 UTC, and 1800 UTC) prior to 1990, hourly since 1990, and every 10 minutes since mid-2008

- The gust wind sensor was modified in 2006
- The sustained wind sensor was modified in 2007
- Prior to 2008 no gust wind information except daily maximum gusts are available via open web page access to JMA records
- Sustained wind observations are 10 minute averages of the time immediately up to and including posted observation time
- Wind direction values are reported online in 1 of 16 cardinal values, for example: North (N), North Northeast (NNE) :

Table 1. Cardinal wind direction numeric values in which standard meteorological convention is followed of winds coming from each direction.

AMEDAS Cardinal Wind Direction	Central Wind Direction	Included Numeric Wind Directions
N	0	348.75 to 11.25
NNE	22.5	11.25 to 33.75
NE	45	33.75 to 56.25
ENE	67.5	56.25 to 78.75
E	90	78.75 to 101.25
ESE	112.5	101.25 to 123.75
SE	135	123.75 to 146.25
SSE	157.5	146.25 to 168.75
S	180	168.75 to 191.25
SSW	202.5	191.25 to 213.75
SW	225	213.75 to 236.25
WSW	247.5	236.25 to 258.75
W	270	258.75 to 281.25
WNW	292.5	281.25 to 303.75
NW	315	303.75 to 326.25
NNW	337.5	326.25 to 348.75

Further details are available from Japanese Meteorological Agency (2013a – 2013d). Such factors are critical for where and when any empirical forecasting scheme would be considered valid. Although operationally used for CFAS, the original nomogram forecast tool for Sasebo was based primarily on JMA observations from Sasebo and other nearby stations. The nomogram creators explicitly state it is technically only valid for the pre-2002 AMEDAS station location (Jarrell 1988). They note the size

of their database and the coarseness (i.e., large and irregular spacing between stations) of their grid, as reasons not expect major differences at CFAS (Jarrell 1988).

All AMEDAS data were obtained from Japanese Meteorological Agency (2013e). To maximize possible case studies, wind data since 1990 have been examined. However, notable differences exist between 1990–2000 AMEDAS data and 2003 to 2010 data. Note that no TC impacts on Sasebo were available for analysis during 2001. Since the AMEDAS station was moved in early 2002, the TCs occurring in 2002 were set aside for validation of the forecast schemes. When the Sasebo AMEDAS station was moved in 2002 (from marker A to marker B in Figure 11), it became more exposed to Northerly and Southerly winds. That is, easterly and westerly winds had occurred much more frequently than any other directions during 1990 to 2000 (Figure 13), but this is not true from 2003 to 2010 (Figure 14).

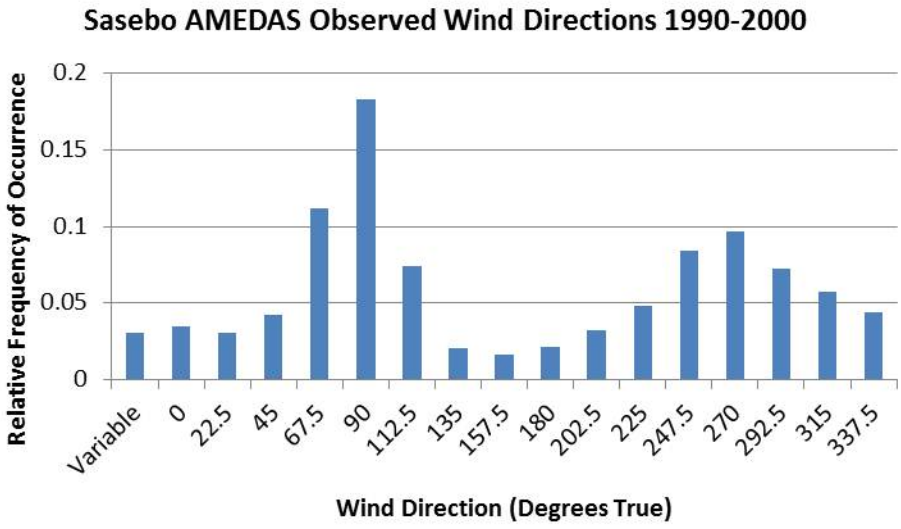

Figure 13. Distribution of observed hourly wind directions in Sasebo from 1990–2000. All hourly AMEDAS observations from that time period have been included. Note that AMEDAS hourly wind observations are 10 minute averages, e.g., a 1300 local time observation is the average of winds from 12:51–13:00.

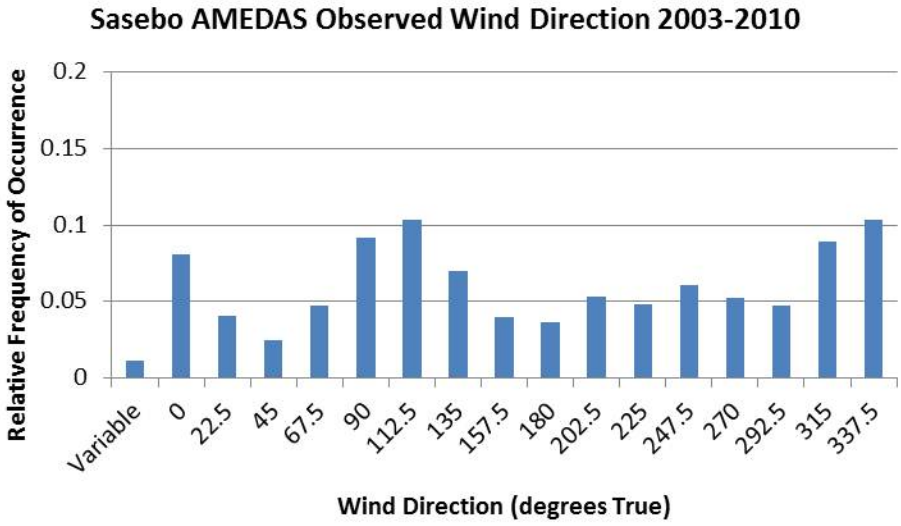

Figure 14. Distribution of observed hourly wind directions in Sasebo from 2003–2010. Note that all AMEDAS hourly wind observations are 10 minute averages, e.g., a 1300 local time observation is the average of winds from 12:51–13:00.

In the 2003–2010 sample set, more NNW winds in particular were observed, which is likely attributed to more exposure to winds through the terrain gap between Mt. Eboshi and Mt. Yumihari. Additionally, the maximum sustained wind speeds observed from each direction were higher in the 2003–2010 timeframe (Figure 16) than during 1990–2000 (Figure 15). Notice the maximum observed speed was from the NNE and the winds with southerly components had noticeably higher speeds during 2003–2010 than during 1990–2000. It should be noted that these observations are hourly values, so higher winds have been recorded at intermediate times.

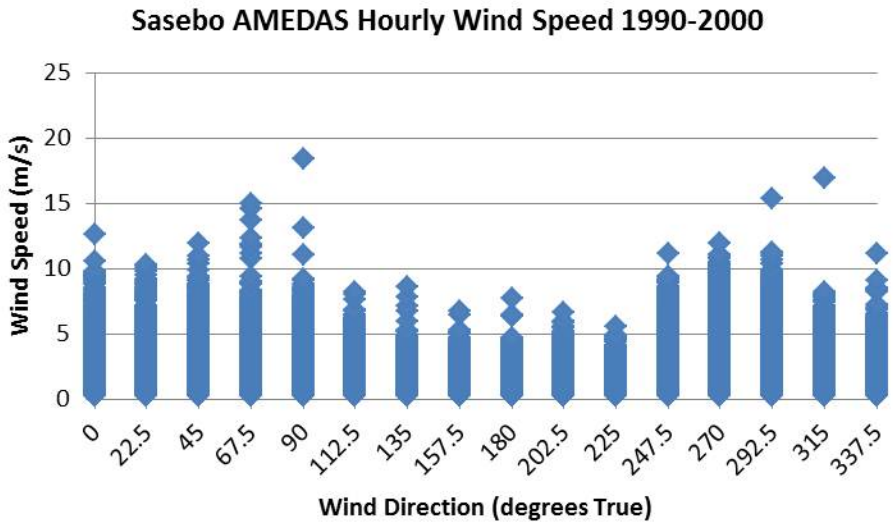

Figure 15. Distribution of hourly observed wind speeds by observed wind direction during 1990–2000. Note that these are the same observations depicted in Figure 13.

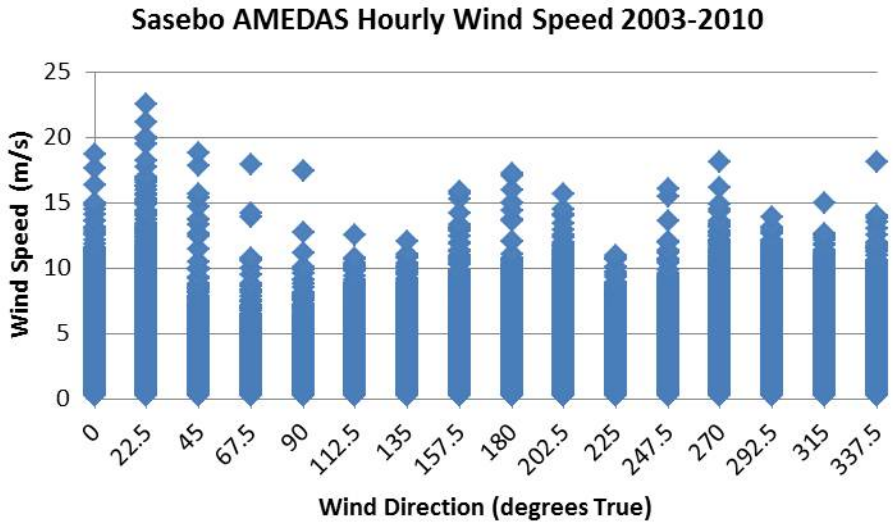

Figure 16. Distribution of hourly observed wind speeds by observed wind direction during 2003–2010. Note that these are the same observations depicted in Figure 14.

Superposing the 16 cardinal directions relative to the current AMEDAS sensor (Figure 17), note that the gap between Mt. Eboshi and Mt. Yumihari overlaps portions of both the N and NNW directions. However, no cardinal direction aligns well with the long N to S axis of open water in Sasebo harbor immediately south of CFAS.

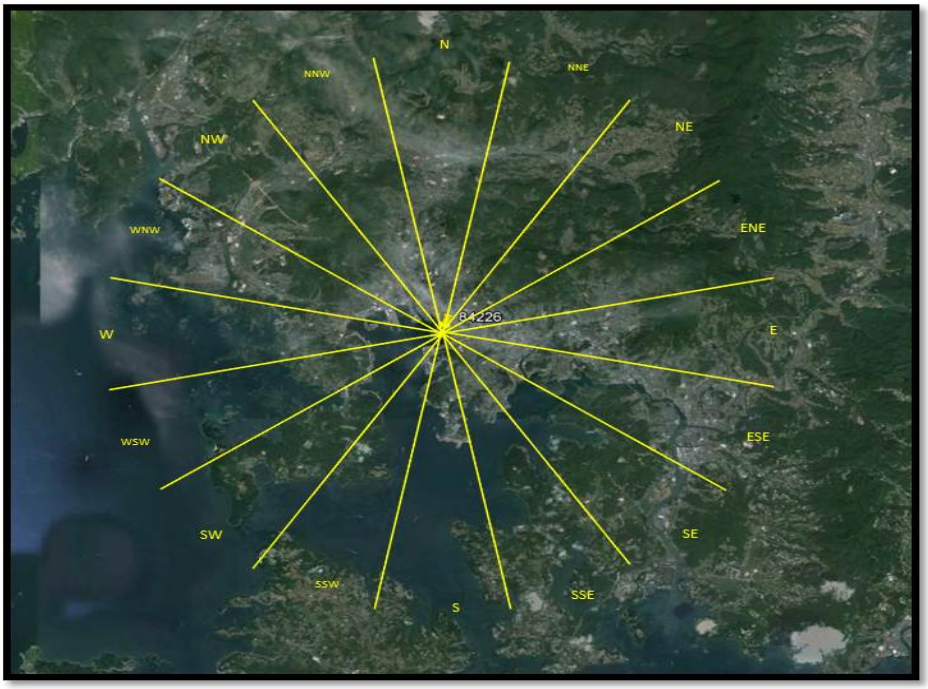

Figure 17. Depiction of cardinal wind directions centered on current Sasebo AMEDAS station. Note that Mt. Eboshi dominates the NNE upstream area. The N upstream area includes the western flank of Mt. Eboshi, and part of the gap between Mt. Eboshi and Mt. Yumihari. The NNW upstream area includes part of the gap between Mt. Eboshi and Mt. Yumihari, and the eastern flank of Mt. Yumihari (after Google Inc. 2013).

2. U.S. Naval Observations

a. Manual Observations

Although U.S. Navy observation records are available from the National Climatic Data Center (NCDC) and other sources, several issues should be noted:

- The number and experience level of Navy Meteorology and Oceanography (METOC) personnel stationed in Sasebo has varied significantly over the past 25 years. Therefore the frequency and quality of observation reporting has also varied. Manning constraints are most evident from the larger numbers of observations at synoptic times that fell

during local daylight hours, on Mondays–Fridays, and only occasional additional reports during significant weather.

- Multiple overlapping observation records, with the same reported position. See for example National Climatic Data Center (2013).
- As noted in the Sasebo Forecaster's Handbook (Naval Pacific Meteorology and Oceanography Detachment Sasebo 2001), multiple anemometers, including geographically dispersed (and therefore potentially subject to different terrain impacts) Davis Weatherlink sensors, and an ASOS have been available to Sasebo personnel. It is therefore not always clear from what exact location winds were being reported.

Given the above, manual U.S. Navy observations from Sasebo are only used for limited comparisons.

b. Automatic Observations

(1) Davis Weatherlink Sensors. A Davis Company weather sensor is currently located in the main base area of CFAS at approximately 120 ft above sea level. Although the last several days of various weather data are posted online, historical or detailed raw data from this sensor were not easily available. The same is true of the Davis sensor in Iorizaki (see location in Figure 11). Therefore, observations from these Davis sensors are only used for specific times, when a screenshot was saved, for comparison with other observations.

(2) Vaisala. A Vaisala MAWS110 weather station with a WXT510 anemometer is positioned in the southeast corner of CFAS main base. The station elevation is approximately six ft above sea level, and the anemometer is 10 m above the ground (Vaisala 2013). This station has been in operation for approximately six years. When these data are available, they will be used for the primary comparison of wind differences between the AMEDAS station and at CFAS. Unfortunately, only one complete calendar year, 2012, of observations was readily available to the author to examine systematic differences from AMEDAS. Limited data were available from other time periods.

A comparison of all available Vaisala sustained wind observations from 2012 with simultaneous AMEDAS observations (both 10 minute mean values) is presented below. Note that the wind directions at the two observing locations are within $\pm$

one cardinal point approximately 80% of the time (Figure 18), and speed differences are generally less than 4 m/s (Figure 19). The mean absolute difference between sustained wind observations in the data sets is 0.81 m/s with a 0.74 m/s standard deviation. Some additional variability is evident when separating the data by AMEDAS direction (Figures 20 and 21).

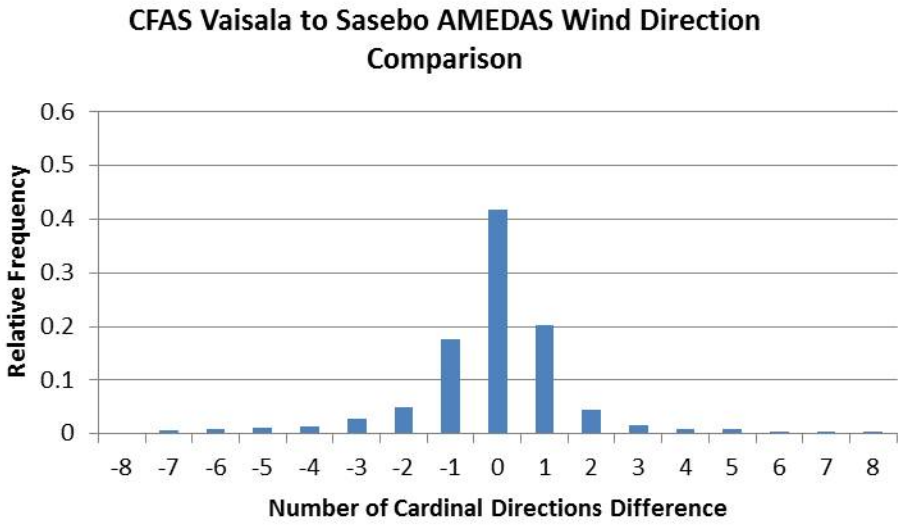

Figure 18. Wind direction differences between the Sasebo JMA sensor and the CFAS Vaisala sensor for all available 10 minute average sustained wind observations during 2012 after excluding light and variable readings. After the Vaisala wind directions were converted to cardinal directions, the quantity (Vaisala direction—AMEDAS direction)/22.5 degrees was calculated to give the number of cardinal point differences between wind directions. Negative numbers indicate the wind backs (turns cyclonically) from the AMEDAS sensor to the Vaisala sensor, positive numbers indicate veering (turning anticyclonically). For example an AMEDAS N wind was associated with a Vaisala N wind approximately 41% of the time, a Vaisala NNE wind 20% of the time, and a Vaisala NNW wind approximately 18% of the time.

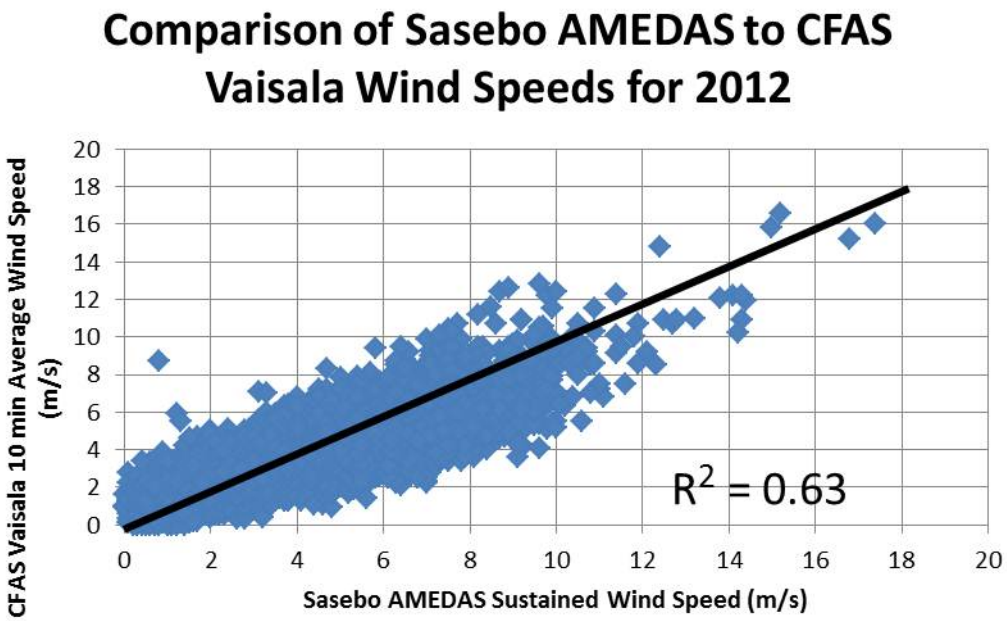

Figure 19. Depiction of all available simultaneous 10 minute average observed wind speeds from Sasebo AMEDAS vs. CFAS Vaisala during 2012. The heavy black line has a slope of 1 and is meant to depict a theoretical perfect match of wind speeds. The given R^2 value was calculated assuming the AMEDAS wind speed was a perfect predictor for Vaisala wind speed.

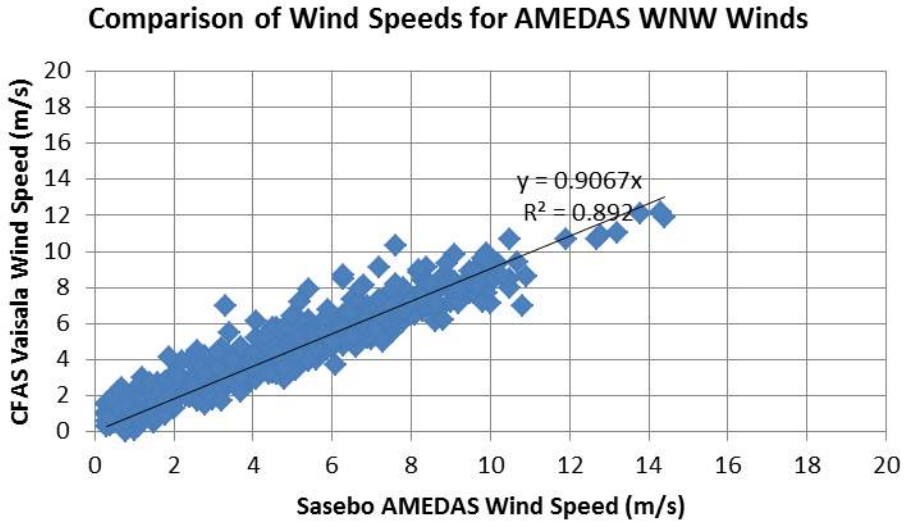

Figure 20. Depiction of all available simultaneous 10 minute average observed sustained wind speeds from Sasebo AMEDAS vs. CFAS Vaisala when AMEDAS 10 minute average direction was WNW. Displayed equation is a linear fit of AMEDAS to Vaisala wind speed with an imposed zero intercept.

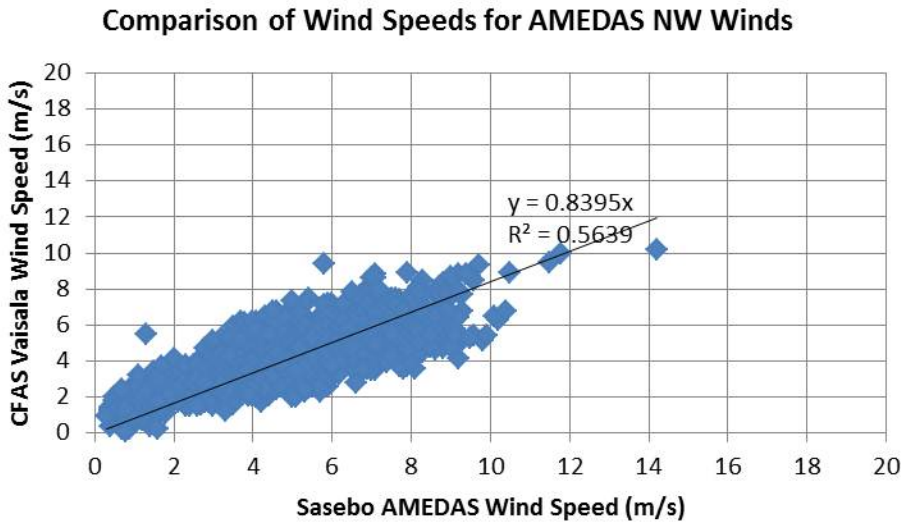

Figure 21. As in Figure 20, except for AMEDAS sustained NW winds. Note the lower R^2 value, and a larger spread of wind speeds around the regression line than that in Figure 20.

The coefficient of determination R^2 displayed in Figures 19–21 is calculated as

$$1—SSE/SST,$$

where SSE is the sum of the squares of the differences between an observed and an expected value, and SST is the sum of the squares of the differences between observations and the mean of the observations. The general interpretation of R^2 is that it is the fraction of the variation of a predictand that is described by the regression of a predictor. So an R^2 of 1 would indicate a perfect match between predicted values and observed values. It is important to note that "described" does not equate with explained (Wilks 1995). However, R^2 values close to 1 do increase confidence that variations in one dataset are related to variations in the other dataset.

A linear fit of Vaisala observations to AMEDAS observations (i.e., the slope of a fit with an imposed zero y-axis intercept as displayed in Figure 20 and 21) provides the typical ratio of Vaisala to AMEDAS wind speed for each cardinal direction as shown in Table 2:

Table 2. Comparison of CFAS 10 minute average wind speeds to Sasebo AMEDAS 10 minute sustained winds sorted by AMEDAS wind direction.

AMEDAS Sustained Wind Direction	Vaisala Wind as a fraction of AMEDAS wind	Coefficient of Determination (R^2)	Number of Observations Compared
N	0.82	0.52	857
NNE	0.84	0.64	430
NE	0.72	0.33	340
ENE	0.71	0.32	603
E	0.76	0.68	1044
ESE	0.80	0.80	1072
SE	0.95	0.85	629
SSE	1.06	0.90	322
S	1.18	0.90	257
SSW	1.11	0.84	371
SW	1.14	0.73	330
WSW	0.86	0.73	448
W	0.81	0.85	407
WNW	0.91	0.89	598
NW	0.84	0.56	1397
NNW	0.77	0.43	1503

The values in Table 2 were determined using Microsoft Excel functions for creating scatter plots and linear trend fitting. A y-intercept of 0 was imposed in all cases so no negative wind speed predictions could occur. Higher R^2 values, especially with larger number of observations, would suggest higher confidence in the results. However interpretation of higher R^2 with a lower number of observations could suggest confidence in that result, or be an anomaly. Results were grouped by AMEDAS observed wind direction, so the simultaneous Vaisala wind direction may or may not have been the same. This convention of grouping by AMEDAS wind direction will be followed throughout unless otherwise indicated. It is interesting to note the spatial

variability. One might expect Vaisala speeds to be higher than the AMEDAS speed for N winds since CFAS is more directly in line with the gap between Mt. Eboshi and Yumihari, but this was not the case (Table 2). Some of the difference might be due to the Vaisala anemometer being approximately 25 m lower in height. Winds at CFAS as a fraction of AMEDAS wind speed when AMEDAS direction was NNW are lower than for most other AMEDAS directions. This is consistent with Mt. Yumihari being NNW from the Vaisala station, which is expected to block winds. The AMEDAS station is more in line with the terrain gap between mountains to its NNW. That SSE to SW winds were generally higher at CFAS than at the AMEDAS station is not surprising since CFAS is more open to the S than the AMEDAS location (see locations in Figure 11).

To further justify the decision to impose a zero y-intercept in the linear fits of scatter plots of AMEDAS to Vaisala winds as displayed in Table 2, linear fits with non-zero intercepts were also considered. For winds from the E, ESE, SE, SSE, S, SSW, SW, WSW, W, WNW and NW, the difference in R^2 values between the two fitting methods are < 0.1 (Figure 22). Although R^2 differences are larger at the other directions, the trend from direction to direction in both sets is the same (e.g., increasing from N to the NNE case, and decreasing from the NNE to NE case). That the R^2 values, in both sets, are smallest for winds generally out of the north indicates greater wind variability from that direction, in keeping with the more complex terrain features in that upstream area.

The decision to use linear fitting was made by visual inspection of all scatter plots. Additionally, all found y-intercept values were < 1.25 m/s, well within typical wind prediction tolerances (i.e., a wind prediction of 0 m/s but a found value of < 2.5 m/s can be considered verified). That, in combination with the trend in R^2 values from wind direction to wind direction being the same whether or not a zero y-intercept is imposed, is motivation to use the simpler-to-interpret linear fits with zero y-intercept.

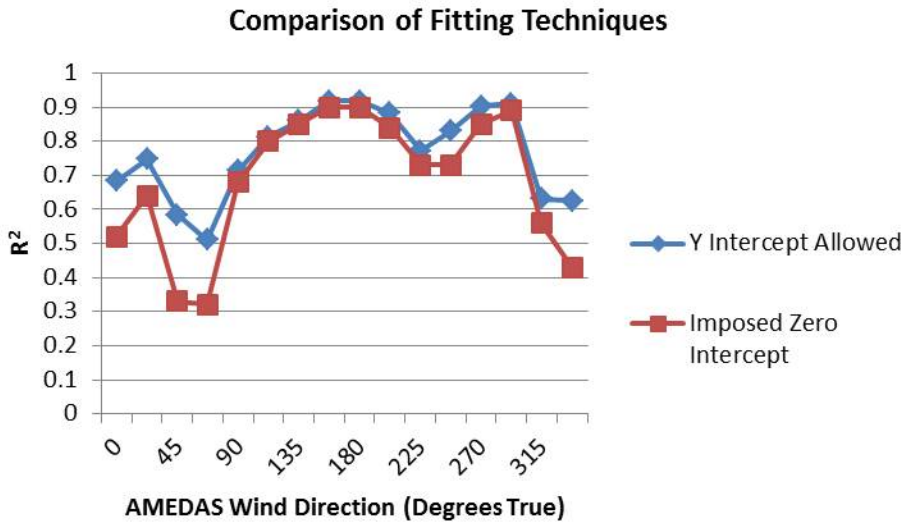

Figure 22. Comparison of R^2 values which result for linear fitting of AMEDAS sustained wind speed to Vaisala 10-minute average wind speed for an imposed zero y-intercept (red squares) and a non-zero y-intercept allowed (blue diamonds).

Comparison of gust wind observations is more problematic than for sustained winds. Observations available from the Vaisala include the maximum gust during the last hour, rather than the maximum gust in the last 10 minutes as is available from AMEDAS records (since 2008). Additionally, the Vaisala data record has multiple irregular gaps in temporal coverage during 2012, with only 10,700 observations available compared to 52,704 AMEDAS observations recorded every 10 minutes for one year. Therefore, for every Vaisala hourly gust observation, the maximum AMEDAS gust speed and direction from the past hour was found. For example, if a Vaisala maximum gust in the last hour observation was available for 1300 UTC, AMEDAS gust readings were examined at 1210 UTC, 1220 UTC, 1230 UTC, 1240 UTC, 1250 UTC, and 1300 UTC and the maximum of those gust observations was selected. This yielded 236 Vaisala to AMEDAS comparisons of maximum gusts in the preceding hour. However, these paired observations may or may not have been at the same 10 minute interval, and only a comparison of cardinal directions can be made.

The hourly maximum gust wind direction at CFAS mostly veers from that at the AMEDAS observation point (Figure 23). Given that the same veering

was not found for the sustained wind observations (Figure 18), the tentative explanation is that this veering may be attributable to the height differences in the anemometers rather than terrain impacts. However, it is difficult to draw firm conclusions due to the possible time differences (as much as 50 minutes) between these observations. It is encouraging that the maximum hourly gust wind at CFAS is roughly 90% of the maximum gusts at the AMEDAS station (Figure 24), where gust observations are available every 10 minutes. Recall from Chapter I.A.1 that operational TCCOR decisions can be based on gust forecasts. Therefore a gust forecast technique might utilize these gust observations at the AMEDAS station with the expectation that the forecast maximum gusts would also apply at CFAS.

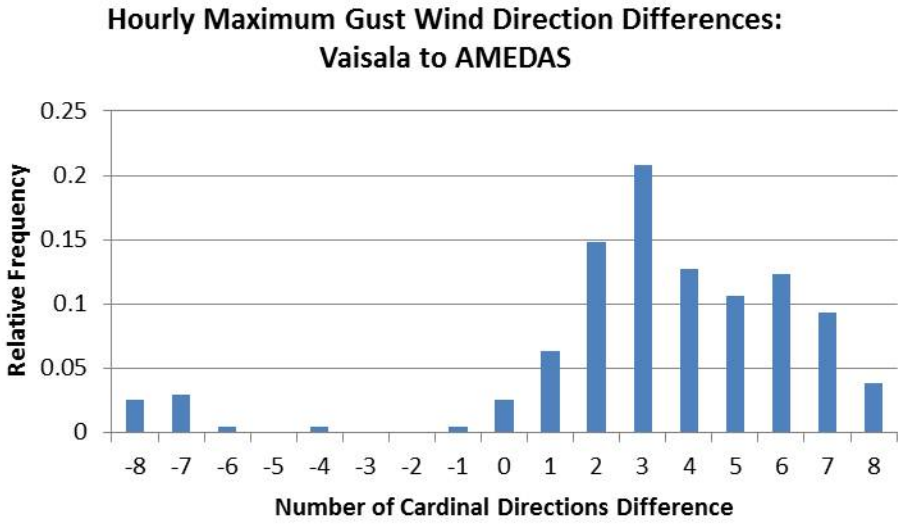

Figure 23. Direction differences between the Sasebo JMA sensor and CFAS for all available hourly maximum gust wind observations during 2012. Vaisala wind directions were first converted to cardinal directions and then the quantity (Vaisala direction—AMEDAS direction)/22.5 degrees was calculated, which gives the number of cardinal point differences between wind directions. Negative numbers indicate the wind backs from the AMEDAS sensor relative to the Vaisala sensor, and positive numbers indicate veering. For example, when AMEDAS gusts were recorded from the E, the most likely Vaisala direction was SSE, or three cardinal directions higher.

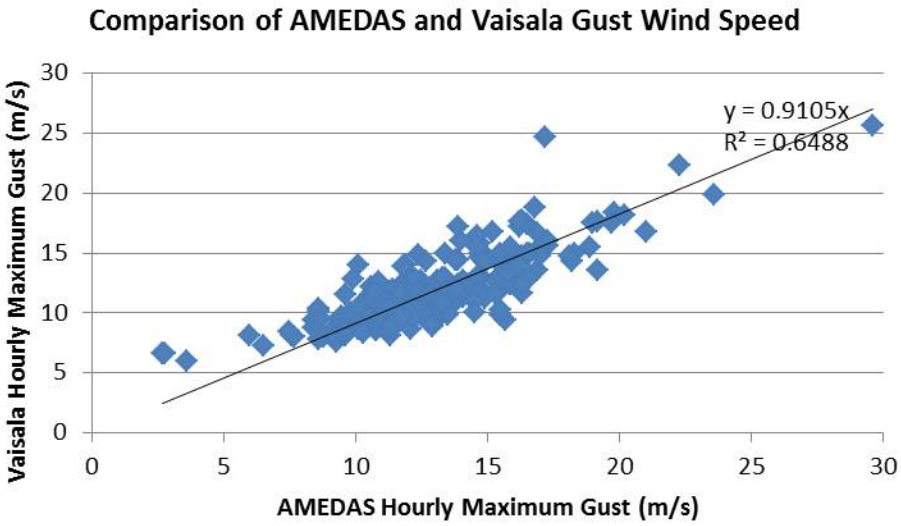

Figure 24. Depiction of all available observed hourly maximum gust wind speeds at Sasebo AMEDAS vs. CFAS Vaisala. The regression equation is a linear fit of the AMEDAS to Vaisala wind speed differences with an imposed zero intercept.

3. Sasebo Fire Department Observations

The Sasebo Fire Department operates a Yokogawa Company Meteorological Data Acquisition System. System output includes 10-minute average wind speed and direction observations on the hour as well as an observed maximum wind gust speed and direction (Y. Sato 2012, personal communication). Although working with translation software and native speakers of Japanese, the author has been unable to verify the gust-averaging interval. Equipment details are available from Yokogawa (2013). The anemometer is mounted on an approximately 1.5 m mast on top of a 3 story tall fire station (Figure 25). Fire station elevation is approximately sea level.

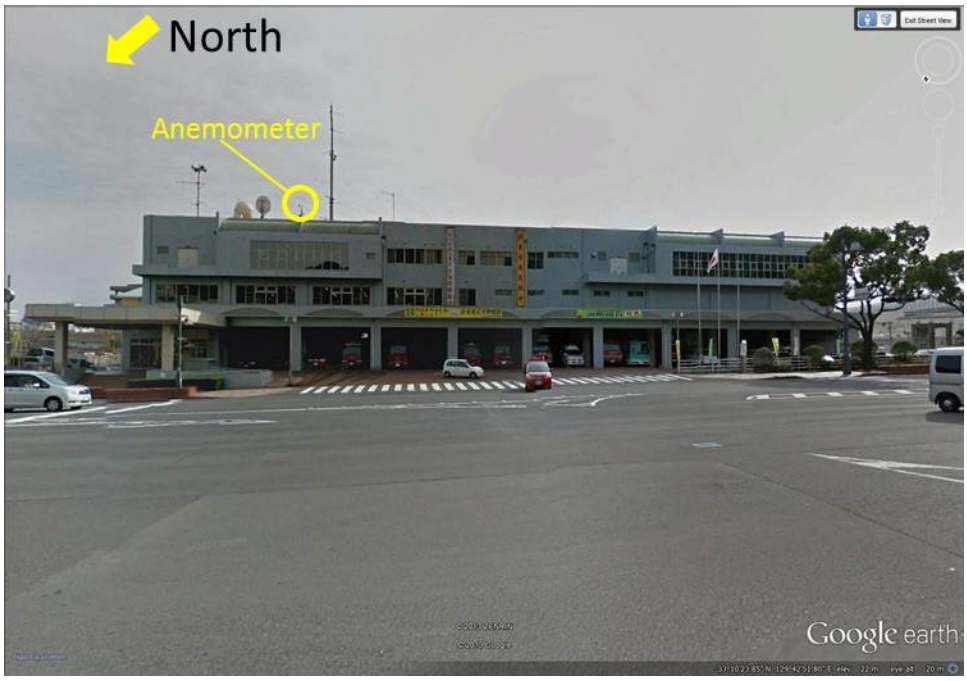

Figure 25. View of Sasebo City, Japan Main Fire Station, which is approximately 1.4 km N of the CFAS Vaisala weather sensor, and 2 km NW of the AMEDAS sensor (after Google Inc. 2013)

Data were graciously provided by the Sasebo Fire Department for approximately 24 hours before and after closest point of approach (CPA) of 17 TCs that passed near to Sasebo from 2007 through 2012. This yielded 1392 observation times for comparison with the AMEDAS observations. The gust observations are of particular interest prior to the 2008 start of regular AMEDAS gust reporting. In particular, it will help to reconstruct if or when Sasebo was really in a destructive wind situation at any time, and how the onset, duration, and offset of significant gusts may vary with direction.

Examining sustained winds first, the hourly wind directions are generally similar between the Fire Station and the AMEDAS station (Figure 26). However the sustained wind speeds at the AMEDAS station are generally 130% of that at the Fire Station for this set of observations (Figure 27). More detailed comparisons by individual cardinal directions such as in Table 2 were deemed of limited use since some directions had as few as 10 wind observations.

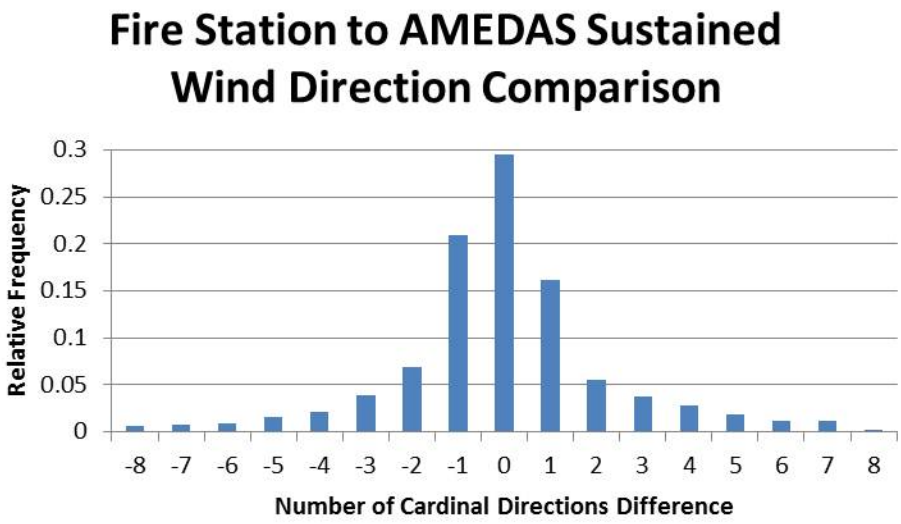

Figure 26. Wind direction differences between the Sasebo Fire Station anemometer and the Sasebo AMEDAS sensor for all available simultaneous sustained wind observations. Note that this figure depicts how much AMEDAS shifts from the Fire Station, vice the convention in Figures 18 and 22 that showed shifts from the AMEDAS direction. This comparison includes data from 2007 to 2012.

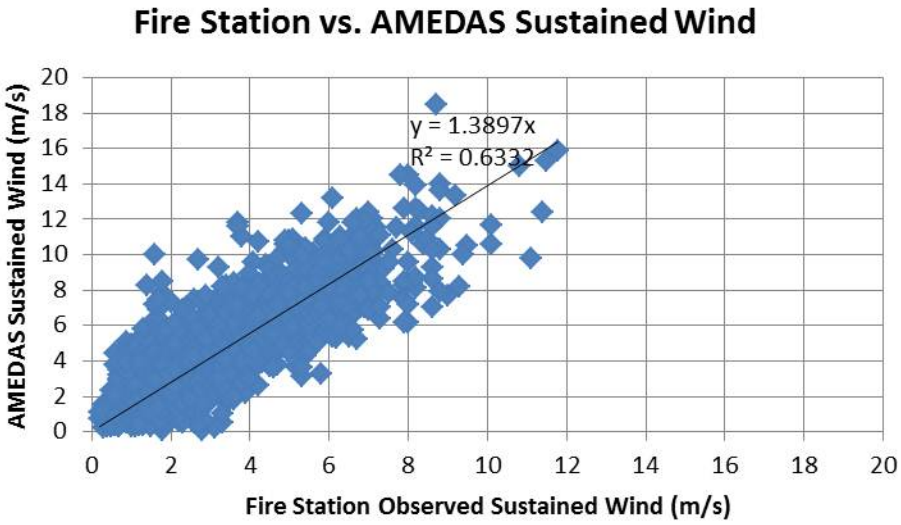

Figure 27. All available sustained wind speeds at the Sasebo Fire Station vs. at the AMEDAS. The regression equation is a linear fit with an imposed zero intercept. This is from the same set of observations as in Figure 26.

Gust wind direction differences between the Fire Station and the AMEDAS (Figure 28) have a larger spread than sustained wind direction differences (Figure 26), but the distributions are clearly centered on 0 for both cases. Furthermore, gust wind speeds (Figure 29) match much closer than for the sustained winds between the observation stations. Although this dataset is too small to draw firm conclusions, the similarity in gusts at these two stations may be due to similar vertical mixing at observation sites at approximately the same elevation. However, the sustained wind speeds at the Fire Station may have been accelerated more than those around the AMEDAS station due to surface roughness differences or flow funneling. Either mechanism could lead to the strong similarity in gust speeds at the two observation locations. Similar to the Vaisala vs. AMEDAS comparisons, it is operationally significant that gust wind speeds at the more inland Fire Station are roughly the same as those at the AMEDAS station despite lower sustained winds. This indicates more care needs to be given to the wind gust forecast to determine if destructive wind criteria are being met for setting the TCCOR at Sasebo.

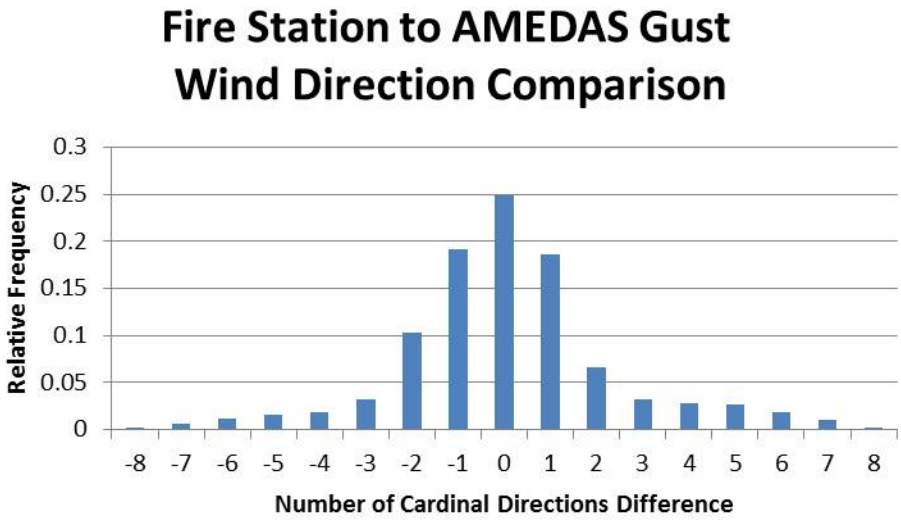

Figure 28. Gust wind direction differences between the Sasebo Fire Station Anemometer and the Sasebo AMEDAS sensor. Note that this figure depicts how much AMEDAS shifts from the Fire Station vice earlier convention, as in Figure 25. The data set is slightly smaller than that of Figures 25 and 26 as regular AMEDAS gust reports only commenced in 2008.

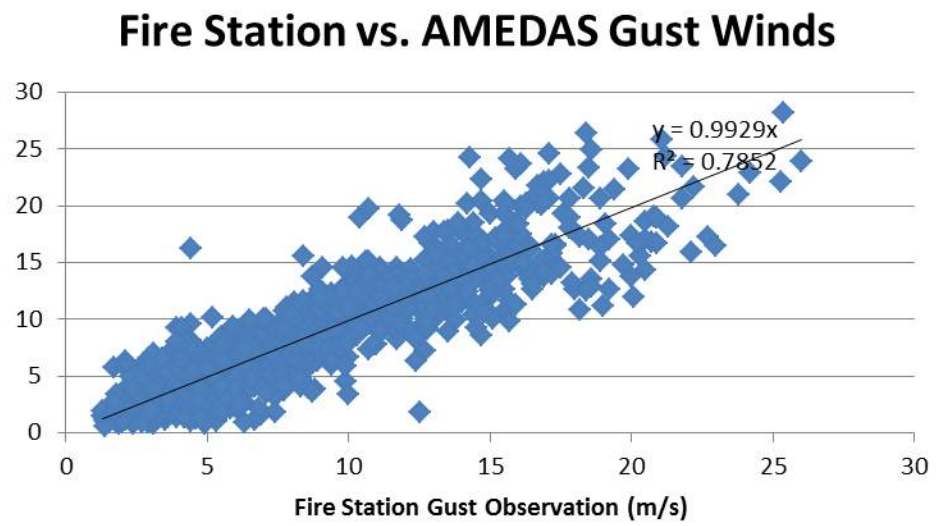

Figure 29. All available gust wind speeds at the Sasebo Fire Station vs. at the AMEDAS station. The regression equation is a linear fit with an imposed zero intercept. This is from the same set of observations in Figure 27.

4. NeWMeK Observations

Researchers from Kyushu University in Fukuoka, Japan graciously provided NeWMeK data they had received from the Kyushu Denki Corporation for time periods around 19 TCs from 2004 to 2012. This yielded 4462 sustained wind observations for comparison to AMEDAS and 3311 gust wind comparisons after 2008. NeWMeK Station 44 is a tower in mostly residential surroundings on the west-southwest slope of Mt. Eboshi (E. Tomokiyo 2012, personal communication) (see Figure 11 and Figure 30). NeWMeK observations include 10-minute average sustained winds and gusts every 10 minutes, so a direct comparison with the AMEDAS observations is possible. The Station 44 anemometer is at 25.5 m above the ground, or approximately 105.5 m above sea level.

Figure 30. NeWMeK Station 44 is located on the power transmission tower indicated above. It is approximately 2.2 km NNE of the CFAS Vaisala sensor and 2.3 km N of the AMEDAS sensor (after Google Inc. 2013)

Cardinal wind direction differences for the AMEDAS relative to NeWMeK Station 44 for sustained winds are shown in Figure 31. These direction differences are fairly well distributed around zero, with perhaps a slight tendency for backing. Although the regression fit implies the AMEDAS sustained wind speeds are virtually the same as NeWMeK winds, the spread of observations around the regression line in Figure 32 is much larger than in the prior inter-station scatter plot comparisons so far presented. Gust wind information is presented in Figures 33 and 34. Although the wind gust direction differences (Figure 33) are similar to those for the sustained winds in Figure 31, the AMEDAS gusts are notably weaker (approximately 85%) than the NeWMeK gusts (Figure 34). It is interesting to note this is opposite to the prior comparison in which the Fire Station sustained winds tended to be weaker and the wind gusts were about the same as at AMEDAS.

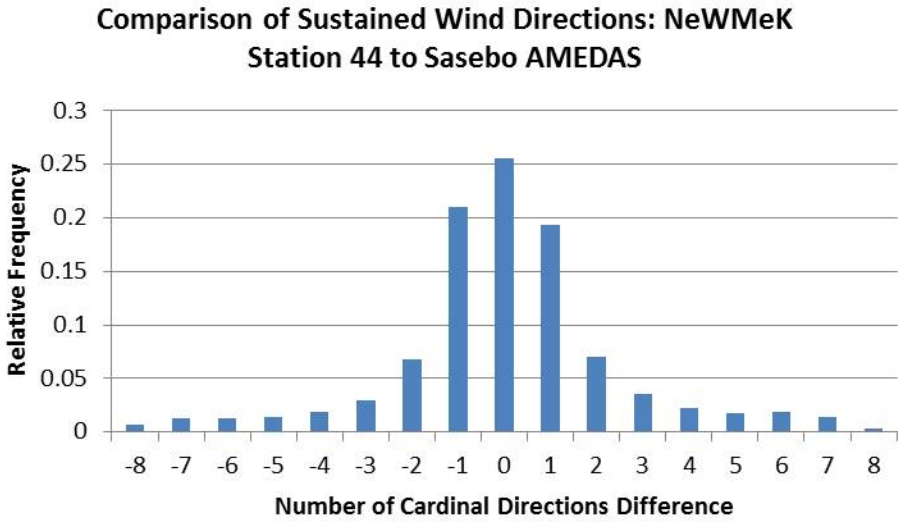

Figure 31. Sustained wind direction differences of the Sasebo AMEDAS sensor relative to the NeWMeK Station 44 for all available simultaneous sustained wind observations.

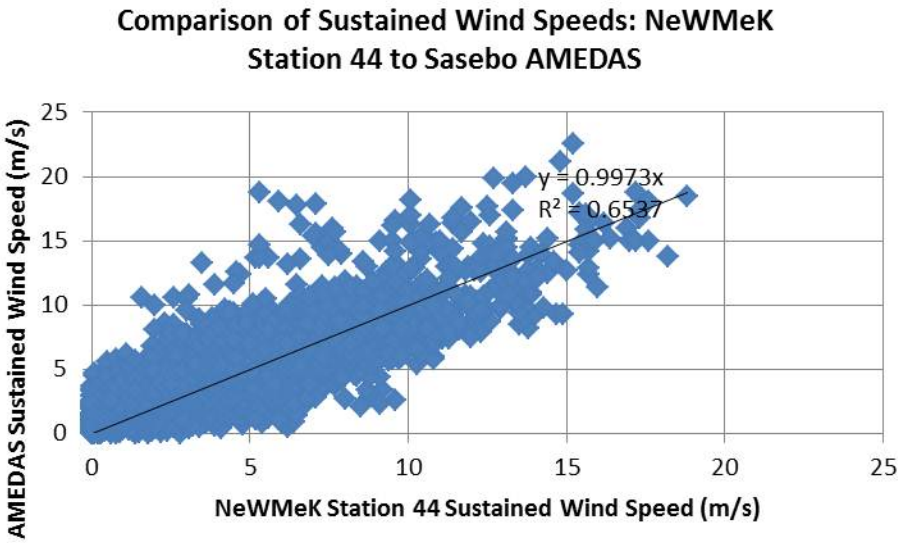

Figure 32. Comparison of all available sustained wind speeds at NeWMeK Station 44 vs. at AMEDAS. The regression equation is a linear fit with an imposed zero intercept. This is from the same set of observations as in Figure 31.

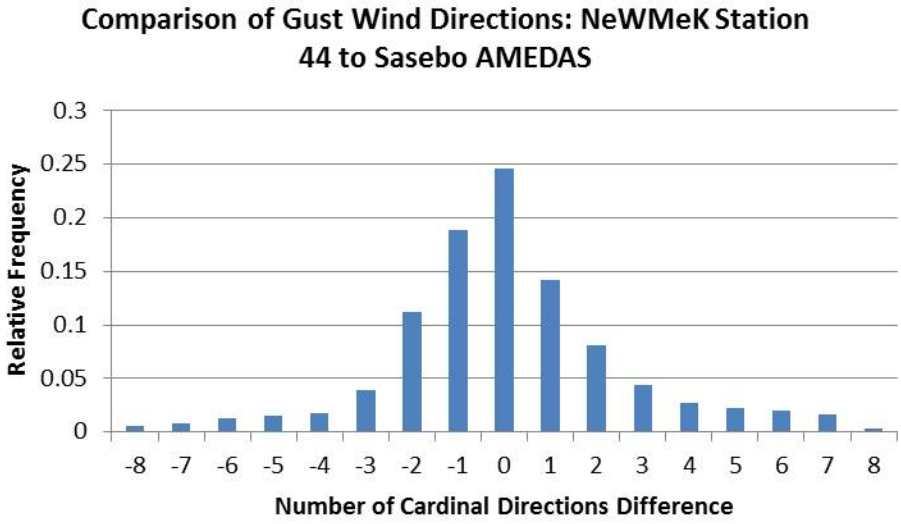

Figure 33. Gust wind direction differences between the Sasebo AMEDAS sensor and the NeWMeK Station 44 for all available simultaneous gust wind observations.

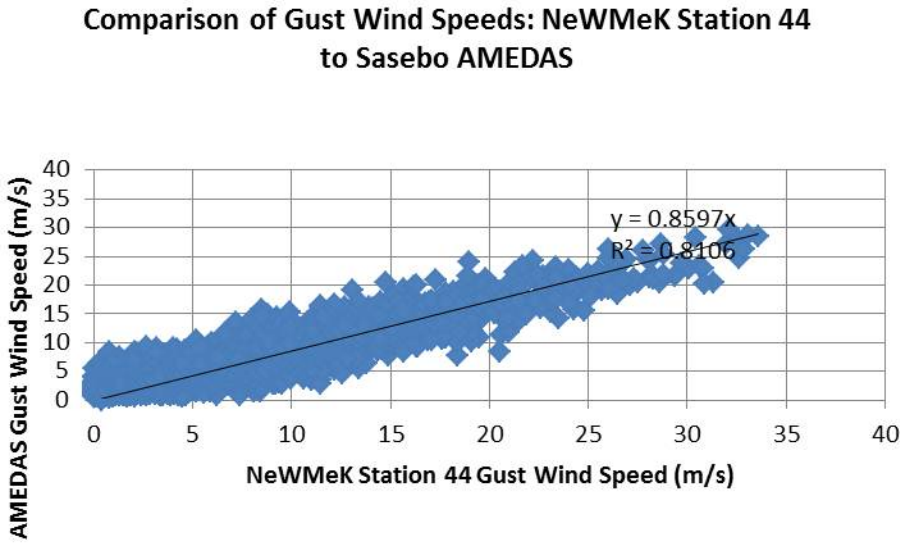

Figure 34. Comparison of all available gust wind speeds at NeWMeK Station 44 vs. at AMEDAS. The regression equation is a linear fit with an imposed zero intercept. This is from the same set of observations as Figure 33.

5. AEROS Sensors

The anemometers at two SORAMAME AEROS sites around Sasebo (see positions D and E on Figure 11) are of interest because the Oono sensor is at the opposite end from downtown Sasebo of the gap between Mt. Eboshi and Mt. Yumihari, which is upstream of CFAS for northerly winds, and the Daitou sensor is east of downtown Sasebo, which is upstream of CFAS in the less well defined east-west gap in terrain. Initial comparisons of AMEDAS data and Oono AEROS data did imply a local acceleration for northerly winds approaching Sasebo. However, there are two major deficiencies for using AEROS data in any significant manner. First, the averaging period for these anemometers has not been confirmed despite repeated author efforts. Most anemometers manufactured in Japan report 10-minute-average winds by default. However, these sensors were installed for pollution monitoring and some of the available documentation implies that the winds reported are true hourly averages, rather than a report every hour of the average winds for the immediately preceding 10 minutes as is done for AMEDAS. Second, it has not been possible to confirm the exact siting of these sensors, particularly with regard to local terrain or buildings. Therefore, AEROS wind measurements will be presented for broad comparison purposes only.

C. TEMPORAL CONSIDERATIONS

1. Primary Time Period for Analysis

Data and cases from 2003 to 2010 will be used to develop empirical relations for sustained winds for forecasting schemes, which allows for internal consistency since the AMEDAS station was in the same location for all of that time. Data from 2009 through 2012 will be used to develop relations for wind gusts. Utilizing all observations from these time periods, rather than just during TC passage, allows for over 70,000 hourly wind observations and over 200,000 every 10-minute gust observations to be compared with other data and predictions. As previously noted, this will allow TCs from 2002 and 2011–2012 to be set aside as test cases for hindcasts using any derived scheme for sustained winds, and any 2013 cases for gust predictions. Cases from 1990 to 2000 are

handled separately, with comparisons to 2003–2010 cases made very cautiously. Data from 1990-1997 will be used to develop relationships based on the earlier data, so 1998–2000 TC activity can be examined.

2. Assumption of Applicability

All empirical schemes for sustained wind derived herein are assumed valid for the same 10-minute averaging period as AMEDAS. Furthermore, any predictions will only be made on the hour. While this is an improvement over the every 3- to 6-hour numerical model predictions local forecasters typically have available, it does not deal with variability on the minute by minute or shorter scale. Gust winds will be assumed to be the maximum wind measured in a 3 second period as available JMA documentation simply refers to maximum instantaneous wind, and 3 seconds is a commonly used period (Harper et al. 2010).

The U.S. Navy differs from most worldwide meteorological services in that it uses a 1-minute averaging period to determine sustained wind (Sampson et al. 1995). Although a variety of empirically-derived conversion factors have been reported, these all must be used with caution. The Navy conversion factor is one-minute mean = 1.14 * ten-minute mean (Sampson et al. 1995). The primary problem with conversion factors is illustrated in the ten minute record of an anemometer sampling at 1 Hz (Figure 35). The ten-minute average wind speed is depicted by a thin horizontal line, with several periods of higher or lower one minute averages depicted by thick black lines.

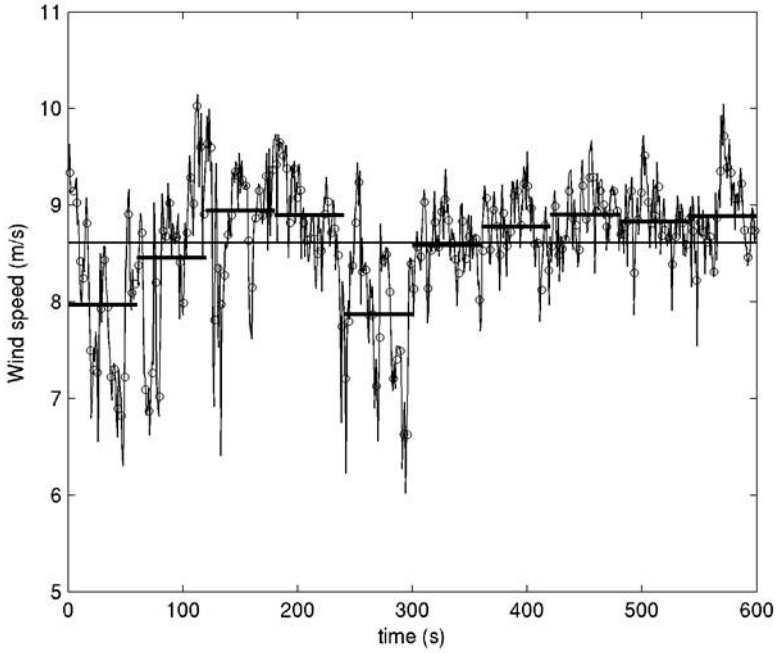

Figure 35. Ten minutes of anemometer readings from Western Australia provided by Harper et al. (2010, Figure 2-3). The thin black horizontal line is the 10-minute average, and the thick black horizontal lines are 1-minute average wind speeds.

If the wind is relatively steady on the scale of ten minutes, the ten-minute average value or one-minute average value should be approximately the same. However, sampling any individual one-minute wind average in a less steady ten minute time window could lead to significant differences from the ten minute average wind. To maintain consistency, Harper et al. (2010) argue that the most valid way to use conversion factors is for gusts at a shorter time period. That is, multiplying a ten-minute average wind speed by a conversion factor for one-minute winds is not the same as one-minute sustained wind speed; rather, it is the maximum average wind speed that should be expected in any one minute sample.

D. WIND MODIFICATION CONCEPT

Regardless of which scheme below that will be used for final predictions, the basic approach here is to treat Sasebo wind as a "black-box." That is, the winds that one would expect from a large TC vortex over open-ocean, possibly modified by other

synoptic forcing, are an input to the forecast technique that will represent the cumulative effects of terrain upstream of and surrounding Sasebo. The wind observed at the AMEDAS station is assumed to be the result of that interaction with the terrain, which can be modeled as the input times an acceleration factor. A schematic of the concept with three steps in the connection between the TC forcing and the Sasebo wind speed and direction is provided in Figure 36.

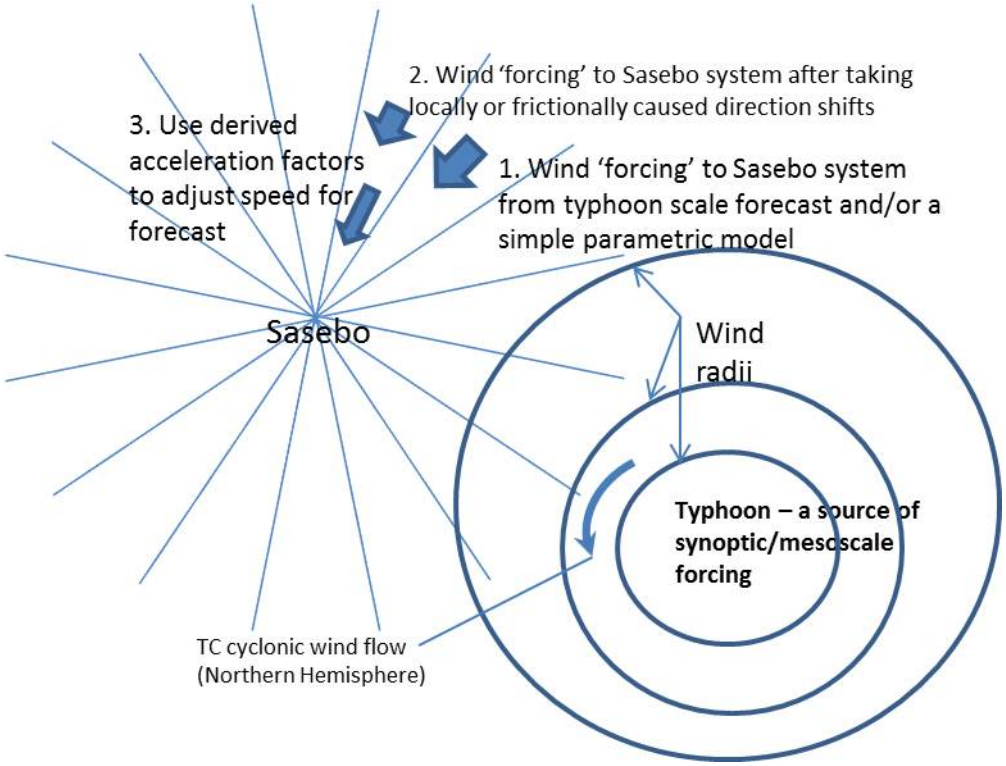

Figure 36. Basic "black-box" concept for Sasebo winds during TC passage. Sasebo is depicted as a point on which the different cardinal directions are centered. The winds generated by the TC are treated as the initial input to a function. While this input has an initial cardinal direction, the interaction with terrain upstream of Sasebo likely shifts the direction, and the cumulative impacts of persistent local features such as terrain cause measurable changes to the wind speed.

The wind field based on JTWC-provided "best-track" analyses will be the primary source for the input winds to the Sasebo black-box. However, only 22 TCs that passed through the basic area of nomogram coverage during 2003–2010 are available for analysis, which yields only a few hundred wind observations. Since terrain based local impacts should be present at all times of the year, it was decided to use non-TC winds

from a reanalysis to compare with the local observations. The advantages of this approach to derive local wind acceleration factors are:

- Tens of thousands of wind speeds from multiple regimes of atmospheric stability, season, time of year, and time of day will be included. While some high-frequency variability in the wind may be averaged out, the most persistent local impacts should emerge.
- Reanalysis models typically have fairly coarse grid spacing (much larger than the ~1 km scale of local features around Sasebo), and would not be expected to capture any local impacts. Thus, differences in observed and reanalysis winds are in part attributable to local terrain. However, the reanalysis may also capture some frictional or land-sea transition impacts.

Ratios of observed wind to reanalysis wind can be calculated each hour (for certain reanalyses), and be grouped into distributions based on observed wind direction (by one of the 16 cardinal points). The means and spreads of these distributions provide an average local acceleration factor and a measure of the uncertainty. The first consideration is to account for the difference between the predicted and observed wind by calculating the likely wind shift and then applying the directional-dependent acceleration factor.

The TC nomogram creation or modification is a separate task, and involves the relationship between the winds observed in Sasebo with the JTWC best-track TC intensity. Details of the TC nomograms are provided in Chapter III.

E. WIND GUST PREDICTION METHODOLOGY

No modeling is necessary to develop an empirical relationship for the wind gust factors in Sasebo. Four complete calendar years (2009 to 2012) with over 200,000 10-minute wind gust observations at the AMEDAS station were examined. Each ten-minute gust wind speed report was divided by the corresponding sustained wind speed to derive a gust factor. Although these were not all hourly (i.e., on-the-hour) reports, they follow the same rules as hourly observations: the sustained wind is the 10-minute average for the 10 minutes immediately preceding the report and the gust wind is the highest wind during the same 10 minutes. Histograms of gust factors were prepared by partitioning the data by sustained wind direction, as well as by sustained wind direction and gust “response” direction. To avoid very high gust factors calculated from very low sustained winds (e.g.,

a 0.1 m/s sustained wind with a gust of 1 m/s yields a gust factor of 10), only sustained winds over 0.5 m/s were initially examined, with later focus on sustained winds over 5 m/s. Higher gusts for sustained wind directions from the N are attributed to funneling between mountain, and from the S to a lack of buildings or other obstructions (Figure 37). Lower gust factors for other sustained wind directions may indicate urban roughness differences rather than terrain impacts.

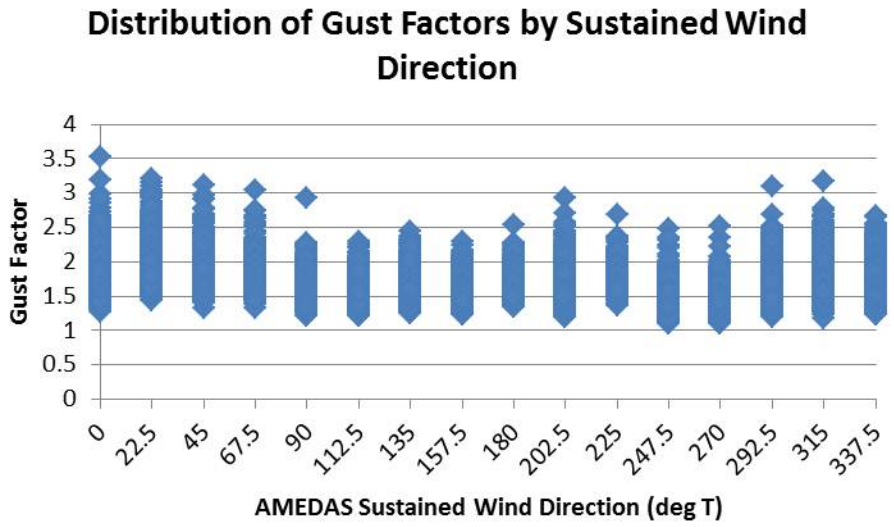

Figure 37. Gust factors calculated as the ratio gust wind/sustained wind for all 10-min AMEDAS sustained wind observations ≥ 5 m/s from 2009 to 2012. Note higher gust factors within a few cardinal points of N and S, and lower gust factors from more easterly and westerly directions.

Note that a strong majority of gust winds are in the same direction as the sustained winds in Sasebo (Figure 38). However, gust winds from a different direction than sustained winds could possibly increase damage. Note that peak gust factor can change by tenths for different gust response directions, which leads to a larger spread of possible responses as sustained wind increases (Figure 39). For example, with a 50 kt input, a N gust response would peak at 1.6 x 50 kt, or 80 kt, while a NNE response could be as high as 100 kt. Further details on the gust factor dependency on the deviation of the gust wind direction relative to the sustained wind direction are given in Table 3. Bold values on the primary diagonal indicate a no-direction shift response, e.g., if a N

sustained wind had a N gust the average gust factor was 1.9, but a WSW sustained wind with a WSW gust had a 1.5 gust factor. Standard deviations for all gust factor values in Table 3 are presented in Table 4.

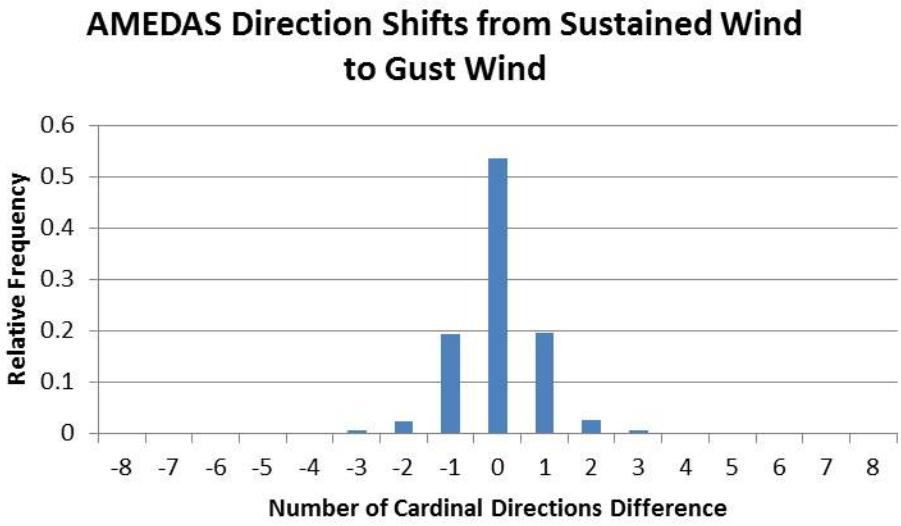

Figure 38. Directional wind difference of the gust wind direction relative to the sustained wind direction at the AMEDAS station in Sasebo from 2009 to 2012.

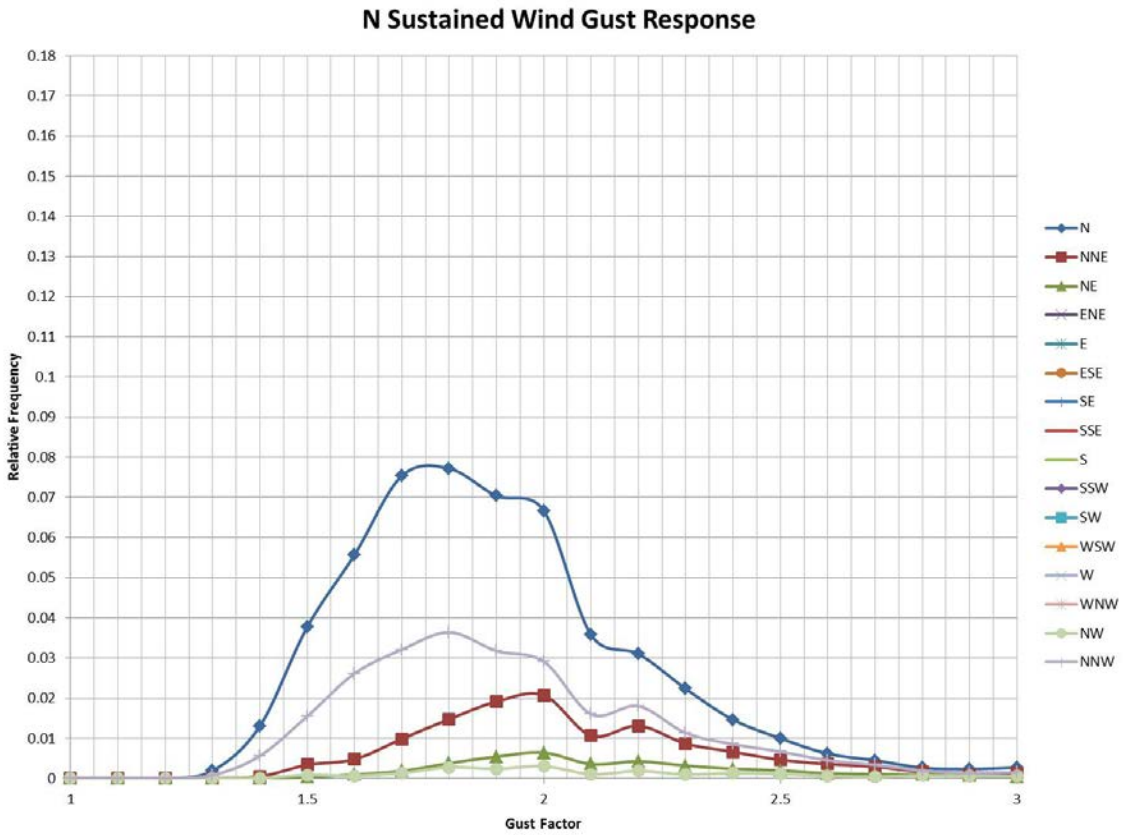

Figure 39. Gust factors as a function of the gust wind direction (key on right) with a N sustained wind observation at Sasebo AMEDAS from 2009 to 2012. Lines connect the centers of histograms binned on every 0.05, or 5%. Such histograms/distributions can be used as an empirical gust forecast tool.

Table 3. Average gust factors for different gust wind directions relative to the sustained wind directions based on AMEDAS observations from Sasebo during 2009–2012. Sustained wind directions are indicated on the left hand column, and gust wind directions along the top row.

	Gust Dir.	N	NNE	NE	ENE	E	ESE	SE	SSE	S	SSW	SW	WSW	W	WNW	NW	NNW
Input Dir.																	
N		**1.9**	2	2.1	2.3	2.5	2.3	2.6	2.4	2.7	2.8	3	2.4	2.8	2.4	2.1	1.9
NNE		2.2	**2.1**	2.1	2.2	2.3	2.4	2.7	2.5	2.5	2.6	2.3	3.3	2.4	2.2	2.4	2.2
NE		2.2	2.1	**2**	1.9	2.1	2.3	2.6	2.6	2.7	2.5	2.4	2.6	2.5	2.5	2.5	2.4
ENE		2.3	2.1	1.8	**1.6**	1.7	2	2.2	2.3	2.7	3.3		2.3	2.2	2.2	2.5	2.3
E		2.3	2.4	2	1.7	**2**	1.7	2	2.1	2.1	2.2	2.7	2.3	2.3	2.6	2.3	2.4
ESE		2.5	2.4	2.3	1.9	1.7	**1.6**	1.7	1.9	2.2	2.5	2.4	2.3	2.1	2.1	2.6	2.6
SE		2.6	2.7	2.6	2.2	2	1.7	**2**	1.7	2	2.1	2	2.5	2.4	2.3	2.5	2.6
SSE		2.9	2.6	2.6	2.6	2.4	2	1.7	**1.6**	1.8	2	2.1	2.2	2.5	2.5	2.5	2.3
S		2.5	2.6	2.4	2.4	2.3	2.4	2.1	1.8	**2**	1.7	1.9	2.2	2.3	2.5	2.6	2.5
SSW		2.9	2.7	3.1	2.4	2.9	2.4	2.3	2	1.7	**1.7**	1.8	2	2.2	2.2	2.4	2.3
SW		2.4	2.5	2.3	2.7	3.1	2.8	2.3	2.1	1.9	1.7	**2**	1.7	2	2.2	2.2	2.4
WSW		2.8	2.5	2.9	2.8	2.5	2.4	2.6	2.1	2.1	1.9	1.6	**1.5**	1.6	2.1	2.3	2.4
W		2.6	3	2.9	2.4	2.6	3				2.1		1.5	**2**	1.6	2.1	2.3
WNW		2.6			3.3			2.4					1.9	1.7	**1.6**	1.7	2
NW		2			2.6									2	1.8	**2**	1.8
NNW		1.8	2.1	2.3	2.3				2.5						2	1.8	**1.7**

Table 4. Standard deviation for gust factors listed in Table 3.

	Gust Dir.	N	NNE	NE	ENE	E	ESE	SE	SSE	S	SSW	SW	WSW	W	WNW	NW	NNW
Input Dir.																	
N		0.1	0.4	0.4	0.5	0.6	0.4	0.4	0.4	0.4	0.4		0.5	1.3	0.7	0.5	0.4
NNE		0.4	0.1	0.4	0.5	0.6	0.6	0.7	0.4	0.7	0.6	0.0	0.6	0.4	0.5	0.5	0.5
NE		0.5	0.5	0.4	0.4	0.5	0.5	0.8	1.2	1.2	0.4	0.7	0.5	0.6	0.5	0.6	0.5
ENE		0.7	0.5	0.4	0.3	0.4	0.5	0.5	0.5	0.9	0.4		0.4	0.3	0.5	0.6	0.6
E		0.5	0.6	0.5	0.4	0.3	0.3	0.5	0.6	0.5	0.2	0.9	0.3		0.4	0.4	0.6
ESE		0.4	0.4	0.6	0.5	0.3	0.2	0.3	0.4	0.4	0.8	0.4	0.4	0.3	0.3	0.7	0.9
SE		0.7	0.7	0.7	0.5	0.4	0.3	0.3	0.3	0.5	0.5	0.4	0.3	0.7	0.5	0.7	0.7
SSE		0.6	0.6	0.7	0.6	0.6	0.5	0.3	0.3	0.3	0.3	0.4	0.4	0.7	0.9	0.6	0.4
S		0.5	0.6	0.6	0.5	0.6	0.6	0.5	0.3	0.3	0.3	0.4	0.5	0.4	0.7	0.5	0.6
SSW		0.8	0.5	0.5	0.6	1.0	0.6	0.6	0.4	0.3	0.2	0.3	0.4	0.5	0.6	0.9	0.5
SW		0.2	0.3	0.4	0.5	1.0	0.8	0.8	0.5	0.4	0.3	0.2	0.3	0.4	0.5	0.4	0.8
WSW		0.5	0.5	0.6	0.2	0.3	0.6	0.6	0.3	0.4	0.4	0.3	0.3	0.4	0.5	0.5	0.6
W		0.7	1.1	0.7	0.6	0.6	0.8				0.5		0.3	0.2	0.4	0.6	0.6
WNW		0.7			0.9			0.6					0.4	0.3	0.3	0.4	0.5
NW		0.4			0.7									0.3	0.3	0.2	0.3
NNW		0.3	0.5	0.5	0.4				0.7						0.4	0.3	0.3

Because not all combinations of sustained wind direction and gust wind direction response are equally likely, histograms of occurrence were examined and the top direction combinations were selected for later use in hindcasts/forecasts. For example, any gust response beyond two cardinal directions from sustained wind direction in Figure 39 is highly unlikely, which is consistent with the histogram of directional differences in Figure 38. Gust factors as high as 3.3 were noted for some unusual direction combinations such as NNE sustained winds with a WSW gust response, but such events are considered to be outliers unrelated to persistent local impacts on 10-minute average sustained wind.

To examine the utility of these gust factors for TC-related forecasting, a comparison of winds was made near the times of the Sasebo CPA for 18 TCs from 2008 to 2012. To account for possible seasonal impacts, monthly average gust factors for each

sustained wind direction were calculated. In addition, an overall average gust factor from the TC dataset was calculated. That is, an average of all observed gust/observed sustained winds. Other constant gust factors were examined, along with gust factors from Table 3 based on observed sustained and gust wind directions. Observed sustained winds were multiplied by each gust factor, and the difference between the observed and predicted gust was recorded. The mean absolute error for all gusts using each technique was calculated for all sustained winds greater than or equal to 5 m/s (Table 5). Note that perfect knowledge of observed sustained and gust wind directions yields the smallest error, with use of monthly by-direction averaged gust factors performing nearly as well. Use of an overall average gust factor from all gust factors from 2008–2012 also does quite well. The value of 2.2 was examined since that secondary peak gust factor occurred for most combinations of sustained and gust wind directions. The overall results imply that use of direction-specific gust factors is marginally better than monthly or constant gust factors. More detailed analysis will be done in case studies below.

Table 5. Mean absolute errors for multiple gust factor determinations for observed winds at Sasebo during passage of 18 TCs during 2008 to 2012.

Different Gust Factors	Mean Absolute Error (m/s)
Monthly Gust Factors	**1.27**
Known Sust. And Gust Directions	***1.22***
1.5	**2.23**
1.6	**1.72**
1.7	**1.46**
1.8	**1.46**
1.9	**1.70**
2	**2.13**
Overall average: 1.76	**1.43**
2.2	**3.37**

An important result in Table 5 is the overall average gust factor of 1.76. In the nomograms of Jarrell (1988) the gusts are first calculated and then the sustained wind is estimated as 2/3 of the gust speed value. That is, it is assumed that gusts are 3/2 of

sustained wind speed, which implies the overall average gust factor is 1.5. However, a 1.76 gust factor led to smaller absolute errors than using a 1.5 gust factor for this sample (Table 5). This over 20% difference in assumed and calculated gust wind factors is a clear indication that the gust wind forecast in Sasebo needs further scrutiny.

Given a forecast sustained wind speed and direction, the values in Table 3 and Table 4 may be applied to make forecasts of the gust speed with a confidence interval. That is the product:

gust speed = sustained wind speed (gust factor ± gust factor standard deviation)

A test of this approach for TC 17W Sanba, which is one of the most recent TCs to significantly impact Sasebo, is shown in Figure 40. Note that for most times the observed gusts lie between Hindcast—CI and Hindcast + CI, where CI is confidence interval, using Tables 3 and 4. That is, Hindcast—CI is the product of gust factor (for known sustained wind direction and known gust direction response minus the standard deviation for that combination of directions) and the observed sustained wind. It is an important result that the observed maximum gust was ~30 m/s, with the hindcast indicating 25–35 m/s at the same time.

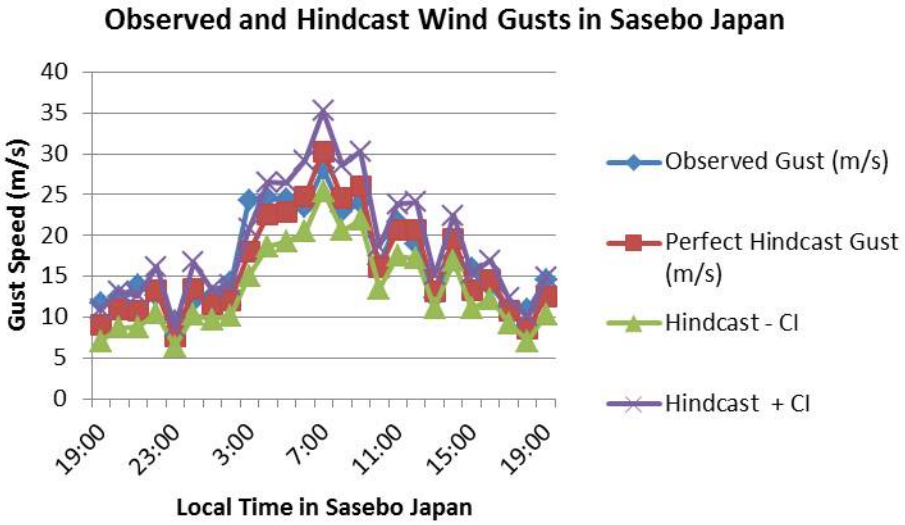

Figure 40. Observed and hindcast gusts in Sasebo during TC 17W Sanba 16–17 Sep 2012.

Of course, a forecaster in real-time does not know the exact sustained or gust wind direction as in Figure 40, and thus has to make certain choices. As described previously, any input wind from a TC to the Sasebo "black-box" in Figure 36 will likely shift the wind direction with some implied uncertainty. The concurrent gust wind direction may also differ from the sustained wind direction (Figure 38). Thus, the forecaster must consider many possible sustained wind directions and gust wind directions to estimate the gust responses. The choices might include a weighted average of all of these options, an examination of all options, or simply choose the most likely case. The author recommends selecting the most likely sustained wind speed and direction at each forecast interval as the input to the gust forecast, and thus forecast the most likely gust speeds and gust directions based on that sustained wind speed and direction. For example, a NE sustained wind from a TC may have a 70% chance of backing to a N wind over Sasebo, with lesser probabilities for other sustained wind directions. The predicted N wind speed would then be multiplied by the gust factor values in Figure 39 (or the values from Tables 3 and 4) to produce a gust forecast for Sasebo. Given the results of Table 5, a good possible alternative is to use monthly gust factors as displayed in Tables 6 and 7.

Table 6. Monthly-average observed gust factors subdivided by sustained wind direction based on observations in Sasebo from January 2009 to December 2012.

	AMEDAS Sustained Wind Direction	N	NNE	NE	ENE	E	ESE	SE	SSE	S	SSW	SW	WSW	W	WNW	NW	NNW
Month																	
All		1.9	2.1	2.0	1.7	1.7	1.6	1.7	1.7	1.7	1.7	1.7	1.5	1.5	1.7	1.7	1.7
Jan		1.9	2.1	2.0	1.7	1.6	1.7	1.8	1.8	1.9	1.9	1.9	1.7	1.7	1.8	1.7	1.7
Feb		2.0	2.2	2.0	1.8	1.7	1.7	1.8	1.9	1.8	1.8	1.8	1.7	1.7	1.8	1.8	1.8
Mar		2.0	2.1	2.1	1.8	1.7	1.7	1.7	1.8	1.8	1.8	1.8	1.6	1.6	1.7	1.7	1.8
Apr		1.9	2.2	2.1	1.7	1.7	1.7	1.7	1.8	1.8	1.7	1.7	1.5	1.5	1.6	1.7	1.7
May		1.9	2.2	2.1	1.8	1.7	1.7	1.7	1.8	1.8	1.8	1.8	1.5	1.5	1.6	1.8	1.7
Jun		2.0	2.3	2.1	1.8	1.7	1.6	1.7	1.7	1.7	1.7	1.8	1.6	1.5	1.7	1.8	1.7
Jul		2.0	2.2	2.1	1.8	1.7	1.6	1.6	1.7	1.7	1.7	1.8	1.5	1.5	1.6	1.8	1.7
Aug		1.9	2.2	2.1	1.8	1.7	1.6	1.7	1.7	1.7	1.7	1.7	1.5	1.5	1.7	1.8	1.7
Sep		1.9	2.1	2.1	1.8	1.7	1.6	1.7	1.7	1.8	1.7	1.7	1.5	1.6	1.8	1.8	1.7
Oct		2.0	2.1	2.1	1.8	1.7	1.7	1.8	1.9	1.9	1.9	1.9	1.6	1.7	1.7	1.8	1.8
Nov		1.9	2.1	2.0	1.8	1.7	1.7	1.7	1.8	1.9	1.8	1.9	1.7	1.7	1.7	1.7	1.7
Dec		1.9	2.1	2.0	1.7	1.6	1.7	1.7	1.9	1.9	1.8	1.8	1.7	1.7	1.7	1.7	1.8

Table 7. Standard deviations for gust factors listed in Table 6.

	AMEDAS Sustained Wind Direction	N	NNE	NE	ENE	E	ESE	SE	SSE	S	SSW	SW	WSW	W	WNW	NW	NNW
Month																	
All		0.4	0.4	0.5	0.4	0.3	0.3	0.3	0.3	0.3	0.3	0.3	0.3	0.4	0.3	0.3	0.3
Jan		0.4	0.5	0.5	0.4	0.4	0.4	0.4	0.5	0.4	0.5	0.5	0.4	0.4	0.4	0.3	0.3
Feb		0.4	0.5	0.5	0.5	0.4	0.4	0.4	0.4	0.4	0.5	0.4	0.5	0.5	0.4	0.3	0.4
Mar		0.4	0.5	0.5	0.5	0.4	0.3	0.4	0.4	0.5	0.4	0.4	0.4	0.4	0.3	0.3	0.4
Apr		0.4	0.4	0.6	0.4	0.4	0.3	0.3	0.5	0.3	0.4	0.4	0.4	0.3	0.4	0.3	0.3
May		0.4	0.5	0.5	0.5	0.4	0.3	0.4	0.4	0.4	0.3	0.3	0.4	0.4	0.4	0.4	0.3
Jun		0.4	0.6	0.7	0.5	0.4	0.3	0.3	0.4	0.4	0.3	0.3	0.4	0.4	0.5	0.5	0.4
Jul		0.4	0.5	0.5	0.4	0.4	0.3	0.3	0.3	0.3	0.2	0.3	0.3	0.3	0.4	0.4	0.4
Aug		0.3	0.5	0.5	0.4	0.3	0.3	0.3	0.3	0.3	0.3	0.3	0.3	0.3	0.4	0.4	0.3
Sep		0.4	0.4	0.5	0.5	0.4	0.3	0.4	0.4	0.4	0.4	0.3	0.4	0.4	0.5	0.4	0.3
Oct		0.4	0.4	0.5	0.5	0.4	0.4	0.4	0.5	0.5	0.5	0.5	0.5	0.5	0.4	0.4	0.4
Nov		0.4	0.5	0.5	0.5	0.4	0.4	0.4	0.4	0.5	0.4	0.4	0.4	0.5	0.3	0.3	0.3
Dec		0.4	0.4	0.6	0.5	0.4	0.4	0.4	0.5	0.5	0.5	0.5	0.5	0.4	0.3	0.3	0.3

THIS PAGE INTENTIONALLY LEFT BLANK

III. CONSTRUCTION AND PERFORMANCE OF EMPIRICAL TECHNIQUES

In this chapter, options will be explored for choosing "input" winds and associated wind direction-dependent acceleration factors during TC passage of Sasebo for use with our "black-box" concept, as previously described. Each particular choice of input winds and acceleration factors, along with decisions on how to consider gusts, is a potential empirical scheme for wind hindcasting/forecasting in Sasebo. The performance of several schemes will be tested with TC cases not included in the development sample. Additionally, the performance of the original nomograms of Jarrell (1988) and the development and performance of a new nomogram (also empirical forecast schemes) will be examined.

A. APPLICABILITY

The nomograms of Jarrell (1988) apply in an approximate 200–300 n mi radius around Sasebo. However, the nomograms do not take differing storm structures into account. Therefore two possibilities for evaluating potential techniques have been selected:

- Whenever a TC is within 200 n mi of Sasebo, which is more conservative than the nomograms in the hope that stronger correlations between TC wind and Sasebo wind could be found than at longer ranges.
- Whenever the range from Sasebo to the center of the TC is less than or equal to twice the reported 34 kt wind radii of the TC. A normalized range will be given by (range/34 kt wind radius). For example, if the 34 kt wind radius is 100 n mi, and the range from Sasebo to TC center is $\leq$ 200 n mi, the normalized range is $\leq$ 2 and a prediction will be made. This is a first-order attempt to handle comparing compact-in-size, but intense, TCs with those larger, but of lesser peak wind strength. It also allows some consideration to a TC center range to Sasebo decreasing, but the wind field contracting, or vice versa.

B. DEVELOPMENTAL DATASETS

As previously mentioned, the primary period to be investigated is since 2003, although data were examined from 1990. The initial criterion for TC selection was a

passage within 3 degrees latitude/longitude of Sasebo, which resulted in a set of 59 TCs with 34 from 1990 to 2000 and 25 from 2002 to 2010. Tracks for these TCs are shown in Figure 41. Testing of empirical or statistical relationships will be with TCs from 2002 and 2011–2012. An earlier set of storms from 1990–1997 was the secondary developmental data set, with TCs during 1998–2000 available for testing. Finally, TCs from 2013 have been reserved for demonstration of this methodology in a forecast mode versus a hindcast mode.

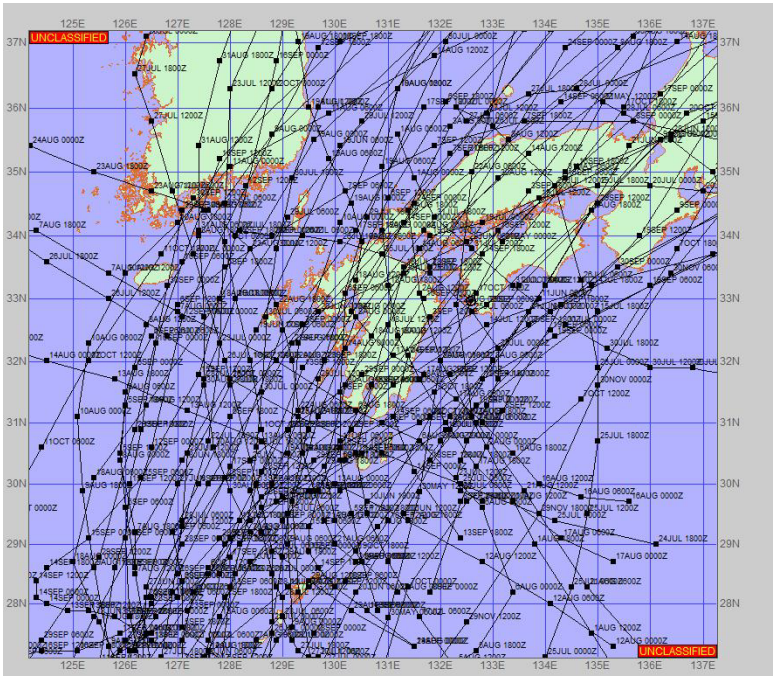

Figure 41. Tracks of 59 TCs during 1990 to 2010 examined in this study (after FNMOC 2013).

C. PARAMETRIC MODEL DEVELOPMENT

As has been utilized in the operational techniques for estimating TC wind probabilities (DeMaria et al. 2009), the modified Rankine vortex parametric model described in Knaff et al. (2007) was used. This parametric model has two basic wind equations for inside or outside the radius (from TC center) of TC maximum winds (r_m):

$$V(r,\theta) = (v_m - a)(r_m/r)^x + a\cos(\theta - \theta_0) \quad \text{for } r \geq r_m \quad (1)$$

$$V(r,\theta) = (v_m - a)(r/r_m) + a\cos(\theta - \theta_0) \quad \text{for } r < r_m \quad (2)$$

with

$$\theta_0 = t_0 + t_1\gamma + t_2 c$$

$$a = a_0 + a_1 c + a_2 c^2 + a_3\gamma$$

$$x = x_0 + x_1 v_m + x_2\gamma$$

$$r_m = m_0 + m_1 v_m + m_2\gamma$$

and

$$\gamma \equiv \text{TC center latitude - } 25^\circ$$

$$c \equiv \text{storm translation speed (in kt)}$$

$$v_m \equiv \text{maximum wind (in kt)}$$

where r is range from TC center to a point of interest (Sasebo), θ is the included angle measured counterclockwise from the bearing 90° to the right of the storm motion vector to the point of interest, x is a size parameter, a is the magnitude of wavenumber-1 azimuthal asymmetry, θ_0 is the degree of rotation of v_m measured in the same manner as θ, and r_m is the radius of TC maximum winds as depicted in Figure 42. The parameters t_0, t_1, t_2, a_0, a_1, a_2, a_3, x_0, x_1, x_2, m_0, m_1, m_2 have been determined in several ways for different ocean basins. For this research, the operational values for the western North Pacific listed in Table 1 of Knaff et al. (2007) (and as further verified by C.R. Sampson 2013, personal communication)) were utilized (Table 8).

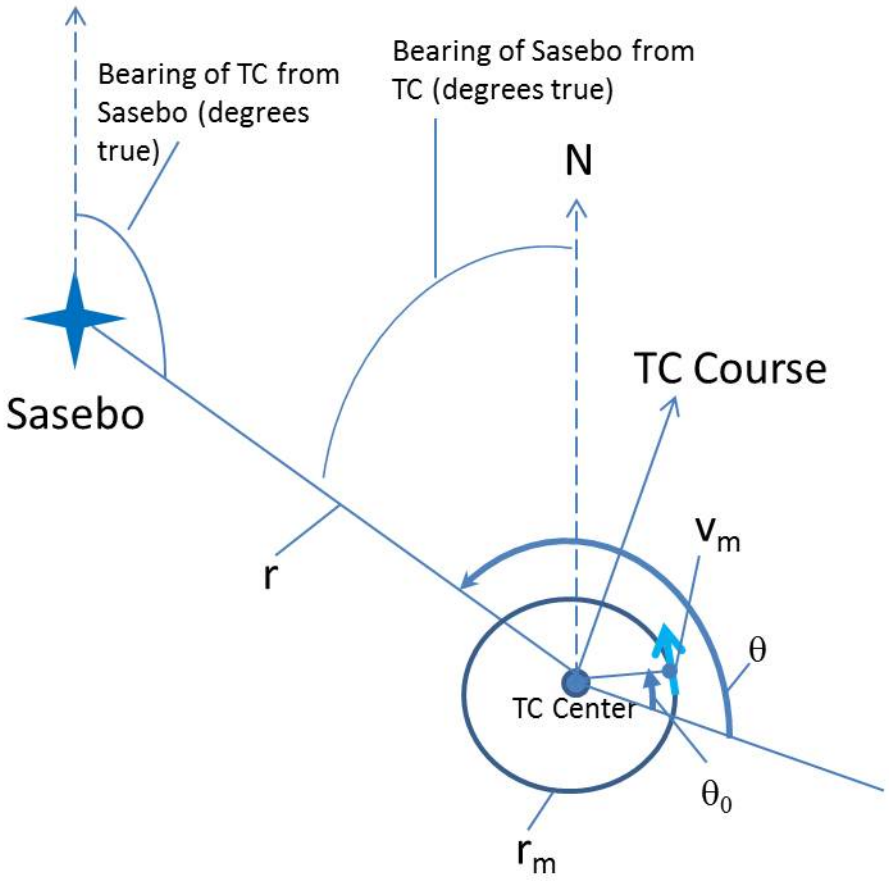

$$\theta = (\text{TC Course} + 90^\circ) - \text{Bearing of Sasebo from TC}$$

$$\text{Add } 360^\circ \text{ if above difference} < 0$$

Figure 42. Schematic of various terms involved in calculating parametric winds at Sasebo. θ and θ_0 are measured counterclockwise from a bearing 90° to the right of the TC direction of motion. In the boxed formula above, all input angles are in degrees true, and the output is a relative angle (e.g., here θ ~ (020 + 90) – 315 + 360 ~ 155 degrees). v_m and θ_0 are determined from JTWC best-track file and an equation from Knaff et al. (2007) respectively. r_m is calculated, unless reported by JTWC.

JTWC best-track reports (or forecasts) from the JTWC website (http://www.usno.navy.mil/JTWC/, Joint Typhoon Warning Center 2013) are used for the 6-hourly fix positions and v_m, as well as r_m for some cases. Storm speed c is also

sometimes provided, or it can be calculated from distance traveled between best track positions. For the hourly wind predictions, linear interpolation is done between the 6-hourly positions, i.e., it is assumed that the course and speed of the TC is constant over the 6-hour interval and the v_m is similarly interpolated.

Table 8. Parameters used for the modified Rankine vortex equations (1) and (2) from Knaff et al. (2007; Table1).

Parameter	Units	Value
t_0	Degrees latitude (°)	15.0000
t_1	None	-0.5500
t_2	° / knot	1.0200
a_0	knot (kt)	0.6300
a_1	None	-0.0100
a_2	1 / kt	0.0006
a_3	kt / °	-0.0300
x_0	None	-0.0059
x_1	1 / kt	0.0055
x_2	1 / °	-0.0031
m_0	Nautical Miles (n mi)	20.0000
m_1	n mi / kt	0.0000
m_2	n mi / °	0.0000

Range and bearing from Sasebo to the TC are calculated via the MathWorks corporation MATLAB program “distance” function, which requires the latitude and longitude of Sasebo (constant) and the hourly latitudes and longitudes of the TC center. Winds calculated from equations (1) or (2) without any adjustment to the parameters in Table 8 will be referred to as parametric unadjusted winds (PUW).

In addition to intensities and positions, the JTWC best track file (or forecasts) may include additional information such as eyewall radius range, radius of maximum wind (r_m), maximum wind gusts, and the 34 kt, 50 kt, and 64 kt wind radii from the TC

center. These wind radii are provided in quadrants around the TC, i.e., the radii of 34 kt winds is not assumed to be symmetric around the TC. JTWC explicitly states that these radii are valid over open water only. However, they will be here used to provide a second wind estimate called parametric adjusted wind (PAW) by modifying the PUW using all JTWC information available. Using the reported r_m vice the calculated values for r_m can obviously change the wind estimates from equations (1) or (2). Inserting wind radii allows a direct solution for the modified Rankine vortex exponent x that is independent of the parameters in Table 8. Inserting r_{34} (the radius of 34 kt winds in the quadrant in which Sasebo lies) and θ_{Sasebo} (the bearing to Sasebo measured counterclockwise from the direction 90° to the right of TC motion) in Equation (1) gives:

$$34 = (v_m - a)(r_m/r_{34})^x + a\cos(\theta_{Sasebo} - \theta_0)$$

which becomes

$$(r_m/r34)^x = (34 - a\cos(\theta_{Sasebo} - \theta_0)) / (v_m - a)$$

and finally

$$x = \log[(34 - a\cos(\theta_{Sasebo} - \theta_0)) / (v_m - a)] / \log(r_m/r_{34}) \quad (3)$$

Similarly, given a 50 kt wind radius (r_{50}) or 64 kt wind radius (r_{64}), the modified Rankine vortex exponent is either:

$$x = \log[(50 - a\cos(\theta_{Sasebo} - \theta_0)) / (v_m - a)] / \log(r_m/r_{50}) \quad (4)$$

$$x = \log[(64 - a\cos(\theta_{Sasebo} - \theta_0)) / (v_m - a)] / \log(r_m/r_{64}) \quad (5)$$

When the range from Sasebo to TC center is between two given wind radii, the MATLAB "fit" function is used to calculate the PAW wind speed estimate at Sasebo. It is assumed that wind speed takes the form of a power function between the two wind radii (i.e., wind speed ~ [range from TC center]^{constant}), which is consistent with equation (1) where $V \sim r^{-x}$. This ensures that when Sasebo's range to TC center is between r_{34} and r_{50} the calculated V at Sasebo will be between 34 and 50 kt. If multiple wind radii are available but the range from TC center to Sasebo is not between these radii, the exponent x from the nearest radii is used. A summary of the calculations for the PUW or the PAW estimates based on available JTWC storm characteristics is given in Table 9.

Table 9. Methods for calculating the PUW or the PAW parametric wind depending on range (r) and wind radii data available from JTWC.

Range Regime	
	Wind Speed Calculation
No wind radii available	
$r > r_m$	V calculated per Equation (1) with parameters from Table 8.
$r < r_m$	V calculated per Equation (2) with parameters from Table 8.
Wind radii available	
$r > r_{34}$	Calculate x per Equation (3), then V per Equation (1) with other parameters from Table 8.
$r < r_{34} < r_m$, no r_{50} or r_{64}	Calculate x per Equation (3), then V per Equation (1) with other parameters from Table 8.
$r_{34} > r > r_{50}$	Use MATLAB to fit a power function for V with wind speed of 34 kt at r_{34} and 50 kt at r_{50}, then solve for V at r.
$r_{50} > r > r_m$, no r_{64}	Calculate x per Equation (4), then V per Equation (1) with other parameters from Table 8.
$r_{50} > r > r_{64}$	Use MATLAB to fit a power function for V with wind speed of 50 kt at r_{50} and 64 kt at r_{64}, then solve for V at r.
$r_{64} > r > r_m$	Calculate x per Equation (5), then V per Equation (1) with other parameters from Table 8.
$r < r_m$	V calculated per Equation (2) with parameters from Table 8. Note no x in Equation (2).

Notes:
1. r is range from TC center to Sasebo.
2. For PAW, when available JTWC best track or forecast r_m is used instead of calculated r_m. PUW always uses x and r_m as calculated in Knaff et al. (2007).

D. SELECTION OF DIRECTIONALLY-BASED ACCELERATION FACTORS

1. Selection and Performance of Reanalysis Model

The Climate Forecast System Reanalysis (CFSR; Saha and Coauthors, 2010) was also used in this study. Reanalysis models retroactively incorporate observations that were not available during operational forecast runs of numerical

weather models. While these techniques do not provide 'perfect' reconstructions of past weather, they provide a physically self-consistent method to examine the past at more regular and higher spatial and temporal resolutions than objective analyses of the raw observations. The CFSR provides 6-hourly reanalysis fields of most variables. CFSR has the added advantages of providing hourly forecast values (i.e., integrating the core model forward between reanalysis times; CFSR uses a variant of the Global Forecast System synoptic-scale numerical weather prediction model), and being available on a grid spacing of 0.5 degrees latitude/longitude.

JTWC reports TC center positions to the nearest tenth of a degree of latitude and longitude. The Sasebo AMEDAS sensor is at 33.2° N, 129.7° E in the ITRF datum, which is virtually identical to the WGS-84 datum used by the Global Positioning System (A. Yamamoto 2011, personal communication; Global Positioning System 2013). CFSR 10-meter u and v wind fields for the grid point 33° N, 130° E from 1979 to 2012 were graciously downloaded and provided to the author by Mr. Robert Creasey, Department of Meteorology, Naval Postgraduate School. For consistency, it was decided to use the 6-hourly forecast fields from the immediately preceding synoptic time, and then the 1–5 hourly forecast fields from the current synoptic time, to acquire wind data for each six-hour block of output. These u and v wind components were then used to calculate a vector wind speed and direction (again following standard convention of the wind coming from a direction), and that wind direction was further converted to a cardinal direction as per Table 1.

The CFSR-derived wind directions, wind speeds as a function of cardinal wind directions, and a comparison of the CFSR wind speed magnitudes with the AMEDAS observations at Sasebo during 2003–2010 are shown in Figures 43–45. Similar comparisons for 1990 to 1997 when the AMEDAS Sasebo sensor was in a different location are given in Figures 46–48.

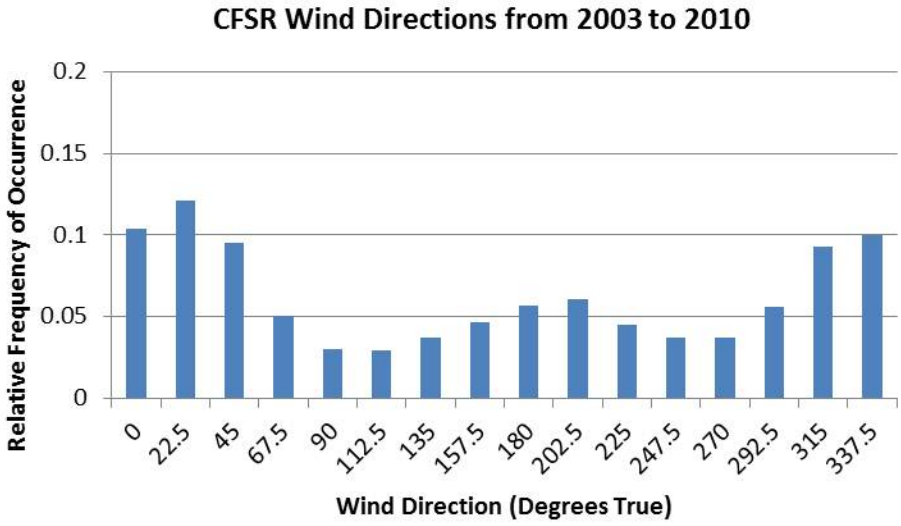

Figure 43. Histogram of calculated cardinal wind direction at CFSR gridpoint 33° N, 130° E for 2003 to 2010. Compare with Sasebo AMEDAS observations in Figure 14.

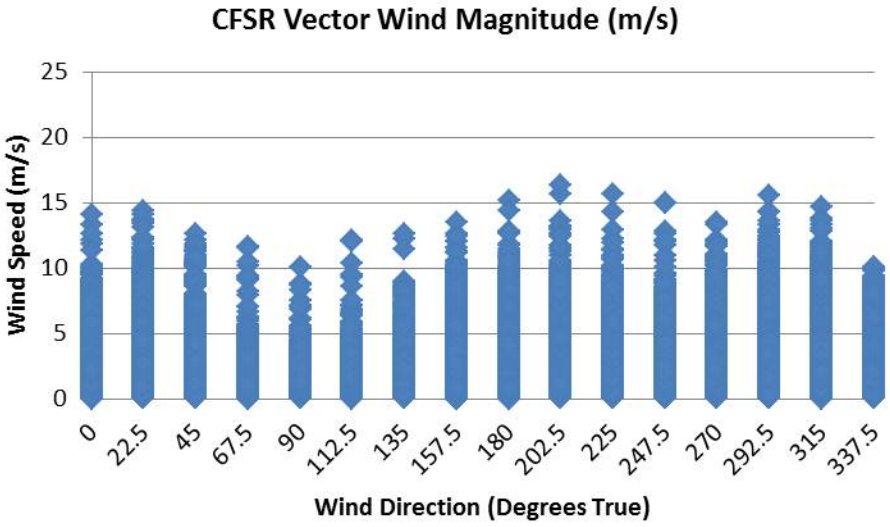

Figure 44. Wind speeds as a function of wind direction at CFSR gridpoint 33° N, 130° E for 2003 to 2010. Compare with Sasebo AMEDAS observations in Figure 16.

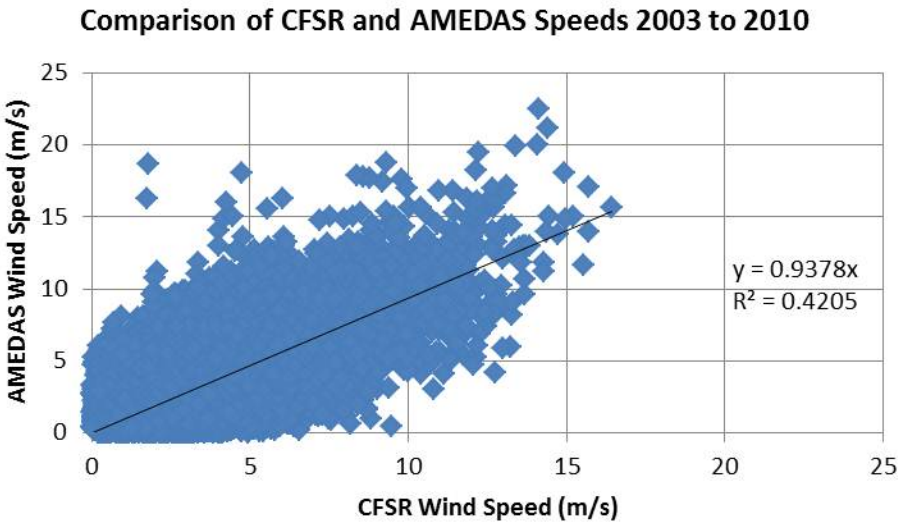

Figure 45. Comparison of CFSR and AMEDAS wind speeds from 2003 to 2010. Note the fitted trend-line suggests AMEDAS winds were typically less than CFSR. AMEDAS and CFSR winds were typically within ± 7 m/s.

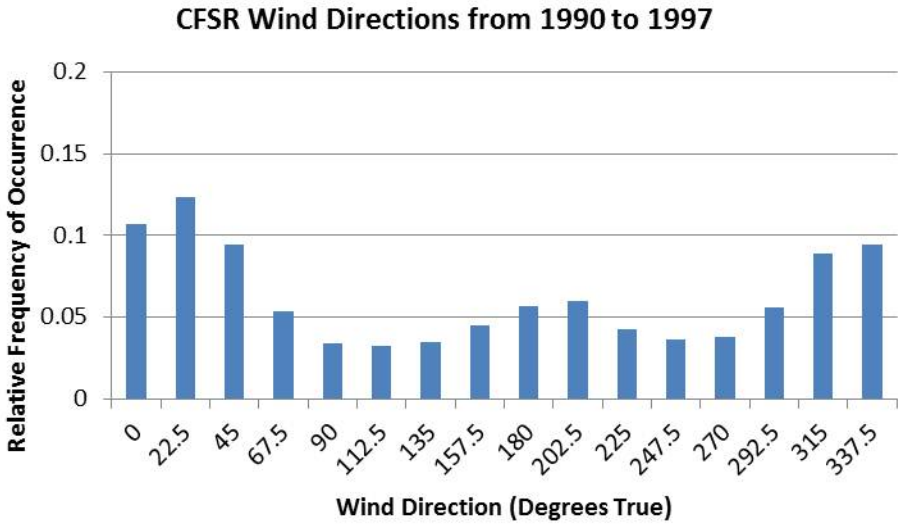

Figure 46. As in Figure 43, except from CFSR 1990–1997 reanalyses. Note the close correspondence with Figure 43, which is expected for same CFSR gridpoint.

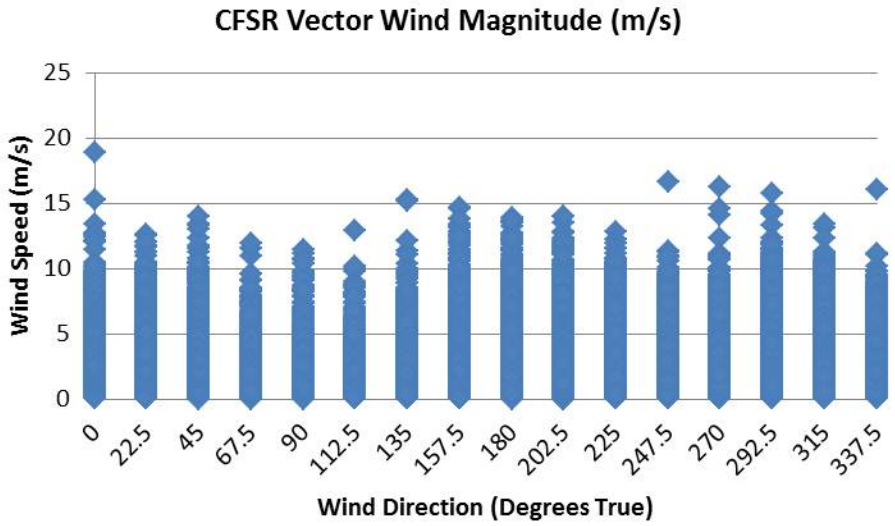

Figure 47. As in Figure 44 except for 1990 to 1997 CFSR reanalyses. Note close correspondence to Figure 44, as expected for same CFSR gridpoint.

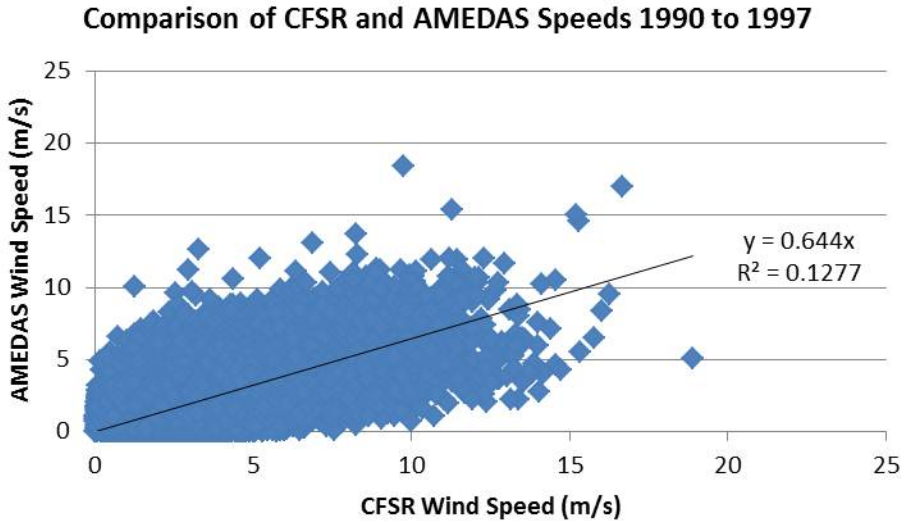

Figure 48. As in Figure 45 except for the 1990 to 1997 Sasebo AMEDAS and CFSR data. Note that AMEDAS speeds during this period were only approximately 64% of CFSR speeds, vice approximately 94% during the 2003–2010 timeframe. This difference is attributable to the AMEDAS sensor change of position.

Compared to the Sasebo AMEDAS wind direction observations in Figure 14, the 2003–2010 CFSR wind directions have a higher frequency of N, NNE, and NE winds and a lower frequency of E winds, which is attributed to Mt. Eboshi's blocking effect being

underestimated in the CFSR, and local channeling factors that favor easterly winds. It should also be noted that peak CFSR winds during 2003 to 2010 tend to be smaller for almost all directions (Figure 44) than in the AMEDAS observations in Figure 16. That is, the CFSR, along with other reanalyses, has a low wind speed bias during 2003–2010 particularly when examining TCs (Schenkel and Hart 2012). However, this low bias does not necessarily apply for the more sheltered AMEDAS location during 1990 to 1997 (Figure 47). This low bias during 2003–2010 will be dealt with in multiple ways to be discussed below. The scatter plot of CFSR and AMEDAS wind speeds from 2003 to 2010 has an R^2 value of only 0.4205 (Figure 45), which reflects a spread of approximately $\pm$ 7 m/s between the data sets. During the 1990 to 1997 period (Figure 48) the AMEDAS wind speeds were notably lower than the CFSR wind speeds.

Histograms of the ratio of the hourly AMEDAS winds to the CFSR winds (i.e., an acceleration factor) were made as a function of the AMEDAS wind direction (Figure 49). Bins were made every tenth of an acceleration factor, so that for a 50 kt wind in TC conditions, each bin would represent a 5 kt change. The histogram for an AMEDAS N wind direction indicates the tendency for frequent acceleration factors < 1, but also a considerable number of acceleration factors of 1.5 and greater.

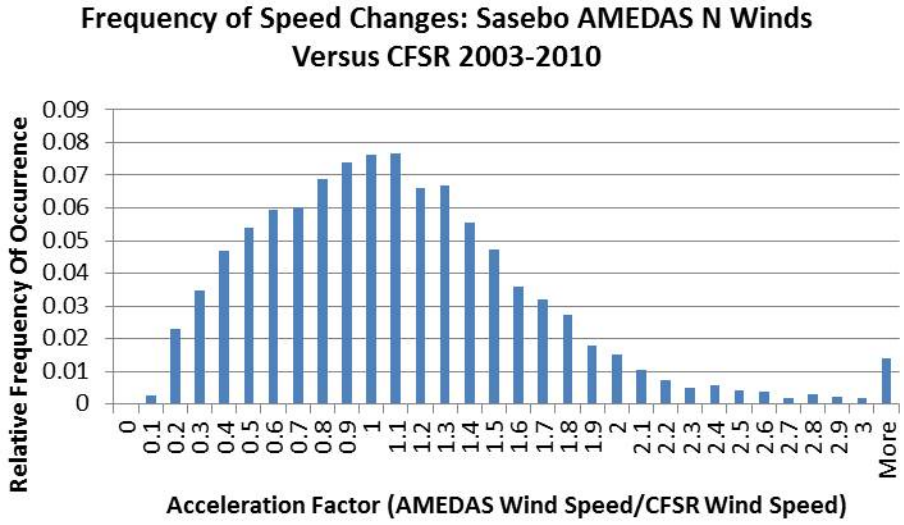

Figure 49. Histogram of the ratio of hourly AMEDAS wind speed in Sasebo to CFSR hourly calculated wind speed at 33° N, 130° E during 2003 to 2010 for all instances when an AMEDAS N wind was recorded.

Histograms for other AMEDAS wind directions showed variations in the most frequently occurring acceleration factors. One caveat in interpreting these histograms is that many fewer comparison pairs are available (especially for infrequently-occurring wind directions in either the CFSR or Sasebo records) than when making gust factor histograms in Chapter II (i.e., ~200,000 10-minute sustained wind observations with accompanying gust observations available from 2009–2012 versus ~70,000 hourly observations from 2003–2010). Therefore, different probability distributions were fitted to the acceleration factor histograms. Fitted normal, log-normal, Weibull, gamma, Rayleigh, and beta distributions were all examined with concurrent chi-squared goodness of fit testing. It was noted that fitting these curves resulted in the distribution peaks generally shifted 0.1 or more. For example, the most frequently occurring acceleration factor in Figure 48 is around 1 or 1.1, but the fitted distributions might have a peak at 0.9 or 1.2. For a CFSR input of 50 kt, multiplying by an acceleration factor of 0.9 yields a 45 kt potential AMEDAS wind vice multiplying by 1.1 for 55 kt. This is operationally significant both for a TCCOR threshold of 50 kt and for typical forecast verification, where a difference of 10 kt between predicted and observed winds is an oft chosen criterion for a forecast "bust." Therefore, a more empirical approach was taken.

One can estimate an empirical probability density function via the kernel function method (Ramlau-Hansen 1983). MATLAB has a built-in function "ksdensity" that takes the raw hourly AMEDAS to CFSR wind ratios and bins and compares that data to produce a probability distribution. This technique has the distinct advantage of keeping the approximate peak of constructed occurrence histograms. For example, as discussed for N AMEDAS winds the peak occurring acceleration factor as determined by histogram (Figure 49 and 50) is around 1. Overlaying the empirical probability distribution function (red dashed line, Figure 50) the corresponding peak value is found near an acceleration factor of 1. The Appendix includes figures for the other cardinal directions.

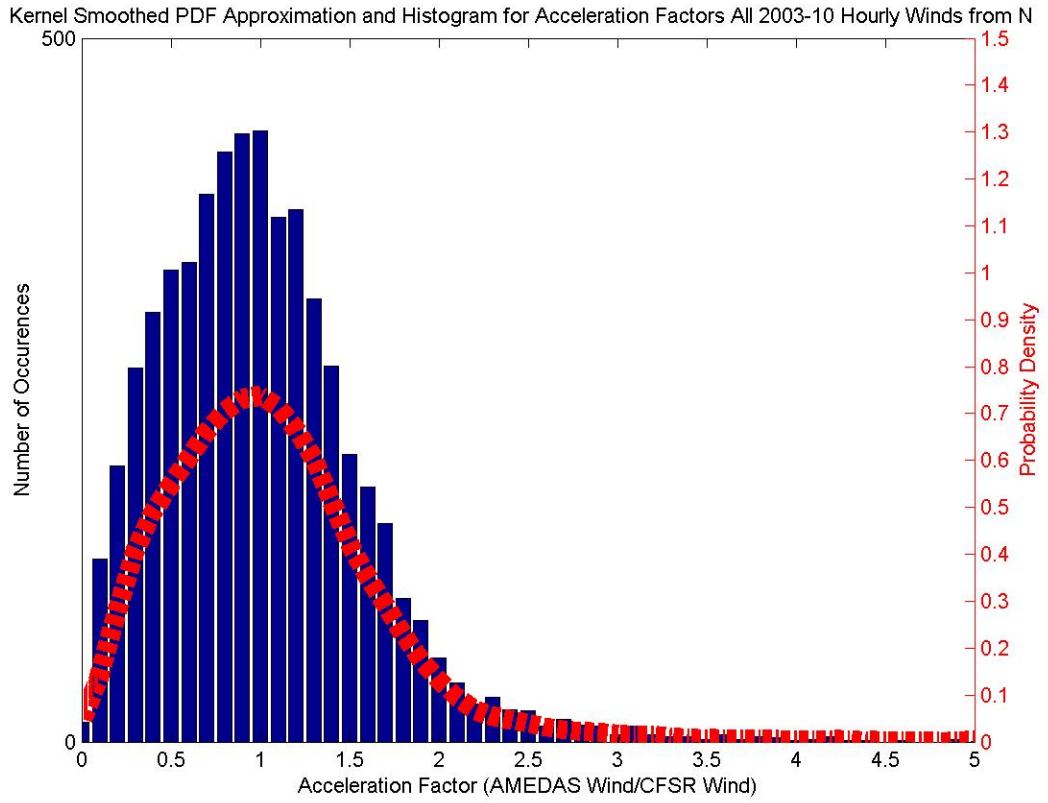

Figure 50. Comparison of histogram of number of occurrences of different acceleration factors (blue bars) to a kernel-smoothed probability density derived from the same data (red dashed line). Here the acceleration factors (AMEDAS wind/CFSR wind) are from all hourly values in 2003–2010 for which the AMEDAS wind was from the N.

As indicated in Figure 14 for AMEDAS data during 2003–2010, not all wind directions had equal numbers of observations available. Therefore, for comparison, histograms and empirical probability distribution functions were also created for the 1000 maximum wind speed observations from each direction. While the smallest number of observations for any cardinal wind direction was 1750, some of these observations had very low wind speeds. Choosing the 1000 maximum wind speeds then assured a sample that might reasonably be expected to have an acceleration factor relevant to TC-related winds at Sasebo. A third set of acceleration factors were calculated from the winds within

± 48 hours of the CPA for each TC examined during the 2003–2010 period. The ± 48 hour time frame was chosen to account for the large variety of TC translation speeds when passing Sasebo.

The three sets of derived acceleration factors are compared in Figure 51. It is interesting to note that for all sets there is a relative maximum for N winds, a decrease for winds from the direction of Mt. Eboshi, and then an increase again as terrain opens up for the more easterly directions. A partially obstructed terrain gap to the west of downtown Sasebo, roughly between Mt. Akasaki (see Figure 10) and Mt. Yumihari, may explain the sharp rise in acceleration factors for W winds. The strong similarities noted here reinforce the idea that comparing synoptic-scale wind fields with local winds can reveal persistent station-specific factors.

However, the trends as winds shift to the south are not so consistent. In particular, for the "All" case one sees a distinct drop in acceleration factors for SSE and S winds. Examining distributions for these directions (see Appendix) one notes a broader, flatter peak shape than for other cardinal directions. This implies the choice to use the most frequently occurring acceleration factor was too simplistic, and after the fact it was realized that a better result might come from calculating the most likely value of the distribution. When this is done (most likely value is taken as the sum of the calculated probability of each acceleration factor times each acceleration factor), a much closer match to the "Top 1000" case occurs (Figure 52).

When choosing acceleration factors for testing, both the "All" case and "Top 1000" cases of Figure 51 were examined. The performance of "Near TC CPA" case acceleration factors was not examined in great detail for two reasons. First, the assumed advantage of using the CFSR was that comparing Sasebo winds to a synoptic scale wind field over as many instances as possible would better capture natural variability than using a much smaller set of comparisons. Therefore we have less confidence in the applicability of "Near TC CPA" acceleration factors. Second, a separate methodology to find acceleration factors derived from winds related to TC passage of Sasebo will be described in the following sections.

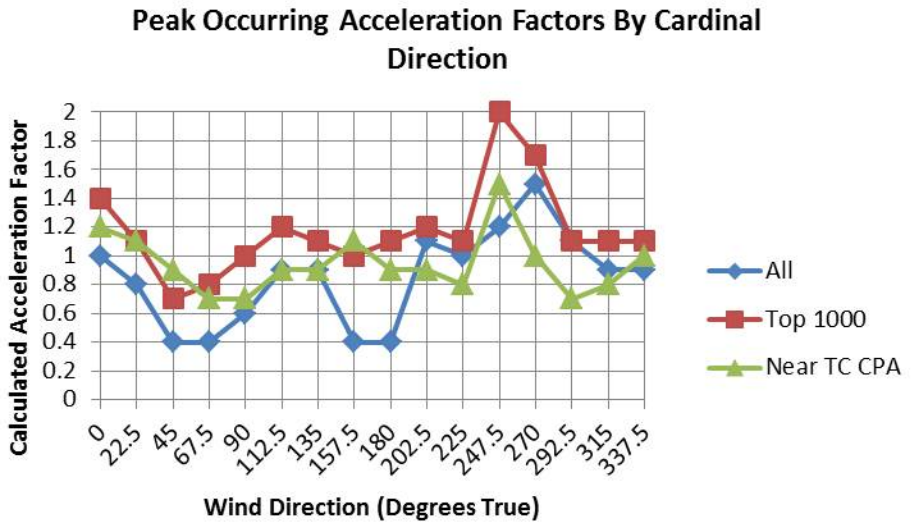

Figure 51. Peak occurring acceleration factors by cardinal direction from empirical probability distribution functions based on three data sets. The acceleration factors were calculated by dividing hourly AMEDAS observed winds at Sasebo from 2003–2010 with CFSR winds for 33° N, 130° E at the same times. The blue diamond line represents "All" data from 2003–2010 being used, the red squares are for the data set of the "Top 1000" wind observations from each cardinal direction were used, and the green triangles are for the data set "Near TC CPA" within ± 48 hours of TC CPA to Sasebo.

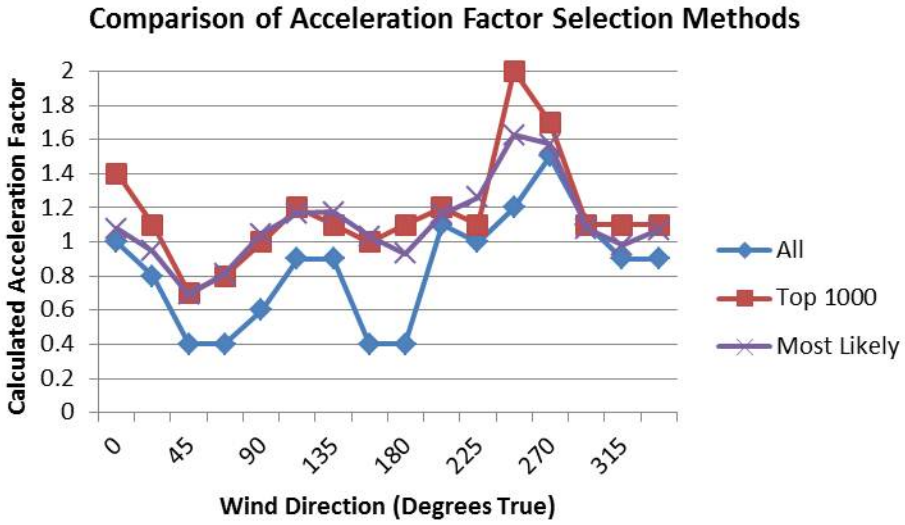

Figure 52. Comparison of peak acceleration factors and most likely acceleration factors by cardinal direction. Colors as in Figure 51 except most likely factors (purple x's).

Given the appropriate acceleration factor from each cardinal direction, this factor is the multiplier on CFSR or other "input" winds to estimate the local winds at Sasebo. An advantage of the large "All" sample and "Top 1000" sample is the ability to estimate from each empirical probability distribution a 66% or 95% confidence interval centered on the most frequently occurring acceleration factor to characterize a range of variability (Tables 10 and 11). Each acceleration factor is rounded to the nearest tenth, and the probability distribution is sampled in steps of 0.1 in both directions from the peak acceleration factor. For example, the peak N acceleration factor in the "All" observations case was 1.0, with 66% of the acceleration factors occurring between 0.5 and 1.5. Therefore, given a 10 m/s input wind with an expected wind from the north, the 66% expectation is that the wind at Sasebo would be between 5 m/s and 15 m/s.

Table 10. Peak acceleration factors (middle column) and upper and lower 66% and 95% occurrence intervals derived from all AMEDAS Sasebo hourly observations during 2003–2010 from each cardinal direction compared to the CFSR wind speed at the same times at 33° N, 130° E.

	Acceleration Factors	Lower 95% Acceleration Factor	Lower 66% Acceleration Factor	Peak Acceleration Factor	Upper 66% Acceleration Factor	Upper 95% Acceleration Factor
Wind Cardinal Direction						
N		0	0.5	1	1.5	2.1
NNE		0	0.3	0.8	1.3	2
NE		0	0	0.4	0.8	1.4
ENE		0	0	0.4	0.8	2
E		0	0.1	0.6	1.1	2.7
ESE		0	0.4	0.9	1.4	2.8
SE		0	0.3	0.9	1.5	2.8
SSE		0	0	0.4	1.1	2.7
S		0	0	0.4	1	2.2
SSW		0	0.6	1.1	1.6	2.6
SW		0	0.4	1	1.6	3
WSW		0	0.4	1.2	2	3.6
W		0	0.6	1.5	2.4	3.3
WNW		0.1	0.6	1.1	1.6	2.1
NW		0.1	0.5	0.9	1.3	1.7
NNW		0	0.4	0.9	1.4	2.1

Table 11. Peak acceleration factors and upper and lower 66% and 95% occurrence intervals as in Table 10, except based on highest 1000 hourly wind speeds from each cardinal direction.

	Acceleration Factors	Lower 95% Acceleration Factor	Lower 66% Acceleration Factor	Peak Acceleration Factor	Upper 66% Acceleration Factor	Upper 95% Acceleration Factor
Wind Cardinal Direction						
N		0.2	1	1.4	1.8	2.6
NNE		0	0.7	1.1	1.5	2.3
NE		0	0.4	0.7	1	1.5
ENE		0	0.4	0.8	1.2	2.2
E		0	0.4	1	1.6	3.5
ESE		0	0.6	1.2	1.8	3.3
SE		0	0.6	1.1	1.6	3.3
SSE		0	0.5	1	1.5	3.2
S		0	0.8	1.1	1.4	2.4
SSW		0.6	0.9	1.2	1.5	1.8
SW		0	0.7	1.1	1.5	2.7
WSW		0.4	1.3	2	2.7	3.6
W		0	1	1.7	2.4	3.5
WNW		0.3	0.8	1.1	1.4	1.9
NW		0.6	0.9	1.1	1.3	1.6
NNW		0.2	0.8	1.1	1.4	2.1

The general applicability of these acceleration factors for the Sasebo area was tested by a similar calculation with the 1990–1997 data (Figure 53) when the AMEDAS station was located ~700 m to the southeast of the 2003–2010 location. Rather than fitting empirical probability distributions for the 1990–1997 data, the relative frequency of occurrence was simply found from a histogram of acceleration factors binned every tenth of one acceleration factor. This different approach was done as experience with the 2003–2010 data had shown that fitting of distributions was not necessarily useful here. A more important difference is that the anemometer height was only 13 m during 1990–1997 versus 35 m during 2003–2010 (Digital Typhoon 2013). That is, lower wind speeds are expected at 13 m height in the surface layer, which may be the explanation for the predominantly lower acceleration factors during 1990–1997 (Figure 53). Additionally,

Table 12 only shows 66% occurrence intervals as the 2003–2010 95% occurrence intervals were so large as to likely be not operationally useful.

The 2003–2010 NE, ENE, and E acceleration factors are lower than for 1990–1997, implying some other factor such as orientation to terrain may be important. Note that the 1990–1997 acceleration factors are $\leq$ 1.0. This is taken as indication of the AMEDAS anemometer being more sheltered than the CFSR grid-point during that time period. However, the broad parallels in the shape of the curves in Figure 53 is taken as evidence that the same terrain features are having similar impacts in Sasebo both during 2003–2010 and 1990–1997. Since CFSR has a known low bias for wind speeds, complications involved in applying CFSR derived acceleration factors will be described in later sections.

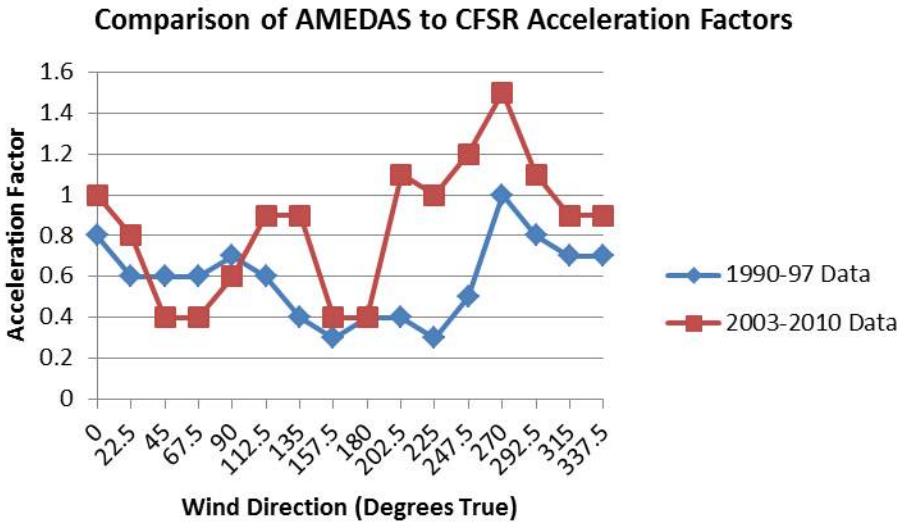

Figure 53. Comparison of 2003–2010 and 1990–1997 calculated AMEDAS to CFSR acceleration factors by AMEDAS sustained wind direction. The AMEDAS station in Sasebo in 1990–1997 was approximately 700 m to the SE of its location during 2003–2010.

Table 12. Peak acceleration factors and upper and lower 66% occurrence intervals found via comparison of Sasebo AMEDAS observations (pre-2002 location) to CFSR winds from 33° N, 130° E for all hourly observations from 1990–1997.

	Acceleration Factors	Lower 66% Acceleration Factor	Peak Acceleration Factor	Upper 66% Acceleration Factor
Wind Cardinal Direction				
N		0.5	0.8	1.1
NNE		0.3	0.6	0.9
NE		0.3	0.6	0.9
ENE		0.2	0.6	1
E		0.3	0.7	1.1
ESE		0.1	0.6	1.1
SE		0.1	0.4	0.7
SSE		0.1	0.3	0.6
S		0.2	0.4	0.6
SSW		0.2	0.4	0.6
SW		0.1	0.3	0.7
WSW		0.1	0.5	1.2
W		0.5	1	1.5
WNW		0.5	0.8	1.1
NW		0.4	0.7	1
NNW		0.4	0.7	1

2. Parametric Wind Direction Based-Acceleration Factors

In this approach, the ratios of AMEDAS wind speed to *parametric wind* speed (as calculated in Table 9), rather than the CFSR wind speeds, are used to calculate the direction-based acceleration factors. While the advantage of this approach is to relate the AMEDAS winds directly to parametric winds, a major disadvantage is the orders of magnitude smaller database of parametric winds from the TCs (Figure 41) passing Sasebo. As a first step, all times when a TC center was within 200 n mi of Sasebo were selected, which is on order of several hundred observation times. After subdividing into cardinal directions at Sasebo, a simple mean and standard deviation of acceleration factors was calculated for each direction. As the parametric winds were generally higher than CFSR winds, the AMEDAS-to-parametric based factors are lower than those for a

CFSR input. For 2003–2010 it was possible to calculate acceleration factors for both the PUW and PAW relative to AMEDAS (Tables 13 and 14). However, very few usable wind radii were available from JTWC for 1990–1997 so only PUW-based acceleration factors are presented for that period (Table 15).

Because the parametric winds are representative of over-water surface winds rather than over land, they do not include the reduction of wind speed and turning of the surface winds due to land frictional effects. Thus, all of the acceleration factors for either the PAW (Figure 54) or the PUW approach (Figure 55) are < 1.0. Here we see different trends than for CFSR based acceleration factors. For 2003–2010, relative highs occur when observed winds in Sasebo are from the NE, SSW, and WNW. The SSW and WNW effects are likely due to the more open exposure of the AMEDAS sensor from those locations, but the NE effect is more puzzling. It may indicate downslope acceleration of winds related to Mt. Eboshi, or insufficient numbers of observations from each cardinal direction for strong comparisons. For 1990–1997, relative highs are seen for ENE and N observed winds, roughly in line with open directions from the AMEDAS sensor at that time (Figure 11).

Table 13. Acceleration factors calculated from AMEDAS to PAW ratios for TCs within 200 n mi of Sasebo from 2003 to 2010. Wind directions are resulting AMEDAS sustained winds.

	Acceleration Factors	Mean Acceleration Factor - One Standard Deviation	Mean Acceleration Factor	Mean Acceleration Factor + One Standard Deviation
Wind Cardinal Direction				
N		0.4	0.6	0.8
NNE		0.4	0.7	1.0
NE		0.4	0.7	1.0
ENE		0.4	0.5	0.7
E		0.3	0.4	0.5
ESE		0.1	0.6	1.3
SE		0.2	0.6	1.1
SSE		0.4	0.7	0.9
S		0.4	0.7	1.0
SSW		0.4	0.6	0.8
SW		0.2	0.4	0.6
WSW		0.2	0.3	0.4
W		0.2	0.5	0.7
WNW		0.3	0.4	0.6
NW		0.3	0.4	0.6
NNW		0.3	0.5	0.6

Table 14. Acceleration factors calculated from AMEDAS to PUW ratios for TCs within 200 n mi of Sasebo from 2003–2010. Wind directions are resulting AMEDAS sustained winds.

	Acceleration Factors	Mean Acceleration Factor - One Standard Deviation	Mean Acceleration Factor	Mean Acceleration Factor + One Standard Deviation
Wind Cardinal Direction				
N		0.4	0.5	0.7
NNE		0.4	0.7	0.9
NE		0.4	0.7	1.0
ENE		0.3	0.5	0.7
E		0.3	0.4	0.5
ESE		0.2	0.3	0.5
SE		0.3	0.4	0.5
SSE		0.4	0.5	0.7
S		0.4	0.6	0.8
SSW		0.4	0.5	0.7
SW		0.1	0.4	0.6
WSW		0.2	0.4	0.5
W		0.2	0.4	0.7
WNW		0.3	0.4	0.6
NW		0.3	0.4	0.6
NNW		0.3	0.4	0.6

Table 15. Acceleration factors calculated from ratio of AMEDAS to PUW winds for all TCs within 200 n mi of Sasebo from 1990–1997. Wind directions are resulting AMEDAS sustained winds.

	Acceleration Factors	Mean Acceleration Factor - One Standard Deviation	Mean Acceleration Factor	Mean Acceleration Factor + One Standard Deviation
Wind Cardinal Direction				
N		0.2	0.3	0.5
NNE		0.2	0.3	0.4
NE		0.2	0.3	0.4
ENE		0.2	0.4	0.5
E		0.2	0.3	0.4
ESE		0.2	0.2	0.3
SE		0.0	0.3	0.5
SSE		0.1	0.2	0.3
S		0.1	0.2	0.3
SSW		0.1	0.2	0.3
SW		0.0	0.1	0.1
WSW		0.1	0.2	0.3
W		0.1	0.2	0.3
WNW		0.1	0.3	0.4
NW		0.1	0.3	0.4
NNW		0.2	0.3	0.4

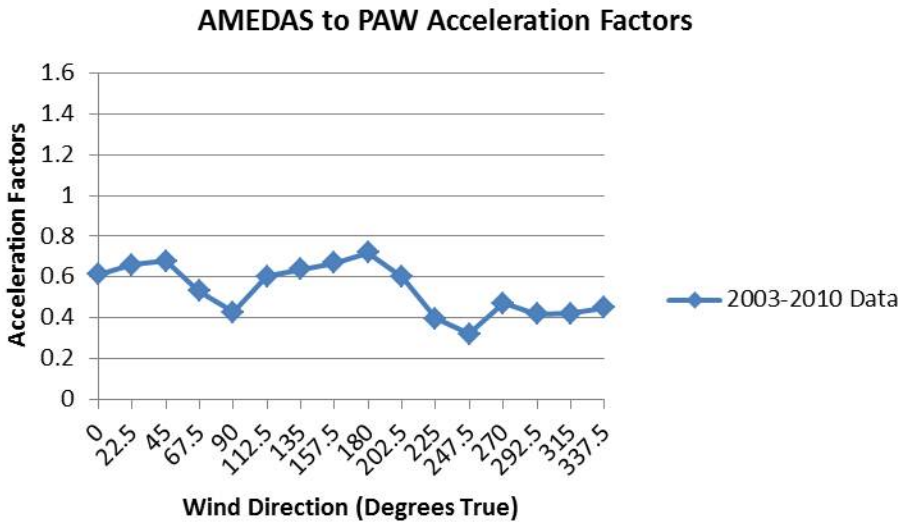

Figure 54. Mean acceleration factors from ratios of AMEDAS to PAW for times when a TC was within 200 n mi of Sasebo during 2003–2010. Wind directions are resulting AMEDAS sustained winds.

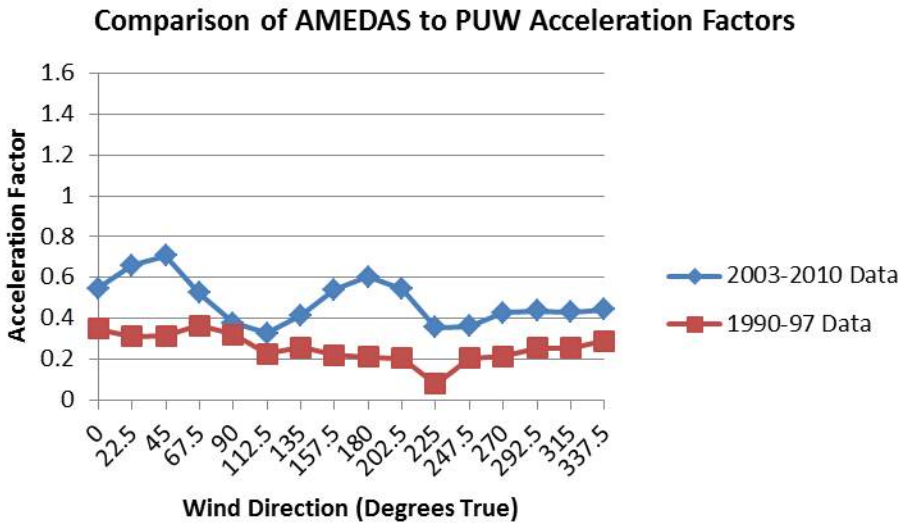

Figure 55. Mean acceleration factors from ratios of AMEDAS to PUW for times when a TC was within 200 n mi of Sasebo during 2003–2010. Wind directions are resulting AMEDAS sustained winds.

These acceleration factors from parametric winds may be used to derive approximate upstream surface roughness values for the cardinal directions surrounding the AMEDAS sensor. As stated above, JTWC winds and wind radii are intended as over-

water values. Therefore, it is assumed that the PUW or PAW represent what the wind would be if the position of Sasebo was open water. If these derived roughness values correspond to the actual terrain, then the confidence in the acceleration factors would be increased. The procedure is based on the classic surface layer logarithmic wind profile as discussed in Harper et al. (2010), although the approach assumes neutral atmospheric stability.

The basic equation for the boundary layer velocity profile V(z) is:

$$V(z) = (u_*/k)\ ln(z/z0)$$

where u_* = friction velocity, which is a function of horizontal and vertical momentum flux, k = von Karman's constant, z = height above ground, and z0 = roughness length.

As indicated above, first assume the parametric wind would be speed at 10 m height (standard height for surface wind measurements) if not over land. Second, assume that the parametric wind and the AMEDAS observed wind at anemometer height (Anem Ht) experience the same u_*, then the ratio

$$V_{AMEDAS}/V_{Parametric} = ln(Anem\ Ht/z0(at\ AMEDAS)) / ln\ (10/z0\ (open\ ocean)\ ) \quad (6)$$

where V_{AMEDAS} is the observed wind, and the $V_{Parametric}$ is calculated as indicated in Table 9.

Harper et al. (2010) provide a typically-used surface roughness called the Davenport roughness classification (Table 16). The open ocean z0 is taken as 0.0002 m, although wind-induced waves could increase expected z0. Since the terrain features vary by direction relative to the AMEDAS station in Sasebo, it is assumed the z0 for the AMEDAS station will also vary by direction, which can be calculated by rearranging Equation (6).

$$ln(Anem\ Ht/z0(at\ AMEDAS)) = ln(10/0.002)\ V_{AMEDAS}/V_{Parametric}$$

$$ln\ z0(at\ AMEDAS) = ln(Anem\ Ht) - ln(50{,}000)\ V_{AMEDAS}/V_{Parametric}$$

$$z0(at\ AMEDAS) = exp(ln(Anem\ Ht) - ln(50{,}000)\ V_{AMEDAS}/V_{Parametric}) \quad (7)$$

Table 16. Representative terrain classes and roughness classifications for tropical cyclone applications from Harper et al. (2010, Table 2.1).

Terrain Class	**Terrain Description**	**Roughness Length z_0 (m)**	**Surface Drag Coefficient C_{10}**
Sea	Open sea conditions for all wind speeds, exposed tidal flats, featureless desert, and tarmac.	0.0002–0.005	0.001–0.003
Smooth	Featureless land with negligible vegetation such as wide beaches and cays, exposed reefs.	0.005–0.03	0.003–0.005
Open	Nearshore water for winds > 30 m s^{-1}, level country with low grass, some isolated trees, airport surrounds.	0.03–0.10	0.005–0.008
Roughly Open	Low crops, few trees, occasional bushes.	0.10–0.25	0.008–0.012
Rough	Lightly wooded country, high crops, centers of small towns.	0.25–0.5	0.012–0.019
Very Rough	Mangrove forests, palm plantations, metropolitan areas.	0.5–1.0	0.019 – 0.032
Closed	Mature regular rainforests, inner city buildings (CBD).	1.0–2.0	0.032–0.065
Skimming	Mixture of large high and low-rise buildings, irregular large forests with many clearings.	> 2.0	> 0.065

Equation (7) may then be applied to the acceleration factor in Tables 13–15 that were derived from all PAW and AMEDAS observations available when a TC was within 200 n mi of Sasebo from 2003–2010. For each cardinal direction, the mean and standard deviation of all acceleration factors were utilized. First, the mean was used to find the approximate z0. Second, the mean acceleration factor minus the standard deviation is expected to represent higher surface roughness in a given direction, and the mean plus the standard deviation is expected to represent lower surface roughness.

The "z0 upper" assuming the 10 m wind at Sasebo is the mean minus standard deviation PAW (Figure 56, green line) is considered to provide an upper bound on the surface roughness values in each cardinal direction from the AMEDAS sensor. By contrast the "z0 lower" (Figure 56, blue line) is considered a surface roughness that implies a maximum local transient acceleration (i.e., some mechanism apparently accelerates the wind above what one might expect from surface roughness values such as

those of a small city center NW of the AMEDAS sensor). Finally, the mean PAW leads to an average equivalent roughness, which is labeled “Approx z0” in Figure 56. Especially noticeable in 2003–2010 are the relatively small z0 values for N to ENE and SSE to SSW directions. This is consistent both with local accelerations occurring from those directions in the 2003–2010 data.

The roughness variations in Figures 56 and 57 are in broad agreement, e.g., both increasing or decreasing at the same wind directions. Note that effectively low roughness values are consistent with northerly winds through the gap. The smaller z0 values for southerly wind directions are consistent with more exposure to the open waters of Sasebo harbor. An unexpected result is the order of magnitude larger roughness values for winds with easterly components. This exception may be due to a smaller number of cases available, or to discontinuities in applying JTWC wind radii in the PAW calculations. For example, a TC passing to the south of Sasebo may suddenly be shifted to a different cardinal direction or the wind radii change from one hour to the next and thus cause an apparent jump in wind speed. Alternatively, one six-hour record may not have accurate wind radii available and then a scatterometer pass is available that causes an apparent jump in wind radii that leads to unrealistic acceleration wind speeds in the PAW.

Examining the red lines for the mean z0, notice much larger magnitudes and greater variability in the roughness values for 2003–2010 data (Figures 56 and 57) than in the 1990–1997 data (Figure 58) for PUW. These small roughness values are attributed to the 1990–1997 AMEDAS station position being much more sheltered than the current station position, which is implied by the generally weaker winds in Figure 15 than Figure 16. As indicated in Figure 11, the 1990–1997 AMEDAS location (position A), is indeed surrounded by suburban/urban development for at least 100 m in all directions. Furthermore, the wind instrument was at 13 m elevation during 1990–1997. These factors are consistent with the majority of mean z0 values in Figure 58 being greater than 0.3 m.

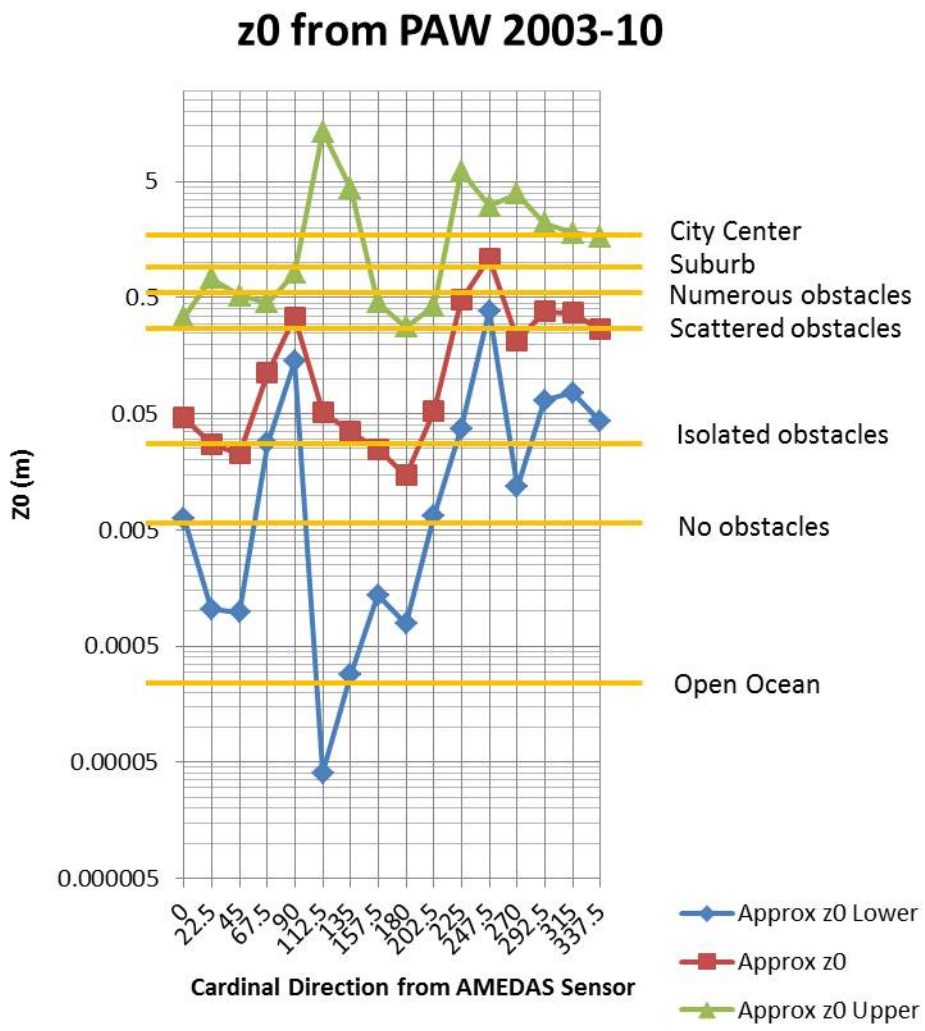

Figure 56. Surface roughness values from Equation (7) assuming the mean (red curve), mean plus standard deviation (blue), and mean minus standard deviation (green) PAW is the 10 m wind at Sasebo with no land present and compared with observed wind at the anemometer height. Typical values of surface roughness (with widely used descriptors) from Table 16 are annotated on the right vertical axis. z0 values that are lower than what might be inferred from terrain effects may indicate a local acceleration.

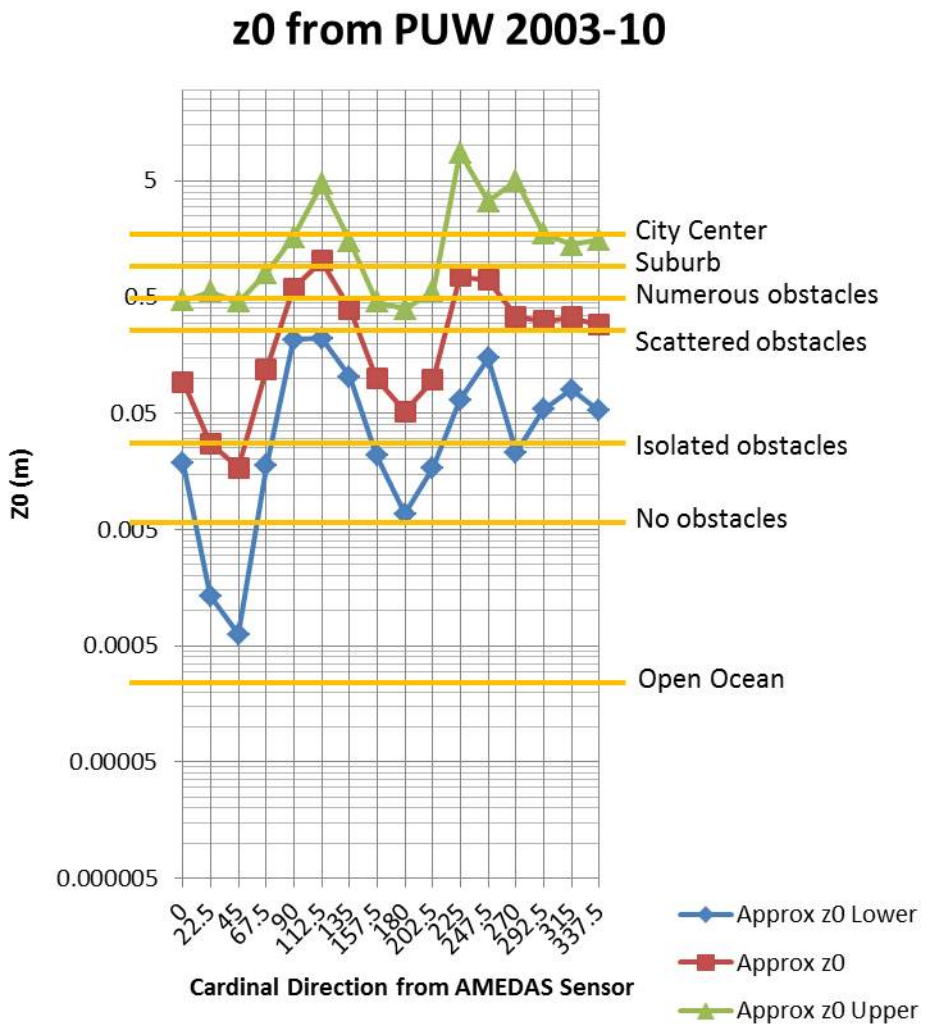

Figure 57. As in Figure 56, except using the mean and standard deviations of PUW for the 2003–2010 data set.

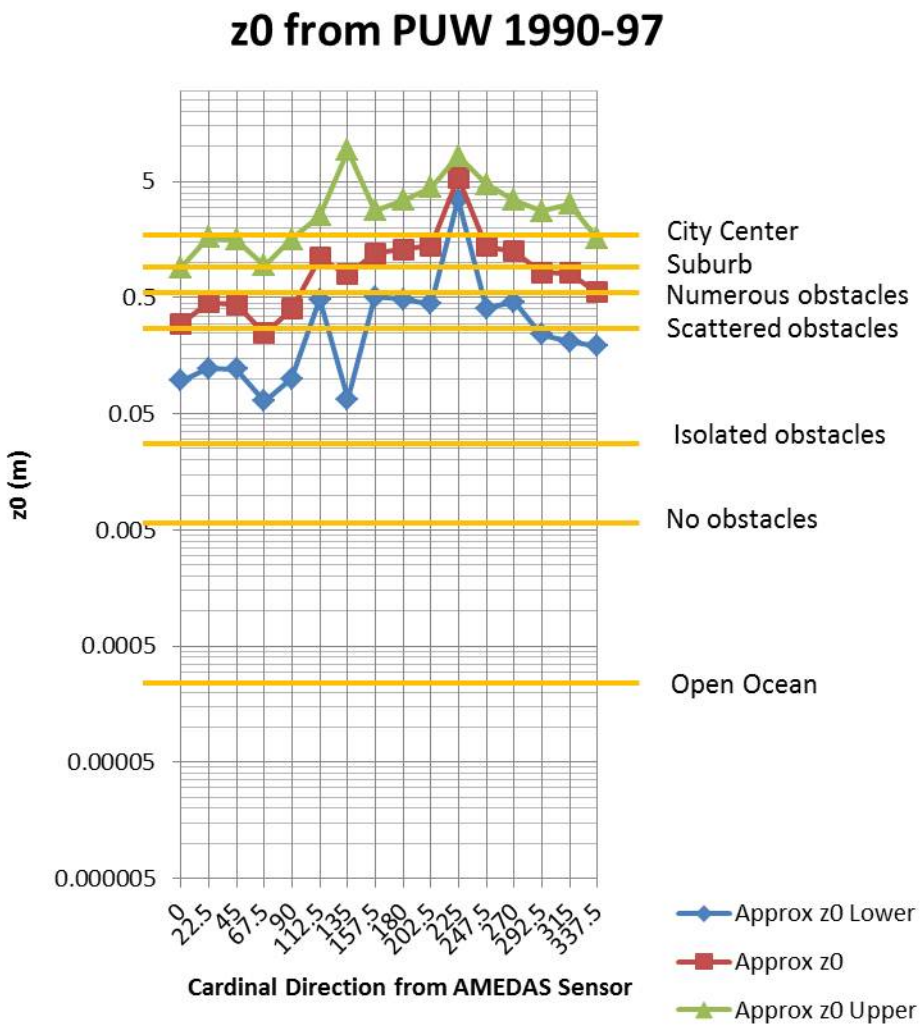

Figure 58. As in Figure 57, except for the PUW and AMEDAS observations for when TCs were within 200 n mi of Sasebo during 1990–1997 rather than 2003–2010.

E. PARAMETRIC MODEL PERFORMANCE

1. PUW and PAW with No Further Adjustments

Parametric models were run for all storm positions within 200 n mi of Sasebo (Figure 41) using the best-track data from the JTWC website, which yielded hourly hindcast parametric predictions for comparison to AMEDAS observations. Note that PUW and PAW do not explicitly take land friction or other land interactions into account. Thus an expected high bias compared to the winds observed in Sasebo is seen (Figures 59–61). As in earlier figures, linear fits of the data are annotated on the graphs. Again, a

zero y-intercept has been imposed. In this case, allowing non-zero intercepts only results in R^2 improvements on order of 0.01.

As indicated by the regression equations in Figures 59 and 60, the local AMEDAS wind speeds are on average 54.37% and 51.83% of the PAW and PUW speeds respectively. Considerable scatter about the regression line exists, particularly in the speed range of 10 m/s (14 m/s) to 20 m/s for the PAW (PUW), so the R^2 values are only 0.3151 (0.3294). The reduction of AMEDAS wind speeds relative to the PUW was markedly larger (only 29.09%) for the 1990-1997 sample (Figure 61) when the AMEDAS site was in a more protected location and the anemometer height was only 13 m (versus 35 m during 2003–2010).

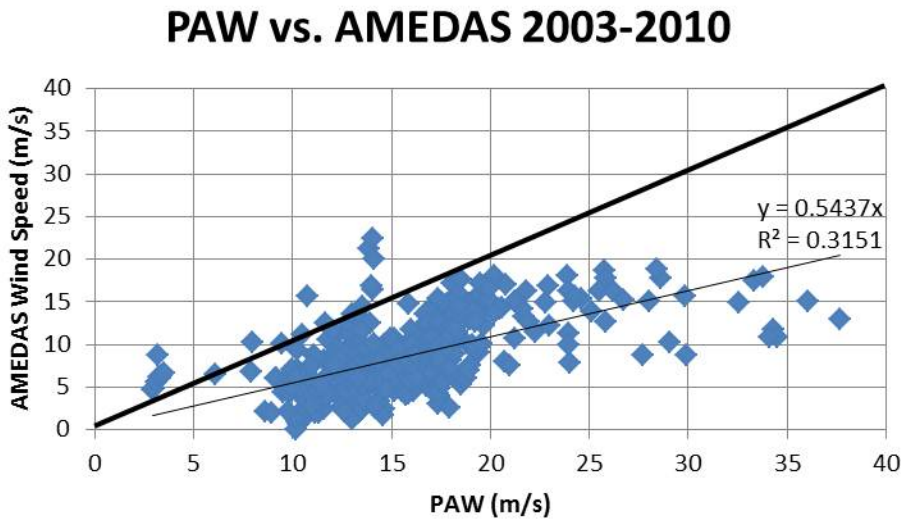

Figure 59. Comparison of 422 PAW speed predictions and corresponding AMEDAS sustained wind observations in Sasebo for TCs within 200 n mi from 2003 to 2010. The thick black line indicates a theoretical one-to-one correspondence, i.e., that the parametric model is a perfect predictor for winds in Sasebo. The thin black line represents the regression equation and R^2 value based on a linear fit of AMEDAS winds to parametric winds with a zero y-intercept imposed to prevent negative speed predictions.

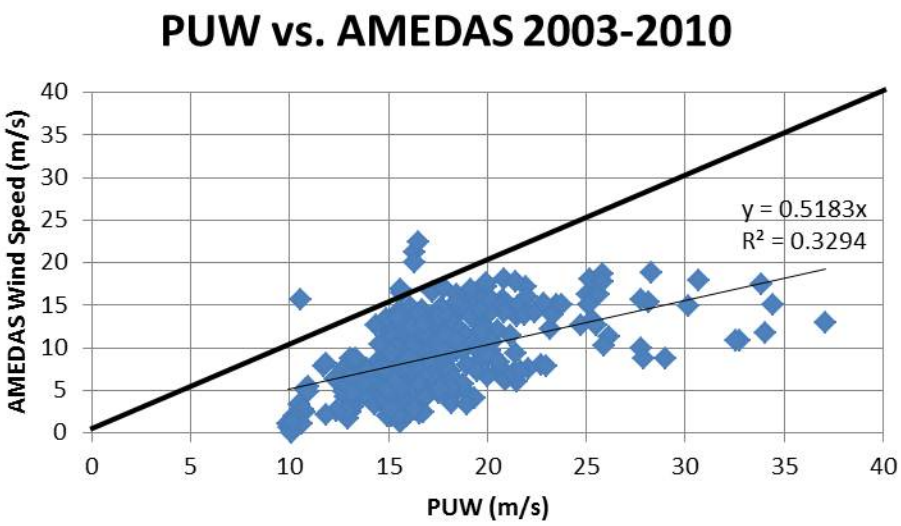

Figure 60. As in Figure 59 except for PUW speed predictions.

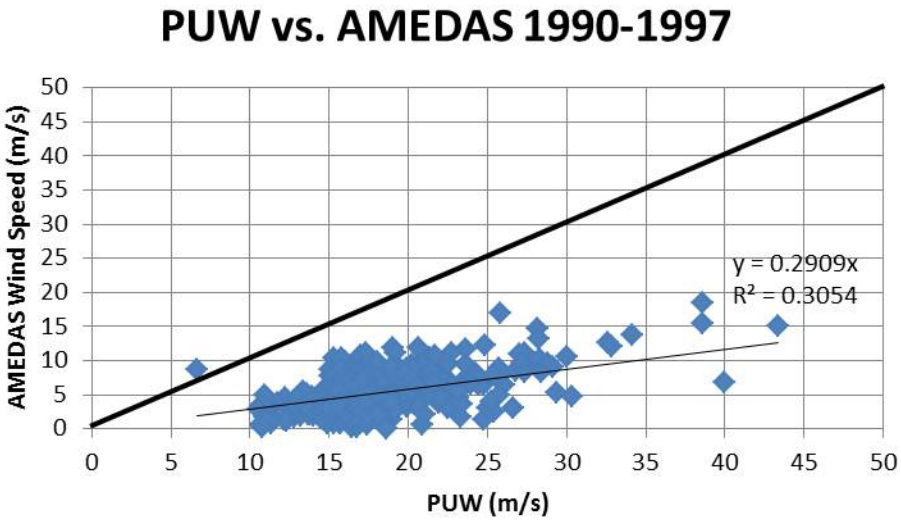

Figure 61. As in Figure 60, except TCs within 200 n mi of Sasebo during 1990–1997, and for 495 prediction-to-observation pairs.

In addition to a wind speed reduction at the AMEDAS site, the local wind direction at Sasebo is shifted relative to the tangential wind of a symmetric vortex assumed in the PAW and PUW equations. As indicated in Figure 62 for the 2003–2010

samples, the Sasebo wind is typically 1–3 cardinal wind directions turned inward relative to the symmetric vortex tangential wind. Whereas the symmetric vortex wind for a storm due south of Sasebo would lead to an easterly wind, an ENE wind is more likely. A very similar directional turning was also found for the TCs during 1990–1997 (Figure 63) with some indication of more frequent shifts of 5–6 cardinal wind directions.

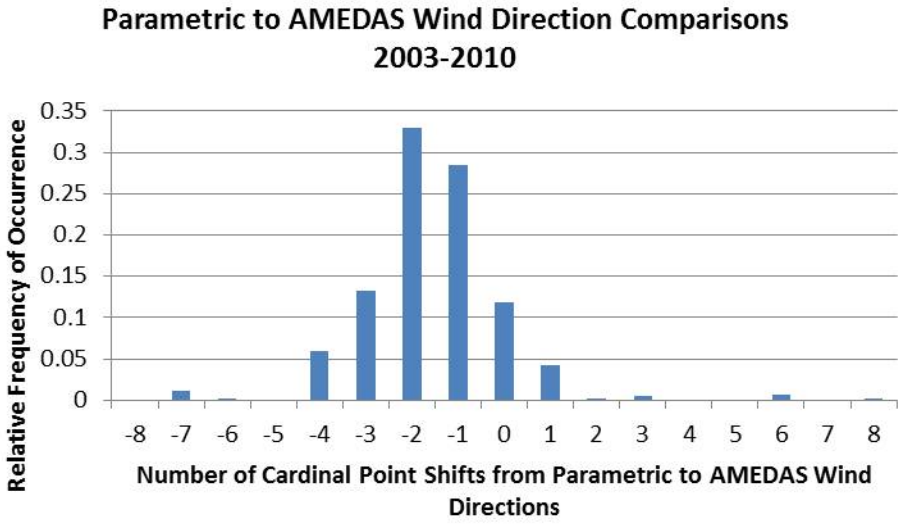

Figure 62. Shift of wind direction from a parametric "prediction," i.e. bearing from Sasebo minus 90 degrees (representing frictionless wind forced by a symmetric vortex) for the sample of TCs as in Figures 59 and 60.

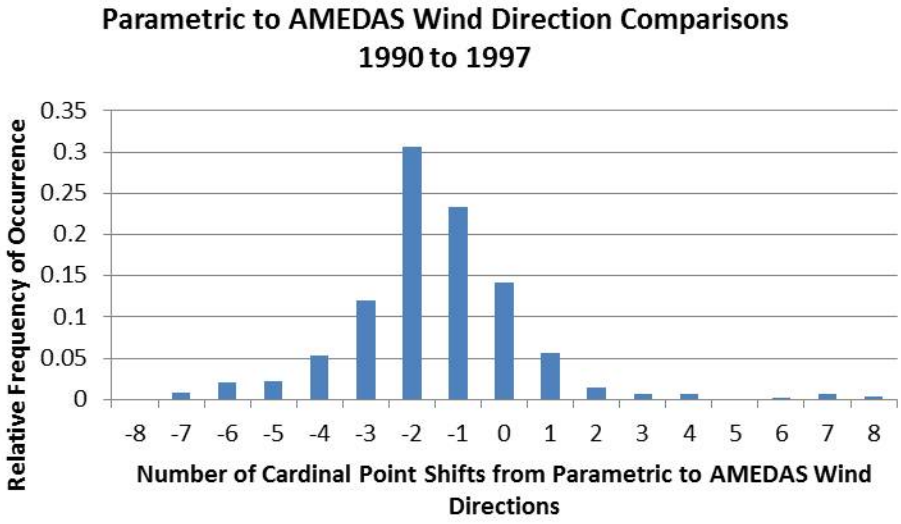

Figure 63. As in Figure 62, except for TCs within 200 n mi of Sasebo during 1990 to 1997, and therefore at the previous Sasebo AMEDAS location.

This wind shift similarity likely indicates a topographic blocking/channeling effect as well as frictional effects. Since the use of these expected wind shift histograms for forecast purposes will be more thoroughly addressed in Chapter IV, the wind direction shifts are also examined for the 2002 and 2011–2012 cases (Figure 64) at the present AMEDAS site and the 1998–2000 cases (Figure 65) at the previous AMEDAS site. Compared to the 2003–2010 cases (Figure 62), smaller wind direction shifts are indicated in Figure 64, which could be stochastic, due to different sample sizes, or be related to TC track variations between the datasets.

The differences in the distribution of the wind direction shifts at the prior AMEDAS site for the 1998–2000 sample (Figure 65) compared to the 1990–1997 sample (Figure 63) are much larger. While this might be attributable in part to the more sheltered anemometer at the prior AMEDAS site, the much smaller 1998–2000 sample (194 observations versus 495 observations during 1990–1997) is a more likely explanation. Such wind direction differences have important operational application of the PAW and PUW profiles since acceleration factors are sensitive to the cardinal wind direction.

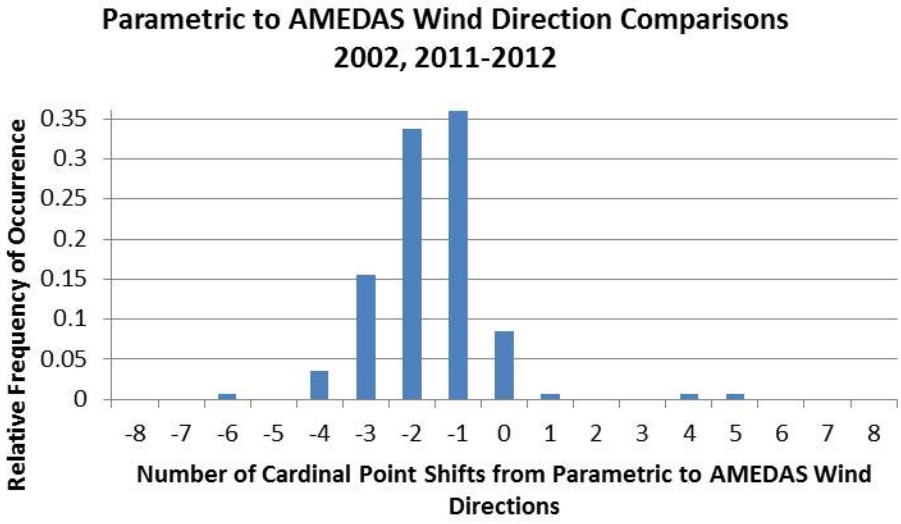

Figure 64. As in Figure 62 except for 142 observations when TCs were within 200 n mi of Sasebo during 2002 and 2011–2012.

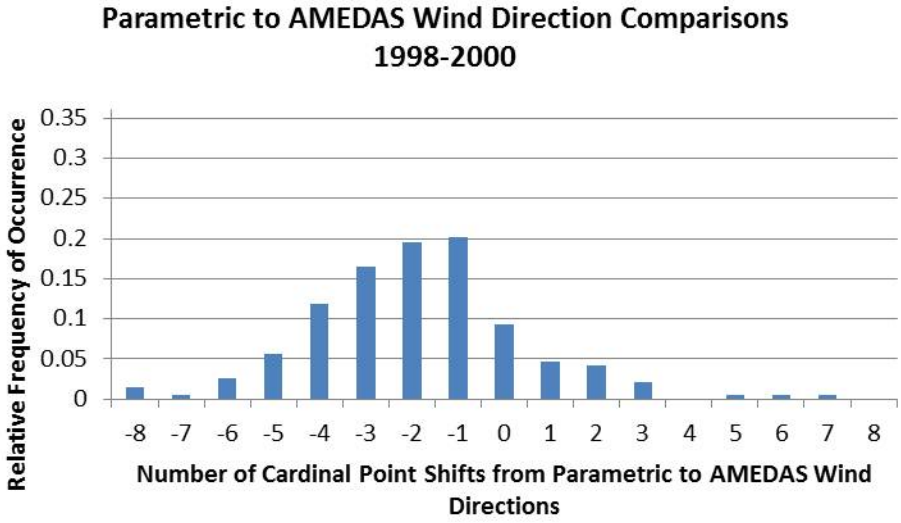

Figure 65. As in Figure 62, except for 194 observation times when TCs were within 200 n mi of Sasebo during 1998–2000, and thus were measured at the prior AMEDAS site.

2. Simplistic Parametric Model Adjustments

Assuming an isotropic (i.e., no topographic or other directional influence) frictional reduction, a simple wind speed correction to the PAW predictions would be that the AMEDAS winds are approximately 0.54 of PAW predictions (see regression equation

in Figure 59). Therefore, the PAW (PUW) for the TCs in the independent 2002 and 2011–12 sample are multiplied by 0.54 (0.52). Similarly, the TCs in the independent 1998–2000 sample for the prior AMEDAS site will be multiplied by 0.29 for comparison to observations, nomogram outputs, and all other modifications to these parametric wind speed estimates.

The optimum result of the application of the parametric wind speed predictions would be a one-to-one correspondence with the AMEDAS at all wind speeds (i.e., a zero intercept and the thick black lines in Figures 66–68). Rather than calculating a linear fit for just pairs of predictions and observations without forcing a zero intercept, it will be assumed that the modified parametric wind speeds will have the same fit for each case (AMEDAS = prediction). Likewise an R^2 with respect to that line will provide a quantitative inter-comparison for all of the empirical techniques. That is, techniques that result in a higher R^2 will be considered to capture more of the full range of variability of the Sasebo wind than lower R^2 values.

The simple modification of multiplying PAW speeds by 0.54 is the best example of this approach with the independent sample (Figure 66). Note that the linear regression with a zero intercept has a coefficient of 0.90 (rather than 1.0). As noted in the dependent sample (Figure 59), there is considerable spread in the predicted wind speeds so the R^2 is 0.43. Less success is achieved in the independent sample by simply modifying the PUW by 0.52 (Figure 67). It is clear that imposing a zero intercept is not appropriate with this sample, even though the slope of the regression line is 0.97 and the R^2 value is 0.34. Multiplication of the PUW speeds for the independent sample during 1998–2000 by 0.29 (Figure 68) is successful in representing the very small AMEDAS wind speeds observed at the prior AMEDAS site with the anemometer height of only 13 m. The slope in the regression is 0.925, but the spread leads to a R^2 of 0.33. However, such small AMEDAS winds are not representative of other Sasebo locations.

It should be noted that for assessing future ensemble forecast potential, evaluation of each technique must also include examination of bias and realism of the spread. For example, points to the right of the thick black lines in Figures 66–68 are high

biased (predictions higher than observations), while those to the left have a low bias. Such an evaluation will be presented later after considering other potential techniques.

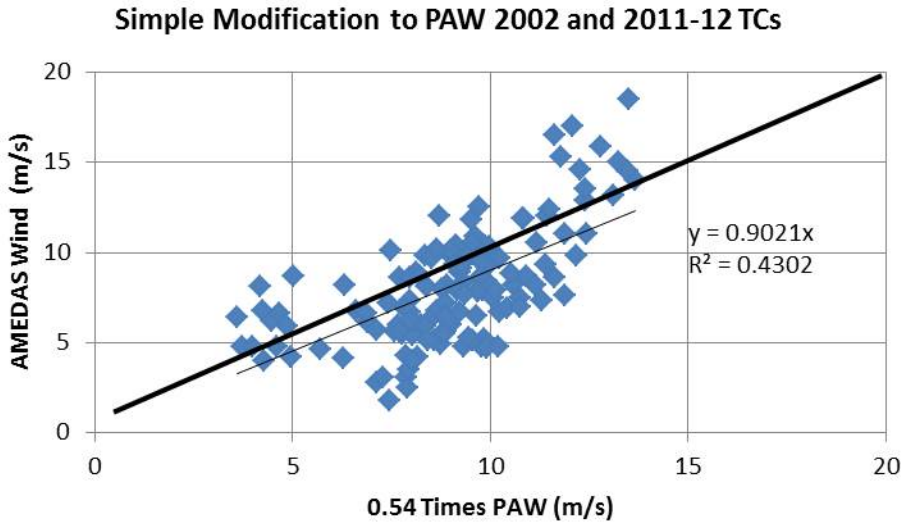

Figure 66. Modified PAW speed versus AMEDAS observed hourly wind values for times when TCs were within 200 n mi of Sasebo for the independent sample of cases during 2002 and 2011–2012. The heavy black line has a slope of 1 and represents a perfect correspondence between the data sets. The thin black line represents the regression equation and R^2 for a linear fit of the data with an imposed zero intercept.

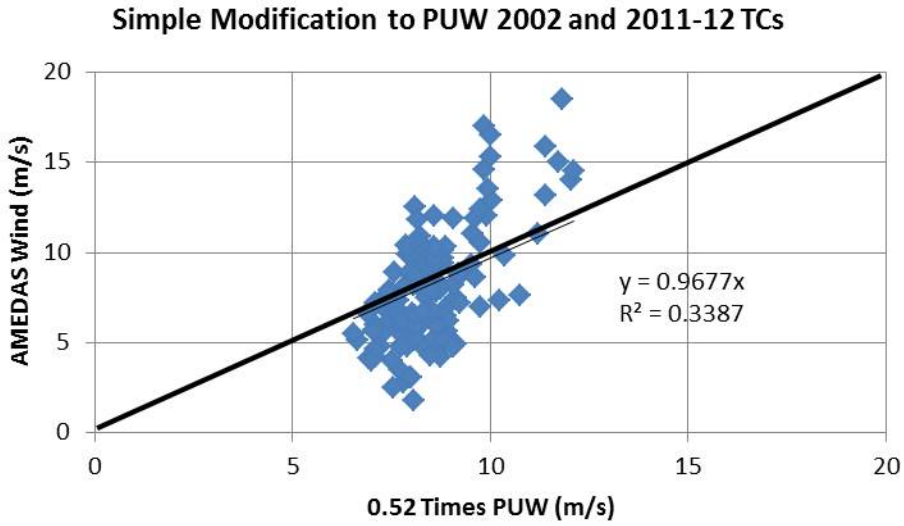

Figure 67. As in Figure 66, except for a modification of the PUW speeds by 0.52.

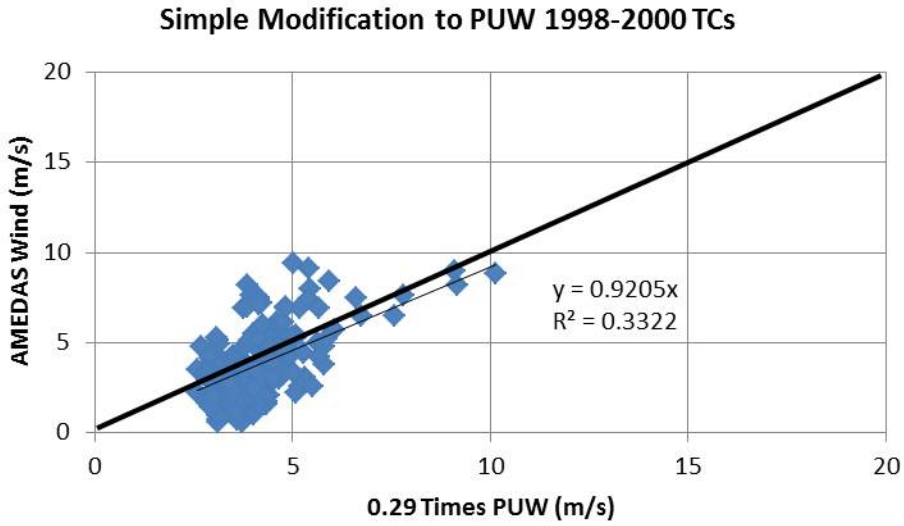

Figure 68. As in Figure 66, except for a modified PUW when TCs were within 200 n mi of Sasebo during 1998–2000.

3. Use of Parametric-Based Acceleration Factors

Comparisons of the Sasebo winds (Figure 70, purple lines) with PAW multiplied with the mean (red lines) and ± one standard deviations (green and blue lines) of the acceleration factors for known Sasebo wind direction indicate the agreement and uncertainty for individual typhoons within 200 n mi during 2002, and 2011–2012. Because the wind direction is known, the agreement between observations and PAW using the mean acceleration factor for that direction is rather good. However, it is noted that the highest hourly wind observation from the TCs during this period was only 17 m/s, so no damaging winds through the mountain gap were included in this sample. Further sub-hourly observed variability exists, with sometimes higher wind speeds, but that is not addressed here. Note that the PAW multiplied by the plus one standard deviation acceleration factor do indicate the potential for winds exceeding 25 m/s for two of the typhoons. By contrast, the enhanced roughness length corresponding to the minus one standard deviation acceleration factor would indicate maximum Sasebo winds of 10 m/s or less for all of these TCs.

The scatter plot of the Sasebo winds during the independent sample during 2002 and 2011–2012 with PUW multiplied by PUW based directionally-dependent acceleration factors (Figure 71) is relatively well fit with the regression line with a zero intercept. However, the scatter about this regression line is quite large with $R^2 = 0.2521$. In particular, the observed AMEDAS wind speeds tend to be much larger in the range of modified PUW of 7–12 m/s, so that a false sense of security would apply for this set of TCs. Overall, the range of modified PUW is considerably smaller than for the modified PAW (Figure 69).

The corresponding comparison of the Sasebo winds with the modified PUW for individual TCs during 2002 and 2011–2012 is shown in Figure 72. As in Figure 71, the range of modified PUW speeds is small, and in most of these TCs the maximum AMEDAS wind observations are larger than the modified PUW winds using the mean acceleration factor corresponding to the known AMEDAS wind direction. Indeed, the maximum AMEDAS wind speeds (purple lines) in two TCs exceed the modified PUW multiplied by the acceleration factor for the plus standard deviation (green line). Again, the modified PUW speeds would lead to a false sense of security for the most intense (and closer approach distance to Sasebo) TCs.

The independent sample to test the acceleration factors for the PUW speeds at the prior AMEDAS site is from 1998–2000 (Figure 73). Nearly all of the TCs during this period led to modified PUW speeds of less than 5 m/s. The regression line with a zero intercept has a slope near 1.0 and $R^2 = 0.42$, which may be attributed to the small range of winds. Comparisons with individual TCs during 1998–2000 of the PUW multiplied by acceleration factors (mean $\pm$ one standard deviation) are shown in Figure 74. While the AMEDAS maximum wind observation generally lies within the uncertainty bounds, it is not clear if this is because the modified PUW speeds are so small or because a good relationship truly exists.

The empirical techniques described in this section may be applied in two ways. Parametric winds multiplied by an appropriate directional-dependent acceleration factor would provide a deterministic forecast. Comparing the scatter plots in Figures 69, 71, and 73, the modified PAW (Figure 69) is clearly superior to the modified PUW (Figure 71)

for the current AMEDAS site. The corresponding PAW comparison for the individual TCs (Figure 70) also indicated a better wind uncertainty range than for the PUW (Figure 72). In addition to such a product that is dependent on the JTWC official track forecast, a similar product could be generated for each member of the ensemble of TC tracks and intensities currently being used to produce wind probability products. This would result in a Sasebo-specific probabilistic forecast of damaging winds.

For operational use, some issues need to be addressed. Note that adjusted PAW appears to have an overforecast bias, whereas PUW errors are spread roughly evenly high and low. A larger spread may be more advantageous in an ensemble approach for capturing a realistic range of variability. Comparing Figures 70 and 72, the PAW has the advantage (for this dataset at least) of always having its predicted upper bound higher than AMEDAS. However, the range between its upper and lower bound is quite large, which is operationally useful only if it represents a realistic range of possibilities. Since the dataset used to calculate parametrically based observed wind direction-dependent acceleration factors was so small (several hundred observation-to-parametric calculation comparison pairs), the variability captured by $\pm$ one standard deviation may not be representative of typical Sasebo-TC situations.

Other important considerations arise in an operational setting. Especially for a deterministic forecast with confidence intervals, there are multiple possibilities of how to proceed. The TC "input" winds to the Sasebo "black-box" can back or veer to multiple directions with varying levels of probability. Gust wind directions may back and veer from the sustained wind direction with different levels of probability. Thus multiple possible scenarios exist. One could focus on the most dangerous, most likely, some weighted average, or other scenario. More discussion of this is presented in Chapter IV.

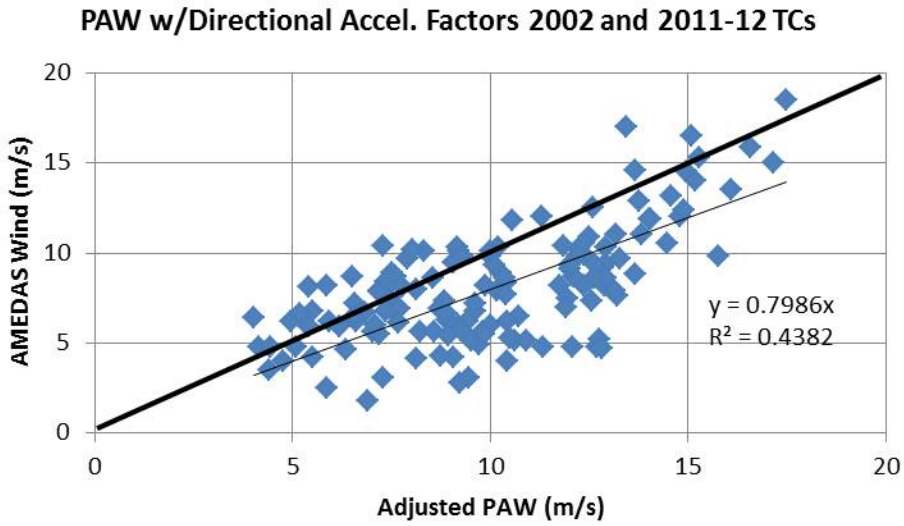

Figure 69. Scatter plot of PAW times acceleration factor vs. AMEDAS for times when TCs were within 200 n mi of Sasebo in 2002 and 2011–12. Acceleration factors were based on PAW vs. AMEDAS in 2003–2010 set of times when TCs were within 200 n mi of Sasebo. Only PAW times the peak acceleration factor is shown. As in Figure 66, thin black line, equation, and R^2 displayed are from an Excel fit of the data. Thick black line represents a theoretical perfect forecast, the R^2 from which is tabulated later.

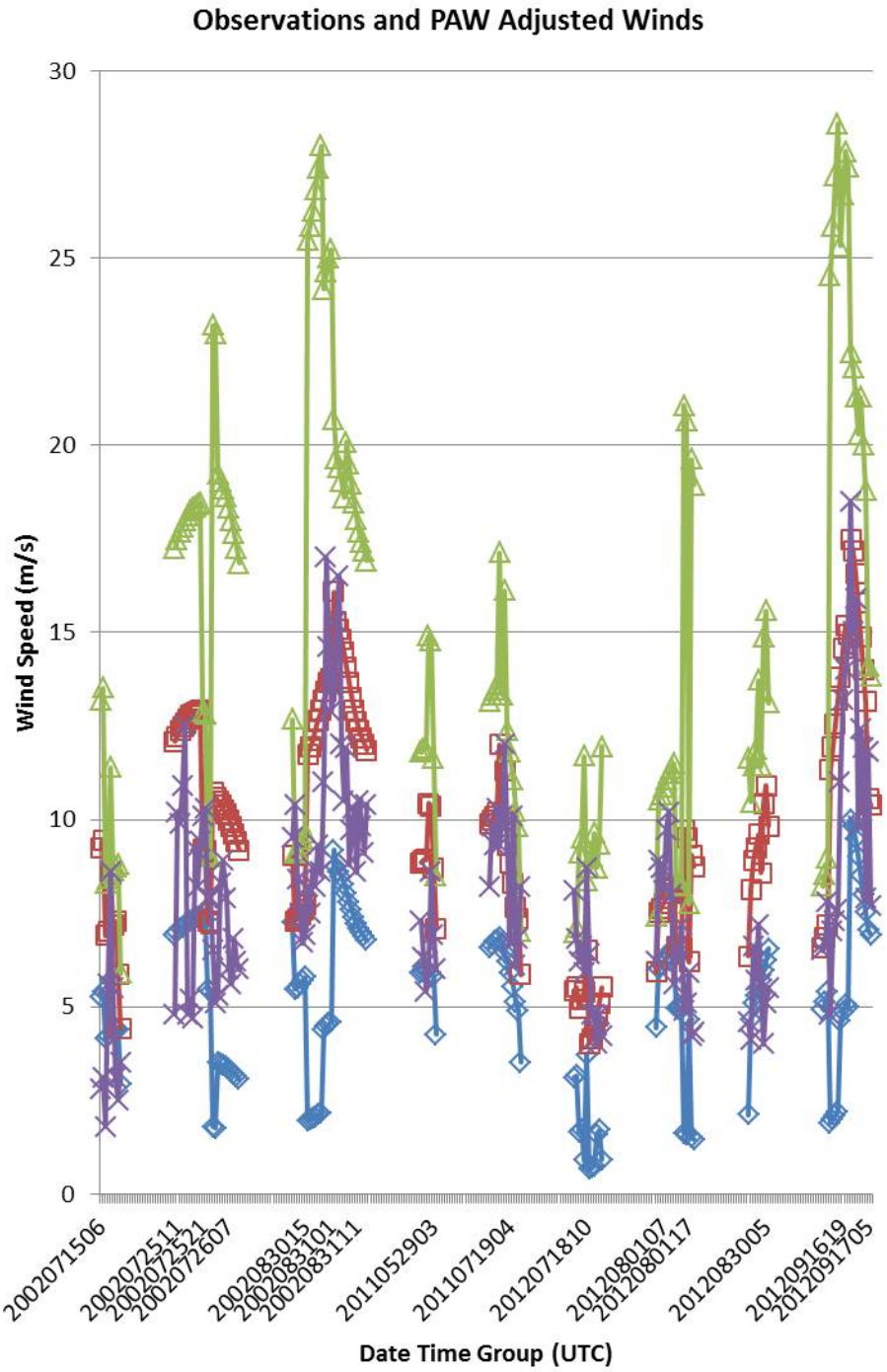

Figure 70. Line plot of all times when TCs were within 200 n mi of Sasebo during 2002 and 2011–12 (YYYYMMDDHH along the abscissa). Purple line is AMEDAS wind speed. Red line is PAW multiplied by directional acceleration factors (same data as plotted in Figure 69). The green and blue lines are PAW multiplied by the acceleration factor ± one standard deviation as shown in Table 13, respectively.

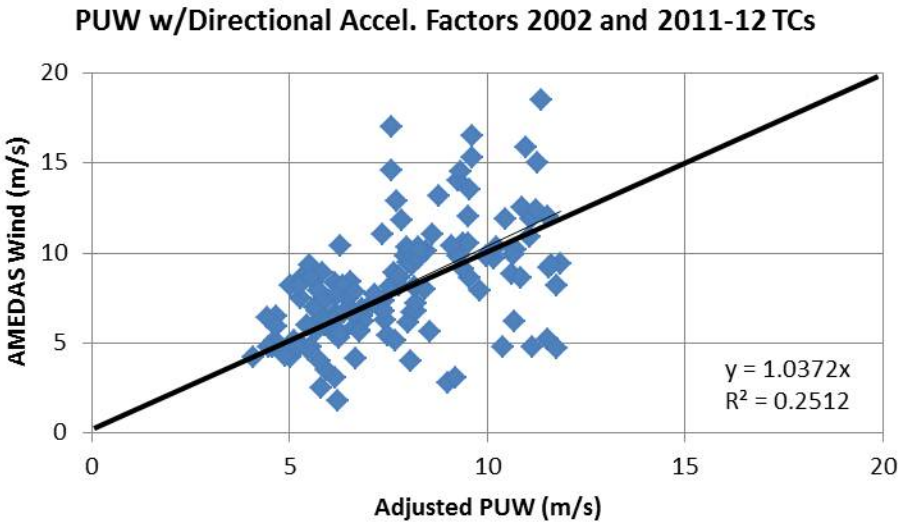

Figure 71. As in Figure 69, except using PUW modified by 2003–2010 PUW-based acceleration factors (Table 14).

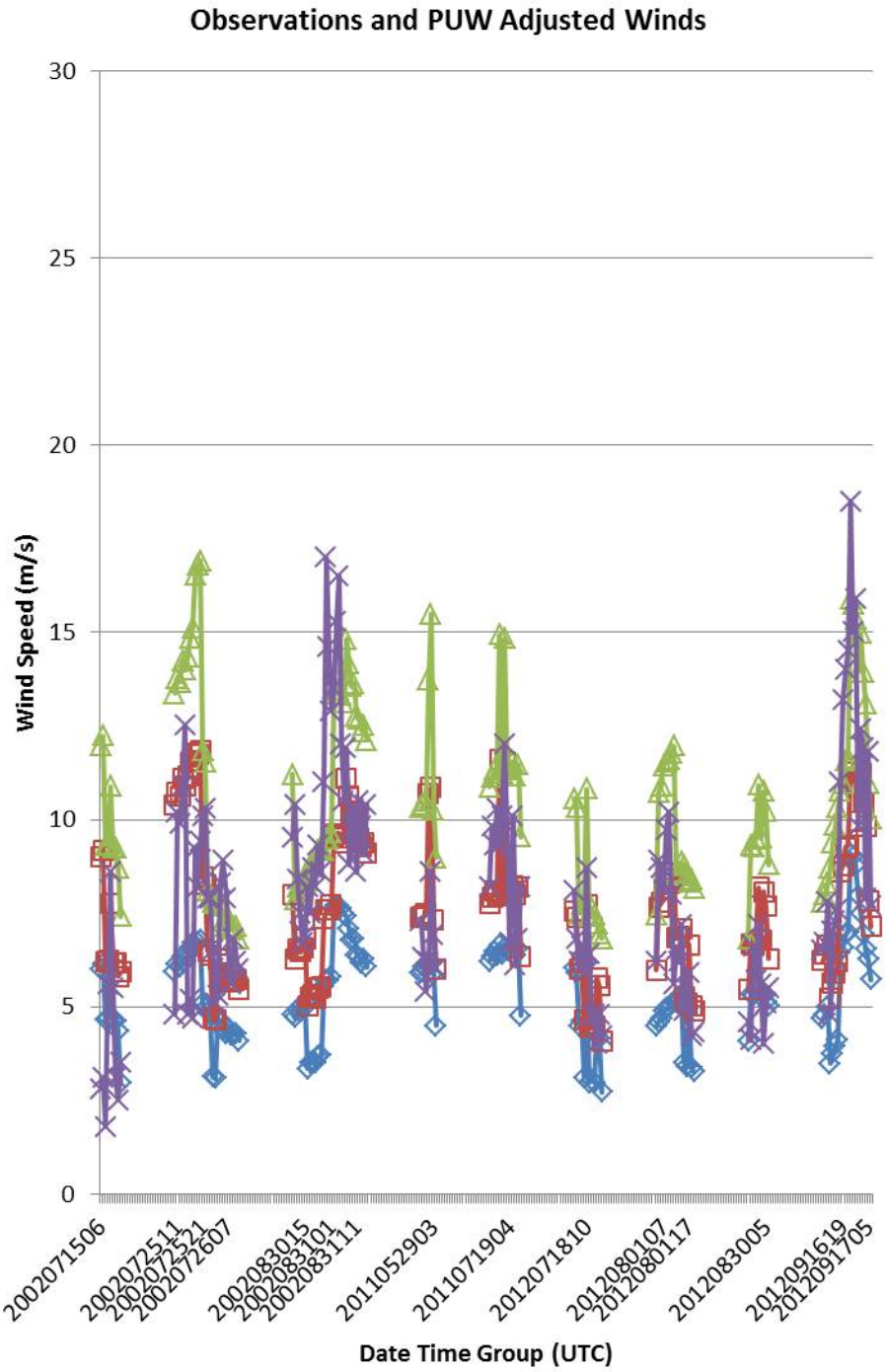

Figure 72. As in Figure 70 except for PUW multiplied by directionally-dependent acceleration factors. Red and purple lines from same data as in Figure 71. Note that the AMEDAS exceeds upper bound expected from adjusted PUW for several observations (purple line above green line).

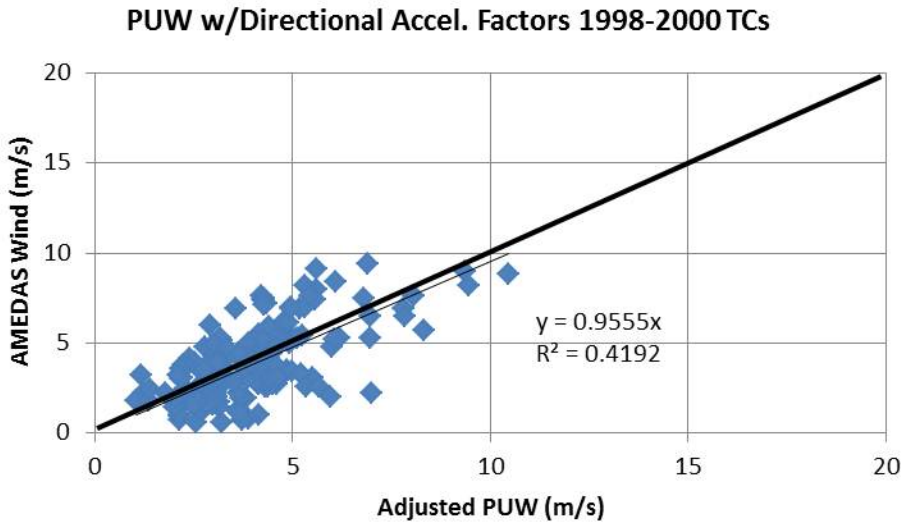

Figure 73. As in Figure 69, except for PUW from 1998 to 2000 modified by directional acceleration factors derived from 1990–1997 PUW to AMEDAS comparison of winds at the prior site (Table 15).

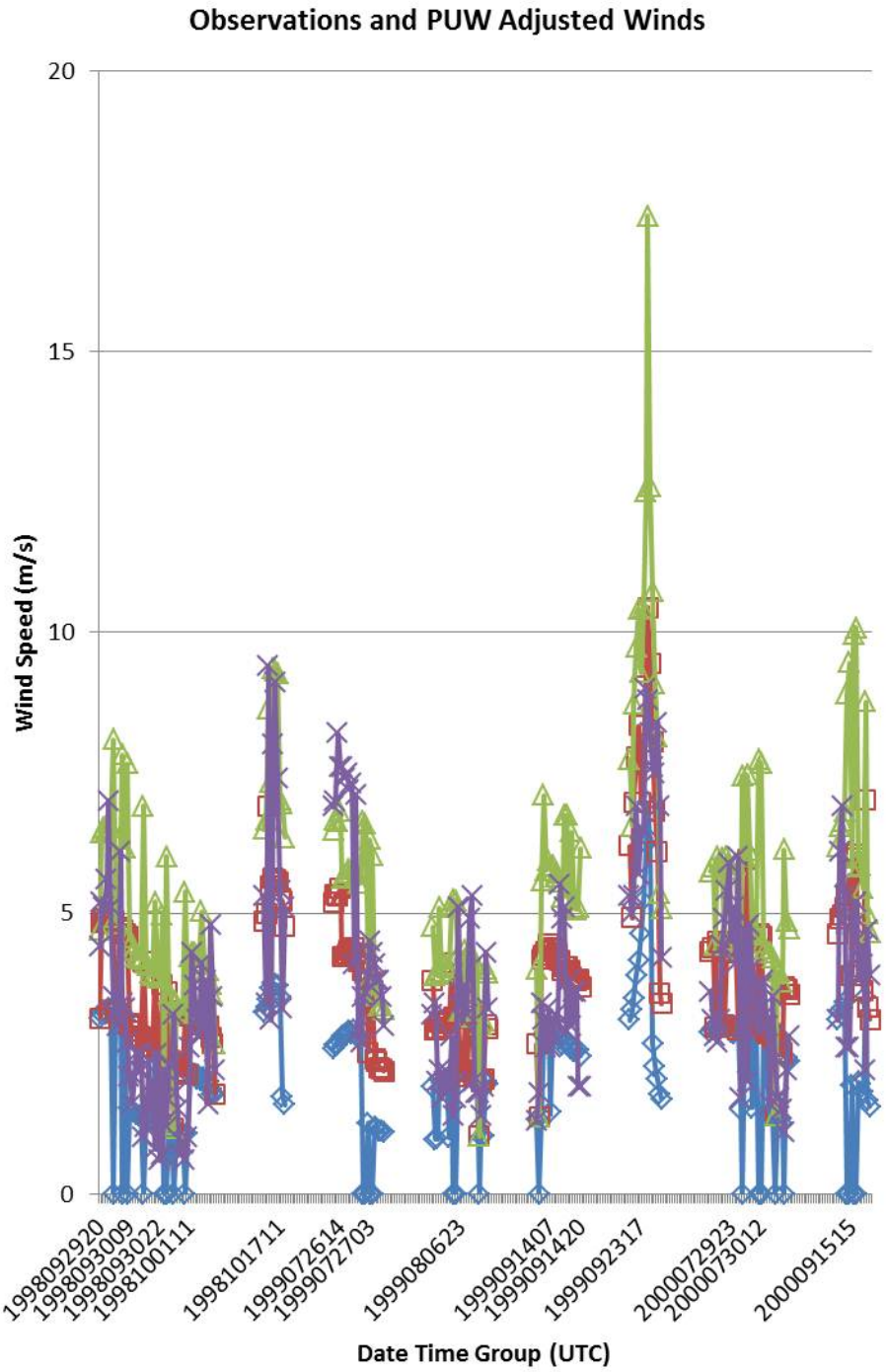

Figure 74. As in Figure 70, except for PUW in the independent sample of TCs during 1998–2000 modified by directionally based acceleration factors. Simultaneous data points from purple and red lines correspond to data points in Figure 73.

4. Use of CFSR-based Acceleration Factors with Parametric Winds

As previously noted, parametric wind speeds are typically much higher than the corresponding CFSR wind speeds, presumably because the land effects have been taken into account via large-scale frictional effects in the CFSR. Therefore a simple correction is applied to the parametric predictions prior to applying the AMEDAS-to-CFSR acceleration factors. That is, the parametric wind speed is multiplied by the average parametric-to-CFSR wind speed ratio before applying the acceleration factors found by comparing CFSR and AMEDAS wind speeds. As in Figures 59–61, a simple linear fit of the CFSR to the parametric winds is calculated with an imposed zero y-intercept.

Note in Figures 75 and 76 that for parametric winds greater than 20 m/s, the CFSR winds tend to decrease, which may represent a physical drag effect at higher wind speed. Therefore, second-order polynomial fits were also calculated for the data in Figures 75–77. While the polynomial fit with the 1998–2000 cases did improve the calculated R^2 value relative to that fitted curve, polynomial-fit corrections with the 2002 and 2011–2012 independent test cases ultimately yielded generally worse performance than using a linear fit. Therefore the polynomial fit results will not be discussed.

Applying the regression equations in Figures 75–77 to the parametric winds in the independent test cases during 2002 and 2011–12, and during 1998–2000, and then applying the acceleration factors from Tables 10–12 did not result in improved predictions of the AMEDAS winds compared to the direct use of parametric winds in Figures 69–74. Quantitative values will be provided later in Table 18.

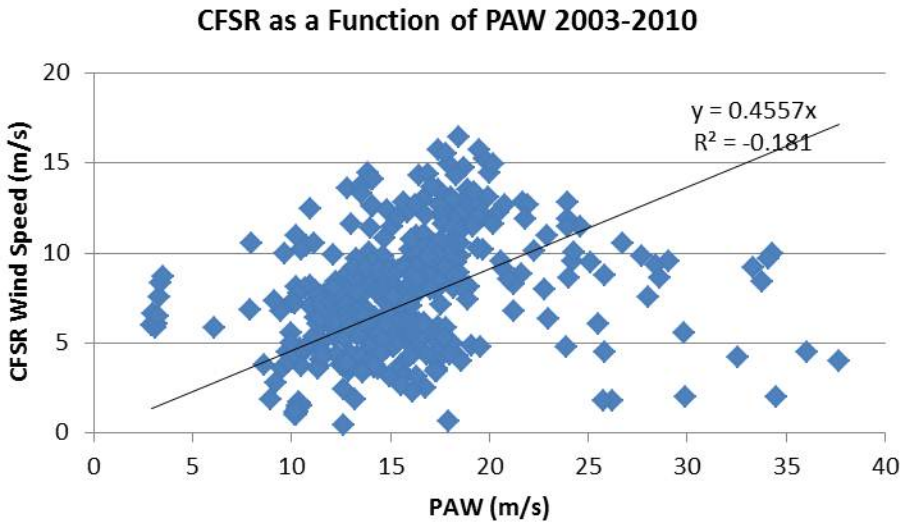

Figure 75. Scatter plot of PAW speeds vs. CFSR for TCs during 2003–10 to define a regression relationship between CFSR and PAW, which will then be applied to the PAW during 2002 and 2011–12 prior to using CFSR-based acceleration factors from Tables 10 and 11.

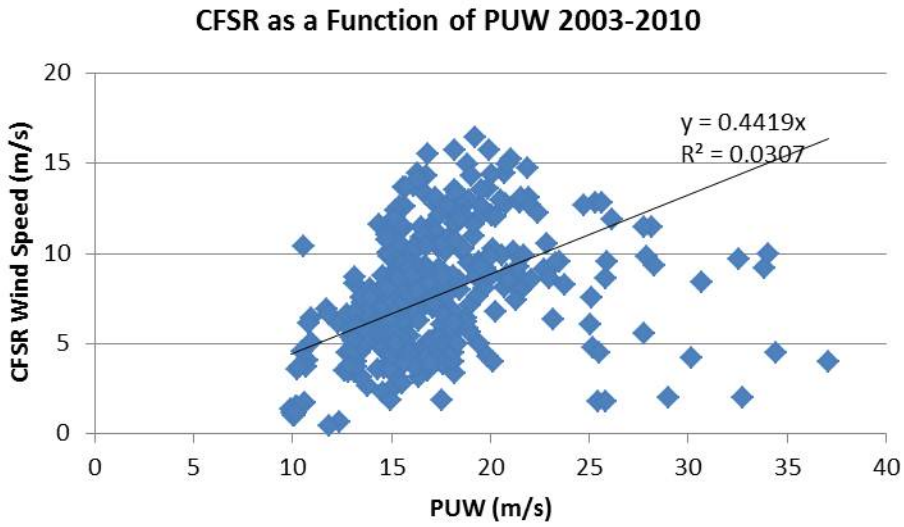

Figure 76. As in Figure 75, except for PUW speeds.

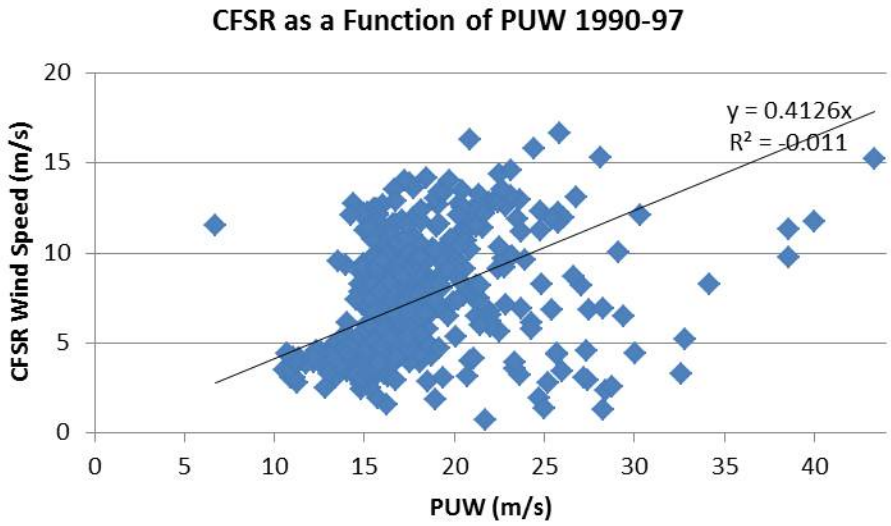

Figure 77. As in Figure 76, except for data from 1990–1997, and the regression relationship is to be applied to the 1998–2000 test cases prior to applying the CFSR-based acceleration factors from Table 12.

F. NOMOGRAM PERFORMANCE

1. Original Nomograms

The nomograms of Jarrell (1988) provide maximum gust wind speed, maximum sustained wind speed, mean gust wind speed, and mean sustained wind speed for any TC position and intensity within their applicable range from Sasebo. When the JTWC wind radii are available, evaluations are made for times when a TC is within two times the 34-kt wind radii range of Sasebo, or two times the range-to-radius ratio (RTRR). Unless otherwise indicated, all nomogram predictions/hindcasts used JTWC best-track data or linear interpolation between best-track reported times. For comparisons with AMEDAS observations via scatter plots, it is the mean nomogram output that is most meaningful.

As indicated in Figures 78–80, the tendencies for the mean sustained wind and mean gust nomograms are to under-forecast at low speeds and to over-forecast at higher wind speeds. However, these figures do represent a limited subset of TC tracks and intensities. For comparison with a larger set of TCs, nomogram hindcasts are prepared for the TCs during 2003–10. Indeed, both the sustained wind (Figure 81) and wind gusts (Figure 82) have better nomogram performance than indicated in Figures 78–79, which is

likely related to more varied TC tracks and intensities. This nomogram performance will be further explored in Chapter IV.

In order to evaluate maximum gust wind speed and maximum sustained wind speed nomogram performance, the focus will be on the 2011–2012 TCs when observations were reported every 10 minutes (Figures 83 and 84). Recall that nomogram maximum sustained wind predictions are simply 2/3 of maximum gust nomogram predictions. Thus it is not surprising to see in Figure 83 large sustained wind differences from the AMEDAS observations at many times. However, note that below approximately 15 m/s there are periods of apparent correspondence. Maximum gust nomogram predictions (Figure 84) generally exceed observed gusts by a large margin. In some other storms (not shown) observed maximum gusts did exceed nomogram predictions. That mean gust wind nomograms appear to correspond well to observations in some times is to be expected as mean gust and mean sustained wind nomogram predictions are different only by a factor of 2/3 and mean sustained nomograms do seem to have some utility (Figure 81).

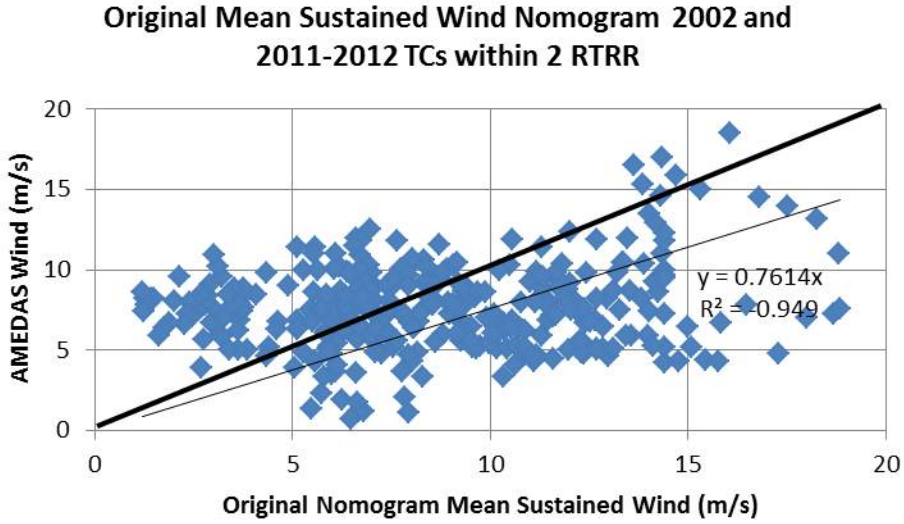

Figure 78. Jarrell (1988) mean sustained wind nomogram predictions vs. AMEDAS observations in Sasebo for the TCs within 2xRTRR of Sasebo during 2002 and 2011–2012.

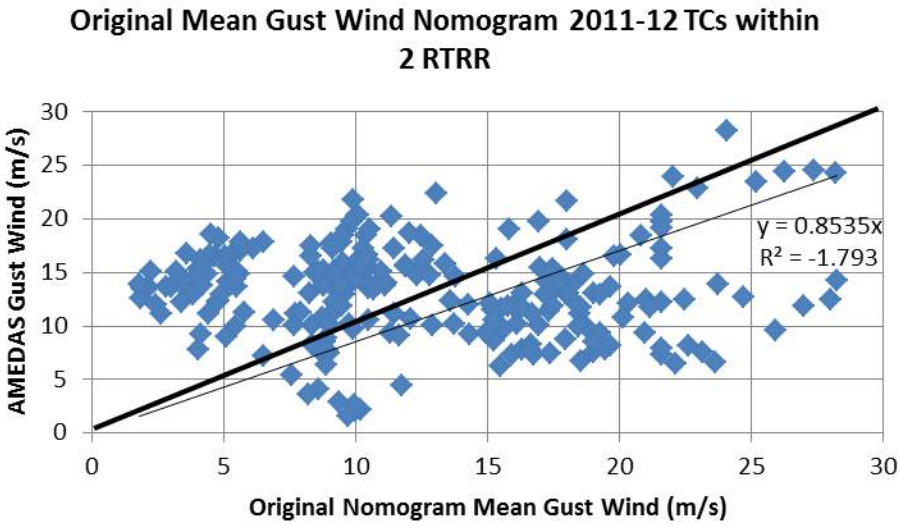

Figure 79. As in Figure 78, except for the mean gust wind nomogram predictions vs. AMEDAS gust observations in Sasebo. Only daily maximum gusts were reported prior to 2008, so only 2011 and 2012 data shown.

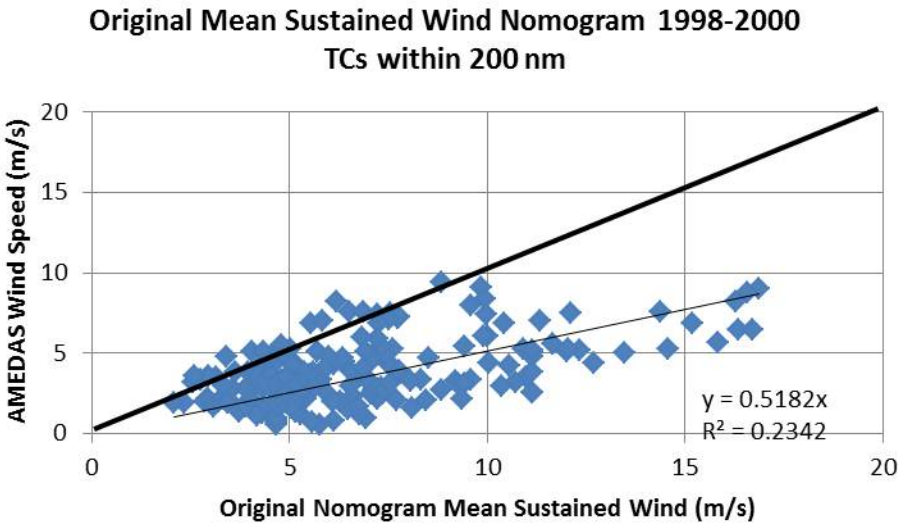

Figure 80. As in Figure 78, except for TCs within 200 n mi of Sasebo during 1998–2000. Note over-forecast tendency with this data from eight TCs.

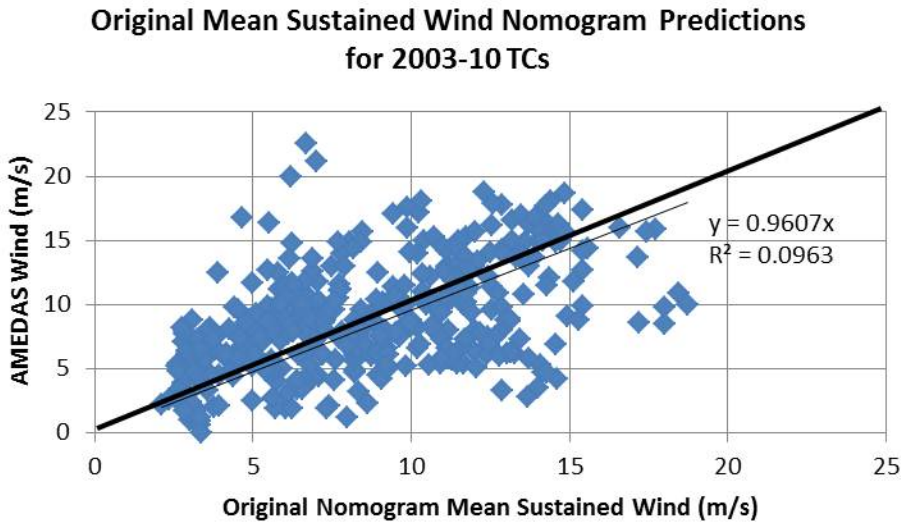

Figure 81. As in Figure 78, except for TCs during 2003 to 2010.

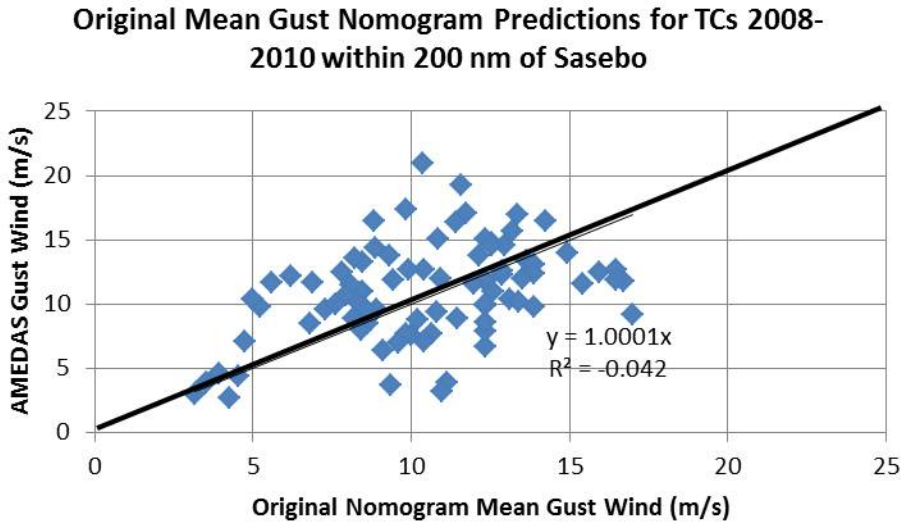

Figure 82. Mean hourly gust wind nomogram performance for limited sample of TCs during 2008–2010. Note the linear fit of data (thin black line, with equation and R^2 displayed, partially obscured) almost exactly matches the one-to-one correspondence line (thick black line).

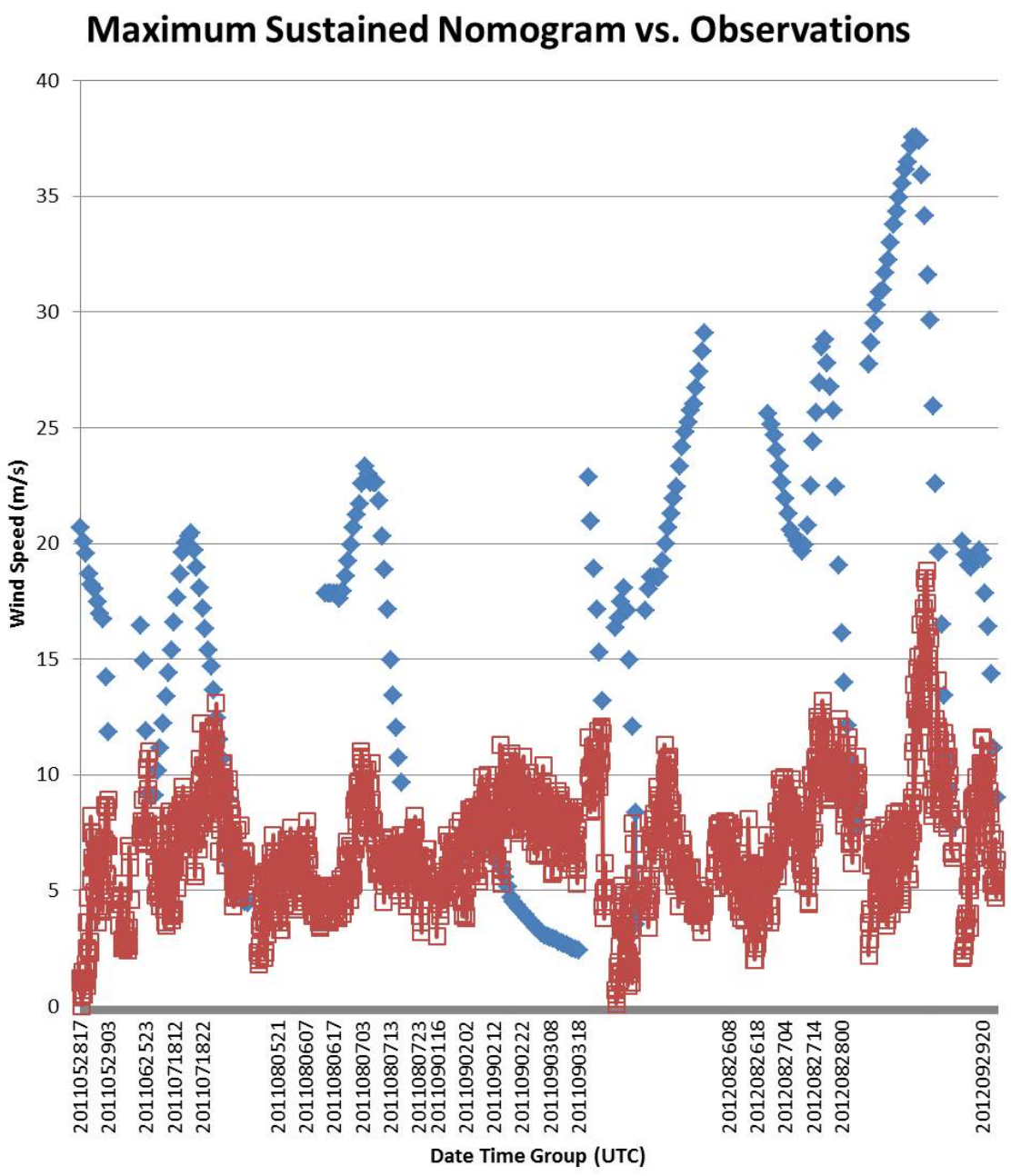

Figure 83. Plot of hourly maximum sustained nomogram wind speed hindcasts (blue symbols) for all times when TCs were within 2xRTRR of Sasebo in 2011–2012 and every 10-minute sustained wind observations (red symbols) from AMEDAS on and between the same hours. One instance of AMEDAS exceeding nomogram values is noted in September 2011.

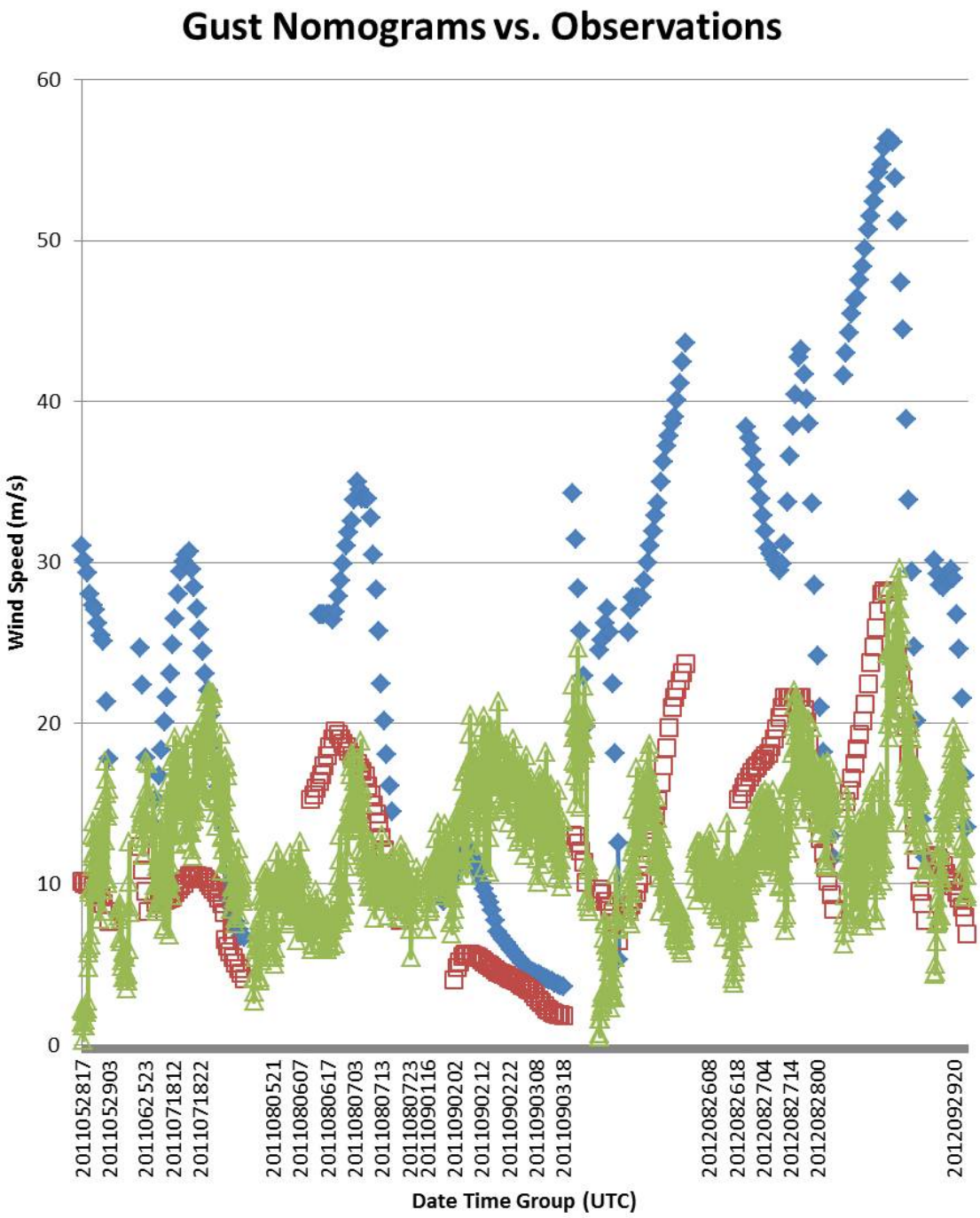

Figure 84. Plot of hourly maximum (blue symbols) and mean (red symbols) gust nomogram hindcasts for same times as in Figure 83, along with AMEDAS 10-minute gust observations (green symbols) on and between the same hours.

2. Alternative Nomograms

a. Derivation

As previously discussed, JTWC best-track wind radii by quadrant (NE, SE, SW, and NW) were available for most reported time steps during 2003 to 2010. Therefore, the quadrant in which Sasebo was relative to the TC center was determined hourly, and the range from TC center to Sasebo was divided by the appropriate 34-kt wind radius to calculate hourly RTRR values. In conjunction with the bearing from Sasebo, the coincident ratio of AMEDAS sustained wind speed to the TC maximum sustained wind speed (as reported by JTWC) was calculated to create a nomogram function (Figure 85). Given the x and y coordinates from Sasebo to the TC the output of the nomogram is a percentage that is multiplied by the JTWC TC intensity to get the Sasebo wind prediction.

While this methodology can also be applied to create a gust specific nomogram, this was not done due to the relatively small number of available gust observations. Instead it is intended that the gust prediction methodology outlined in Chapter II would be used with this new nomogram. Additionally, Jarrell (1988) provides nomograms for TCs of typhoon strength ($\geq$ 64 kt) separately from weaker TCs. As this new nomogram is using a normalized range, i.e., how far Sasebo is from TC center relative to the radius of 34 kt winds, it is taking TC structure into account in a way not done in the original nomograms. Therefore, only one nomogram was produced. A total of 468 individual observation times, with positions calculated in steps of 0.1 x or y coordinate, were used to create the new nomogram, which may lead to "bulls-eyes" caused by strong individual TCs in the dataset. No further smoothing was done after the use of the MATLAB TriScatteredInterp function, so some contour modification might be useful.

Comparison of Figure 85 with an original nomogram (Figure 3) indicates relatively higher values for TCs to the west of Sasebo. A notable relative maximum in contour values also exists southeast of Sasebo. By contrast, only a slight hint of a maximum is found in that region in Figure 3. Predictions from this nomogram will be

examined as an alternative for handling TC structure impacts using a normalized range that describes where Sasebo lies in the TC structure.

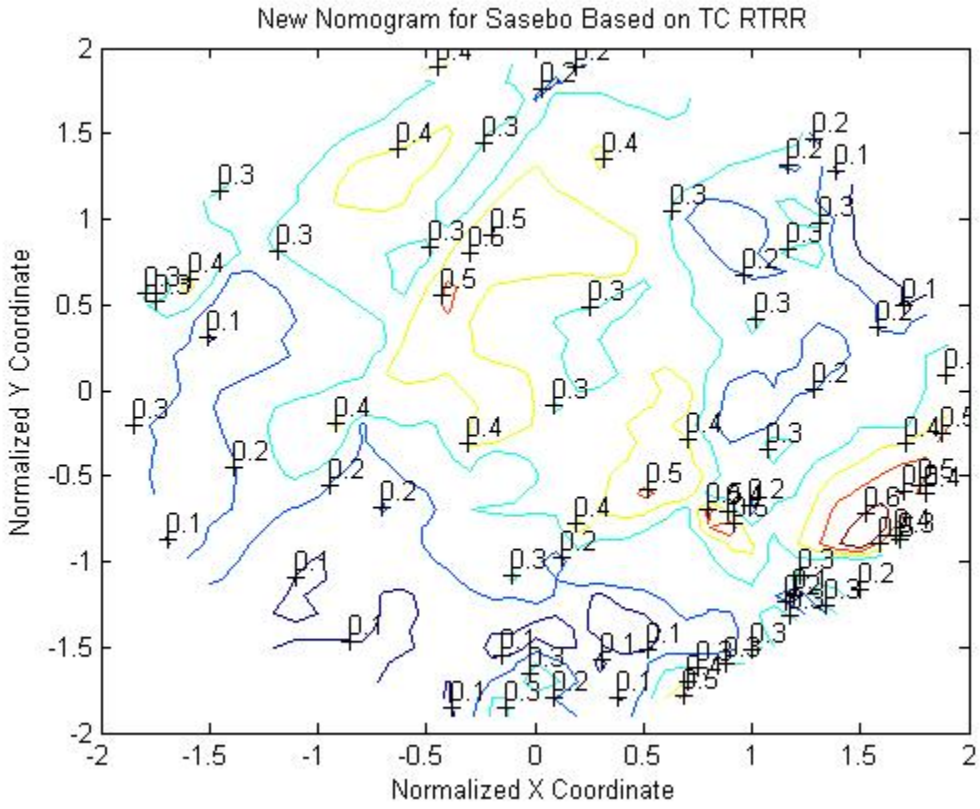

Figure 85. New nomogram for maximum sustained winds at Sasebo created from the data base of 2003–2010 TCs within 2 RTRR of Sasebo. The origin is centered on Sasebo and the x and y coordinates (positive values to the east and north) determine the contour value on which the TC center lies. Compare with sample original nomogram shown in Figure 3. The fraction of the JTWC intensity for the TC at a given time us an estimate for the Sasebo maximum sustained wind.

b. Results

The new nomogram in Figure 85 is tested with the independent sample of 2011–12 TCs within 2 RTRR of Sasebo (Figure 86). While the new nomogram performed similarly to the original mean sustained wind nomogram of Jarrell (1988), the new nomogram over-predicts the AMEDAS sustained wind speeds, e.g., by a factor of 3–4 for a few nomogram wind speeds of 30–40 m/s. Consequently, the R^2 value is near

zero, which may indicate that the predominant TC tracks in 2011–12 fell in relatively inaccurate portions of the new nomogram. This will further be explored in Chapter IV, both by looking at persistent errors for all empirical methods as related to the TC track, and by using the new nomogram for a 2013 storm.

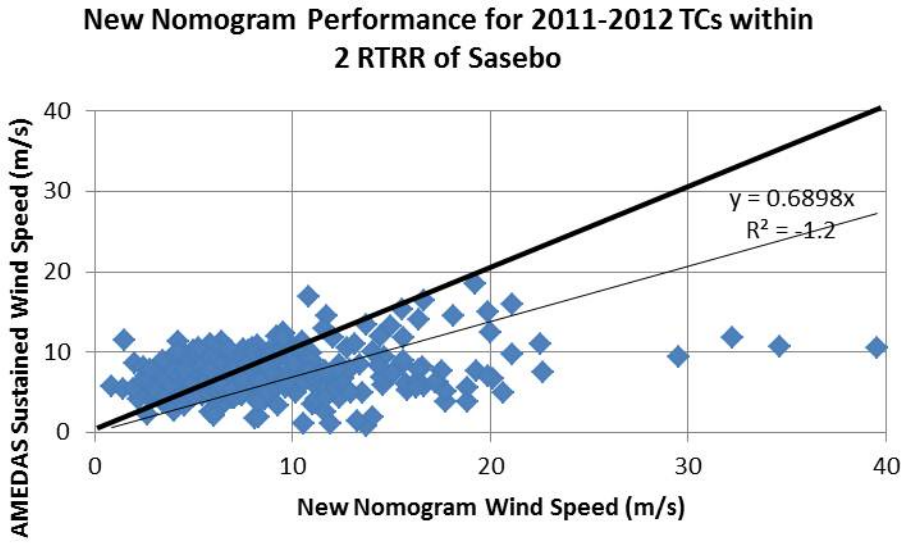

Figure 86. Scatter plot of new nomogram sustained wind predictions vs. AMEDAS observations for hourly observation times when a TC was within 2 RTRR of Sasebo during 2011 and 2012.

G. SUMMARY OF PERFORMANCE OF EMPIRICAL TECHNIQUES

Summarizing first the performance of the techniques for the prior AMEDAS site with the independent 1998–2000 cases, the largest R^2 of 0.41 was obtained when modifying the PUW with the PUW-to-AMEDAS derived directional acceleration factors (Table 17, row 2). The use of CFSR-derived acceleration factors yielded a slightly lower R^2 of 0.38 (Table 17, row 3). The smallest R^2 was the simple technique of PUW multiplied by a constant, which was basically a proxy for assuming all variability in the wind comes from the TC (Table 17, row 1). That is, the PUW times a constant is for the JTWC forecast extrapolated to Sasebo, and then reduced for friction. The percent of observations that fall between the upper and lower bounds (i.e., upper and lower range of acceleration factors from Tables 12 and 14) is larger for the CFSR-derived acceleration

factors (81%) than for PUW-derived acceleration factors (which was approximately 66% by design). While this appears to indicate that the range of CFSR acceleration factors better captures the variability of the Sasebo wind, the ranges are actually too large as they were also designed to capture 66% variability. Note that negative R^2 values in Table 17 rows 3, 5, 7, 9, and 10 simply indicate the variability relative to an assumed perfect forecast for that empirical technique is greater than the variability of the observations from their common mean. Nomogram R^2 performance is unimpressive, but that 60% of observations were within 5 kt of nomogram predictions suggest the nomogram technique is feasible for certain circumstances. More discussion follows in the case studies in Chapter IV.

The performance of empirical techniques in terms of R^2 for the independent sample of 2002 and 2011–12 cases at the current AMEDAS site appears to be most successful for the approach of simply multiplying PAW (Table 18, row 1) or PUW (row 2) by a constant (again as a proxy for isotropic friction). It also should be noted that both sets of CFSR-derived acceleration factors (i.e., those from all comparisons in 2003–2010 and those from the top 1000 observations from 2003–2010) were used, and that the 66% occurrence interval was used for "upper and lower bounds."

The larger R^2 value for PAW times a constant (Table 18, row 1) than for PUW times a constant (row 2) suggests that taking JTWC wind radii into account is beneficial. In addition, the percentage of observations within $\pm$ 5 kt is also higher (66%) for the PAW speeds. Whereas PAW multiplied by the PAW-to-AMEDAS directional acceleration factors (Table 18, row 3) has an over-forecast bias (Figure 69) that is reflected by the -0.02 R^2 shown, 86% of observed winds were within its predicted range, which suggests usefulness as a stand-alone forecast tool. Since the over-forecast bias for that particular method may be due to the limited set of TC tracks available for analysis during 2011–12, there may still be viability for using the technique in probabilistic forecasting. Considering all three right-hand columns of Table 18, PUW speeds adjusted by PUW-to-AMEDAS based acceleration factors has the best overall performance. Therefore, it may also be a good choice for probabilistic forecasting, e.g., applying the technique to each member of existing TC track/intensity ensembles.

For the 2002 and 2011–2012 test cases, the use of CFSR-derived acceleration factors (Table 18, rows 5–8) showed no obvious advantage over those derived from the much smaller set of AMEDAS to parametric wind comparisons. Nomogram performance was also not as good as for the 1998–2000 cases. The new nomogram (Table 18, last row) slightly outperformed the original mean sustained wind nomogram (Table 18, next-to-last row) in that more of its predictions (56% vs. 42%), were within 5 kt of observed winds.

Table 17. Summary of empirical techniques tested on independent sample of 1998–2000 TCs within 200 n mi of Sasebo. The three right hand columns summarize three performance metrics. The "R^2 from Perfect Deterministic Forecast Assumption" column is for the peak acceleration factor times PUW (e.g., red line in Figure 74) as a deterministic forecast. The "Percent of Deterministic Predictions within $\pm$ 2.5 m/s" column summarizes how often a technique treated as a deterministic forecast verified within 5 kt. The "Percent of OBS Between Upper and Lower Bounds" column summarizes how frequently an observed wind fell between the upper and lower bound of the acceleration factors times PUW (e.g., between the blue and green lines in Figure 74).

					Perform. Metrics	R^2 from Perfect Deterministic Forecast Assumption	Percent of Deterministic Predictions within $\pm$ 2.5 m/s	Percent of OBS Between Upper and Lower Bounds
Empirical Method	**Model/ Variant**	**Parametric Model Modified before Acceleration Factors Applied**	**TC Center Range from Sasebo**	**Source of Accel. Factors**				
Parametric	PUW	Multiplied by average AMEDAS/PUW from 1990-97	$\leq$ 200 n mi			0.30	87	
Parametric	PUW		$\leq$ 200 n mi	1990-97 PUW vs AMEDAS		0.41	89	67
Parametric	PUW	Multiplied by average CFSR/PUW from 1990-97	$\leq$ 200 n mi	1990-97 CFSR vs AMEDAS		0.38	90	81
Nomogram	Orig. Mean Sust.		$\leq$ 200 n mi			-3.17	60	

Table 18. As in Table 17, except for the independent 2002 and 2011–2012 test cases, with empirical factors derived from 2003–10 TC cases. Modifications to PAW speeds as well as PUW speeds are shown. Note RTRR was not widely available for 1998–2000 test cases.

					Perform. Metrics	R^2 from Perfect Deterministic Forecast Assumption	Percent of Determ. Predictions within ± 2.5 m/s	Percent of OBS Between Upper and Lower Bounds
Empirical Method	**Model/ Variant**	**Parametric Model Modified before Acceleration Factors Applied**	**TC Center Range from Sasebo**	**Source of Accel. Factors**				
Parametric	PAW	Multiplied by average AMEDAS/PAW from 2003-10	≤ 200 n mi			0.35	66	
Parametric	PUW	Multiplied by average AMEDAS/PUW from 2003-10	≤ 200 n mi			0.33	61	
Parametric	PAW		≤ 200 n mi	2003-10 PAW vs AMEDAS		-0.02	58	86
Parametric	PUW		≤ 200 n mi	2003-10 PUW vs AMEDAS		0.24	75	75
Parametric	PAW	Multiplied by average CFSR/PAW from 2003-10	≤ 200 n mi	2003-10 CFSR vs AMEDAS		-1.04	48	64
Parametric	PAW	Multiplied by average CFSR/PAW from 2003-10	≤ 200 n mi	2003-10 CFSR vs AMEDAS, top 1000 obs		0.16	61	72
Parametric	PUW	Mult. by avg. 2003-10 CFSR/PUW	≤ 200 n mi	2003-10 CFSR vs AMEDAS		-1.27	49	63
Parametric	PUW	Mult. by avg. 2002-10 CFSR/PUW	≤ 200 n mi	2003-10 CFSR vs AMEDAS, top 1000 obs		0.05	55	68
Nomogram	Orig. - Mean Sust.		RTRR ≤ 2			-1.68	42	
Nomogram	New		RTRR ≤ 2			-2.53	56	

IV. COMPARISONS, PERSISTENT ERRORS, AND FORECASTING APPLICATIONS

To illustrate the utility of the empirical techniques developed in Chapter III, the techniques will be applied to a TC in the Atlantic as well as TCs impacting another western North Pacific site without surrounding terrain. In addition, simultaneous observations from Sasebo and adjacent open-ocean buoys will be examined to demonstrate how well the parametric technique can predict different parts of the same TC at the same time. Next, two TC hindcasts are examined in detail to possibly detect persistent errors and propose conditional forecast rules that might be derived for Sasebo. Finally, analysis of a recent TC during 2013 demonstrates how the empirical techniques might be used in "real-time" forecast mode, including for use with existing ensembles to create TC wind probability products.

A. NAVAL STATION NORFOLK: HURRICANE IRENE 2011

Naval Station Norfolk, Virginia, is the largest naval facility in the world (Commander Navy Installations Command 2013), and is surrounded by relatively flat terrain when compared to Sasebo (Figure 87).

Figure 87. View of Naval Station Norfolk, Virginia, to the east, with the entrance to Chesapeake Bay just beyond the upper right corner of the photograph. Main base area depicted is approximately 4 km by 4 km. Note the multiple U.S. Navy ship piers in the foreground and the lack of terrain height differences within several kilometers of the piers. The areas immediately adjacent to this photograph are also at low elevation (from Commander Navy Installations Command 2013).

In August 2011, the forecast for Hurricane Irene caused the sortie of 27 U.S. Navy ships from Norfolk and extensive on-base preparations (U.S. Navy 2013). The CPA of Irene to Norfolk was approximately 30 n mi to the east at 0000 UTC 28 August (Figure 88). Knaff et al. (2007, Table 1) provides parameters for the North Atlantic, in addition to those for the western North Pacific values reported in Table 8. Using the geographical position of the Norfolk Naval Station sensor (available from the U.S. National Climatic Data Center), and the best-track position and intensity data for Hurricane Irene from the NHC best-track, computer code was modified to hindcast the PUW and PAW for this case (Figure 89).

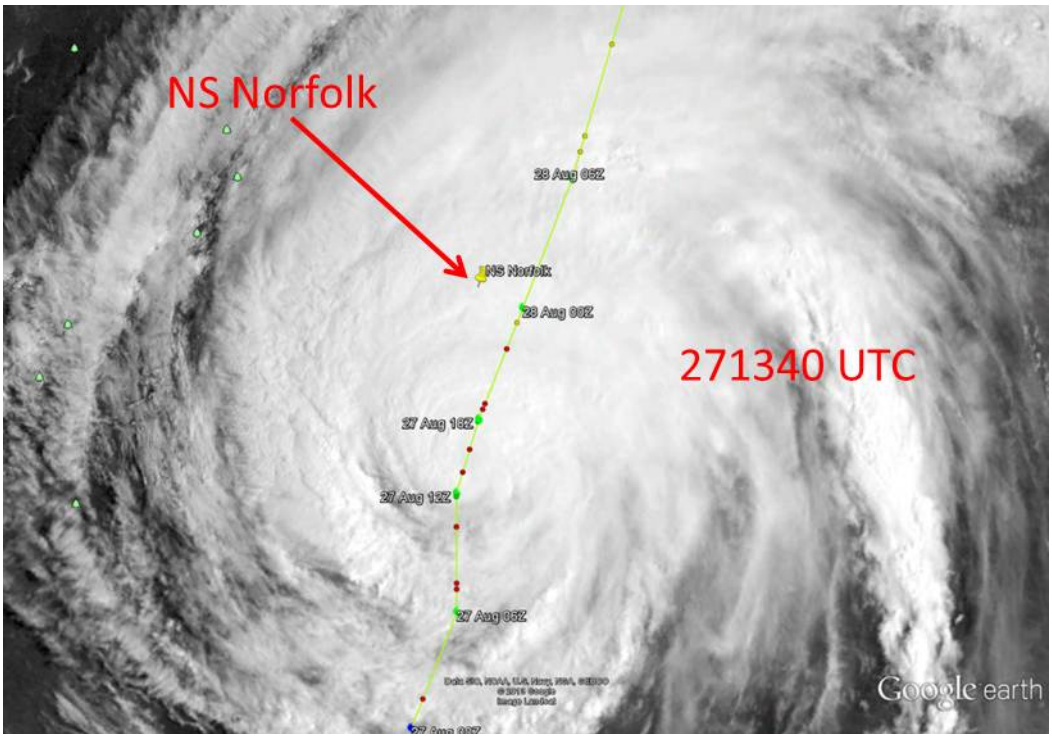

Figure 88. GOES 13 visual satellite imagery of Hurricane Irene approximately 10 hours before CPA to Norfolk, VA on 27 August 2011. NHC best track is displayed as the green line (after Naval Research Lab 2013 and Google Inc. 2013).

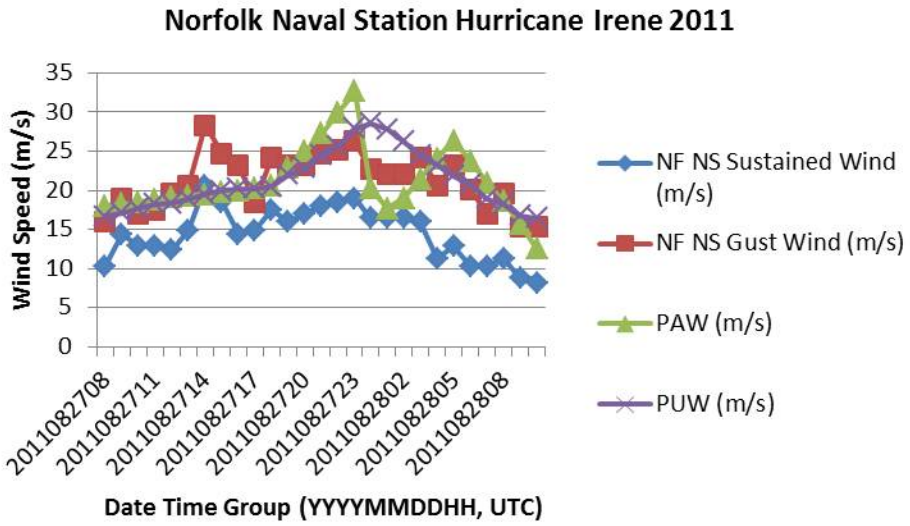

Figure 89. Hourly PAW and PUW hindcast speeds (m/s) for Naval Station, Norfolk from best-track Hurricane Irene position and intensity for comparison with reported sustained and gust wind observations. No terrain-based adjustments have been made.

Four noteworthy features in Figure 89 will be described. First, both PUW and PAW are within a few meters per second of observed gust speeds at the majority of time steps, which indicates the parametric models are representing gusts from vertical mixing of the winds above the boundary layer. Second, a "surge" in observed sustained and gust winds at approximately 1400 UTC 27 August is not represented in either the PUW or PAW speeds. Third, PAW speeds match observations much better than PUW speeds for the relative wind maximum followed by relative minimum and then a secondary maximum in winds between 2300 UTC 27 August – 0500 UTC 28 August. Indeed, this pattern is completely absent in the PUW time series. Fourth, the difference between sustained wind observations and PUW and PAW is roughly constant. As with the Sasebo cases an isotropic frictional effect can be represented by calculating average sustained wind to PUW or PAW ratios, and then multiplying the parametric winds by those values (Figure 90).

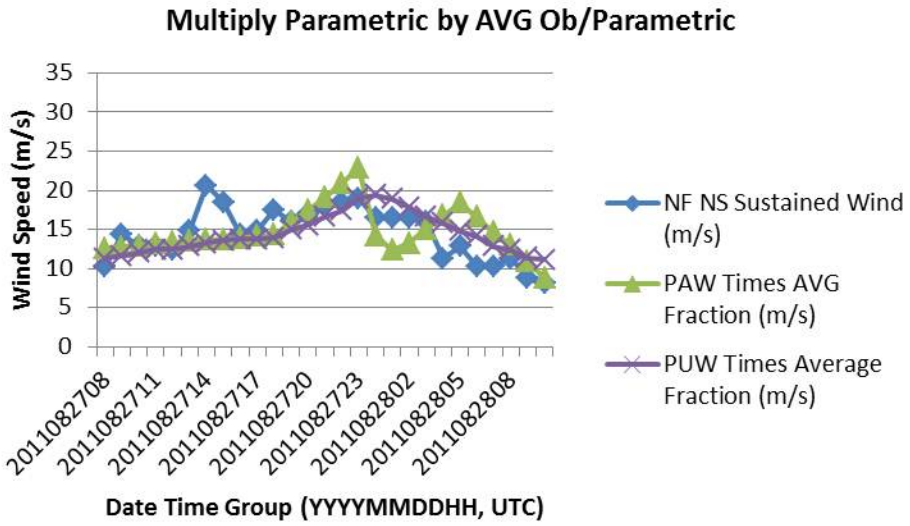

Figure 90. Adjusted PUW and PAW hindcast speeds for Naval Station Norfolk after multiplying by an average of hindcast to PUW or hindcast to PAW ratios, respectively, for the same time period in Figure 89. Note the surge in winds from 1400–1600 UTC is not hindcast.

With the exception of the wind surge at approximately 1500 UTC on 27 August, either PUW or PAW speeds multiplied by a constant is a viable forecast technique for Naval Station Norfolk. As was described in Chapter I, this is the approach used by the National Weather Service and the U.S. Navy for stations in flat terrain on the east coast of the U.S. This wind surge was likely caused by a TC rainband around 1400 UTC 27 August, and a local tornado warning was in effect at 1445 UTC (Figure 91). At 1900 UTC, Norfolk appeared to be in between rainbands and thus did not experience convection related wind enhancement (Figure 92).

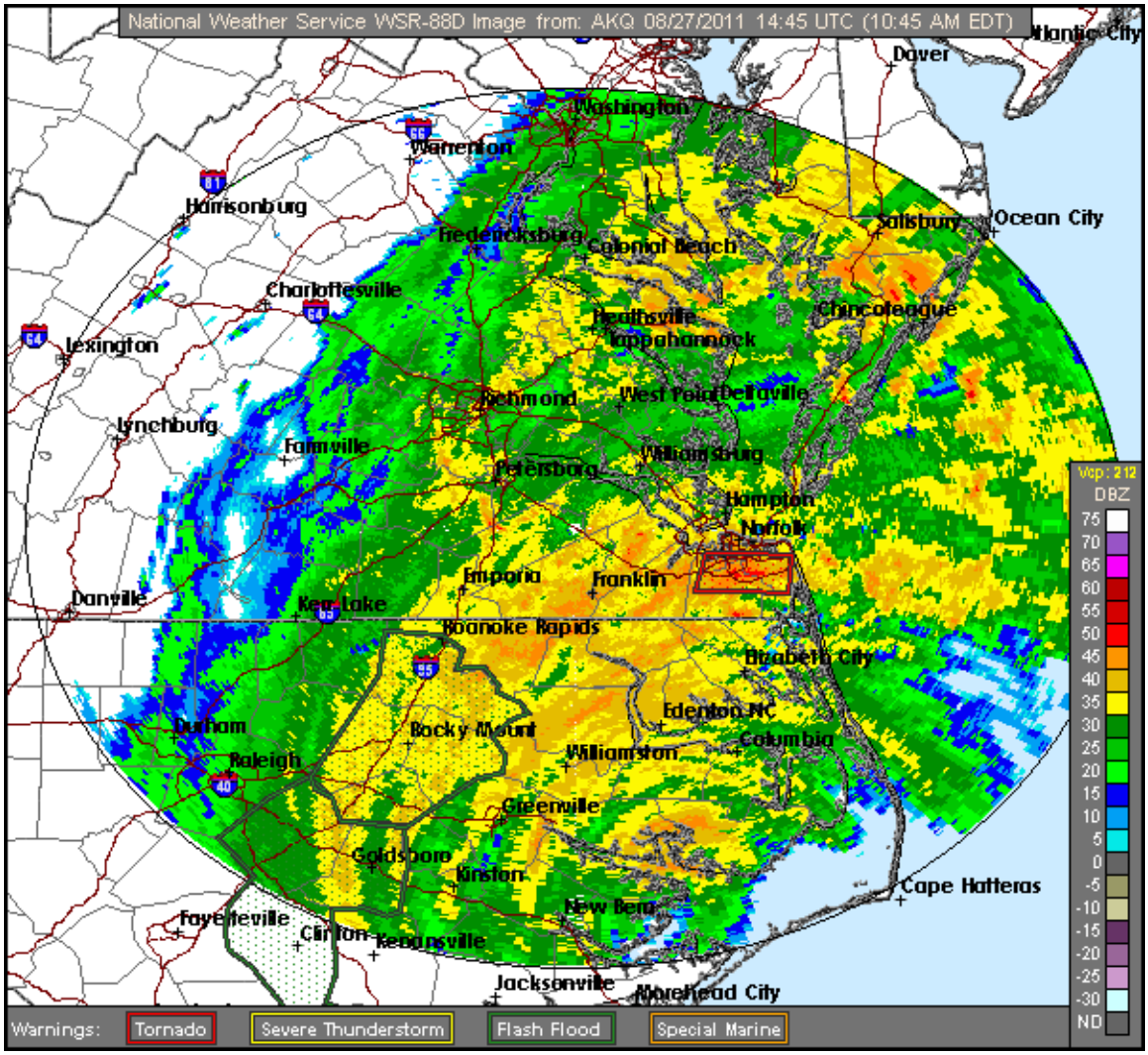

Figure 91. NWS radar imagery at 1445 UTC 27 August 2011 during Hurricane Irene. Hurricane center appears to be north of Morehead City (bottom center right of image). Note the relatively high DBZ values around Norfolk (middle right of the image), and the red Tornado warning box near Norfolk, which was during the wind "surge" noted in Figures 89–90, and approximately one hour after the image in Figure 88 (from National Weather Service 2013).

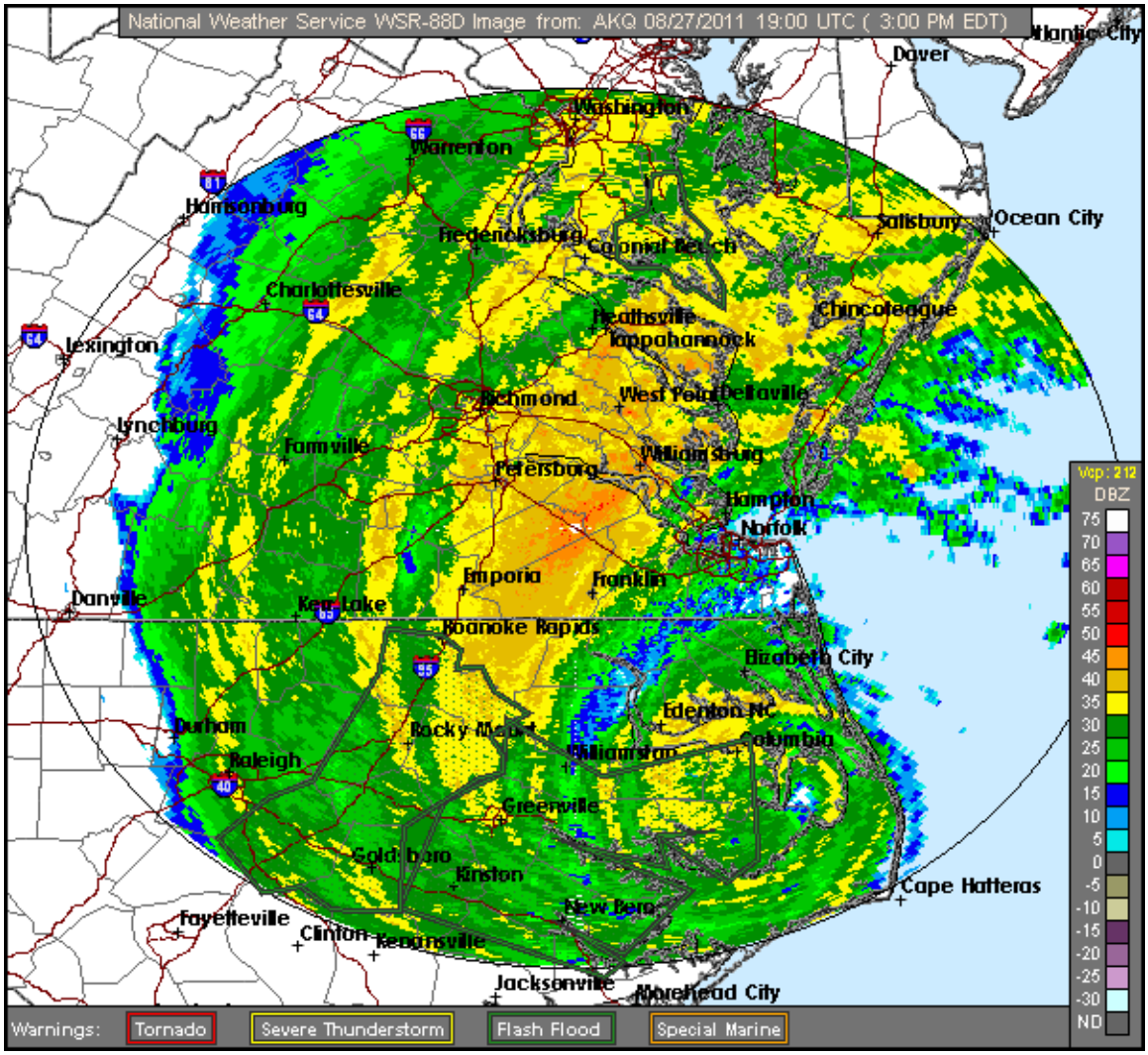

Figure 92. NWS radar imagery at 1900 UTC 27 August 2011, which is approximately 5 hours before CPA to Norfolk, Virginia. The geographic area shown is the same as for Figure 91. Note that the center of Hurricane Irene just southeast of Columbia, North Carolina, is continuing to approach Norfolk. However, Norfolk is between TC rainbands as suggested by higher radar reflectively in bands to the south and north of Norfolk.

B. MINAMITORISHIMA

As a contrast to the terrain-influenced Sasebo, consider the remote island of Minamitorishima at 24.3° N, 154° E in the western North Pacific. This small island is part of Japan, has an AMEDAS sensor installed, and is extremely flat (Figures 93–94). Thus, minimal terrain impacts on wind observations will be assumed, apart from a land-sea surface friction contrast, and possible sea breeze modifications.

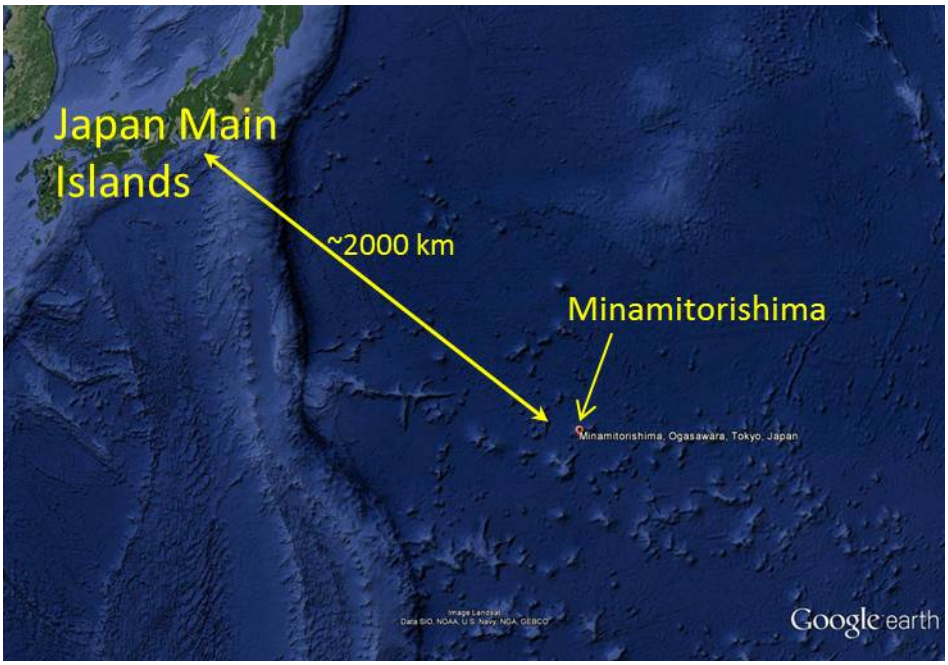

Figure 93. Broad area view of the position of Minamitorishima in the western North Pacific (after Google Inc. 2013).

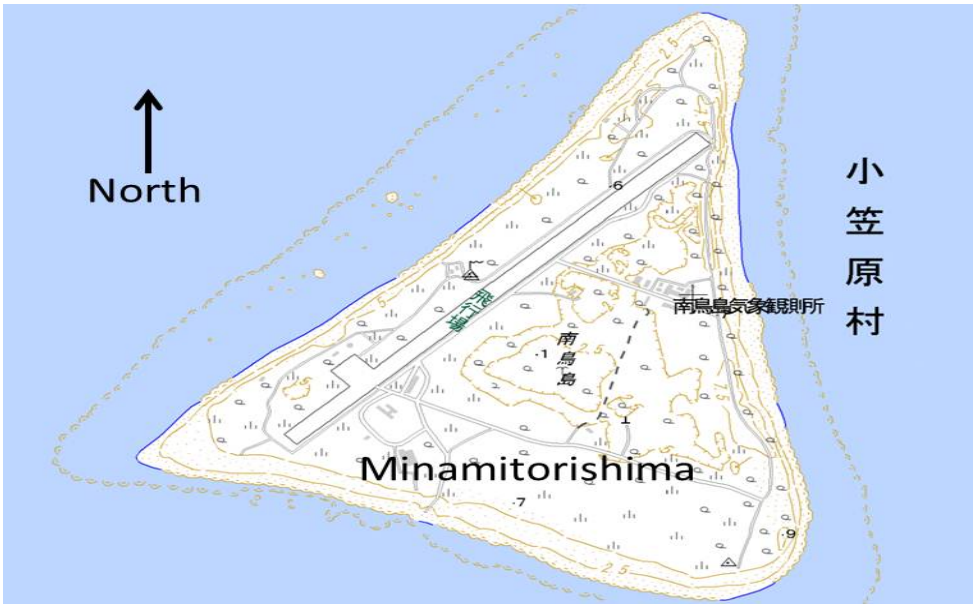

Figure 94. Topographic map of Minamitorishima for which the highest elevation contour is 5 m above sea level. Note the airstrip running from southwest to northeast on the west side of the island. The sides of the island are each approximately 1.5 km long (after Geospatial Information Authority of Japan 2013).

Eight TCs that influenced the weather on Minamitorishima were selected from 2002–2009, which is a period for which JTWC wind radii are readily available so that PAW as well as PUW can be tested. As the island is in the same ocean basin as Sasebo, the only change to the core parametric computer code was the location of the station, but no directionally-based acceleration factors were applied. PUW and PAW calculated for times TCs were within 200 n mi or 2 RTRR tend to be higher than observations, which indicates frictional effects are not adequately considered (Figures 95–98). Moreover, the parametric and observed wind directions are within one cardinal point at all times with the parametric directions often higher (Figure 99), which is consistent with frictionally-based wind in-turning.

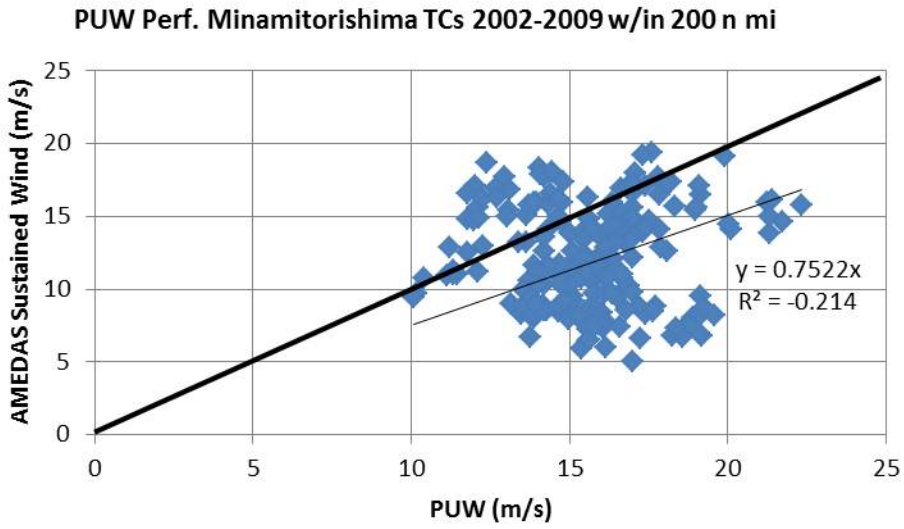

Figure 95. PUW vs. Minamitorishima AMEDAS sustained wind observations (m/s, 10 minute average) for TCs within 200 n mi during 2002–2009. Thick black line represents theoretical perfect correspondence. Thin black line is linear fit of data with imposed zero-intercept.

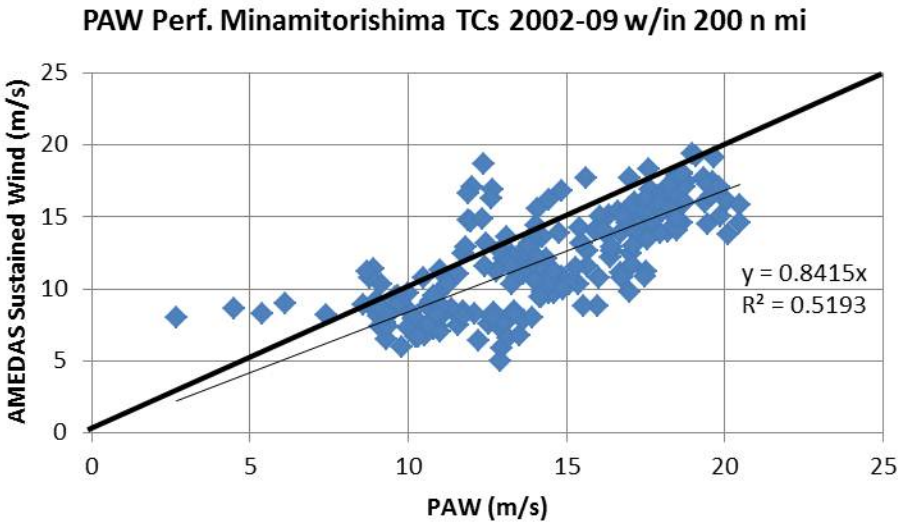

Figure 96. As in Figure 95, except for PAW. Note more linear appearance of Figure 96 plotted points, and higher R^2 value displayed.

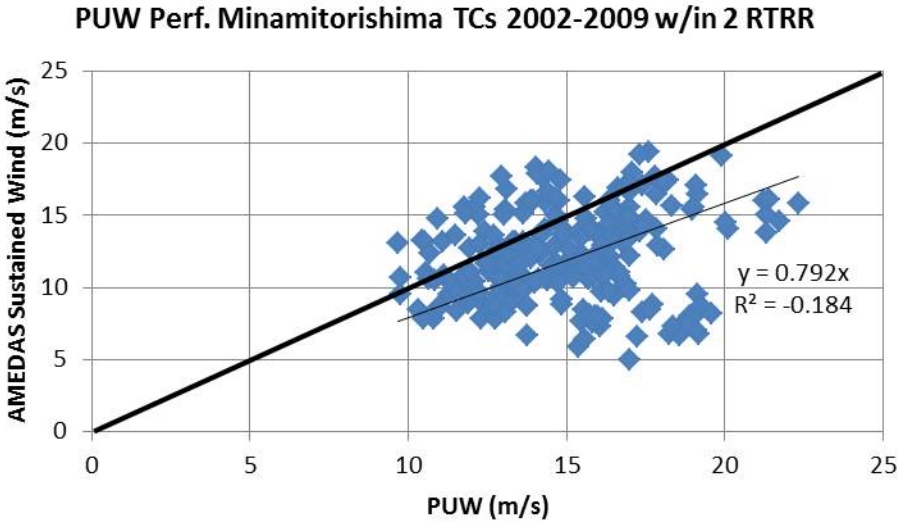

Figure 97. As in Figure 95, except for times when TCs were within 2 RTRR of Minamitorishima. Note that the times and values of AMEDAS observations overlap with, but do not exactly match, those in Figures 95–96.

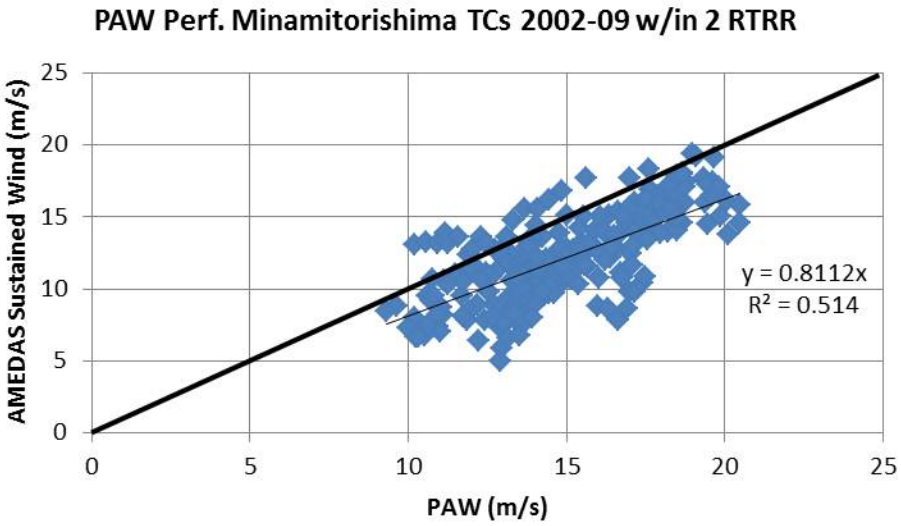

Figure 98. As in Figure 96, except for times when TCs were within 2 RTRR of Minamitorishima. Times and values of AMEDAS observations match those in Figure 97.

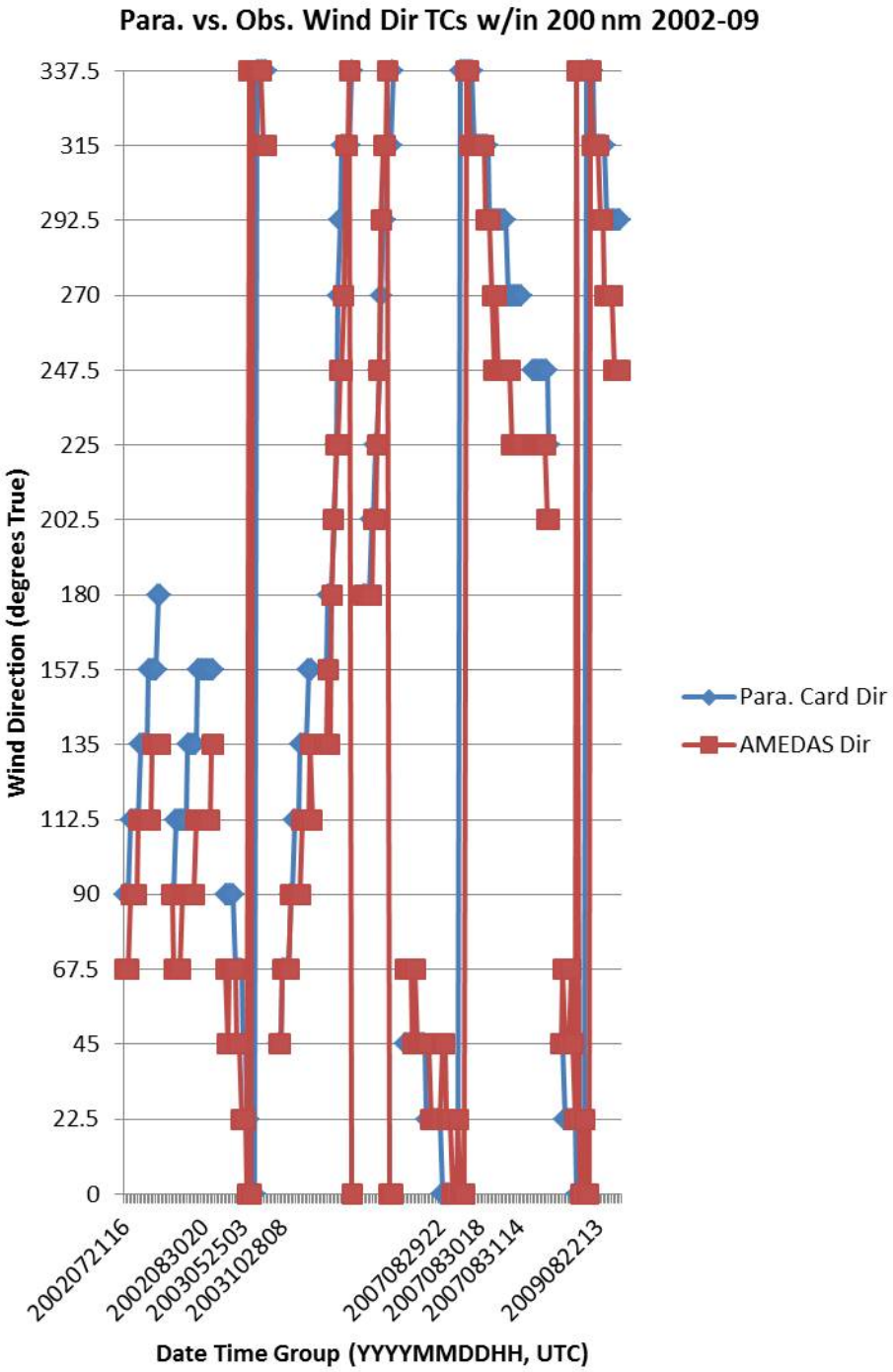

Figure 99. Parametric wind directions (bearing from Minamitorishima minus 90 degrees, blue line) and observed AMEDAS wind direction (red line) for eight TC passages. Both sets of wind directions are one of 16 cardinal points.

The improvement from including the JTWC analyzed wind radii in the PAW model (Figure 96 and Figure 98) versus the PUW model (Figure 95 and Figure 97) is confirmed by the larger regression coefficients and smaller spreads about the regression lines. Furthermore, multiplying PAW by a constant reduction factor as a first-order method of handling friction yields a better match with observed winds (Figure 100). Note that approximately 71% of these adjusted PAW values are within 2.5 m/s of AMEDAS winds. In combination with the close agreement between the parametric and observed wind directions (Figure 99), these results reinforce that the PAW technique are useful (indeed essential) for estimating the local winds caused by a TC in the western North Pacific. However, even for "non-complex" terrain more wind variability occurs than is accounted for by the TC intensity and track in the parametric wind relationship. As with Hurricane Irene, localized enhanced convection could be the cause of higher wind speeds, or TC wind asymmetries during extratropical transition (ET), or other factors that a simple vortex equation cannot account for. For Sasebo, these same sources of wind variability may be present with the additional effects of terrain blocking and gap winds.

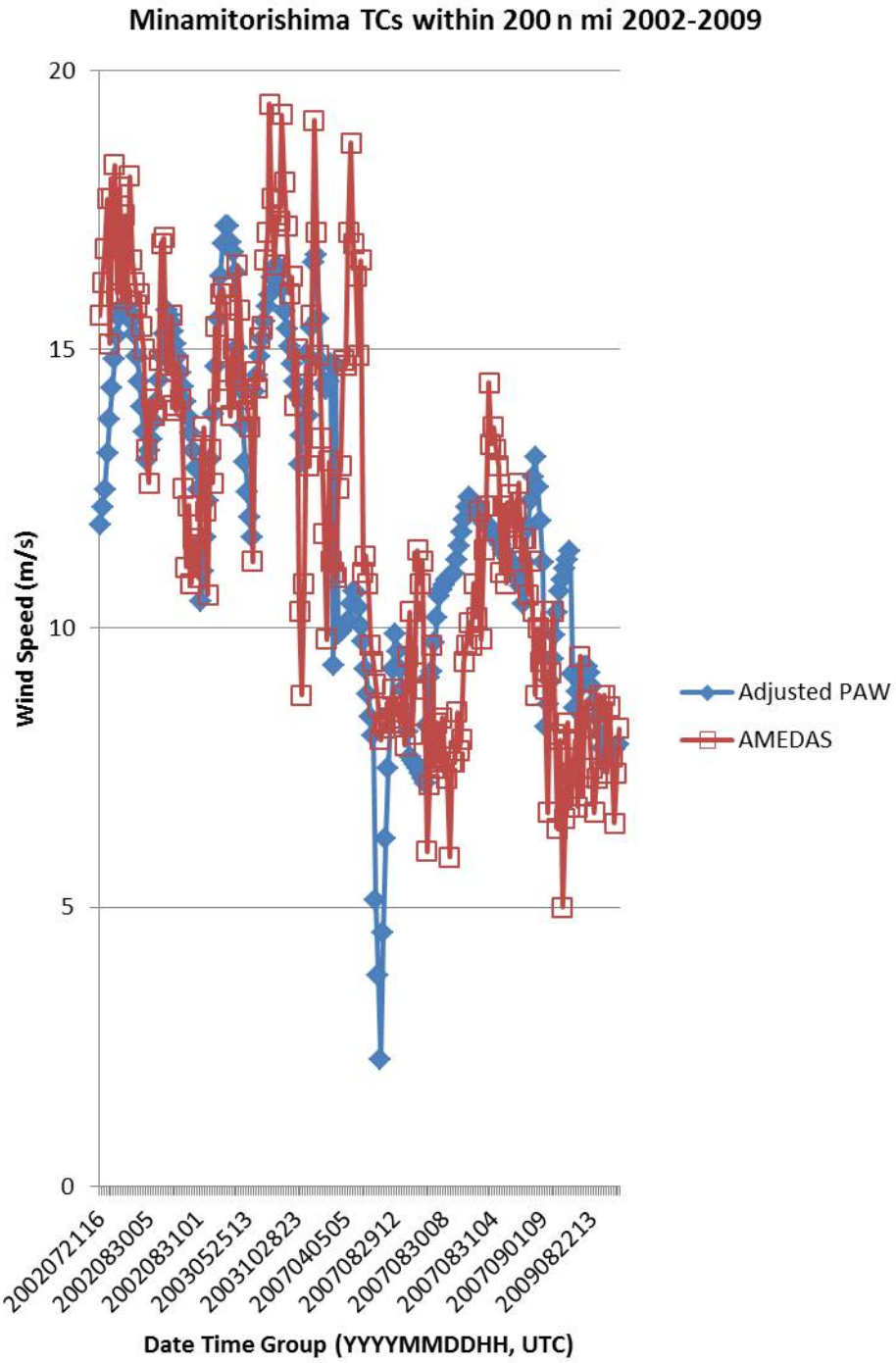

Figure 100. PAW adjusted by multiplying by a constant (blue line) and AMEDAS sustained wind observations at Minamitorishima for times when TCs were within 200 n mi during 2002–09.

C. SIMULTANEOUS OPEN-OCEAN OBSERVATIONS

The JMA maintained several fixed open-ocean observation buoys from 1978–2000 (Japanese Meteorological Agency 2013f). Although these buoys were all located quite far from Sasebo (Figure 101), there were times when TCs were approximately equidistant from Sasebo and a buoy. Similar to Minamitorishima observations, this buoy data are especially interesting due to no local terrain impacts. However, surface friction is still a factor, and can be enhanced by larger waves generated by a TC. The first case examined here is TC Bolaven in 2000, whose track passed Sasebo to the west (Figure 102).

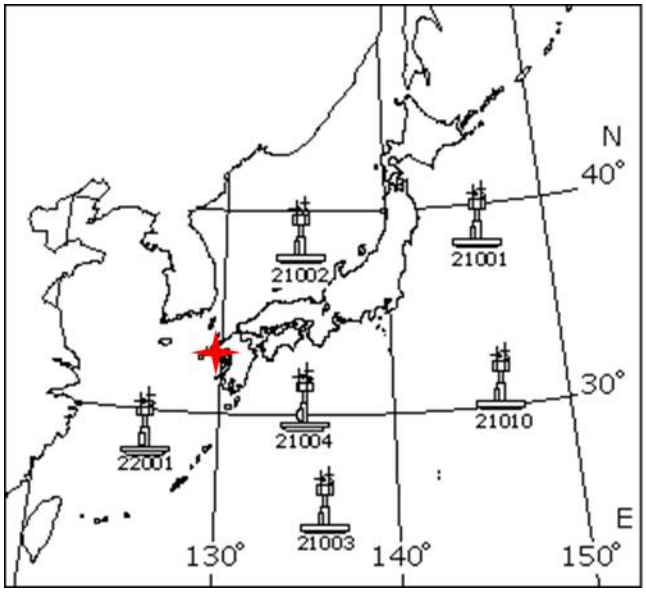

Figure 101. Position of JMA observation buoys relative to Sasebo (red star). Buoy 22001 is at approximately 600 km distance, while buoy 21004 is approximately 700 km from Sasebo (after Japanese Meteorological Agency 2013f).

Figure 102. .JTWC best track of TC Bolaven in 2000is shown as thin black line, Sasebo is at the red star, and buoy 22001 is at the yellow star. The thick yellow line indicates the portion of the track where the difference in range from the TC to Sasebo and from the TC to the buoy is ≤ 100 n mi. TC range to Sasebo during this time was approximately 230 to 130 n mi.

As previously noted PUW tends to be an overestimate of the local wind speeds, especially with no frictional reduction (Figure 103). Except for these offsets of the observed winds being smaller, buoy observed winds and buoy PUW generally decrease during this time and the Sasebo observed winds and Sasebo PUW have a moderate increase as TC Bolaven moves poleward. Additionally, good agreement exists between the predicted and observed wind directions with the 1 or 2 cardinal point differences being consistent with frictional in-turning (Figure 104).

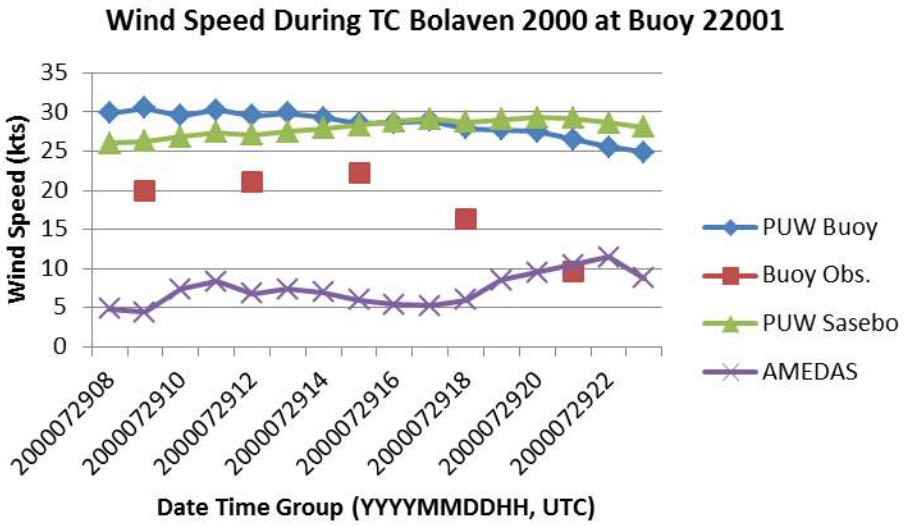

Figure 103. Parametric (PUW) and observed wind speeds at JMA buoy 22001 and at Sasebo during TC Bolaven in 2000. Note buoy parametric wind prediction (blue line) and buoy observations (red squares) both decrease over time. Sasebo parametric winds (green line) and observations (purple line) both show overall increases.

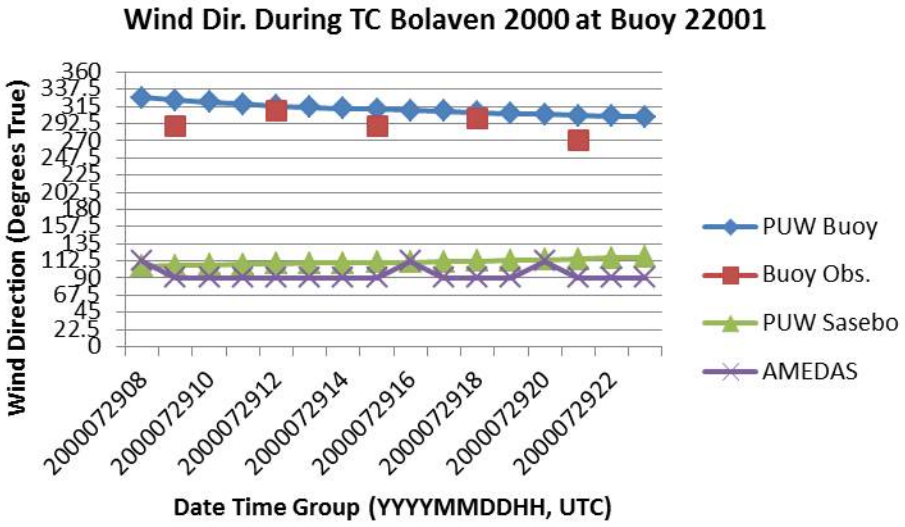

Figure 104. Parametric (PUW) and observed wind directions at JMA buoy 22001 and Sasebo during TC Bolaven in 2000. Note observed wind directions are within 1-2 cardinal points (22.5-45 degrees) of predictions at all times.

TC Kent during 1992 passed between Sasebo and buoy 21004 on a notably different track than Bolaven 2000 (Figure 105). As with TC Bolaven, observed wind

speeds at both buoy 21004 and in Sasebo follow the trend of the PUW speed (Figure 106), but with observed wind speeds notably lower. AMEDAS wind speeds in Sasebo during the approach of TC Kent have more variability than in the Bolaven case, which may be directly related to greater wind direction variability than in TC Bolaven (compare Figures 104 and 107). This direction variability is likely caused by TC Kent passing directly over the long axis of Kyushu with extensive terrain interaction causing asymmetric winds. Note a near-simultaneous cyclonic turning in observed wind directions at both the buoy and Sasebo around 0000 UTC 18 August 1992 (Figure 107). While this shift could be caused by some TC scale asymmetry or internal structure, it may be related to the relatively more complex terrain to the immediate NE of Sasebo since this was the predicted TC Kent wind direction, and corresponds to an increasing fraction of the TC circulation interacting with land as the storm continues northward.

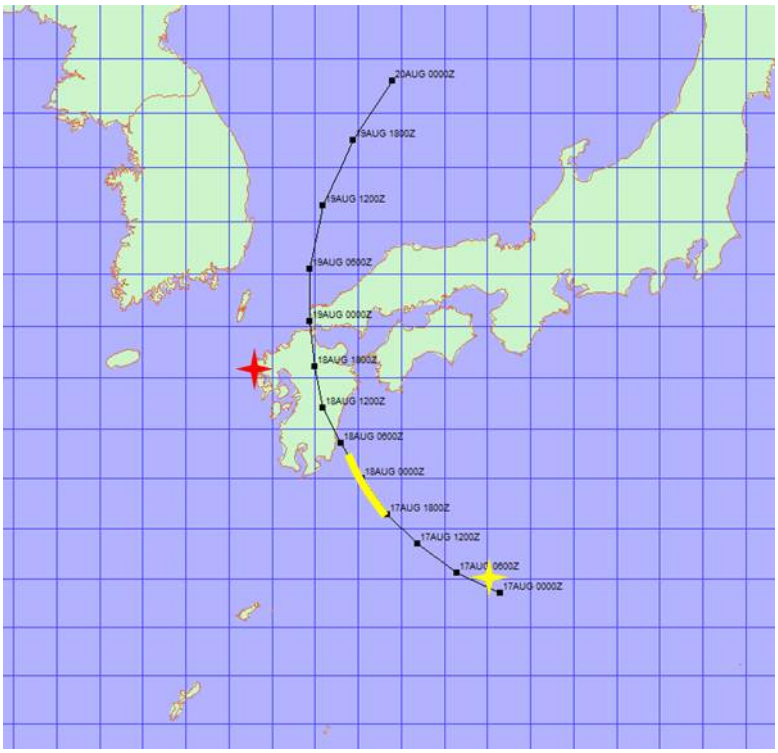

Figure 105. As in Figure 102, except for TC Kent in 1992 with yellow star at the position of JMA buoy 21004 and the thick yellow line the time period during which the difference in range from Sasebo to TC and the range from buoy to TC was $\leq$ 100 n mi. Range of TC to Sasebo was approximately 240 to 150 n mi.

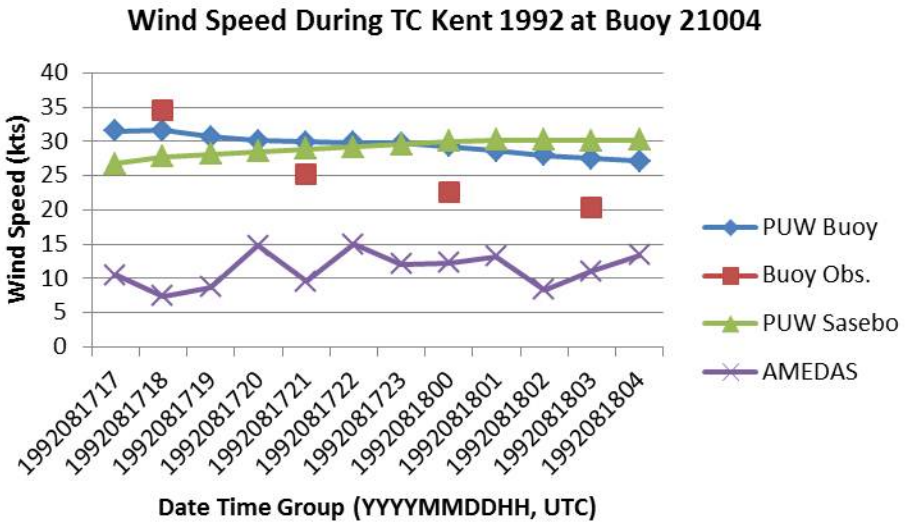

Figure 106. As in Figure 103, except for TC Kent 1992 and buoy 21004.

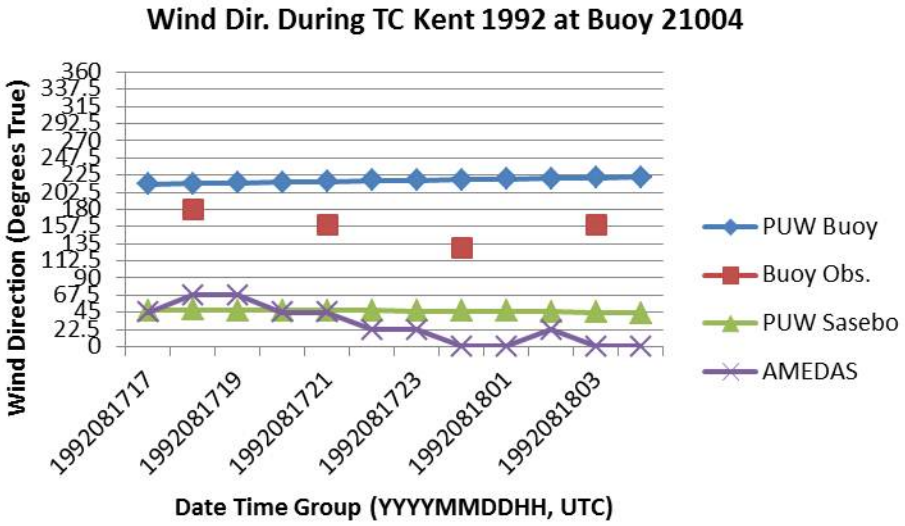

Figure 107. As in Figure 104, except for TC Kent 1992 and buoy 21004.

It is encouraging that a parametric technique can capture the trend of variability over several hours simultaneously in different parts of the same TC. Other storms (not shown) had PUW speeds at the buoys during eyewall passage with the general trend of increases and decreases as a TC passed. Since JTWC wind radii were not readily available for the cases, a comparison with the PAW values was not made. If a frictional

reduction to the wind was taken into account, PUW predictions at the buoys worked well for many, but not all, storms. This is not too surprising as the modified Rankine vortex utilized for PUW can only handle limited asymmetries, so the technique would be expected to work best for well organized, midlife-cycle TCs, which should be considered when predicting wind variability in Sasebo.

D. HINDCASTS EXAMINED IN MORE DEPTH

1. Confidence Intervals

Confidence intervals were calculated for the various directional acceleration factors that were intended to capture natural variability, and provide forecasters with an alternate probabilistic product. In some instances, the confidence intervals were too large to be operationally useful, e.g., giving a forecast range from 5 to 30 kt. Therefore, the range of observed wind variability at Sasebo is examined in more depth in this section to gauge the plausibility of these confidence intervals, as well as to provide an alternate representation of uncertainty estimates.

The MATLAB "smooth" function, which uses a moving average, was applied to the time series of AMEDAS 10-minute sustained and gust wind observations from 2009–2012. All observed winds within 2.5 m/s were binned every 2.5 m/s (i.e., bin centers at 1.25 m/s, 3.75 m/s, 5.25 m/s, etc.). Histograms of the speed difference between actual observations and smoothed winds (sampled in steps of 0.1 m/s) were calculated to include 95% of the speed differences. This sustained wind variability in each bin is shown in Figures 108–109, and Table 19. For the sustained winds (Figure 108), this method of specifying the expected wind speed range increases from 0.6 m/s for an AMEDAS wind speed of 2.5 m/s to 1.7 m/s for a wind speed of 12.5 m/s. The gust wind variability (Figure 109) increases more rapidly from 0.7 m/s at 2.5 m/s to 3.1 m/s at 20 m/s. Sustained wind variability and gust wind variability over a larger range of wind speeds and gust winds are provided in Table 19.

It is proposed that these wind and gust variability estimates may be more useful than the confidence intervals calculated in Chapter III. In an operational setting, the forecast sustained wind from the parametric technique would be entered in Table 19 to

provide the expected sustained wind variability. Similarly, the forecast gust wind would be entered in Table 19 to provide the gust wind variability.

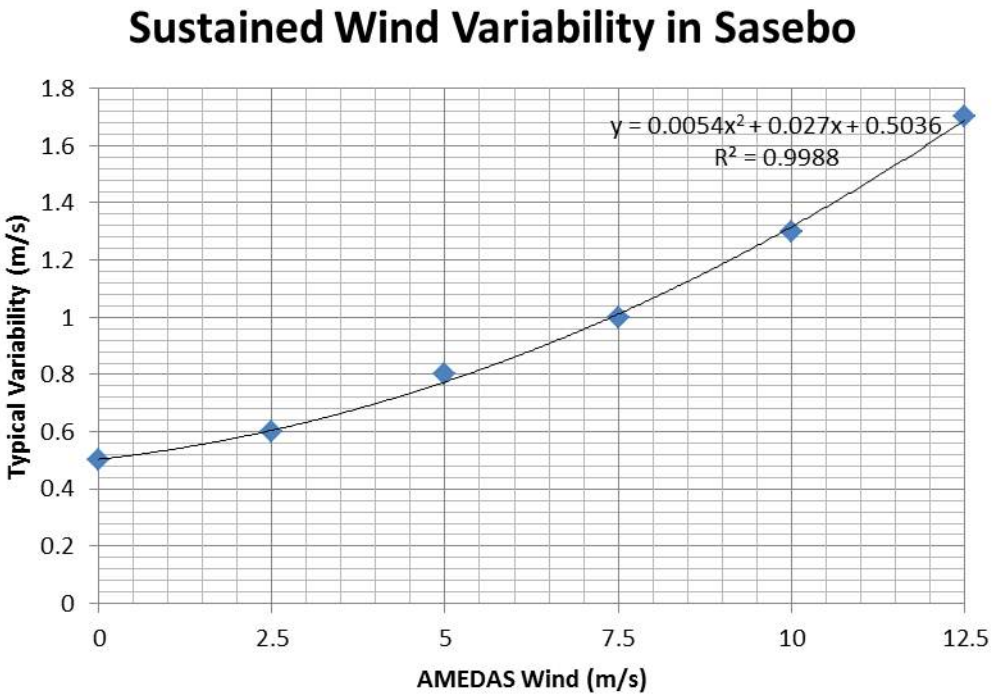

Figure 108. Expected variability of sustained winds in Sasebo as derived from all (not just TC-related) 10-minute AMEDAS observations during 2009–2012 compared to a smoothed wind time series.

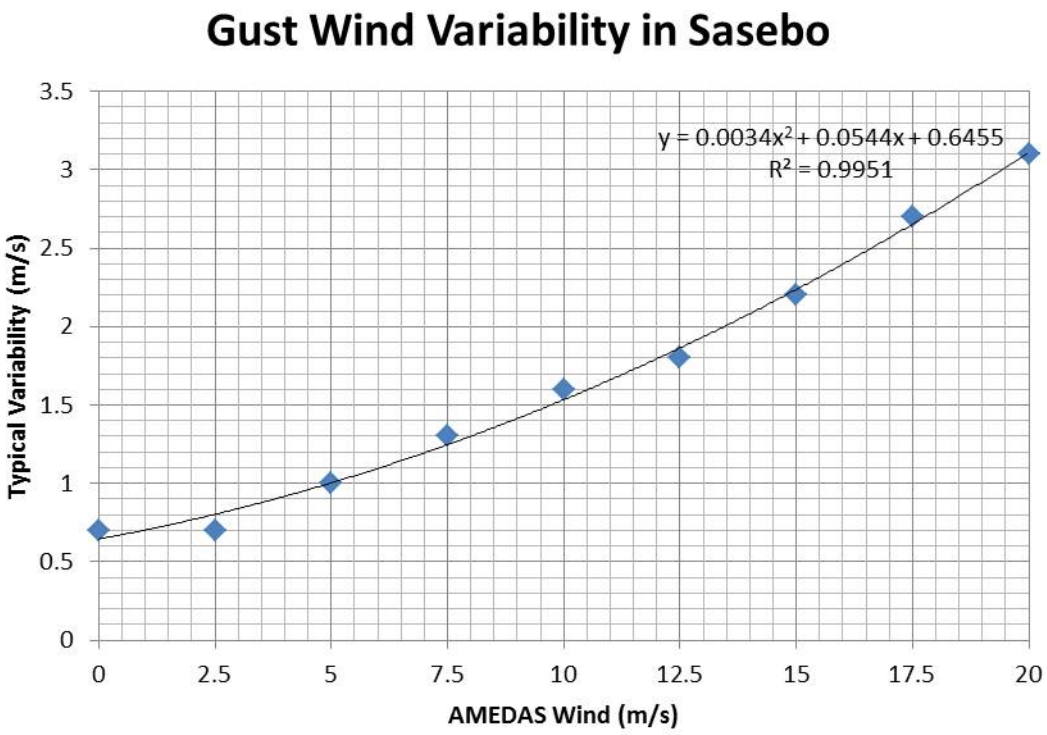

Figure 109. Expected variability of gust wind in Sasebo as derived from all (not just TC-related) every 10-minute AMEDAS gust wind observations during 2009–2012 compared to a smoothed gust wind time series.

Table 19. Expected variability of sustained and gust winds in Sasebo as calculated from the procedure for Figures 108 and 109 but extended to a large range of sustained winds and gust winds.

Sustained Wind (m/s)	Typical Variability (m/s)	Gust Wind (m/s)	Typical Variability (m/s)
0	0.5	10	1.6
2.5	0.6	12.5	1.8
5	0.8	15	2.2
7.5	1.0	17.5	2.7
10	1.3	20	3.1
12.5	1.7	22.5	3.6
15	2.1	25	4.1
17.5	2.6	27.5	4.7
20	3.2	30	5.3
20.5	3.3	32.5	6.0
21	3.5	35	6.7
21.5	3.6	37.5	7.5
22	3.7	40	8.3
22.5	3.8	42.5	9.1
25	4.6	45	10.0
27.5	5.3	47.5	10.9
30	6.2	50	11.9

2. TC Grouping

As part of the analysis of the various empirical techniques developed and tested in Chapter III, some common errors were detected for recognizable, recurring situations. For example, errors are expected due to asymmetries in wind structure as TCs under-go ET, or due to local terrain interactions with TCs at certain bearings relative to Sasebo. Thus, five track categories were created (Figure 110): (Track 1) TCs approaching Kyushu from the SW and making landfall along the W coast of Kyushu, which includes the direct hits on Sasebo; (Track 2) TCs passing roughly parallel to the W coast of Kyushu, but generally did not make landfall in Japan; (Track 3) TCs passing from SW to NE south of Kyushu, and thus often making landfall on Shikoku or Honshu (refer to Figure 1), but only rarely grazing the southern edge of Kyushu; (Track 4) TCs passing S of Kyushu while moving from SE to NW, with possible brief landfall on the SW coast of Kyushu;

(Track 5) TCs approaching from SE to NW, and either making landfall on the E coast of Kyushu or on Shikoku or Honshu.

While ideally the developmental and testing data sets in Chapter III would contain multiple examples of each track type, this was unfortunately not the case (Figure 111). For example, no Track 1 TCs were available in the 2002 and 2011–12 data, no Track 4 TCs were available in the 2003-2010 data, and no Track 5 cases were available for 1998–2000. This lack of comprehensive TC track data sets may be an additional source of errors in the nomogram development and especially the acceleration factor specifications for the Sasebo site.

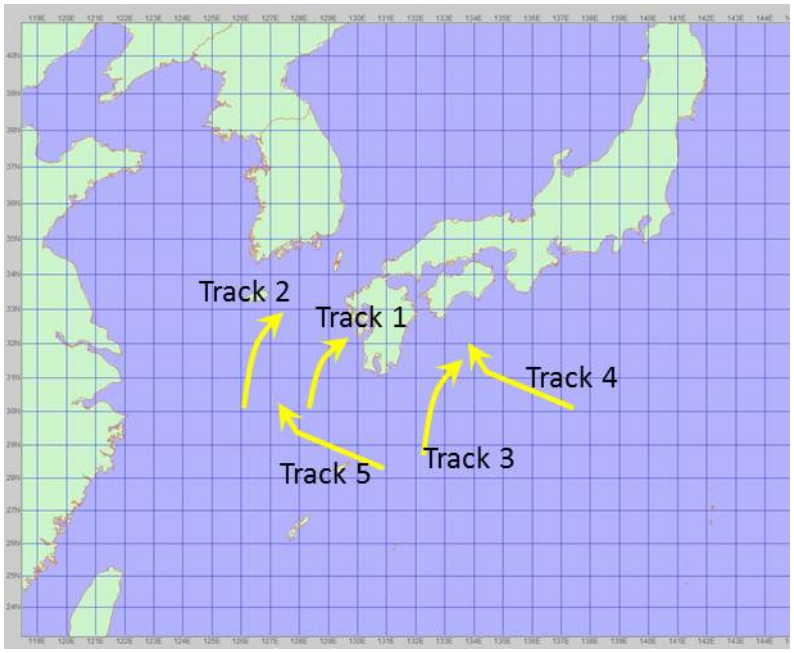

Figure 110. Schematic of the five track categories defined in this research.

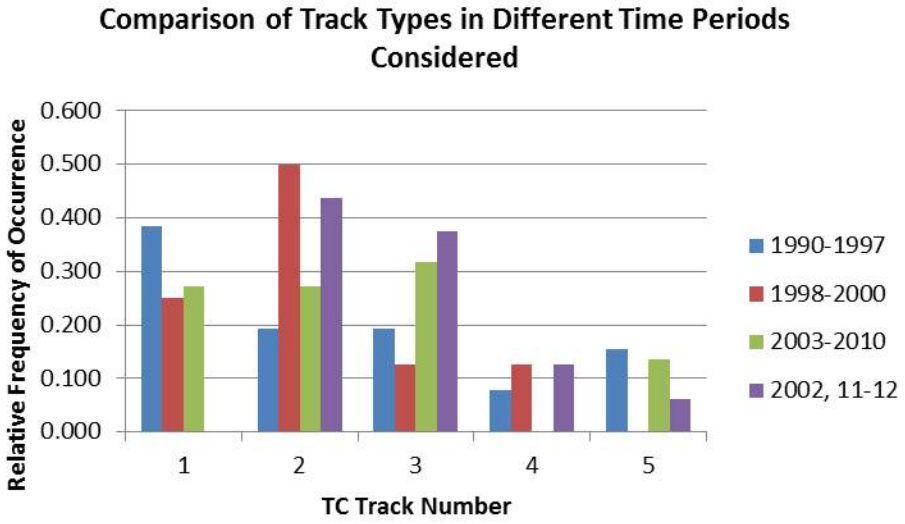

Figure 111. Availability of the five TC track categories in Figure 110 during the time periods of the developmental and testing data sets for the empirical techniques examined in Chapter III.

The Jarrell (1988) mean sustained wind nomogram predictions are taken to be the baseline for judging the improvement from the empirical techniques examined in Chapter III, with a focus on the TCs from 2002–2012 in comparison with the AMEDAS observations at the current site. The nomogram mean sustained wind hindcasts minus AMEDAS observations in relation to the TC center bearing from Sasebo is shown in Figure 112. For most bearing directions, the nomogram winds are under-forecasts. However, a particular tendency is for higher nomogram winds than observations (i.e., over-forecasts) when TCs are located SW (202.5 to 270 degrees True) of Sasebo. TCs in the Track 1, Track 2, and Track 5 categories would fall into this geographic area.

For times when the absolute difference between AMEDAS and nomogram mean sustained nomograms winds was > 2.5 m/s (Figure 113), a distinct tendency for over forecasts occurs when TCs are SW of Sasebo. At times when TCs were at approximately 180 to 292.5 degrees True from Sasebo (Figure 114), both under- and over-forecasts occurred, especially when the TCs were WSW to WNW (247.5 to 292.5 degrees True)

from Sasebo. Within the bearing 180–292.5 True, those TCs farther from Sasebo tended to be over-forecast, while those closer to Sasebo were over- and under-forecast (Figure 115).

It is interesting here to compare the applicable original nomograms (Figures 116–117) to the new nomogram shown in Chapter III (Figure 85). The relatively high percentage contours in the original nomograms to the west of Sasebo might be shifted eastward and possibly increased. For TCs passing Sasebo to the west, this would have the net effect of lowering predictions for TCs at greater ranges, while keeping the same or raising predictions for more closely passing TCs. These changes are somewhat reflected in Figure 85 since relatively high contours do exist to the west of Sasebo, but at relatively close RTRR values. Small RTRR values correspond to a TC passing close to Sasebo, or to Sasebo being well within the 34 kt wind radius of a medium to large TC.

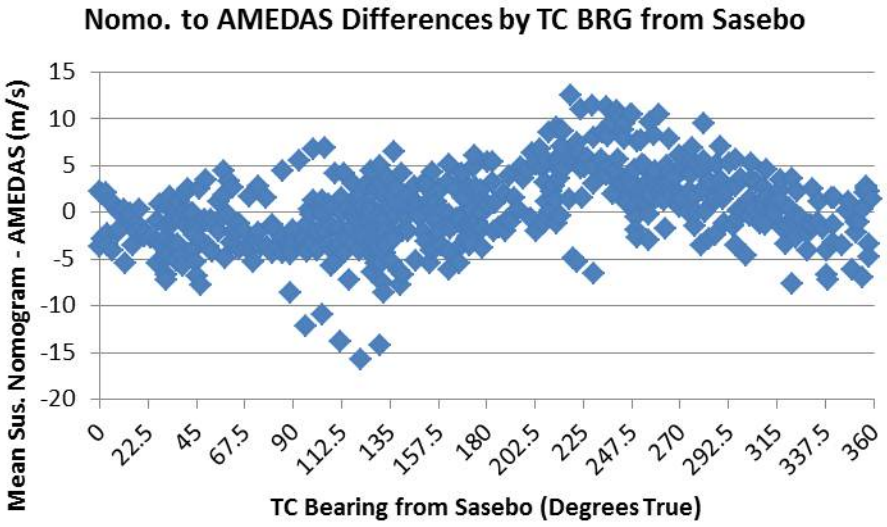

Figure 112. Jarrell (1988) nomogram mean sustained wind hindcasts minus AMEDAS sustained wind observations as a function of TC bearing angle for all TCs passing within 200 n mi of Sasebo during 2002–2012. TC positions and intensities from JTWC best-track files with hourly linear interpolation between 6-hourly reports.

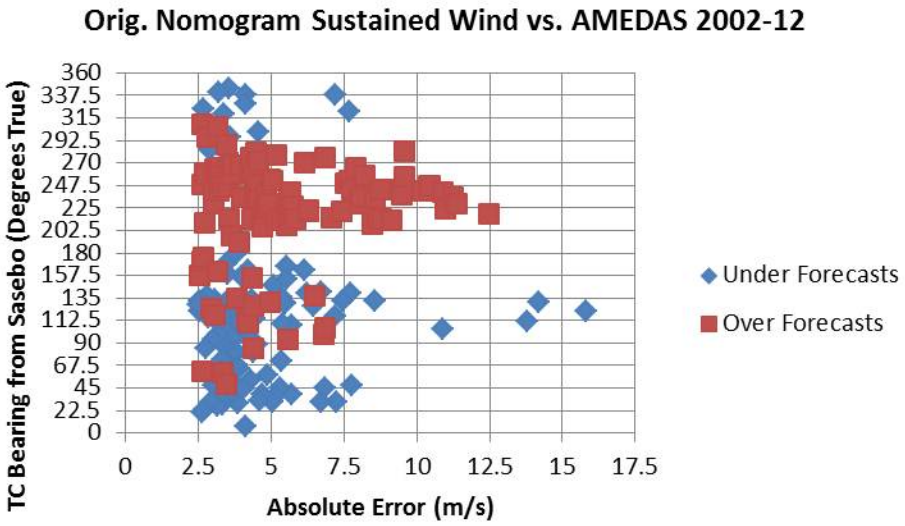

Figure 113. Absolute value of Jarrell (1988) nomogram minus AMEDAS wind speeds of at least 2.5 m/s for all TCs passing within 200 n mi of Sasebo during 2002–2012. Under-forecasts (over-forecasts) by the nomogram are indicated by blue (red) symbols.

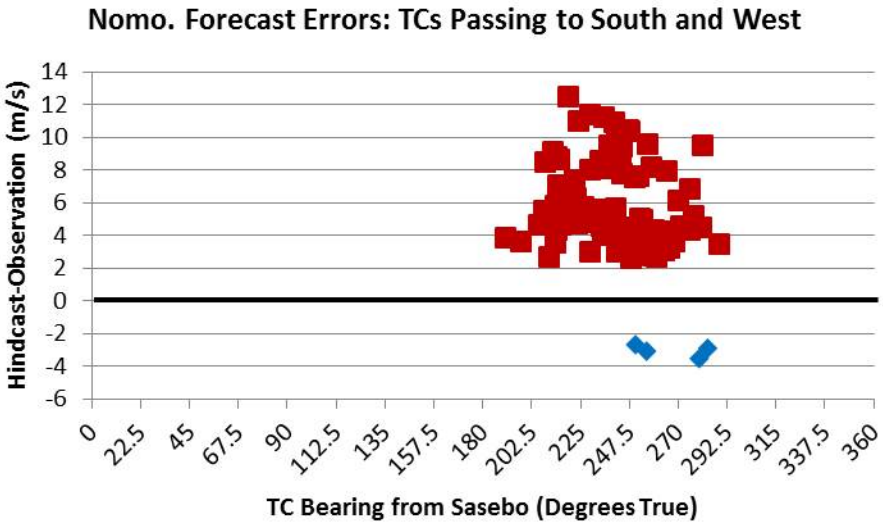

Figure 114. Distribution of over- and under-forecasts for TCs passing roughly 180 to 292.5 degrees True from Sasebo. These points are a subset of those shown in Figure 113. Note under-forecasts (below thick black line) more constrained to TCs bearing from WSW to WNW.

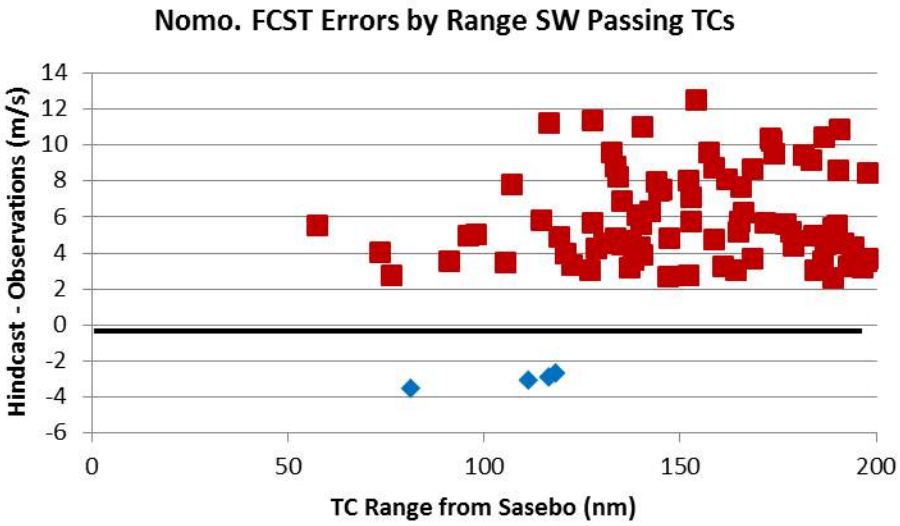

Figure 115. Forecast errors of Jarrell (1988) nomograms by range of TC to Sasebo for TCs passing roughly 180 to 292.5 degrees True. These points correspond to those in Figure 114.

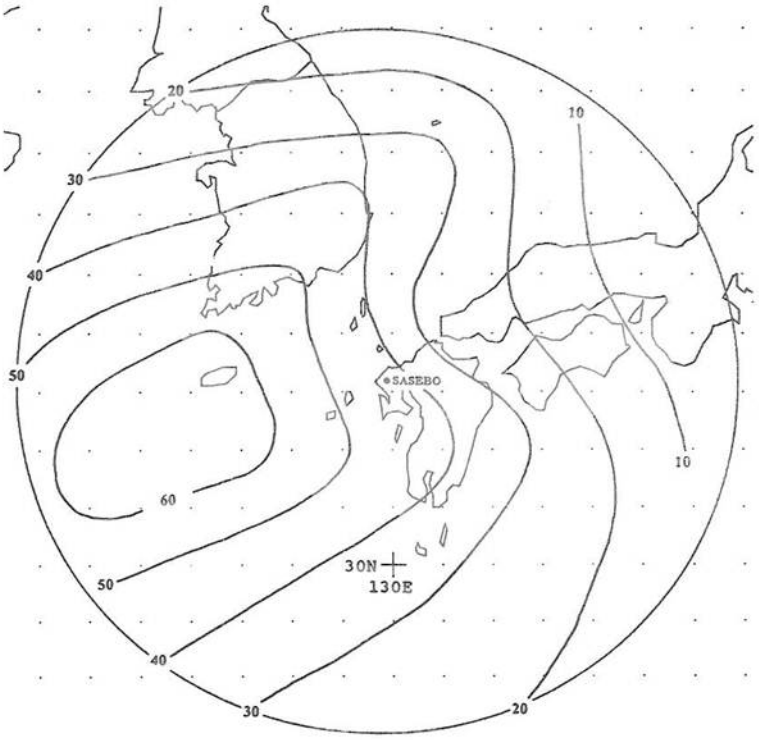

Figure 6. Mean Gust Ratios (labelled as percentage) for Sasebo when a tropical cyclone of less than typhoon strength (<64 kt) is centered within 360 nm of the station. Locate the tropical cyclone center by latitude and longitude and interpolate the ratio (percentage) value. Multiply the tropical cyclone center wind speed by this percentage to get the wind speed value of the maximum gust expected with the given center position and wind speed. Multiply the mean gust speed by 0.67 to find the mean one-minute average sustained wind speed.

Figure 116. Mean gust nomogram from Jarrell (1988, Figure 6) for Sasebo for less than typhoon strength (64 kt intensity) TCs. Mean sustained winds are taken to be 2/3 of the mean gusts corresponding to the TC position relative to Sasebo.

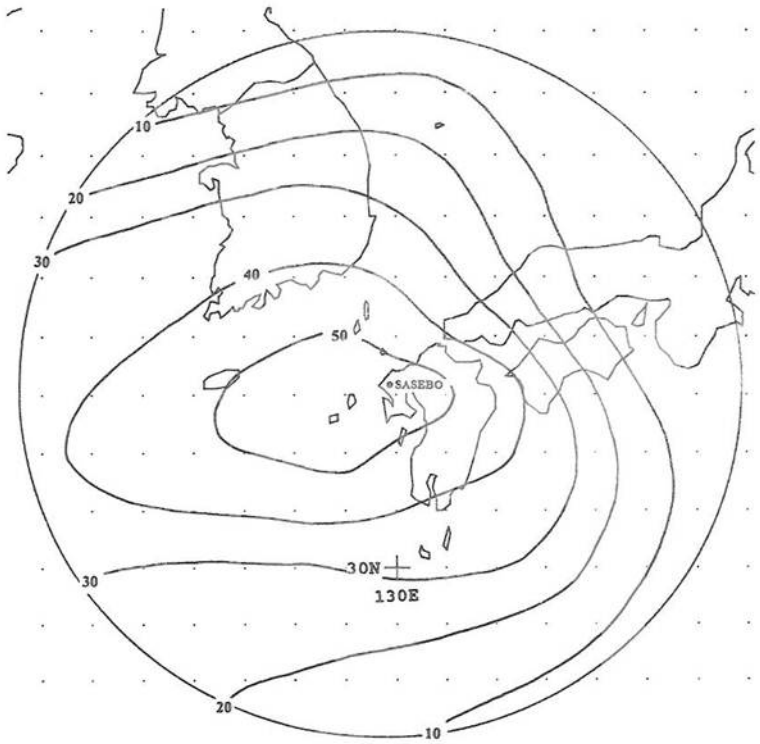

Figure 8. Mean Gust Radios (labelled as percentage) for Sasebo when a tropical cyclone of typhoon strength (≥ 64 kt) is centered within 360 nm of the station. Locate the typhoon center by latitude and longitude and interpolate the ratio (percentage) value. Multiply the typhoon center wind speed by this percentage to get the wind speed value of the mean gust expected with the given center position and wind speed. Multiply the mean gust speed by 0.67 to find the mean one-minute average sustained wind speed.

Figure 117. Mean gust nomogram from Jarrell (1988, Figure 8) for typhoon strength TCs. Mean sustained winds are taken as 2/3 of the mean gusts.

As discussed in Chapter I, TCCOR criteria may be met with gust winds as in Figure 116 and 117 or by multiplying these gust winds by 2/3 to obtain a sustained wind. Using the NeWMeK and Sasebo Fire Station data a reconstruction of AMEDAS gust winds can be calculated for dates prior to 2008. Specifically, NeWMeK observed gusts are reduced by 14% and the Fire Station gusts are used directly in accordance with the analysis in Chapter II. These reconstructed gust winds for multiple (but not all) TCs during 2003–2010 are shown in Figure 118. First, note the two cases of observed gust wind over 30 m/s (TCCOR criterion). Since the graph has only hourly gust winds, it is highly likely that additional sub-hourly variability also exists. Second, the corresponding

PAW speeds are generally similar to the observed gusts except for the under-forecasts for the TCs during 2004 (especially during Typhoon Tokage, which will be discussed later), and for three TCs with high gust winds. These TCs with high PAW speeds were Songda (2004), Nabi (2005), and Shanshan (2006), which were all Track 1 type TCs that had almost direct hits on Sasebo. As described in this section, TCs approaching Sasebo from the southwest tend to be associated with larger prediction errors. If the TC also is a near-direct hit, the eyewall interaction with the complex terrain around Sasebo undoubtedly led to a highly complicated gust wind field. With these notable exceptions, the PAW predictions may be a useful first-order gust forecast tool for Sasebo.

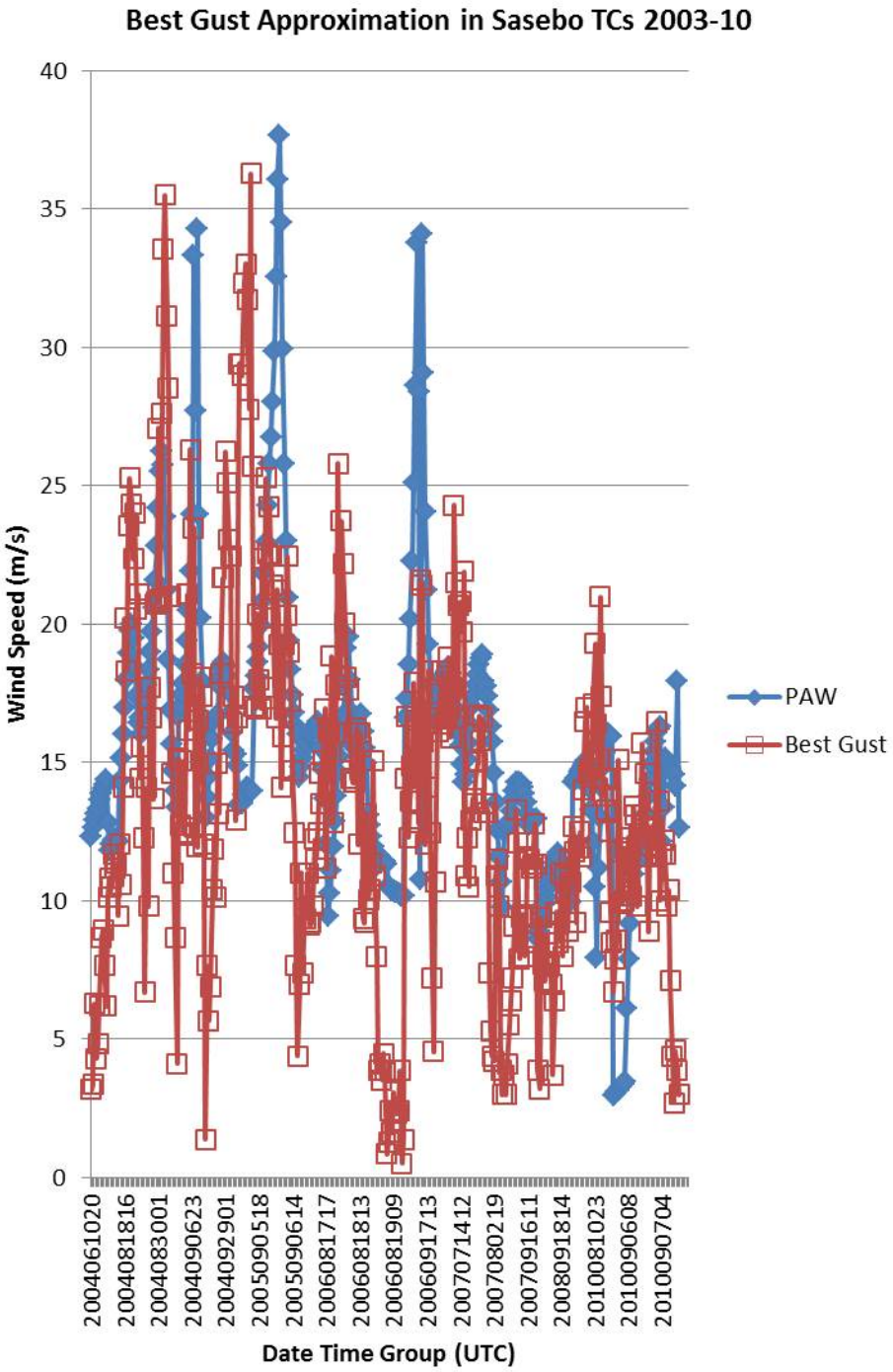

Figure 118. Hourly gust winds from the PAW approach (blue) and observations at Sasebo when selected TCs were within 200 n mi of Sasebo for times (YYYYMMDDHH) along abscissa. Note the "best gust" line (red) consists of AMEDAS observations after 2008, reduced NeWMeK observations when only those were available, and Fire Station observations when those were what were available.

Some of the Track 2 type TCs also had relatively large sustained and gust wind errors (for certain wind directions) among the multiple empirical techniques developed and tested in Chapter III (not shown). However, these errors were not consistently high or low among the various techniques. The recent Track 2 type Typhoon Sanba during 2012, which caused Sasebo to proceed completely through the TCCOR process, will be discussed in detail in the next subsection.

Track 3 TCs, which are recurving storms passing east of Kyushu, are of particular interest because after affecting Sasebo they often affect the U.S. base in Iwakuni (southwest Honshu) and multiple bases in the greater Tokyo area including Yokosuka. These TCs generally have SE to NE bearings from Sasebo during their passage, which may then have under-forecast errors (Figure 113). The Track 3 type Typhoon Tokage during 2004, which as mentioned in Chapter I caused remarkable and not well-forecast winds in Sasebo will be discussed in detail in Chapter IV.D.4.

3. Typhoon Sanba 2012

According to the JTWC best-track file, Typhoon Sanba had a CPA to Sasebo of approximately 88 n mi at a bearing of 274 degrees True on 2012091621 UTC (note YYYYMMDDHH). At that time, the intensity of Sanba was approximately 90 kt, and Sasebo was just beyond the range of the Sanba 50 kt wind radius, but well within the 34 kt wind radius (RTRR value of 0.48). Peak AMEDAS sustained winds were 18.3 m/s at 09162230 UTC (MMDDHHmm) with an hourly AMEDAS peak gust at the same time of 29.6 m/s. A satellite image of the TC in relation to Sasebo is shown in Figure 119. The Vaisala sensor at CFAS recorded similar peak values as at the AMEDAS site, while the Davis sensor at Building 98 (see Figure 11) recorded slightly higher values (Figure 120). Overall, the winds at CFAS were very similar to the AMEDAS winds (Figure 121), so the verification will be based on the AMEDAS winds.

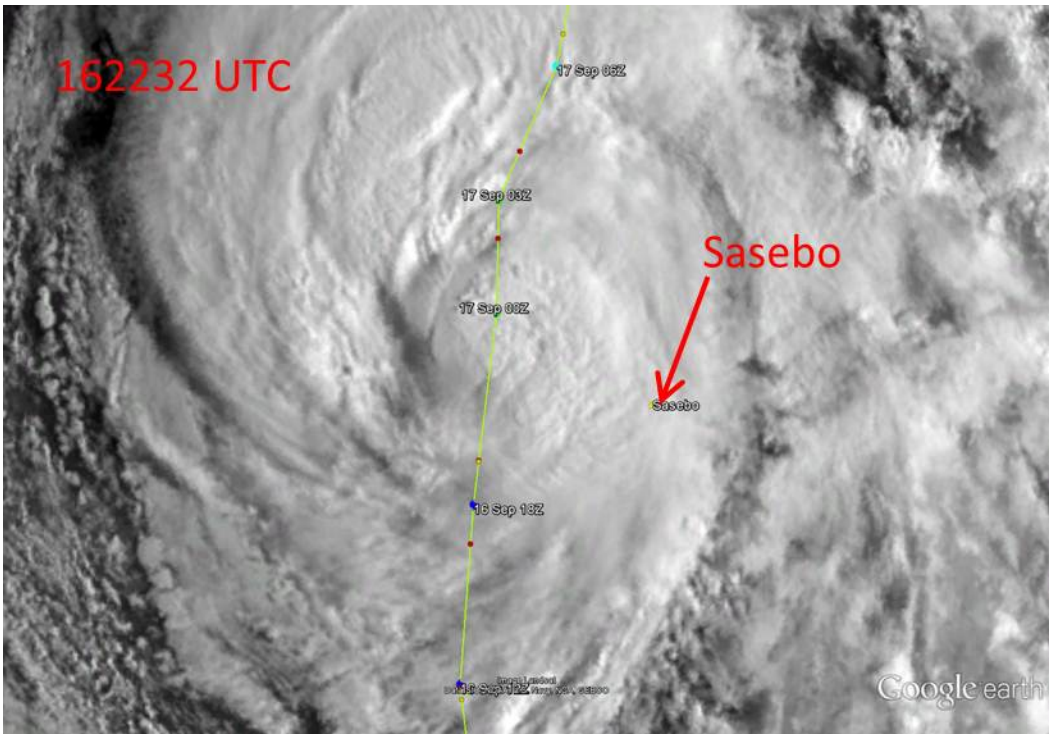

Figure 119. MTSAT visual image of Typhoon Sanba at 2232 UTC 16 September 2012 (0732 JST 17 September), which was about one and a half hours past CPA and at the approximate time of maximum winds recorded in Sasebo. The center of Sanba was approximately 90 n mi WNW of Sasebo, which is designated by the red arrow (after Naval Research Lab 2013; Google Inc. 2013).

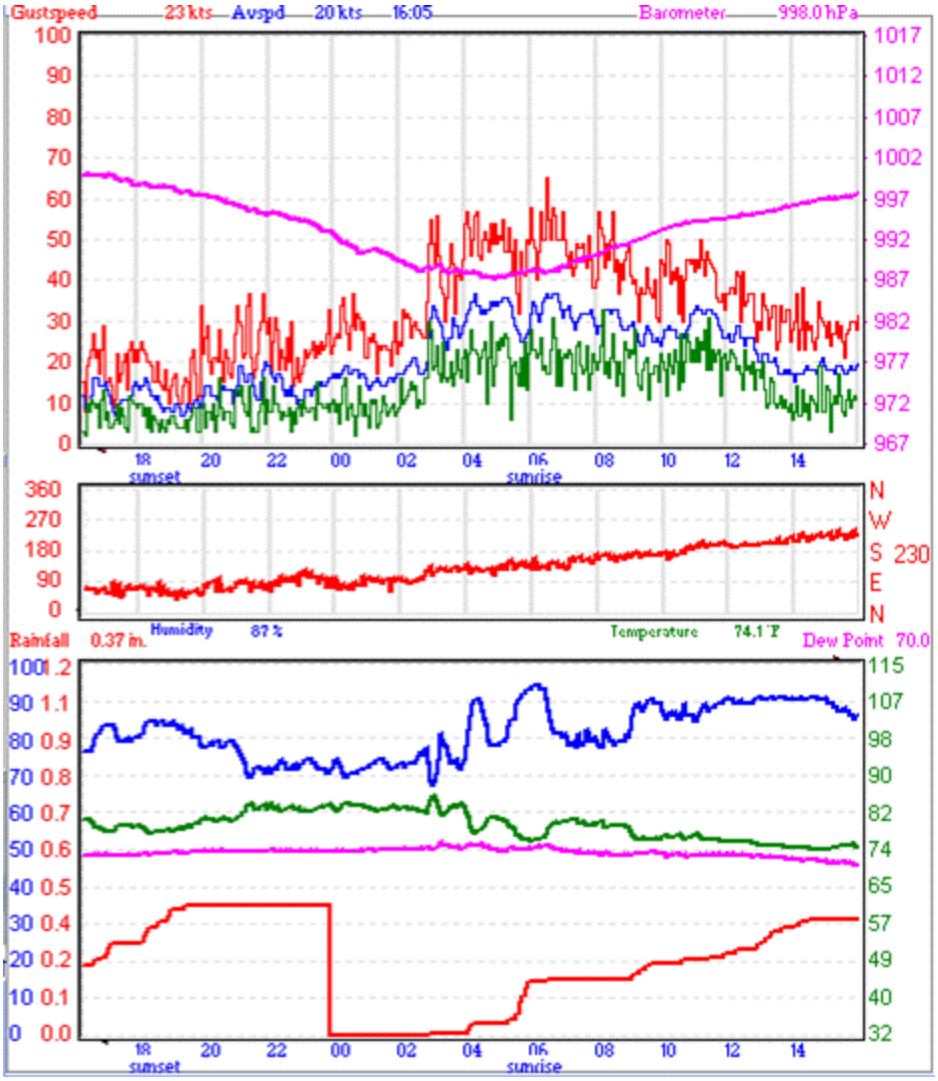

Figure 120. CFAS main base Davis sensor data during Typhoon Sanba 2012 with wind speed in kt and local time. Blue line in top panel is average wind speed, green line is instantaneous wind, and red line is wind gusts. Maximum gust reported at this site was 65.2 kt (~33.5 m/s) at approximately 0730. Note that this wind sensor is placed higher than the AMEDAS or Vaisala sensors) (from Naval Oceanography Antisubmarine Warfare Center Yokosuka 2012).

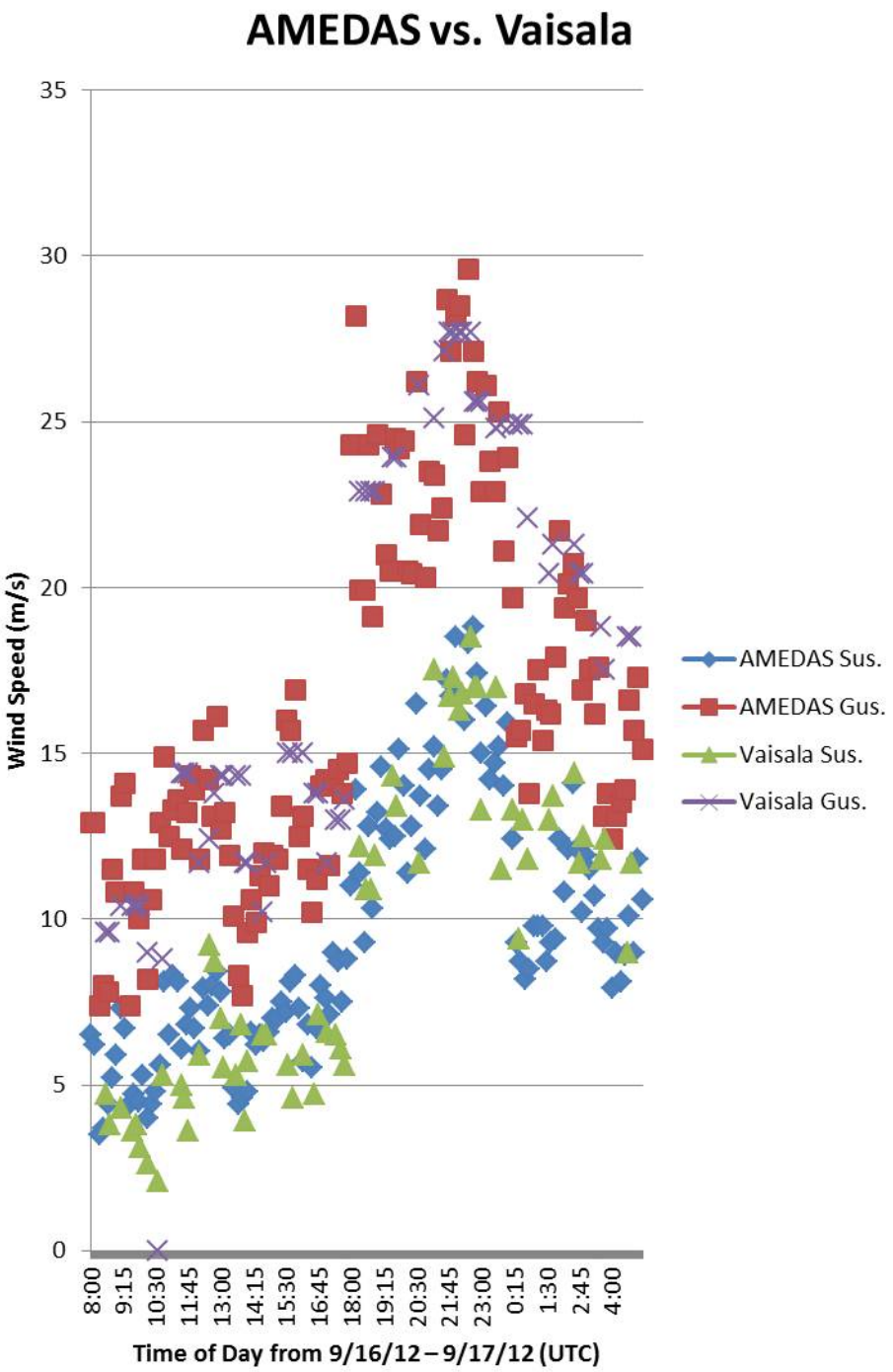

Figure 121. Comparison of CFAS Vaisala winds (green, 10-min mean for sustained; 1-min mean winds were very close but not shown) and gusts (purple) with Sasebo AMEDAS winds (blue) and gusts (red). Both data sets are within 2.5 m/s for the majority of times, except for a brief period between 0:15 and 1:30 UTC on 9/17 when the on-base winds were higher than AMEDAS. Wind direction was generally SSE at those times.

For Typhoon Sanba, both the maximum gust and maximum sustained wind nomogram (Jarrell 1988) predictions were 10s of meters per second higher than observations prior to CPA, and the predicted time of peak winds is approximately 2 hours early (Figure 122). The CPA and time of peak winds occurred when TC was W to WNW from Sasebo. While over-forecasts by the Jarrell (1988) nomogram was indicated for TCs located SW of Sasebo by the analysis in Chapter IV.D.2, the magnitude of the over-forecasts are noteworthy. The mean sustained and mean gust nomogram predictions perform somewhat better, although they too over-forecast on order of 5 m/s prior to the time of peak observed winds, and also predict the time of peak winds too early.

The new nomogram performs much better than the Jarrell (1988) nomograms prior to CPA, but predicts the time of peak winds several hours too late, and slightly over-predicts winds past the time of peak observed winds. Thus, the new nomogram is successful in using the RTRR as a proxy for storm structure for TCs SW of Sasebo. RTRR values here ranged from about 1.98 to 0.56 since the JTWC-analyzed 34 kt wind radii varied from ~175–197 n mi in the same quadrant as Sasebo. Since Knaff et al. (2007) used basin-specific statistically-determined structure parameters, PUW is a proxy for an average TC structure at a given latitude and intensity. The Sanba PUW estimate had < 34 kt winds at Sasebo for 2 hours after RTRR was already less than 1 (i.e., best track indicated Sasebo within the 34 kt wind radius), and had < 34 kt winds 2 hours earlier than when RTRR re-increased to over 1.0 (not shown). This comparison with PUW speeds suggests Sanba had a slightly larger wind field than an average Track 2 TC. While the track of an average sized Track 2 TC would have to be moved eastward from the best-track for a similar portion of the wind field to affect Sasebo, it is unlikely that would notably improve the forecast for the original nomogram.

At the time of peak winds at Sasebo, the observed gust factor was approximately 1.62 since peak observed gust of 29.6 m/s from the SSE is divided by peak sustained observed winds of 18.3 m/s from the SSE at same time. The approach with the new nomogram is to multiply its output by an appropriate gust factor for a gust hindcast. As previously discussed, the Jarrell (1988) nomograms assume an average gust factor of 1.5, which would yield a peak gust ~2 m/s too low. Assuming a SSE sustained wind with a

SSE gust response, the average September SSE gust factor from Table 6 is 1.7, which would yield a slightly too high gust hindcast. The overall average gust factor of 1.76 times the new nomogram output would also have yielded an over-predicted peak gust hindcast here.

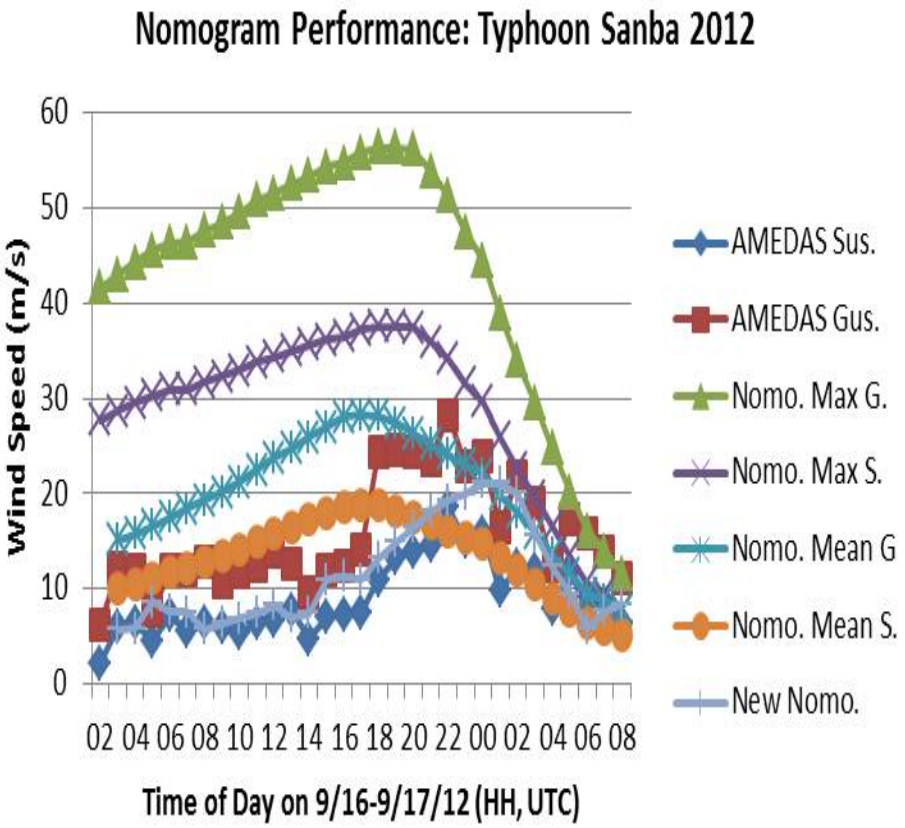

Figure 122. Hourly AMEDAS and nomogram-predicted winds and gusts (see index on right) values in Sasebo during the time period when Typhoon Sanba 2012 was within 2 RTRR of Sasebo. Note Figure 121 shows all available observations, including every 10 minutes and some every 5 minutes.

As a first evaluation of parametric technique performance, the mean parametric predictions without their associated confidence intervals are considered to be deterministic forecasts (Figure 123). The PAW speeds agree with the observed gusts to within a few m/s, although the peak gust is under-forecast by close to 5 m/s and the peak wind is predicted to occur earlier than observed. Multiplying the PAW speed by a

constant as a proxy for isotropic friction, the sustained winds tend to be over-forecast at early times and the maximum wind is predicted too early. Adjusting the PAW with directionally-dependent acceleration factors, over-forecasts continue to occur before the time of peak winds, but the timing and magnitude of peak winds are better predicted. This also holds for multiplying the adjusted PAW by the average overall Sasebo gust factor of 1.76 (see Chapter II) for comparison with the AMEDAS gusts.

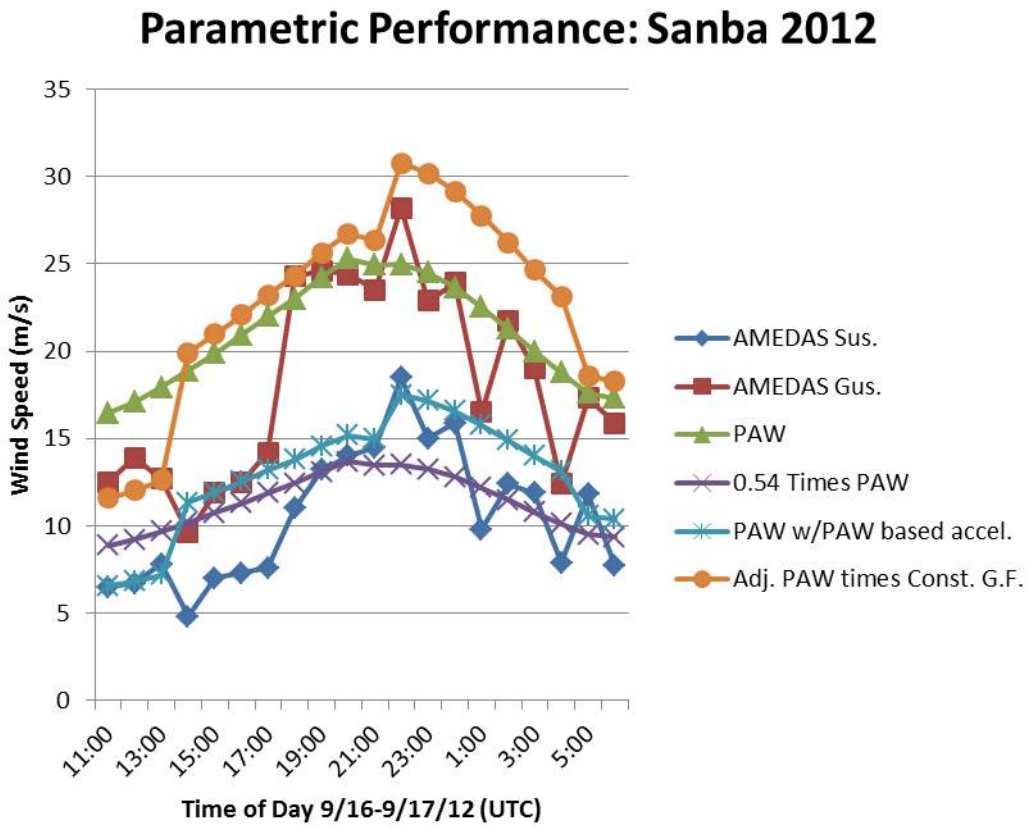

Figure 123. Performance relative to the AMEDAS sustained winds and gusts of the PAW technique as a deterministic forecast for the times when Sanba was within 200 n mi of Sasebo. The purple x's are a constant times PAW, which represent a simple frictional reduction to JTWC best-track wind structure utilized in the PAW. The light blue asterisks are PAW modified by the acceleration factors from Table 13. The orange circles are the light blue asterisks multiplied by the overall average gust factor (G.F.) of 1.76.

Confidence intervals added to the parametric wind predictions are also provided for PAW (Figure 124) and CFSR based acceleration factors (Figure 125). Note that the PAW adjusted by PAW-based acceleration factors outperforms PAW adjusted by CFSR-based acceleration factors, i.e., the purple line is closer to the dark blue line in Figure 124 than in Figure 125. A wide range between the high confidence and the low confidence interval are noted at some times. Because the wide range for PAW-based acceleration factors for certain wind directions may have little operational usefulness, use of Table 19 might be more beneficial here. By contrast, the CFSR-based acceleration factors perform reasonably well prior to and after time of peak winds. Around the time of peak winds, the wind directions were generally S or SSE. As discussed in Chapter III, taking maximum value in the empirical distributions versus the maximum likelihood value may have resulted in too low acceleration factors for these directions.

These “perfect-prog” hindcasts assume knowledge of the observed wind direction in selecting the acceleration factors for Sasebo. Thus the observed wind directions are compared with the parametric wind directions in Figure 126. Note the large width of PAW-based acceleration factor confidence intervals for ESE and SE winds (Table 13), and recall that the CFSR-based factors are most inaccurate for S and SSE winds. Prior to the time of peak winds, the AMEDAS wind direction is within 1-2 cardinal points of the parametric wind, but from 0000–0400 UTC on the 17th, the wind direction differences are as much as three cardinal points. This difference may be related to Sasebo terrain effects, or to the fact that after CPA to Sasebo TC Sanba rapidly decreased in intensity to 45 kt by 0600 UTC and then proceeded through ET.

Inverse bearing, which is defined as the bearing of Sasebo from the TC, is also shown in Figure 126. This inverse bearing is considered to be a proxy for an ageostrophic pressure gradient-induced wind from relatively high pressure in Sasebo toward the TC center, versus being in-line with the TC vortex rotation. For some TC passages of Sasebo this pressure gradient may be strong enough, and/or align with terrain gaps, to deflect the flow relative to the “direct” TC wind field. Thus, this ageostrophic component may be a source of error in the empirical methods that assume a symmetric wind field. In such a situation, the inverse bearing will be closer (in terms of the magnitude of cardinal point

difference) to AMEDAS observed winds than the parametric wind direction. For the independent sample of 2002 and 2011–12 TCs when the TC was within 200 n mi, 27 of 142 (~19%) hourly wind direction observations were within 1 cardinal point of inverse bearing. These cases occurred for all AMEDAS directions except WSW, W, WNW, and NW. Winds blowing from these directions toward a TC center would have to travel generally across more land than winds from other directions, which may play a factor here.

In this TC Sanba case, PAW multiplied by directionally-dependent acceleration factors, and using a very basic gust prediction methodology, reasonably hindcast the time and magnitude of peak winds in Sasebo. Thus, accounting for the directionally-dependent acceleration factors at a single station can explain local wind variability not related to just the TC intensity or separation distance.

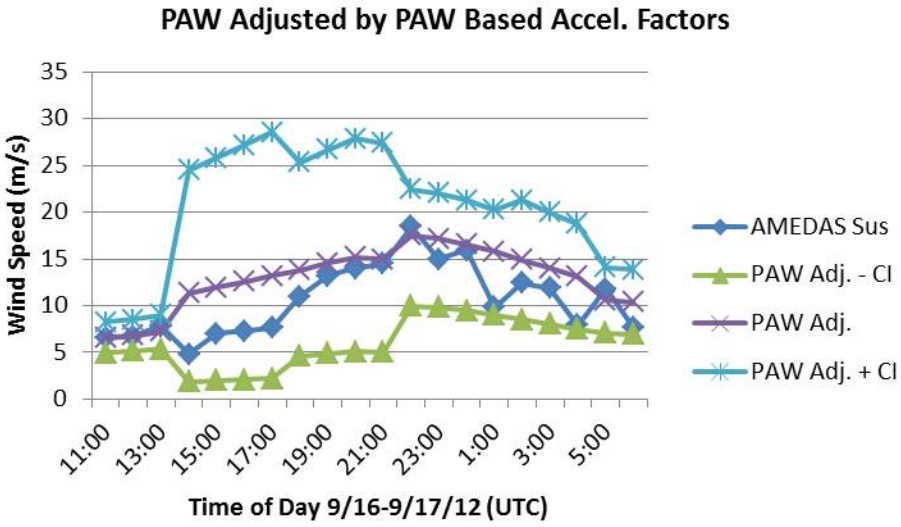

Figure 124. PAW speeds multiplied by PAW-derived directionally-dependent acceleration factors, and with the confidence intervals based on Table 13 during Typhoon Sanba.

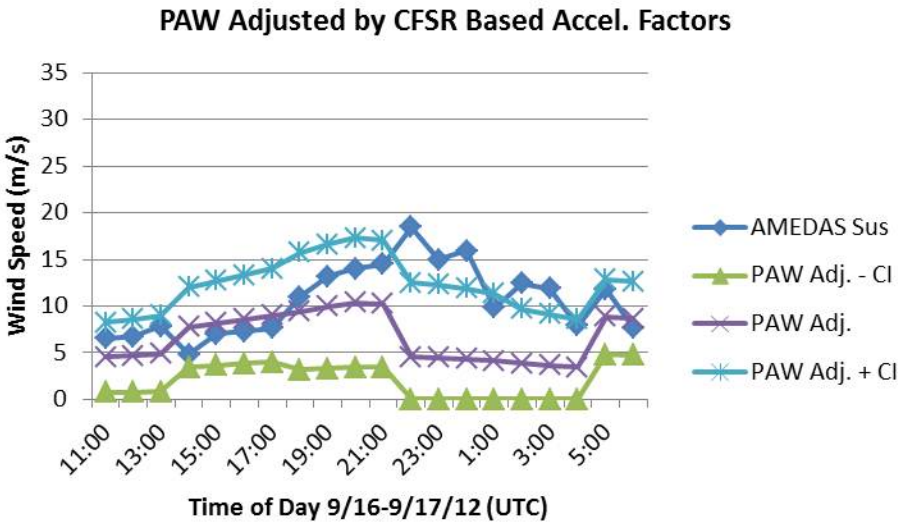

Figure 125. PAW speeds multiplied by CFSR-based directionally-dependent acceleration factors, and with 66% confidence intervals based on Table 10 during Typhoon Sanba.

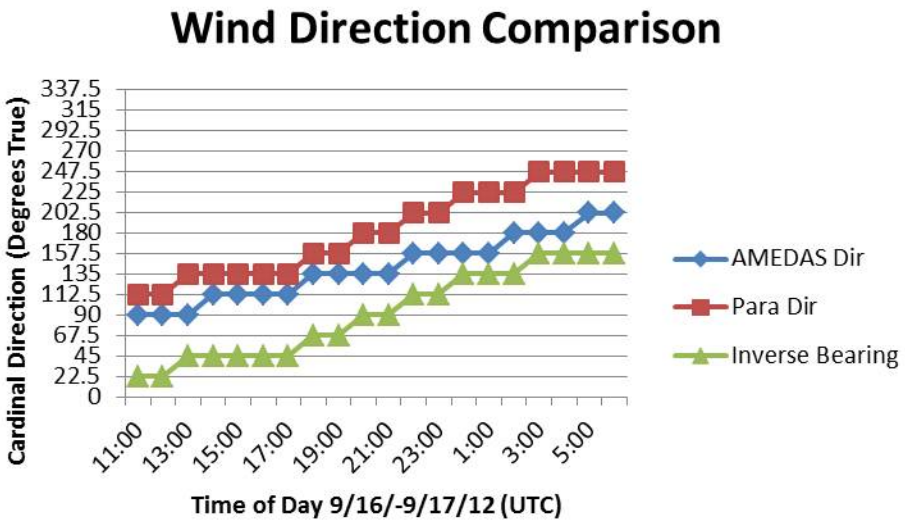

Figure 126. Observed wind direction in Sasebo (blue line), with parametric wind direction (red line), and the inverse bearing, or the bearing of Sasebo from the TC (green line). Inverse bearing is a proxy for an ageostrophic wind along the pressure gradient from Sasebo to the TC.

4. TC Tokage 2004

Based on the JTWC best-track data, TC Tokage had a CPA to Sasebo of approximately 159 n mi at a bearing of 121 degrees True at 0200 UTC 20 October 2004 (Figure 127). At that time TC intensity was approximately 62 kt after having been at typhoon strength (64 kt) just two hours earlier. The 34 kt wind radius in the quadrant in which Sasebo lay was approximately 90 n mi, and Sasebo was at greater than 1.5 RTRR from Tokage at all times in this case study. While the daily maximum AMEDAS sustained winds were 22.8 m/s, and the daily maximum AMEDAS gust was 49.3 m/s, the times of these events are not available. Hourly AMEDAS sustained winds peaked at the time of CPA. U.S. Navy observations recorded a peak wind of 57 kts (~29 m/s) at 0239 UTC 20 October. Both the AMEDAS and the NeWMeK observations are shown in Figure 128.

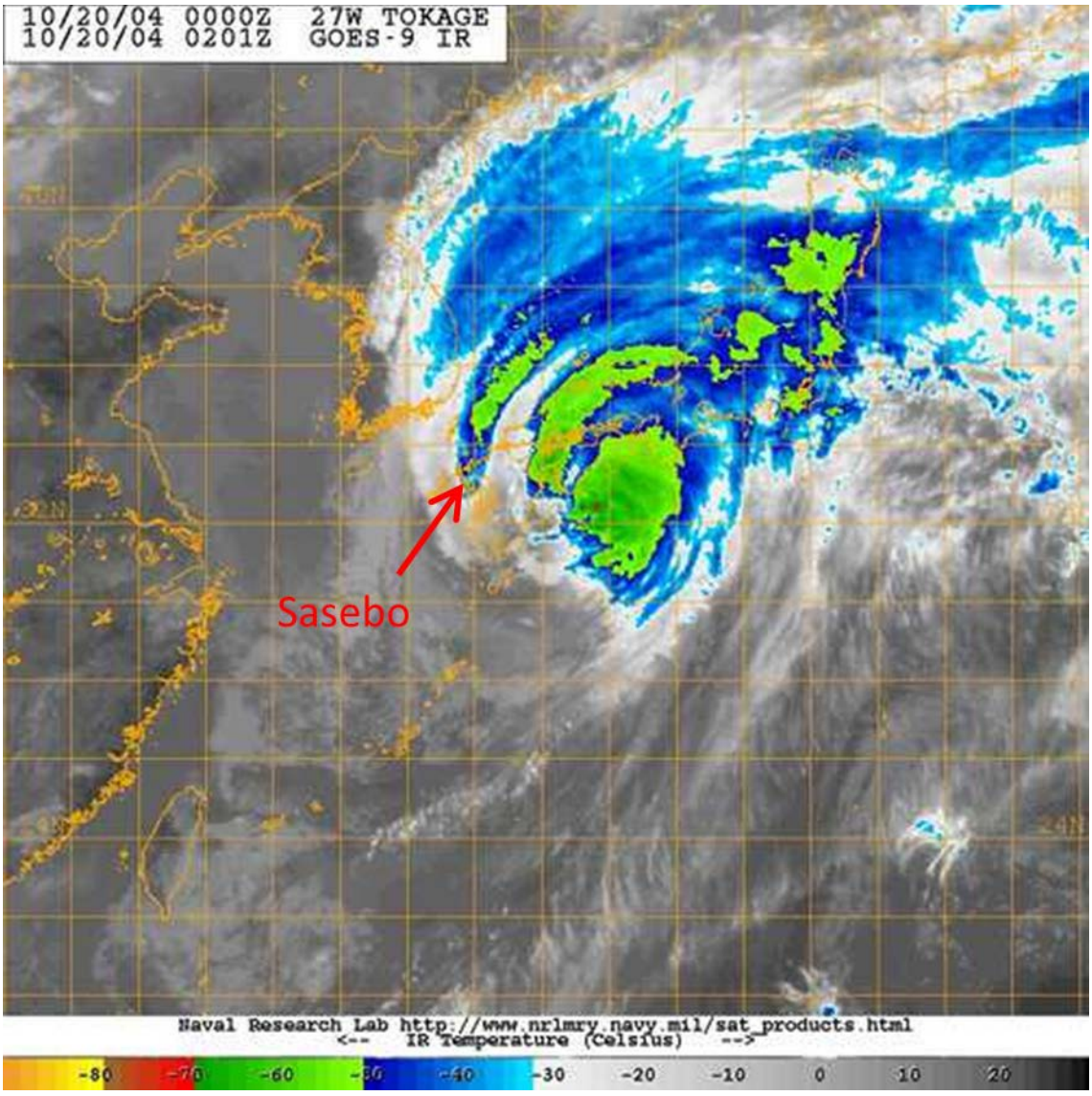

Figure 127. Satellite enhanced infrared image of TC Tokage (2004) in relation to Sasebo (red arrow) at the approximate time of CPA to Sasebo. Note the band of low infrared temperatures (green and blue) extending NE from Sasebo, which implies a rainband had recently passed over Sasebo as Tokage had moved generally SW to NE (after Naval Research Lab 2013).

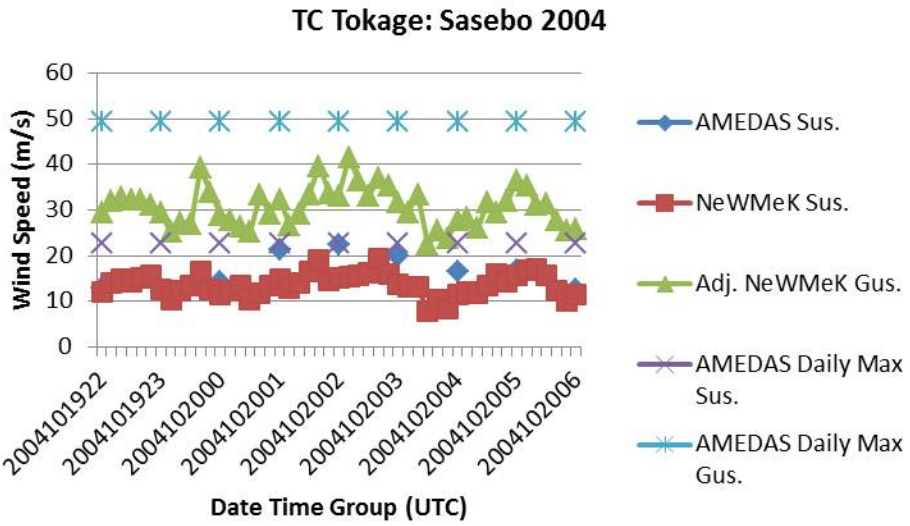

Figure 128. Observations from Sasebo during the passage of TC Tokage: dark blue diamonds are AMEDAS hourly observations, red squares are NeWMeK sustained wind observations every 10 minutes, and green triangles are NeWMeK gusts every 10 minutes. Also plotted is the AMEDAS daily maximum gust and sustained winds, for which no time was available.

As TC Tokage occurred during the development sample period (2003–2010) from which PAW- and CFSR-based acceleration factors were derived, using those adjustments here is problematic. The Jarrell (1988) nomogram predictions (Figure 129) for the magnitude of winds and the timing of maximum winds were not useful. Surprisingly, the PAW and PUW speeds without any adjustment (i.e., not even a reduction for friction) were both good approximations for observed sustained winds for some periods (Figure 130). The exceptions were for the hours immediately preceding, during, and after the peak winds. This agreement is unusual as experience with other TCs has shown that PAW and PUW speeds must be multiplied by a constant reduction factor to have values comparable to observed sustained winds.

Several not necessarily conflicting factors may be contributing in the Tokage case. While the JTWC best-tracks are a valuable resource, they are not necessarily perfect. Decisions made in real-time may have influenced the post-storm analysis and lead to too low TC intensity and too small wind radii, which might be inferred from the satellite scatterometry winds compared to best-track wind radii (Figure 131). At least at

2100 19 October, greater than 50 kt winds appear to be present well outside the JTWC 34 kt wind radius. While such winds may be erroneous, these winds may have been caused by an interaction with an adjacent synoptic feature. For example, Kitabatake (2008) suggests Tokage interacted with a pre-existing surface frontal zone extending SW to NE through the middle of Kyushu. Additionally, Tokage may have become more asymmetric with associated wind field distortions. However, it was also noted that observed winds were within 2 cardinal points of the parametric wind direction during this time period. Note that observed winds at the times shown were all either NNE or N. Whereas the JTWC best-track file indicates Tokage as completed ET 16 hours after CPA, other sources such as Kitabatake (2008) indicate Tokage had completed ET much sooner (but still after CPA to Sasebo). Thus it is likely the wind asymmetries associated with the ET process were beginning or well under way during the time of interaction with Sasebo.

The enhanced infrared image in Figure 127 appears to indicate that a TC rainband had passed over Sasebo in the hours immediately prior and following CPA. As in Hurricane Irene (Chapter IV.A) this rainband may have caused localized accelerations although no obvious wind direction shifts in the AMEDAS observations would support that supposition. Some U.S. Navy observations indicate showers, occasionally heavy, during the time of interest, but detailed radar imagery is not readily available. The most likely scenario is that best-track intensities for Tokage are too low, as evidenced by un-adjusted PAW and PUW matching sustained observations prior to and after the period of peak winds. In addition, localized convection from the rainband passage possibly in combination with wind field changes associated with ET likely caused a peak in winds from approximately one hour before CPA to one hour after CPA. This peak does not seem present in NeWMeK sustained wind observations in Figure 128, but that may be due to a blocking effect from Mt. Eboshi (sensor is on SW slope and AMEDAS winds were generally northerly).

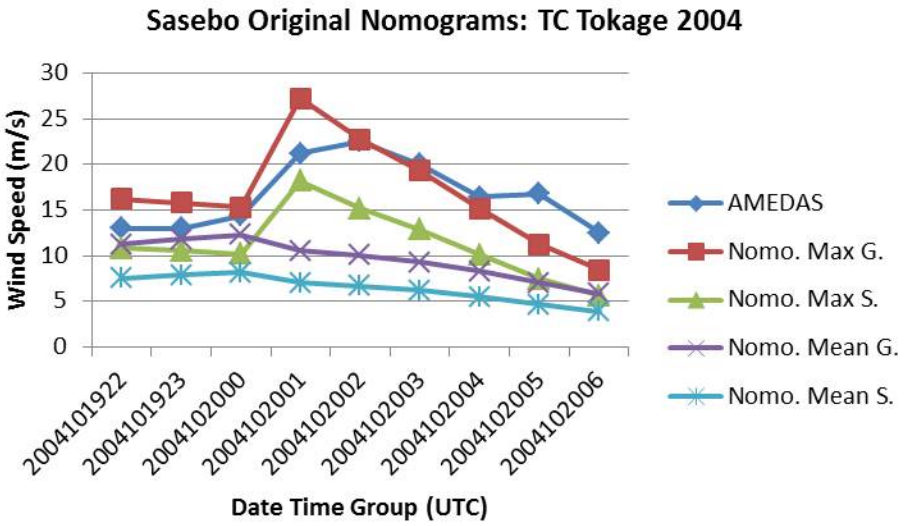

Figure 129. Jarrell (1988) nomogram performance in Sasebo during passage of TC Tokage 2004 calculated from JTWC best track data. Note that hourly AMEDAS sustained wind observations exceeded all of the nomogram wind speeds at all times, except the maximum gust prediction. Maximum observed gust on this day was 49.3 m/s.

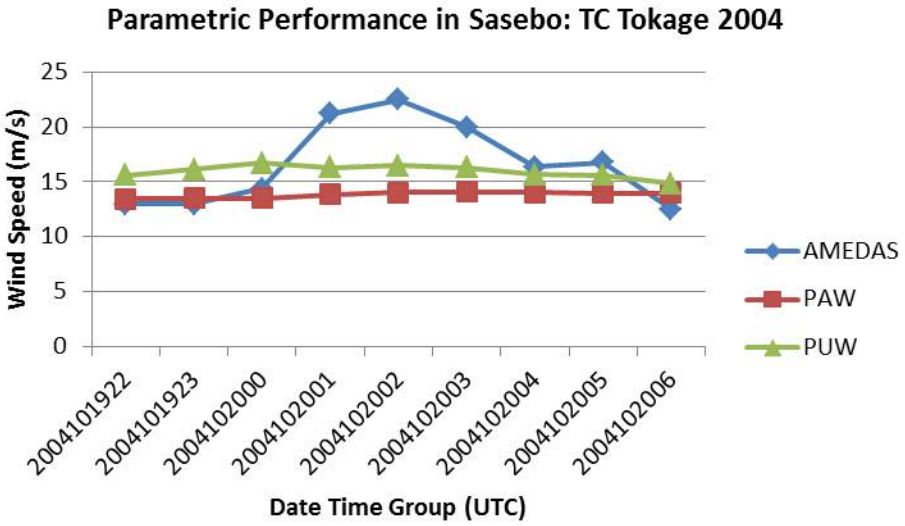

Figure 130. Performance of the raw PAW (red) and PUW (green) parametric models with no directional or isotropic frictional adjustments relative to the AMEDAS wind speeds (blue) during TC Tokage 2004.

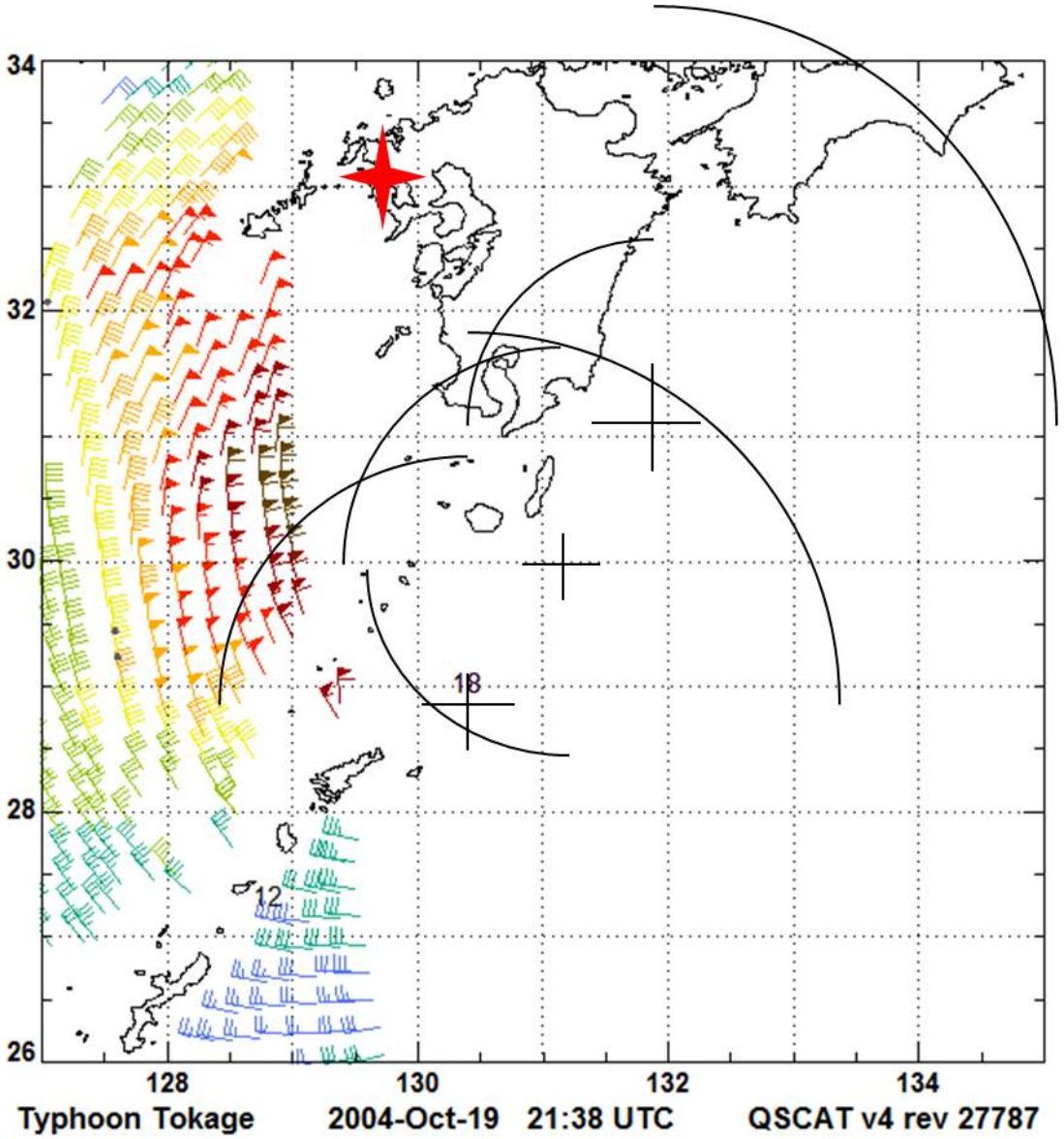

Figure 131. Scatterometry-based winds (colored wind barbs) during Typhoon Tokage, overlaid with JTWC best-track 34 kt wind radii (arcs) at 1800 UTC 19 October and 0000 UTC 20 October, relative to the TC centers (upper and lower + symbols). Interpolated wind radii at 2100 UTC 21 October are centered on the middle + symbol. Sasebo is located at red star. Note that 50 kt (barbs with full flags) or greater winds lie outside the 34 kt wind radii (after Remote Sensing Systems 2013).

Another procedure is available to calculate the wind variability during Tokage, and thus supplement an existing probabilistic TC wind product produced by Naval Research Lab-Monterey. Recall from Chapter I.A.1 that for selected storms, 1000

member ensembles of TC tracks and intensities are created that essentially create a PUW wind field at forecast time steps for each member. Occurrences of winds reaching a certain threshold at a given point are counted and divided by the size of the ensemble to give the probability of winds exceeding that threshold. By design, such ensembles attempt to capture the range of natural variability in the atmosphere. C.R. Sampson of NRL-Monterey provided such an ensemble run valid at 0000 UTC 19 October (not best track), or approximately 24 hours before Tokage CPA to Sasebo. Each ensemble member has positions and intensities that can be used to calculate range and bearing to Sasebo at forecast times, which may then be interpolated to hourly values. Thus the PAW and PUW speeds as well as the Jarrell (1988) nomogram winds may be calculated for each ensemble member. The ensemble average nomogram output is shown in Figure 132. Note that speeds in Figure 132 are in kt as probability of 34 and 50 kt wind is regular wind probability product output. Ensemble average parametric winds are virtually identical to Figure 130 and thus are not shown. Because not all ensemble tracks passed through the area covered by nomograms, less than 1000 realizations may have been available at any given time step in Figure 132.

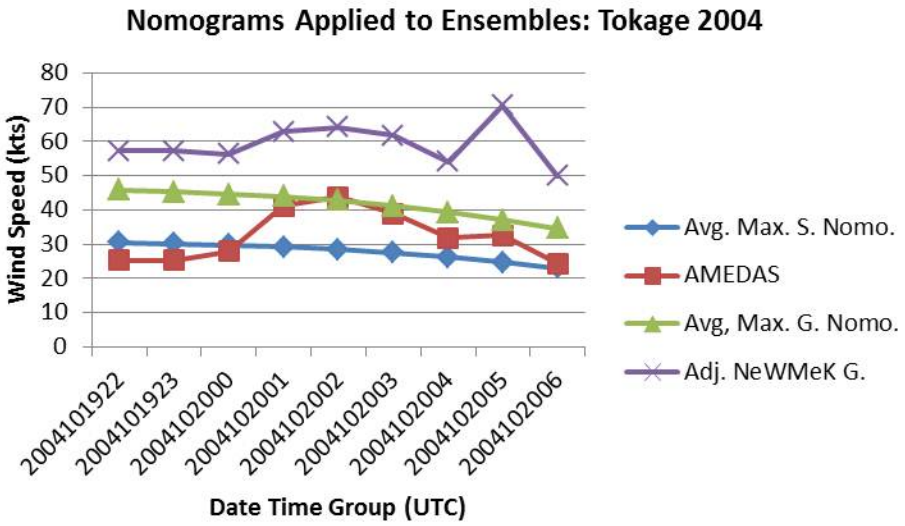

Figure 132. Average of the Jarrell (1988) nomogram maximum gust (green triangles) and sustained wind (blue diamonds) nomograms applied to all 0000 UTC 19 October ensemble members versus the AMEDAS sustained wind observations (red squares) from Sasebo, and NeWMeK gust observations (purple x's; reduced to be a best guess for AMEDAS gust values, procedure as previously explained).

It is important to note that maximum wind nomogram output is provided in Figure 132 rather than the earlier mean wind nomograms. It is interesting that this ensemble average nomogram maximum gust output does agree with observed sustained winds for a period of time. As nomograms are based on TC center intensity, if the ensemble average TC center intensity was increased, both the ensemble average maximum sustained nomogram and maximum gust nomogram output would also increase. Thus it is likely that the intensity of Tokage is systematically under-forecast in the ensemble, with the same result as the proposed under-analysis of the intensity in the JTWC best-track. As previously considered, the Tokage wind field may also be distorted and not easily representable in the PAW and PUW calculations due to the constraints of the ensemble members.

Presenting parametric-based ensemble probabilistic outputs is somewhat challenging in this instance. The PAW and PUW ensemble outputs (with individual members unadjusted in any way) indicate positive probabilities for > 34 kt, > 40 kt, > 50 kt, and > 60 kt winds. However if these PAW and PUW ensemble outputs are adjusted at

least for an assumed isotropic friction, those probabilities at each time step are then reduced to virtually zero. Similarly, nomograms for the mean (maximum) winds applied to the ensemble have zero (4% and smaller) probability for observed conditions to occur. While TC Tokage may have been an outlier, additional factors that could not be handled by parametric or nomogram techniques may also have contributed. As indicated previously such factors as rainband passage over Sasebo, Tokage beginning ET, and interaction with a pre-existing surface front are possible contributors.

E. REAL-TIME FORECAST APPLICATIONS

The biggest difference between the parametric technique "perfect-prog" hindcasts and real-time forecasting is that the AMEDAS wind direction is not known ahead of time. This is critical as selections of the directional-dependent acceleration factors have assumed knowledge of actual wind direction in Sasebo. Several ways to deal with this uncertainty in the wind direction are possible. For each parametric wind direction (i.e., TC bearing from Sasebo minus 90 degrees), or each CFSR direction, histograms of observed wind "response" occurrence were prepared and then combinations of parametric wind directions and observed directions at Sasebo are calculated. For example, an N parametric wind might be associated with a NNW observed wind 20% of the time (values illustrative only). In addition to the most likely direction combination, several of the most likely combinations, or some weighted average of combinations can be extracted from the histograms. Because the majority of observed wind directions were 1 or 2 cardinal points less (i.e., backed) from the parametric wind, it was decided to test acceleration factors determined by simply subtracting 1 cardinal point from the parametric wind direction.

TC Danas was a Track 2 TC with a CPA to Sasebo on 8 October 2013 that triggered the TCCOR warning procedures. The 1200 UTC 6 October 2013 ensemble used for the current wind probability product was kindly provided by C.R. Sampson. This is a particularly interesting case study as a near direct hit on Sasebo had been predicted, but the actual track was shifted rather west. As noted in Chapter I, useful decisions as to ship sortie or TCCOR have to be made well in advance, despite the limitations of our

forecasts. If the observed winds at the required forecast intervals for these sorties or warnings fall within the confidence intervals specified by the empirical forecast techniques, or by Sasebo-specific ensemble outputs, greater confidence in that approach is justified.

Both deterministic and probabilistic forecasts will be presented. Nomogram predictions (based on the 1200 UTC 6 October 2013 warning) are shown in Figure 133. Note that the Jarrell (1988) mean sustained and mean gust nomograms reach maximum values too early, but accurately predict the observed peak wind speeds that occurred around 1100 UTC 8 October. However, the Jarrell (1988) nomograms for the maximum winds are far too high. While the new nomogram predicts a peak after the observed time, the overall trend is a closer match to the observations than the Jarrell (1988) nomogram mean sustained wind predictions.

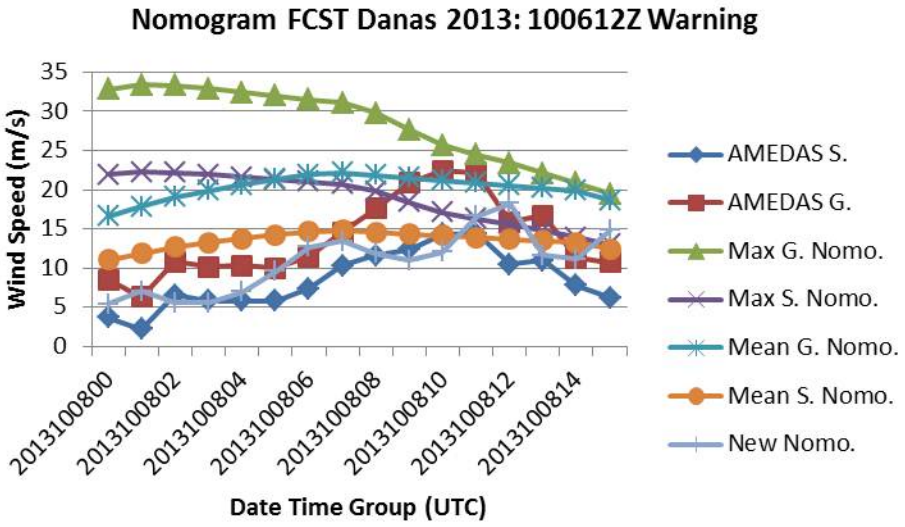

Figure 133. Nomogram derived maximum and mean sustained winds and gusts and with the new nomogram (see index on right side) based on the 1200 UTC 6 October 2013 forecast compared with observations in Sasebo on 8 October.

Only the adjustments to PAW predictions with directional-dependent acceleration factors based on the 2003–2010 PAW-to-AMEDAS comparisons will be presented (Figure 134). Note that the PAW prediction of the mean sustained wind is generally 5 m/s

higher than what was observed, and the maximum value was predicted several hours later than what occurred. At several forecast intervals, the lower limit of the PAW confidence interval did come close to the observed wind. It is emphasized that these wind forecasts are based on a forecast TC track and intensity initiated approximately 48 hours before the peak winds, and that the actual track was shifted to the west of Sasebo. Thus, the differences between the parametric (and nomogram) wind predictions and the observations are in part due to the track forecast error.

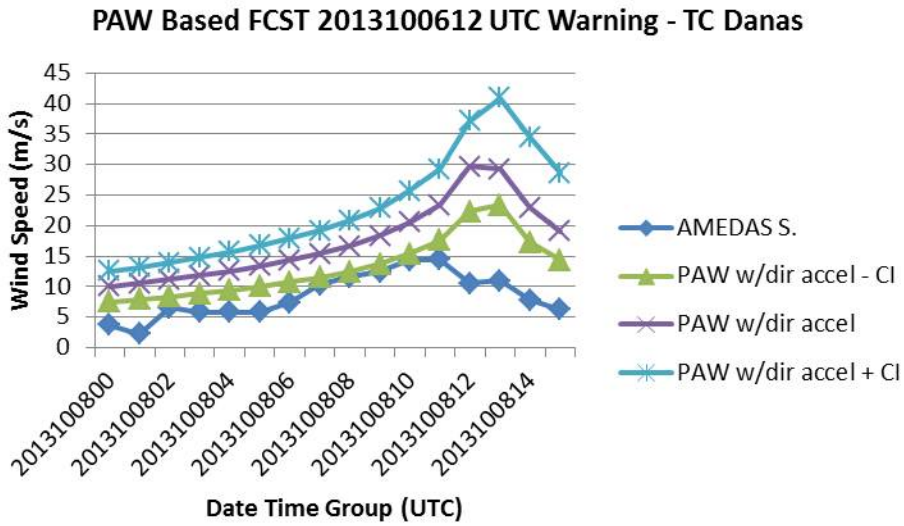

Figure 134. PAW forecast for Sasebo based on the 1200 UTC 6 October 2013 JTWC warning and using the directional-dependent acceleration factors determined from 2003–2010 PAW to AMEDAS comparisons. The forecast wind directions were taken as parametric wind direction minus one cardinal point. Note AMEDAS sustained wind observations are dark blue diamonds, the PAW deterministic prediction is the purple x's, and the low and high confidence intervals (see Ch. III) are plotted as green triangles and light blue x's.

The nomograms and parametric technique are also applied to the 1200 UTC 6 October 2013 wind probability ensemble. First, the chance of winds meeting TCCOR criteria (probability of 34 kt or 54 kt winds is most often depicted) would be one useful product. Here, a calculation of TCCOR level gusts ($\geq$ 60 kt) occurring is calculated with the nomogram for each member of ensemble. At each hour, the number of occurrences meeting the criteria is counted (Figure 135). As in Figure 132, not necessarily all 1000

members of the ensemble passed through the area of the nomogram. While none of the hourly observed gusts exceeded 30 m/s or approximately 60 kt, only the Jarrell (1988) nomogram maximum gust derived from the ensemble indicates a relatively high chance for TCCOR level gusts occurring, with the highest probability values several hours before actual peak observations. Additionally, TCCOR level sustained winds, ~> 25 m/s, were not seen in hourly observations. However, it is interesting that the probability of TCCOR level winds from the new nomogram peaks near the time observations peaked. That is, the probability values for the new nomogram (Figure 136, green line) reach their maximum between 0800–1400 UTC on 08 October, which is the period of maximum AMEDAS sustained wind and gust observations (Figure 133, dark blue and red lines).

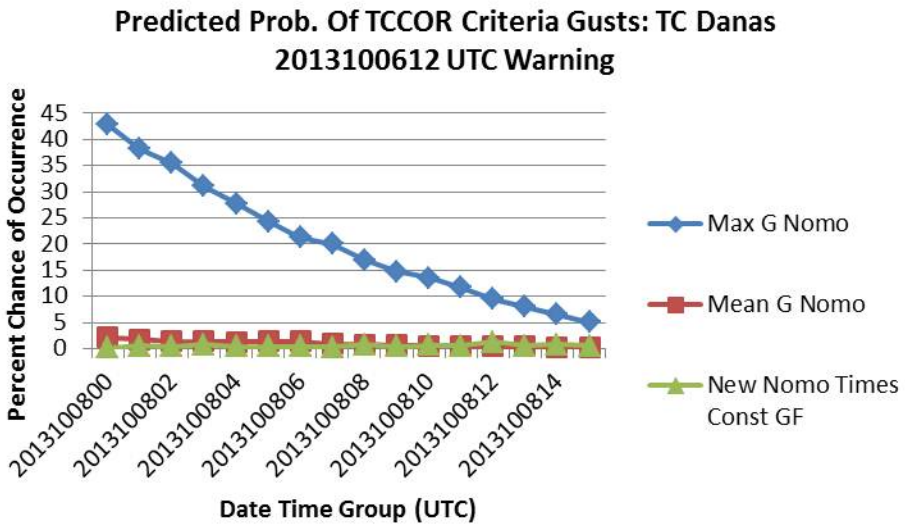

Figure 135. Probability of the TCCOR gust wind (≥ 60 kt) criterion occurring which is calculated by running each member of the 1200 UTC 6 October 2013 ensemble forecast through individual nomograms (see index on right). Jarrell (1988) nomogram maximum gusts are the blue line, nomogram mean gusts are the red line, and the new nomogram times a constant gust factor (GF) is plotted as the green line.

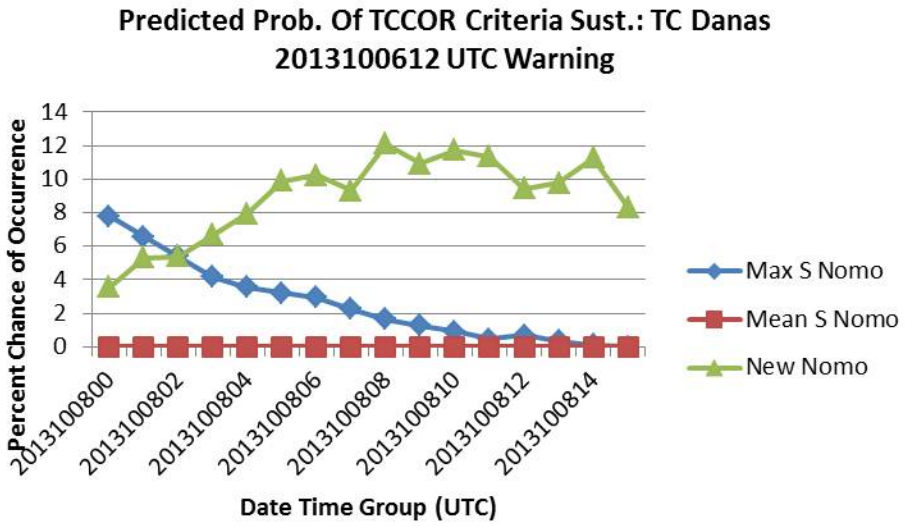

Figure 136. Probability of TCCOR sustained wind (≥ 50 kt) criterion occurring, which is calculated by running each member of the 1200 UTC 6 October 2013 TC ensemble through individual nomograms (see index on right). Line colors are as in Figure 135.

Finally, the PAW modified by directional-dependent acceleration factors derived from PAW-to-AMEDAS comparisons in 2003–2010 is also applied to 1200 UTC 6 October 2013 ensemble members. Only the mean (i.e., not considering the confidence intervals as shown in Figure 134) acceleration factor times PAW is examined as the track and intensity variations among the ensemble members is assumed to capture natural variability. Hourly probabilities of 34 kt or 50 kt winds based on the PAW ensemble are shown in Figure 137. The probability of attaining 50 kt winds is low, but a small relative maximum probability is predicted at nearly the same time that the maximum wind was observed (1100 UTC 08 October; Figure 133).

Sampson et al. (2012), used the existing wind probability products to examine a 6% probability of 50 kt winds on station at 48 hours lead time as a threshold for an objective TCCOR level recommendation. Since their probabilities are based on the same equations from DeMaria et al. (2009) used in this research, but without any terrain considerations, it is not too surprising that ensemble members modified (mostly reduced) by PAW-based directional-dependent acceleration factors yield low probabilities at 48 hours lead time. It should be noted that for historical-operational TCCOR settings, human

factors such as risk perception by individual commanders is a contributing factor, as well as winds actually observed on station. Threshold settings were also noted to require a trade-off between probability of detection and false alarm rate; weighing the relative costs of not forecasting a destructive event against the costs of preparations should no damage occur (Sampson et al. 2012). Ultimate use of an adjusted PAW in an ensemble-probabilistic manner would require a re-examination of thresholds for recommending TCCOR.

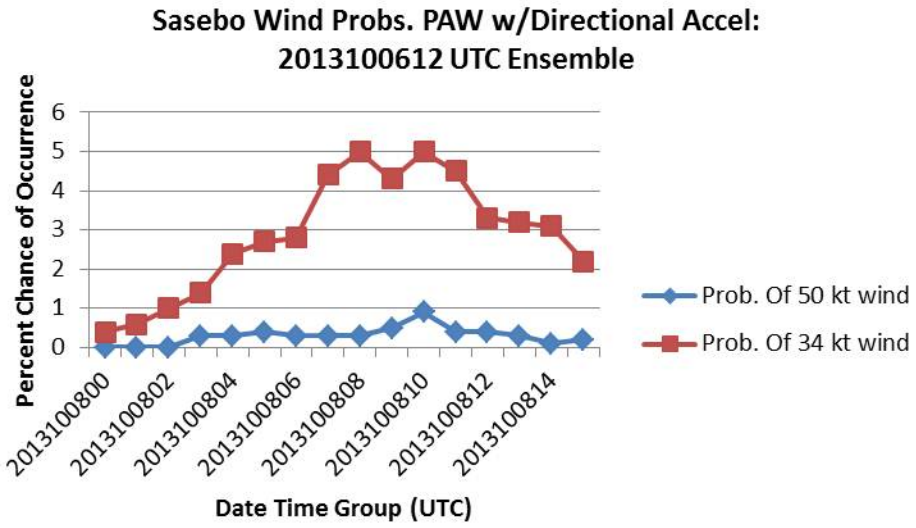

Figure 137. Probability of 50 kt (blue) and 34 kt (red) winds occurring based on running each member of the 1200 UTC October 6 2013 ensemble through the PAW model with directional-dependent acceleration factors.

V. DISCUSSION AND CONCLUSIONS

In this chapter, the results of the development and testing of the various empirical techniques will be discussed in relation to the six hypotheses from Chapter I.C. Finally, some suggestions for future research and how this research might be transitioned to operational use will be presented.

A. STATION-SPECIFIC FACTORS FOR WIND VARIABILITY

Hypothesis 1 posited that a substantial fraction of the wind variability in Sasebo is caused by persistent and identifiable station-specific factors. In Table 17 in Chapter III, a clear improvement in the independent 1998–2000 wind hindcasts was achieved when the directional-dependent acceleration factors were applied. For example, the high bias in PUW hindcasts was reduced by including an isotropic friction reduction term and a better representation of the variability (i.e., larger R^2 values) could be achieved by applying CFSR- or PUW-based directional acceleration factors.

For the independent sample of 2002 and 2011–2012 test cases, the PAW adjusted by directional-dependent acceleration factors still had a high bias and a relatively small vertical spread of the winds around the regression line (Figure 69). Thus an additional reduction in the PAW speeds would result in a higher R^2 value than for any other technique in Tables 17 or 18. While this bias may be a statistical artifact of the limited number, or limited maximum wind speeds for the TCs in the independent sample of cases, the PAW to AMEDAS comparisons from the 2003–2010 development sample used to derive directional acceleration factors may have resulted in a high bias.

In this analysis it has been implicitly assumed that the PAW to AMEDAS derived directional-dependent acceleration factors already included land frictional effects. An alternate approach would be to include an isotropic frictional reduction term before any directional acceleration factors are used. Such a simple approach for the PAW, which includes interpolation between JTWC best track wind radii, multiplied by a reduction factor of 0.54 is shown in Figure 138 (red line). Note that this simple approach results in sustained wind predictions that generally follow the trend of the Sasebo observations

(Figure 138, blue line), but underforecast (overforecast) many maximum (minimum) wind observations. However, applying the directional-dependent acceleration factors then results in better agreement (Figure 138, green lines) with the observations, and especially for the observed maximum winds that are the key input to the TCCOR/sortie-related forecast.

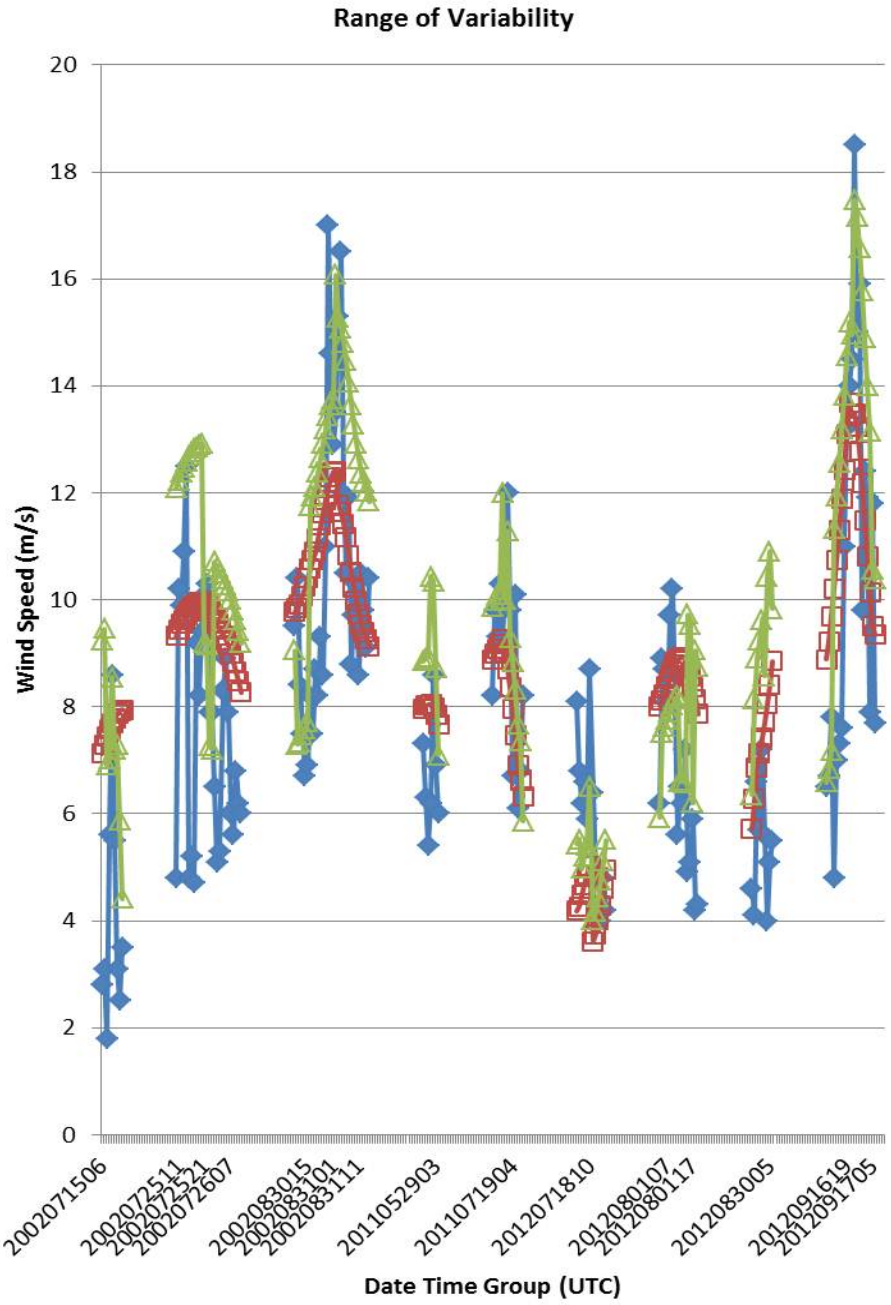

Figure 138. AMEDAS sustained wind observations (blue lines) and predictions for selected TCs within 200 n mi of Sasebo in the 2002 and 2011–12 independent sample. The red boxes are for a simple model that assumes Sasebo winds are caused only by changes in TC intensity and range that is represented by 0.54 times the PAW. The green triangles are PAW adjusted by directional-dependent acceleration factors based on the 2003–2010 AMEDAS to PAW comparisons.

The requirement for the frictional reduction factor for the PAW was demonstrated in Chapter IV in the case study for the small, flat island Minamitorishima. That is the raw PAW speeds had a high bias without the frictional reduction factor. The improvement in Sasebo to the wind forecast by applying direction-dependent acceleration factors during the passage of TCs may be attributed to wind interacting with local terrain features, as those features are always present. Although it is speculated that terrain features such as Mt. Eboshi and Mt. Yumihari are the primary contributors to blocking and channeling effects, this study has only demonstrated that wind direction must be considered when forecasting TC impacts in Sasebo. More detailed observational and numerical studies are required to identify the Sasebo terrain-specific physical mechanisms.

B. DETERMINATION OF DIRECTIONALLY-DEPENDENT WIND VARIABILITY

Hypothesis 2 posits that synoptic-scale wind forcing to Sasebo could be represented by a reanalysis model, such as the CFSR. The advantage to using the CFSR is that a large number of hourly wind estimates over several years would be available to compare with AMEDAS hourly sustained winds for representing the direction-dependent terrain modifications of the winds in Sasebo. This includes multiple synoptic situations vice just a small number of TC cases. For simplicity, only the closest CFSR grid point was used to make comparisons with Sasebo observed winds. Because CFSR may include some terrain effects at its resolution, it may have been better to take the four grid points surrounding Sasebo and interpolate to obtain a more representative wind at Sasebo. That is, the CFSR-based acceleration factors calculated in this study are likely more representative of wind differences between two locations 30 km apart, rather than differences between synoptic-scale and local-scale winds.

The disadvantage of the CFSR winds is the tendency for a low bias, particularly for TC-related scenarios. Consequently, the acceleration factors derived from parametric wind comparisons to the Sasebo observations are expected to be more appropriate than those derived from the CFSR. Because of the CFSR low wind bias, the CFSR-derived acceleration factors are larger than the parametric acceleration factors, but they both might be expected to have similar variations with cardinal wind direction (Figure 139).

Note the decrease of acceleration factors from NNE to ENE, increase from E to ESE, no change from ESE to SE, decrease from SSW to SW, increase from WSW to W, and decrease from W to WNW. However, some differences for the SSE and S cardinal wind directions are attributed to the CFSR-based acceleration factors being too low.

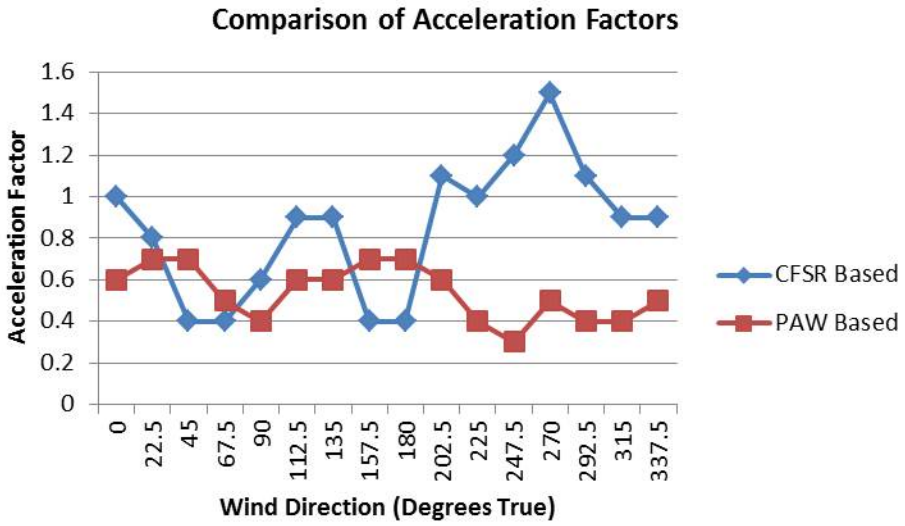

Figure 139. Comparison of directional-dependent acceleration factors derived from comparisons of the CFSR winds to the Sasebo AMEDAS wind during 2003–2010 (blue diamonds) and similar comparisons of PAW speeds to AMEDAS wind for times when a TC was within 200 n mi of Sasebo.

Application of the CFSR-derived and parametric wind-derived directional-dependent acceleration factors did improve Sasebo wind speed magnitude and the timing of maximum wind predictions relative to raw PAW wind calculations (i.e., just interpolating between TC wind radii). Therefore these empirically-derived acceleration factors do represent directional-dependent wind response in Sasebo to synoptic-scale forcing, and specifically for TCs within 200 n mi.

C. VARIABILITY IN SUSTAINED AND GUST WIND FORECASTS

Hypothesis 3 posits that directional variability is also important for gust winds in Sasebo during TC passage. Since gust strength varies with the gust direction relative to sustained wind direction (Tables 3 and 5), improved gust forecasts will result if both

directions are known. However, both an overall average gust factor and a seasonally dependent gust factors performed well for various test cases.

If terrain is a key factor for gust magnitude, those same terrain features will also be responsible for PAW sustained speed direction dependency. Indeed the trends of gust acceleration factors and PAW based acceleration factors broadly parallel (Figure 140). Thus, it is concluded that wind direction must be taken into account to explain gust wind variability in Sasebo.

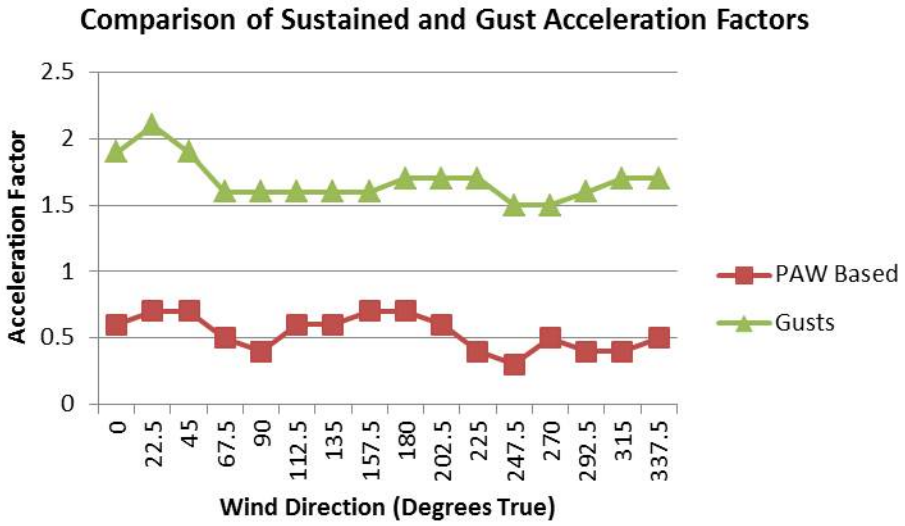

Figure 140. Gust acceleration factors derived by comparing observed gusts and observed sustained winds from 2009–2012 (green triangles) compared with acceleration factors derived from comparisons of PAW to observations (red triangles) when TCs were within 200 n mi of Sasebo from 2003–2010.

D. NOMOGRAMS AND TC STRUCTURE

It is well known that the Jarrell (1988) nomograms for Sasebo do not take into account variations in TC size for a given intensity. For example, a strong but relatively small storm at a given range from Sasebo would not be expected to have the same impact as a TC of the same intensity but with a much larger wind field. To include such TC size effects, a new nomogram was created that used the position of Sasebo relative to the TC 34-kt wind radii as a normalized range from the TC. As demonstrated in Chapters III and

IV, independent tests of the new nomogram have been encouraging, which tends to validate Hypothesis 4 that posited a need to account for wind variability caused by TC structure as well as by terrain. However, further improvement in this technique is proposed with a larger database to refine the nomogram contours, and perhaps with better smoothing techniques applied.

E. PARAMETRIC MODELS WITH MODIFICATION

Modifying the parametric model of Knaff et al. (2007) to utilize the wind radii from JTWC (when available) is another way to take into account variations in TC structure. The PUW model basically provides an average size wind field for a given TC intensity and latitude. A clear improvement in the Sasebo (and other sites) winds from the PAW model vs. the PUW model has been demonstrated in this study, and that the PAW directional-dependent based acceleration factors are typically superior to the PUW acceleration factors. However, further refinement of the existing acceleration factors may be required, especially as limited cases with the JTWC wind radii were available to determine the PAW to AMEDAS based acceleration factors.

As posited in Hypothesis 5, it is concluded that TC structure-related modifications to the basic parametric model have merit for improved descriptions of the wind variability during TC passages near Sasebo.

F. PERSISTENT ERRORS

Sources and impacts of persistent errors for the empirical techniques developed and tested in this research have been described in Chapter IV. It is clear that TCs passing SW of Sasebo are less well handled by these techniques. Some case studies suggest that rainband passage and TC structure changes during extratropical transition may lead to local winds that are not explained by this directional-dependent acceleration factor approach. Further research is required to identify the sources of that deficiency, e.g., influence of specific terrain features, ocean currents, sea-surface temperatures, or other factors.

In both the nomogram and parametric model approaches it is assumed that an almost symmetric TC wind field exists. When accurate JTWC wind radii are available by quadrants, asymmetry effects can be included. The parametric models tested here also have an advantage because the direction-based acceleration factors are assumed to represent the terrain-influenced wind asymmetries.

G. OPERATIONAL APPLICATIONS

Several methods for operational application of these research results are proposed. First, in the near term:

- More focus should be on the original nomograms for the mean sustained winds. At least during the author's last operational tour in Japan, only maximum wind nomograms were in use for Sasebo. Forecasters should be aware of potential over-forecasts particularly when TCs are SW of Sasebo.
- Place less emphasis on the nomogram gust forecasts, and instead use the overall average gust factor of 1.76, or monthly directional-dependent gust factors times mean sustained wind nomogram predictions.
- Make gust forecasts at a higher frequency as the historical record shows Sasebo winds met TCCOR criteria more frequently for gusts than for sustained winds.
- Make use of the typical Sasebo wind variability presented in Table 19 to modify empirical forecasts.

Additional applications might be achieved in the mid to longer term. As previously noted, both the PAW and PUW appear to provide good estimates for observed gusts at Sasebo, and perhaps at other locations. Therefore, the existing TC wind probability product might, with slight modifications, be also used to provide a gust wind probability. As mentioned in Chapter I, both forecasters and operational decision makers might benefit from a forecast time series of sustained and gust winds that also includes uncertainty estimates. The parametric models, new nomogram, and automated original nomograms are all run in MATLAB, which is unfortunately not typically installed on Navy computers. However, these codes could be modified to be automatically run at JTWC and provided for every TC. Alternatively, Microsoft Excel based versions could potentially be created for direct forecaster interaction.

It would be beneficial to automatically produce probabilistic forecasts of 34 kt winds, 50 kt winds, and/or TCCOR criteria specific to Sasebo utilizing the Monte Carlo tracks and intensities used for wind probability products (e.g., Figures 135–137). However, further refinements in the directional acceleration factors may be required to reduce the high bias (e.g., Figures 66 and 69), which would also result in a bias in the probabilistic forecasts. Alternatively, the original mean wind nomogram or new nomogram could be used, with some adjustment for TCs SW of Sasebo.

H. FUTURE RESEARCH

Other U.S. bases in Japan have surrounding complex terrain. Iwakuni, Japan is located on the coast of Honshu facing the inland sea between Honshu and another of the main islands of Japan, Shikoku (Figure 1). In addition to the local terrain effects, some local low-level wind enhancement may be caused by the gaps between the main islands. Although Yokosuka, Japan is located on one of the major plain areas in Japan, it is surrounded by low hills on the land side, the gap at the entrance to Tokyo Bay to its southeast, and another bay to its southwest. Mt. Fuji is also in close proximity to the base, which may influence the local wind field. Thus it is proposed to apply the techniques developed and tested in this study for both Iwakuni and Yokosuka (recall they presently utilize nomograms), and then inter-compare the local wind modification for the three different terrain regimes.

Numerical experimentation with mesoscale models of wind acceleration factors for the Sasebo terrain should also be carried out. Sensitivity tests with different terrain features being selectively removed should be examined to provide a better understanding of terrain impacts, particularly for TCs to the SW of Sasebo.

Finally, this study should be expanded to test different parametric models. The modified Rankine vortex was chosen largely because it was already in use for a TC wind probability product and the required inputs are all available in a JTWC warning message. Other parametric models may better represent effects such as eyewall replacement cycles and the frictional reduction due to land interaction. Parametric models for TC

precipitation should also be studied since heavy rainfall is another major TC hazard. It would be interesting to see if these could be applied, likely in an ensemble mode, to improve TC-related rainfall forecasts in Japan.

I. FINAL THOUGHTS

The techniques developed and tested here appear to improve on existing wind and gust forecasts for Sasebo. The basic techniques can be applied at very little computational cost, may be applicable to other stations, and will continue to improve as TC track and intensity forecasts continue to improve. Although the performance of increasingly higher resolution numerical weather prediction models is impressive, such deterministic model integrations capture only one scenario out of a range of natural variability. While in the future similarly high resolution ensembles may be capable of addressing the complex terrain-influenced wind uncertainty, the techniques developed and tested in this study offer a simple and efficient way to describe and potentially predict some of that variability.

APPENDIX CFSR BASED ACCELERATION FACTORS

An example was given in Figure 50 of an empirical probability density function (created using the MATLAB function ksdensity) applied to a histogram of occurrence of acceleration factors (AMEDAS Wind Speed/CFSR Wind Speed) constructed from 2003–2010 Sasebo AMEDAS and CFSR data for hourly times when AMEDAS winds were from the N. The comparisons for Sasebo winds for the remaining 15 cardinal directions are presented in this appendix. Shifts in the peak of each distribution as the AMEDAS wind direction varies suggests wind direction-dependent wind variability in Sasebo.

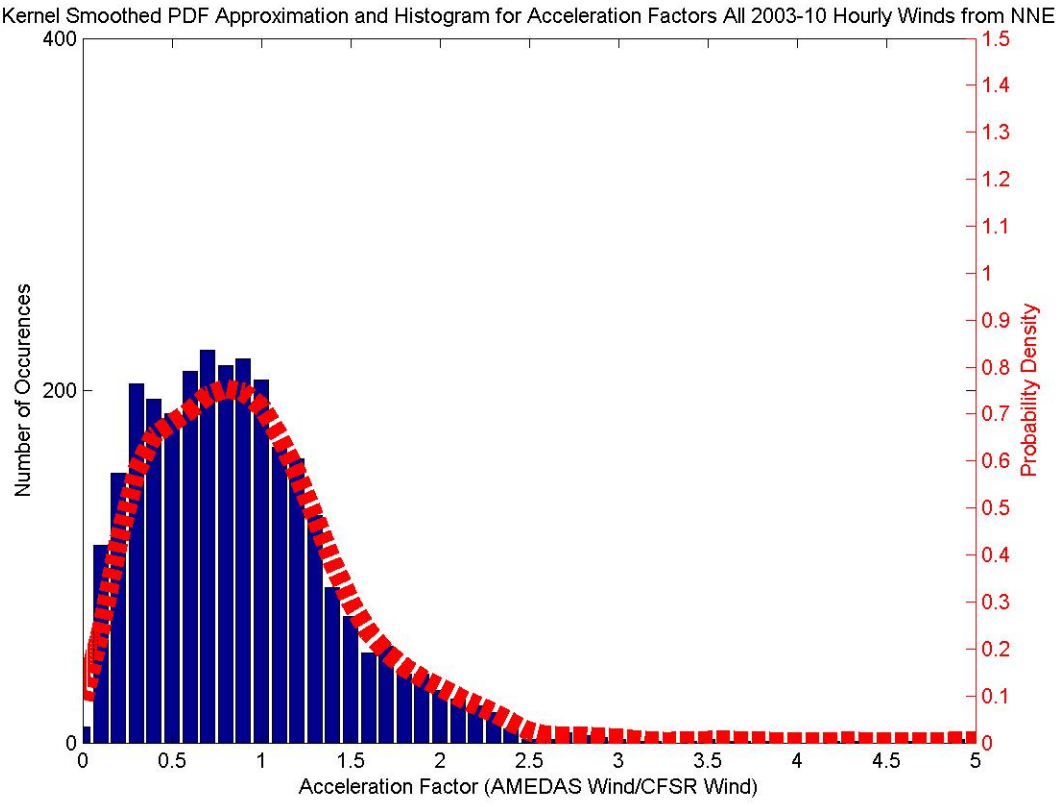

Figure 141. Comparison of histogram of number of occurrence of different acceleration factors (blue bars) to a kernel-smoothed probability density derived from the same data (dashed red line). Here the acceleration factors (AMEDAS wind/CFSR wind) are from all hourly values in 2003–2010 for which observed AMEDAS wind was from the NNE in Sasebo.

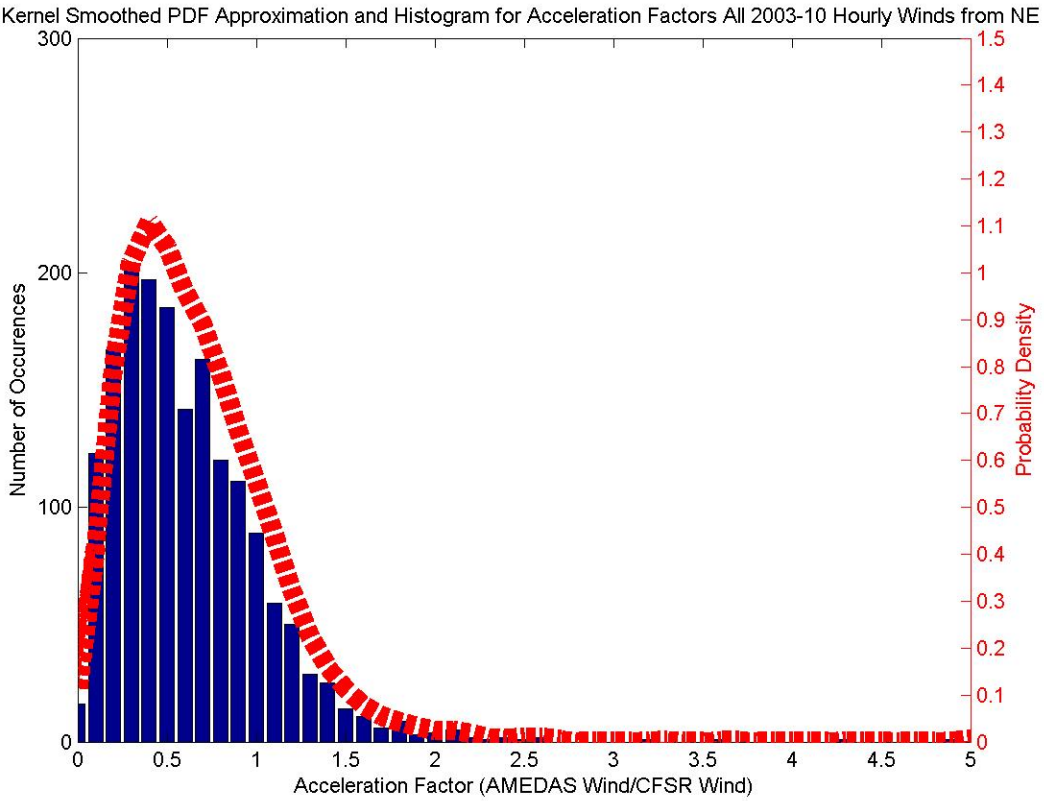

Figure 142. As in Figures 50 and 141, but for AMEDAS NE wind.

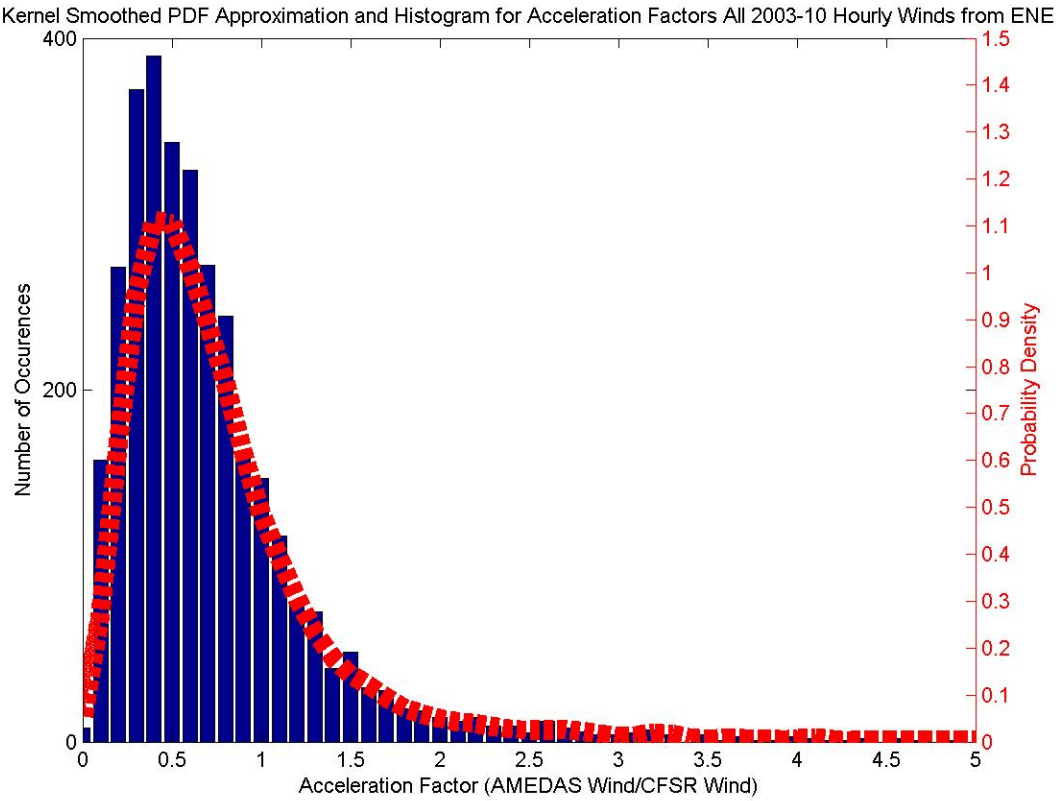

Figure 143. As in Figures 50 and 141, but for AMEDAS ENE wind.

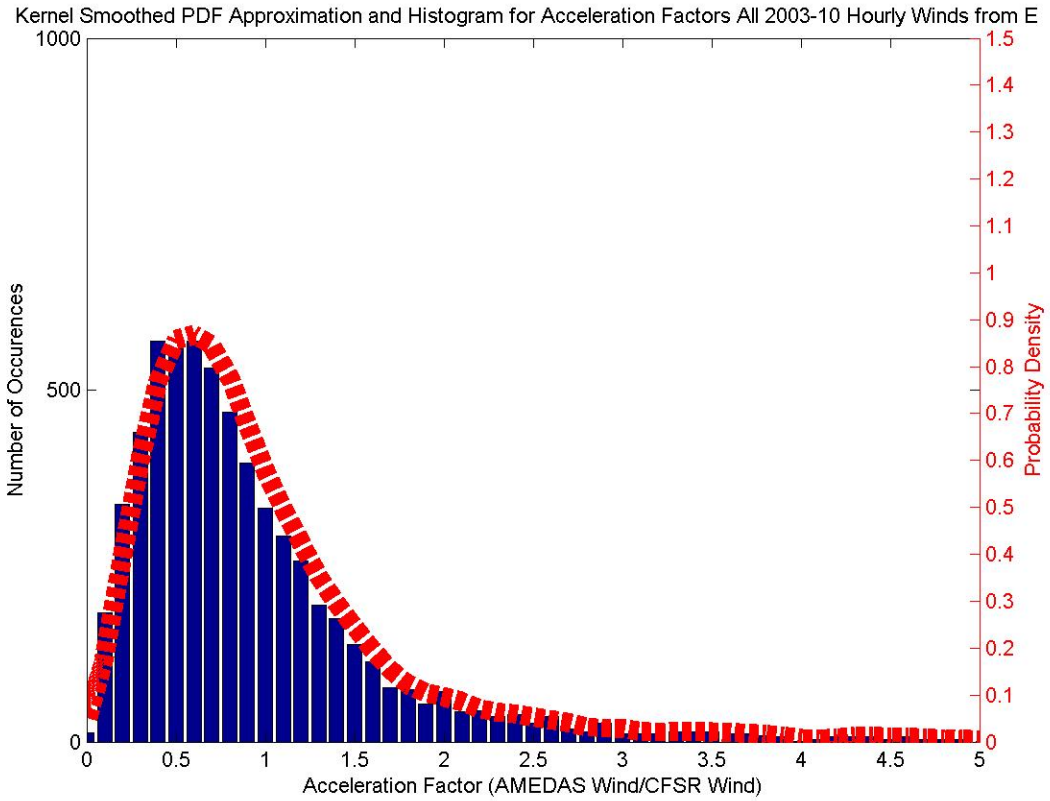

Figure 144. As in Figures 50 and 141, but for AMEDAS E wind.

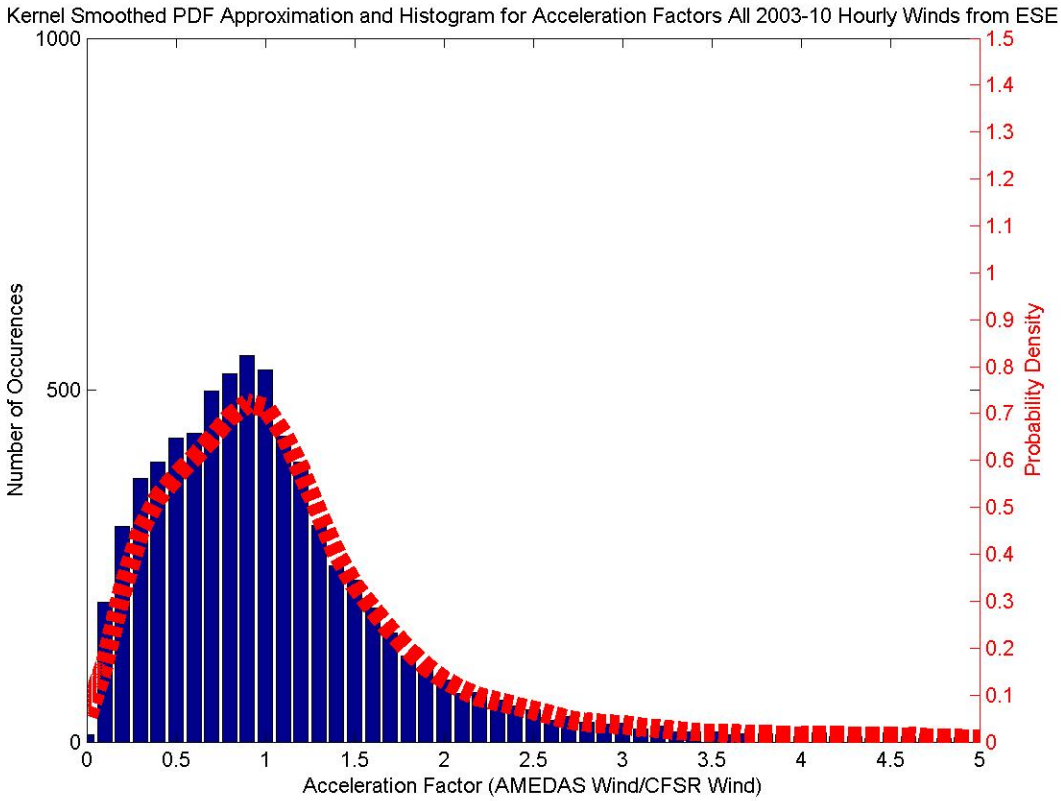

Figure 145. As in Figures 50 and 141, but for AMEDAS ESE wind.

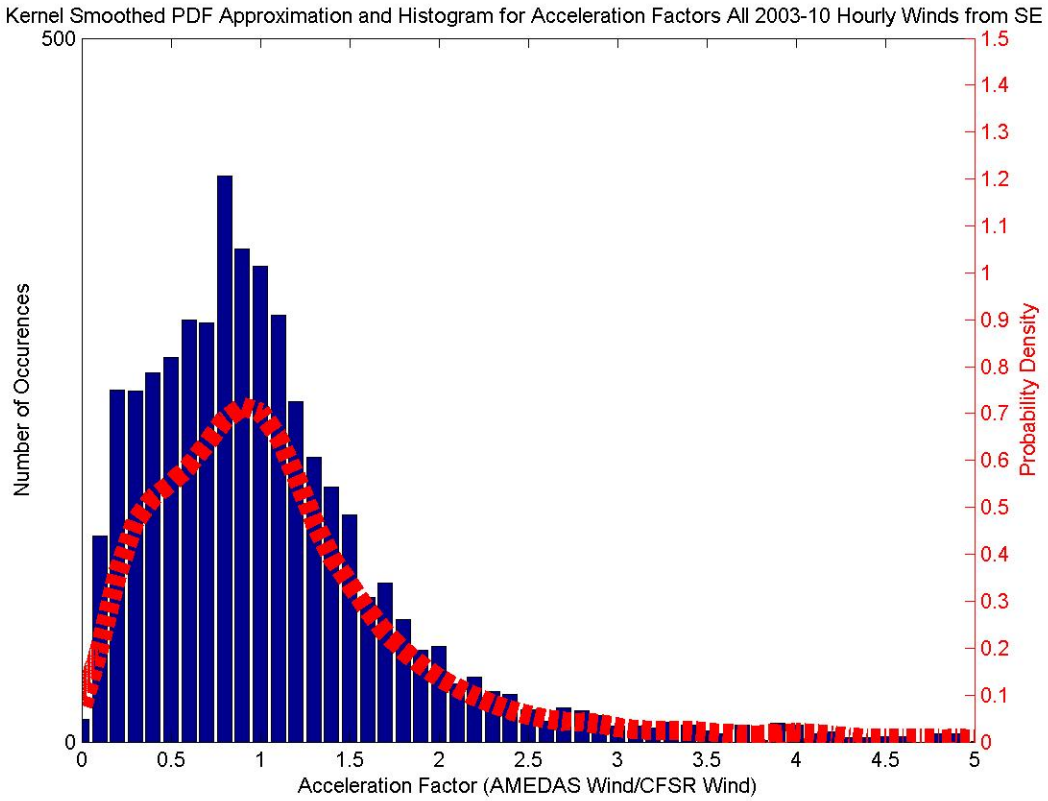

Figure 146. As in Figures 50 and 141, but for AMEDAS SE wind.

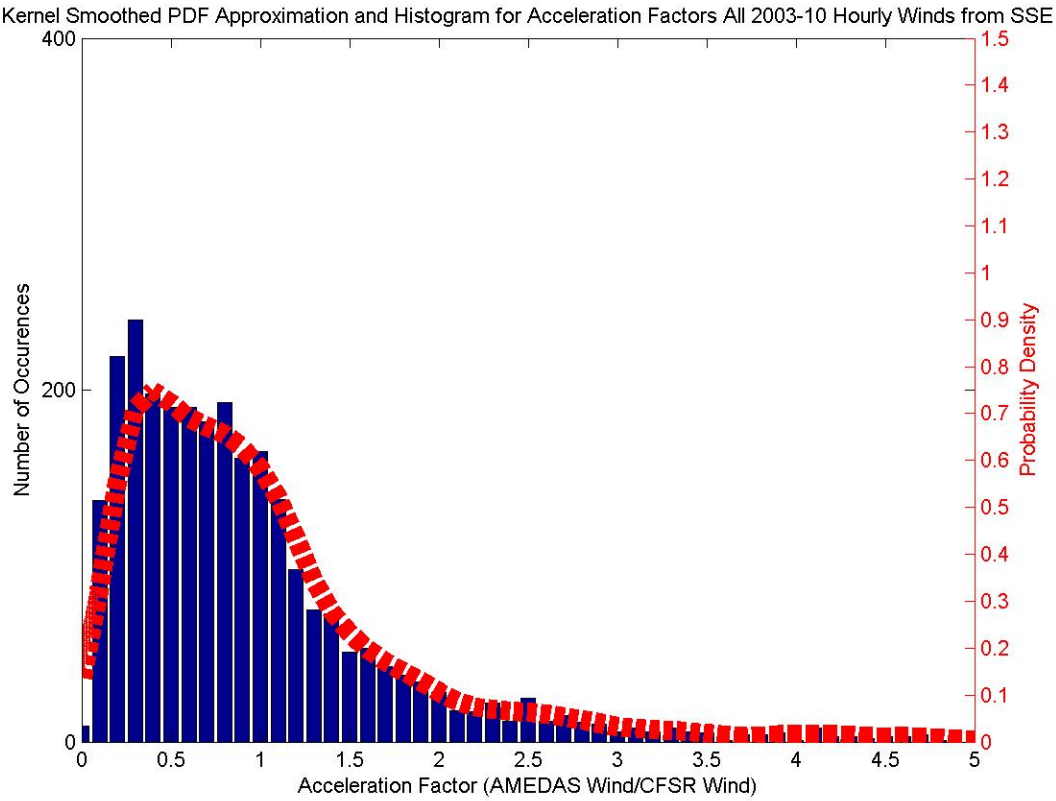

Figure 147. As in Figures 50 and 141, but for AMEDAS SSE wind.

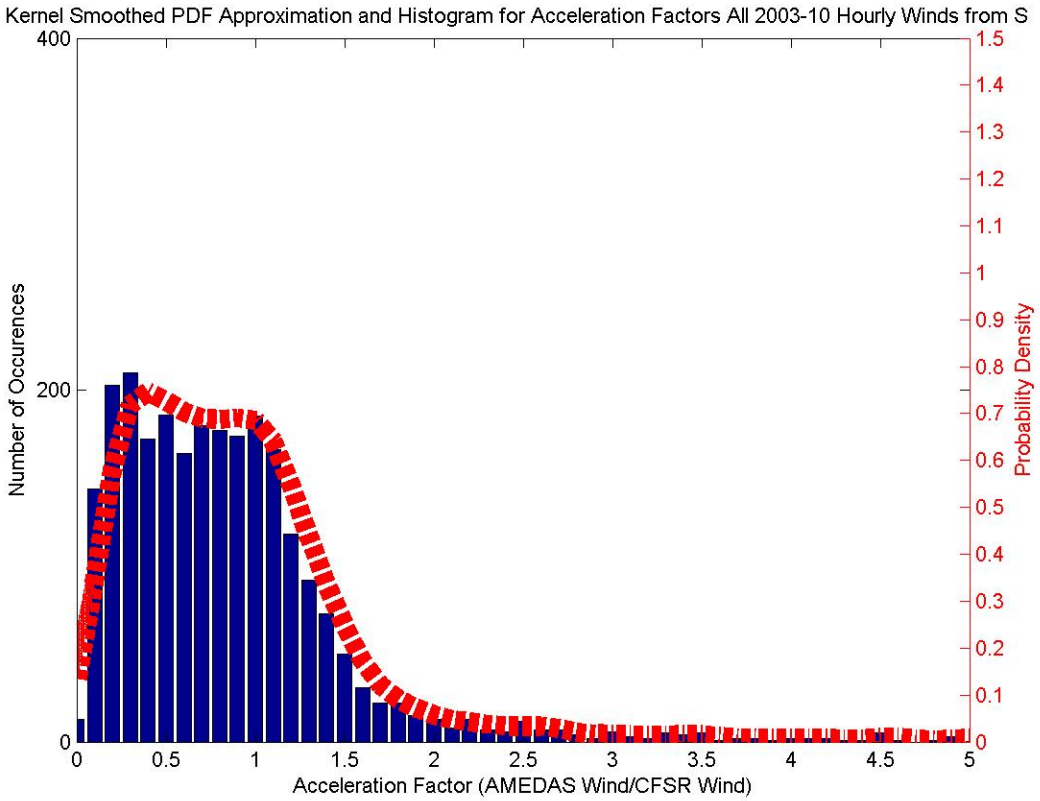

Figure 148. As in Figures 50 and 141, but for AMEDAS S wind.

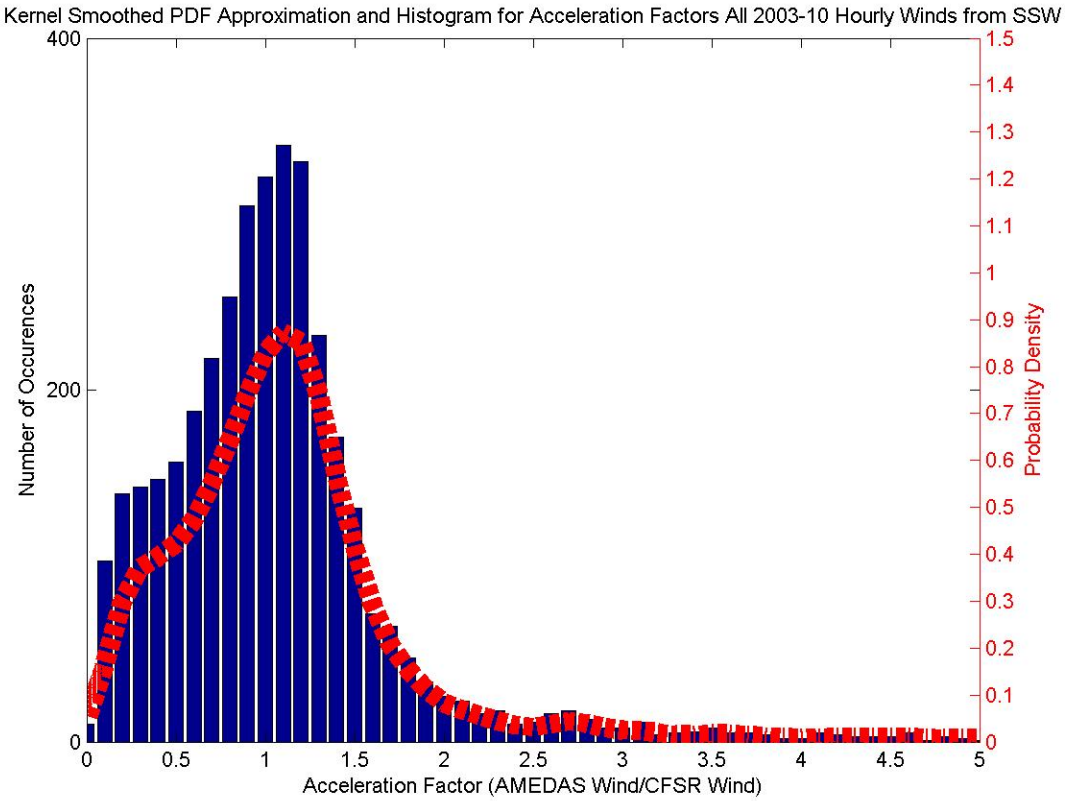

Figure 149. As in Figures 50 and 141, but for AMEDAS SSW wind.

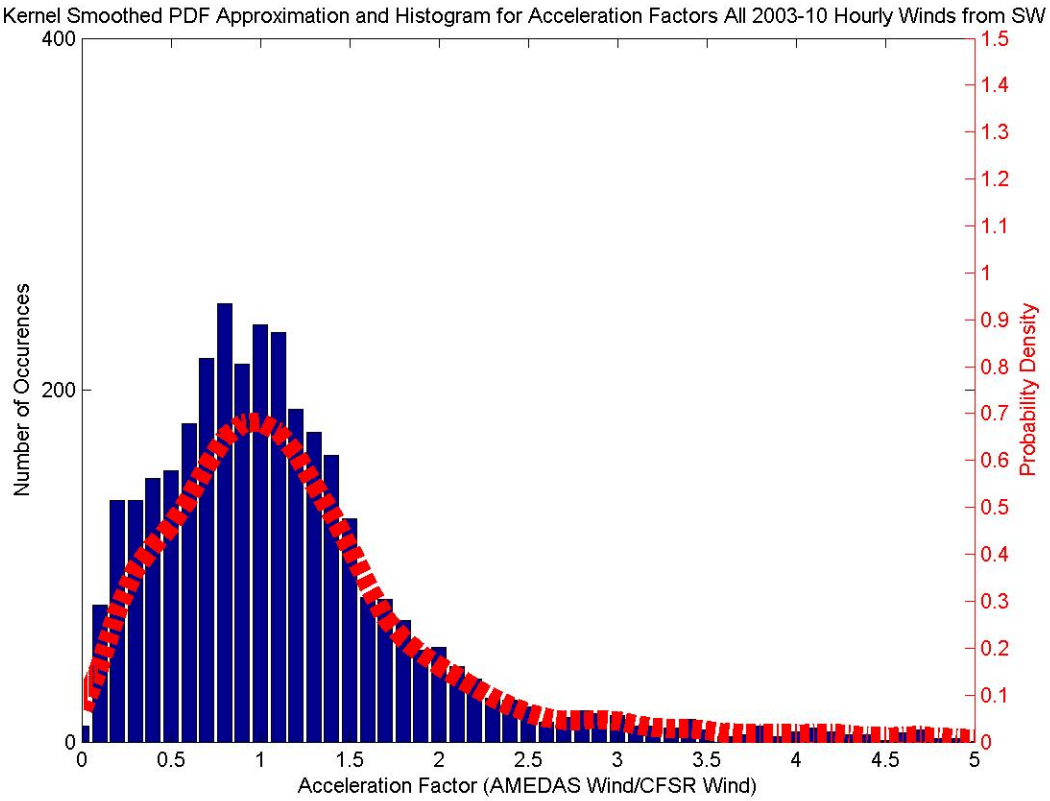

Figure 150. As in Figures 50 and 141, but for AMEDAS SW wind.

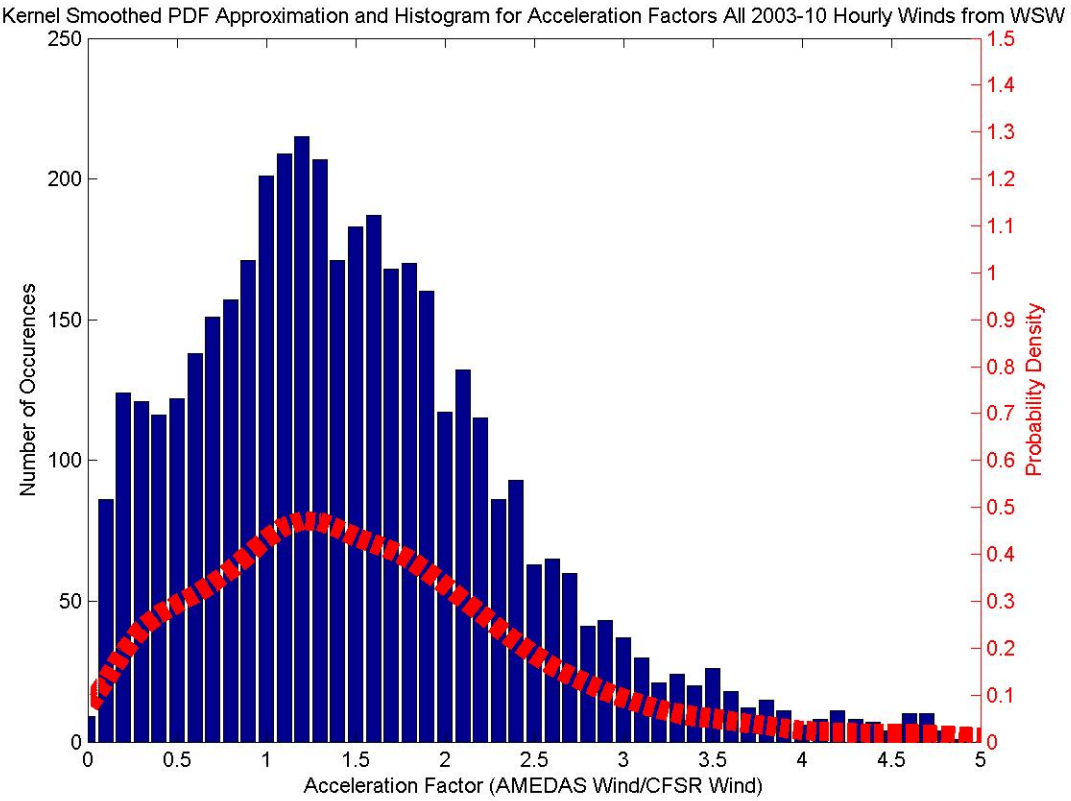

Figure 151. As in Figures 50 and 141, but for AMEDAS WSW wind.

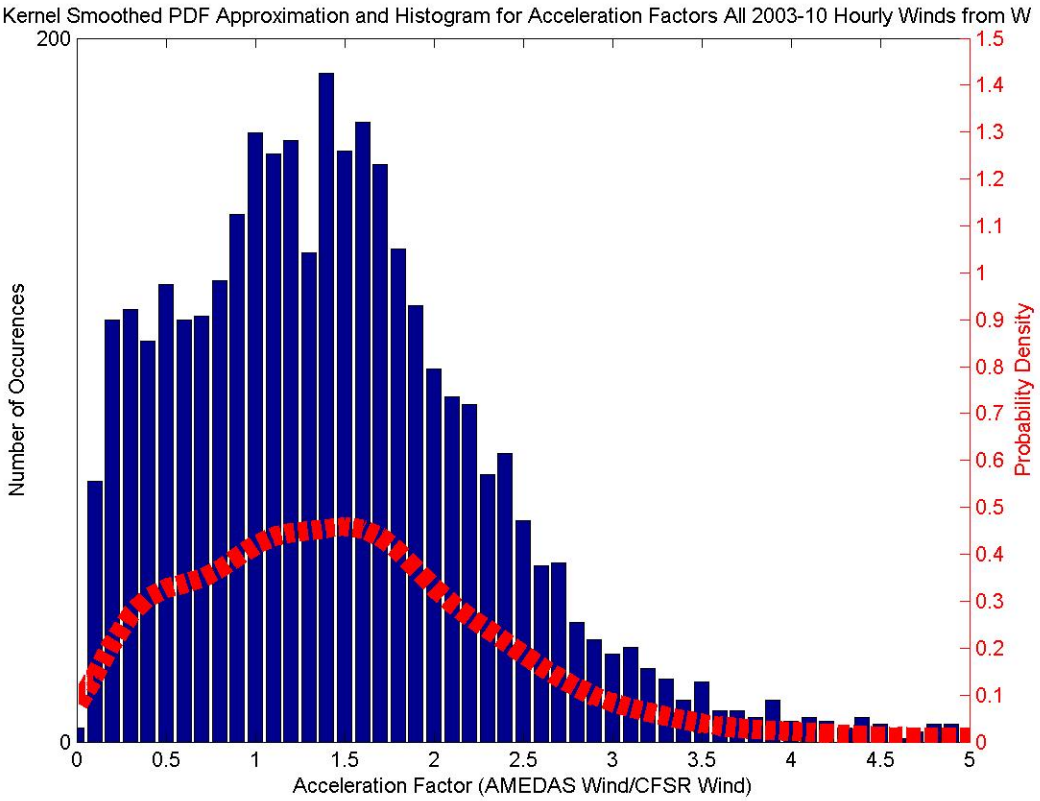

Figure 152. As in Figures 50 and 141, but for AMEDAS W wind.

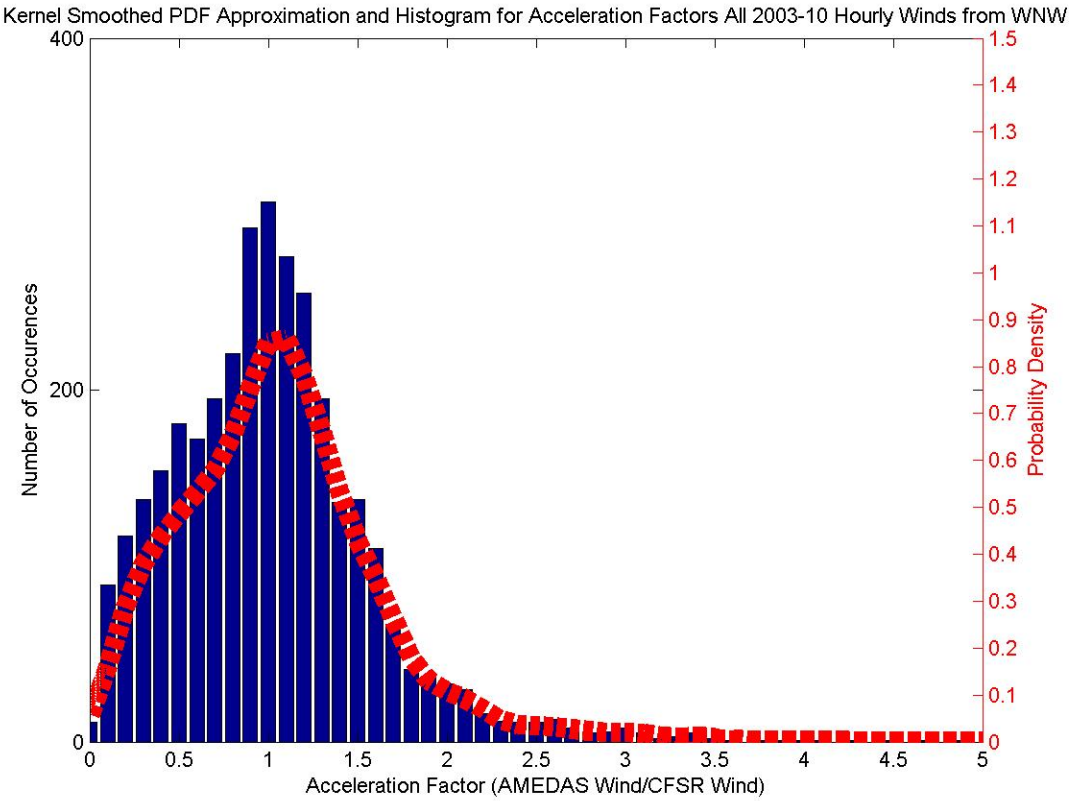

Figure 153. As in Figures 50 and 141, but for AMEDAS WNW wind.

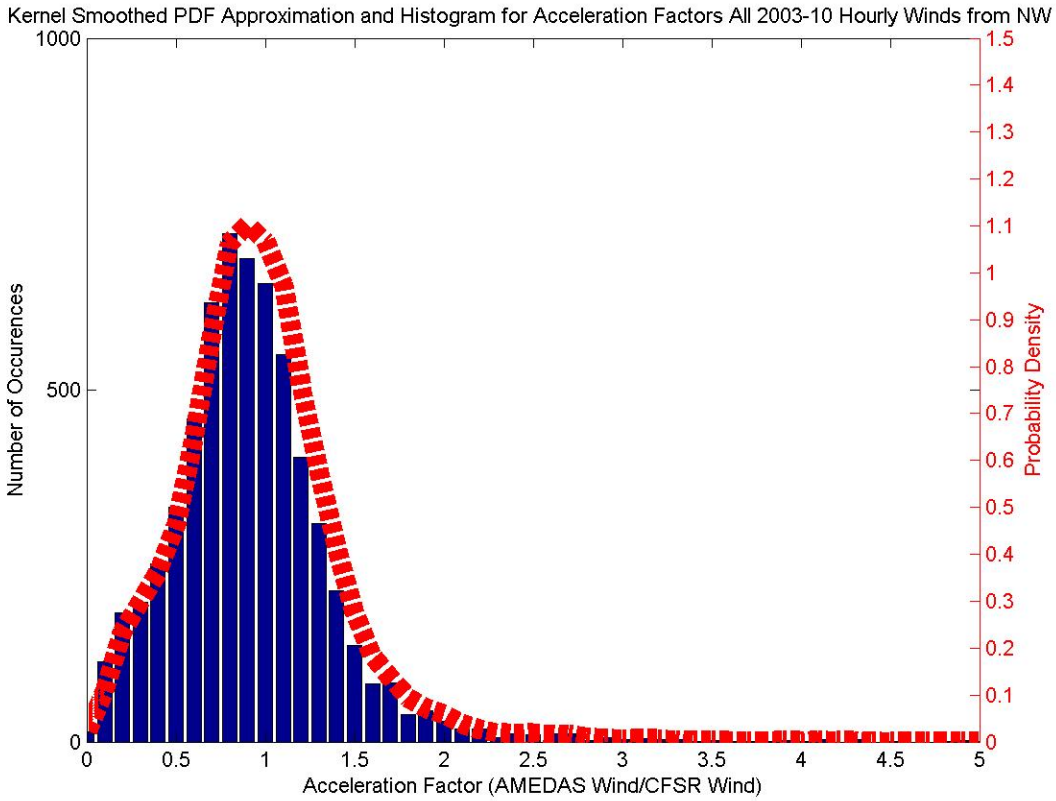

Figure 154. As in Figures 50 and 141, but for AMEDAS NW wind.

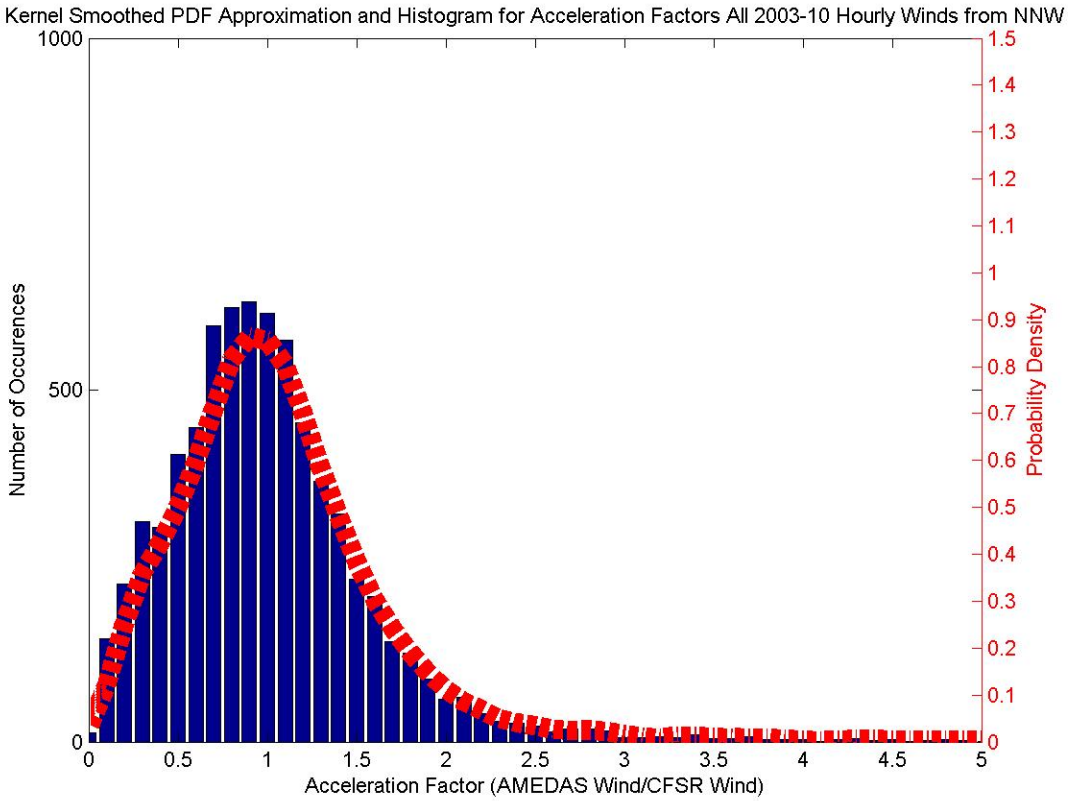

Figure 155. As in Figures 50 and 141, but for AMEDAS NNW wind.

THIS PAGE INTENTIONALLY LEFT BLANK

LIST OF REFERENCES

Commander Fleet Activities Sasebo, cited 2013: History. [Available online at http://cnic.navy.mil/regions/cnrj/installations/cfa_sasebo/about/history.html.]

Commander Navy Installations Command, cited 2013: Naval Station Norfolk. [Available online at http://cnic.navy.mil/regions/cnrma/installations/ns_norfolk.html.]

Commander U.S. Naval Forces Japan, 2010: Hazardous/Destructive Weather Plan. CNFJ Instruction 3140.4A, 15 pp.

DeMaria, M., J. A. Knaff, R. Knabb, C. Lauer, C. R. Sampson, and R. T. DeMaria, 2009: A new method for estimating tropical cyclone wind speed probabilities. *Wea. Forecasting*, **24,** 1573–1591.

Digital Typhoon, cited 2013: Search of AMEDAS stations. [Available online at http://agora.ex.nii.ac.jp/cgi-bin/amedas/search.pl?lang=en&key=sasebo.]

Fenlason, J. W., 2006: Accuracy of tropical cyclone induced winds using TYDET at Kadena AB. M.S. thesis, Dept. of Meteorology, Naval Postgraduate School, 111 pp.

FNMOC, 2013: METCAST Version 1.7.0.5.

Geospatial Information Authority of Japan, cited 2013: Topographic maps. [Available online at http://watchizu.gsi.go.jp.]

Global Positioning System cited 2013: Global Positioning System standard positioning service performance standard. [Available online at http://www.gps.gov/technical/ps/2008-SPS-performance-standard.pdf .]

Google Inc., 2013: Google Earth Version 7.1.1.1888.

Harper, B. A., J. D. Kepert, and J. D. Ginger, 2010: Guidelines for converting between various wind averaging periods in tropical cyclone conditions. World Meteorological Organization, TCP Sub-Project Report, WMO/TD-No. 1555, 64 pp.

Holland, G. J., J. I. Belanger, and A. Fritz, 2010: A revised model for radial profiles of hurricane winds. *Mon. Wea. Rev.,* **138,** 4393–4401.

Japanese Meteorological Agency, cited 2013a: Sasebo statistics all years (in Japanese). [Available online at http://www.data.jma.go.jp/obd/stats/etrn/view/annually_s.php?prec_no=84&block_no=47812.]

Japanese Meteorological Agency, cited 2013b: Observations. [Available online at http://www.jma.go.jp/jma/en/Activities/observations.html.]

Japanese Meteorological Agency, cited 2013c: Regional Meteorological Observatory List (in Japanese). [Available online at http://www.jma.go.jp/jma/kishou/know/amedas/ame_master.pdf.]

Japanese Meteorological Agency, cited 2013d: Recent improvements of integrated observation systems in JMA. [Available online at: http://www.wmo.int/pages/prog/www/IMOP/publications/IOM-104_TECO-2010/2_5_Akaeda_Japan.pdf.]

Japanese Meteorological Agency, cited 2013e: Sasebo observations (in Japanese). [Available online at http://www.data.jma.go.jp/obd/stats/etrn/index.php?prec_no=84&block_no=47812.]

Japanese Meteorological Agency, cited 2013f: JMA data report of oceanographic observations special issue. [Available online at http://www.data.kishou.go.jp/kaiyou/db/vessel_obs/data-report/html/buoy/buoy_NoS2_e.html.]

Jarrell, J. D., 1988: Forecasting aids for setting tropical cyclone conditions: Sasebo and Iwakuni, Japan. NEPRF Contractor Report CR 88-02, 46 pp.

Jarrell, J. D., and R. E. Englebretson, 1982: Forecast aids for predicting tropical cyclone associated gusts and sustained winds for Yokosuka, Japan. NEPRF Contractor Report CR 82-11, 20 pp.

Joint Typhoon Warning Center, cited 2013: Home page. [Available online at http://www.usno.navy.mil/JTWC/.]

Kitabatake, N., 2008: Extratropical transition of Typhoon Tokage (0423) and associated heavy rainfall on the left Side of its track over Western Japan. *Pap. Meteor. Geophys.*, **59,** 97–114.

Knaff, J. A., C. R. Sampson, M. DeMaria, T. P. Marchok, J. M. Gross, and C. J. McAdie, 2007: Statistical tropical cyclone wind radii prediction using climatology and persistence. *Wea. Forecasting*, **22,** 781–791.

MacAfee, A. W., and G. M. Pearson, 2006: Development and testing of tropical cyclone parametric wind models tailored for midlatitude application—Preliminary results. *J. Appl. Meteor. Climatol.*, **45,** 1244–1260.

National Climatic Data Center, cited 2013: Integrated surface hourly (ISH) database station list. [Available online at ftp://ftp.ncdc.noaa.gov/pub/data/inventories/ISH-HISTORY.TXT.]

National Weather Service, cited 2010: TCMWindTool documentation. [Available online at http://www.mdl.nws.noaa.gov/~applications/STR/data/2068/TCMWindTool.pdf.]

National Weather Service, cited 2012: National Weather Service instruction 10-601 tropical cyclone products. [Available online at http://www.nws.noaa.gov/directives/.]

National Weather Service, cited 2013: Wakefield Virginia Weather Forecast Office Hurricane Irene 2011 Event Summary. [Available online at http://www.erh.noaa.gov/akq/wx_events/hur/Irene.]

Naval Pacific Meteorology and Oceanography Detachment Sasebo, 2001: Forecaster's handbook for Sasebo Japan. NAVPACMETOCDETSASEBOINST 3140.1, 26 pp.

Naval Research Lab, cited 2012a: COAMPS-TC tropical cyclone prediction and verification. [Available online at http://www.nrlmry.navy.mil/coamps-web/web/tc.]

Naval Research Lab, cited 2012b: Typhoon havens handbook. [Available online at http://www.nrlmry.navy.mil/port_studies/thh-nc/0start.htm.]

Naval Research Lab, cited 2013: NRL tropical cyclone page. [Available online at http://www.nrlmry.navy.mil/tc-bin/tc_home2.cgi.]

Ramlau-Hansen, H., 1983: Smoothing counting process intensities by means of kernel functions. *Ann. Stat.*, **11**, 453–466.

Remote Sensing Systems, cited 2013: Data archive of past tropical cyclones. [Available online at http://images.remss.com/hurricane/data_archive.html.]

Saha, S., and coauthors, 2010: The NCEP climate forecast system reanalysis. *Bull. Amer. Meteor. Soc.*, **91,** 1015–1057.

Sampson, C. R., R. Jeffries, and J-H. Chu, 1995: Tropical cyclone forecasters reference guide, 6. Tropical cyclone intensity. NRL/PU/7541--95-012, 48 pp.

Sampson, C.R., A. Schumacher, J. Knaff, M. DeMaria, E. Fukada, C. Sisko, D. Roberts, K. Winters, and H. Wilson, 2012: Objective guidance for use in setting tropical cyclone conditions of readiness. *Wea. Forecasting,* **27**, 1052–1060.

Schenkel, B.A., and R. Hart, 2012: An examination of tropical cyclone position, intensity, and intensity life cycle within atmospheric reanalysis datasets. *J. Climate,* **25**, 3453–3475.

Stars and Stripes, cited 2013: Typhoon Tokage creates havoc in Japan. [Available online at http://www.stripes.com/ews/typhoon-tokage-creates-havoc-in-japan-1.25284.]

Tyner, B.P., cited 2012, Tropical cyclone inland wind NWS forecaster questionnaire results. [Available online at http://www4.ncsu.edu/~bptyner/Final_writeup_wind.pdf.]

U.S. Navy, cited 2013: All sortie ships underway in preparation for Hurricane Irene. [Available online at http://www.navy.mil/submit/display.asp?story_id=62403.]

Vaisala, cited 2013: CFAS—Station information. [Available online at http://192.101.77.172/info.php?station=CFAS&form=info.]

Wallace, K.A., 2008: A probabilistic approach to tropical cyclone conditions of readiness (TCCOR). M.S. thesis, Dept. of Meteorology, Naval Postgraduate School, 65 pp.

Wilks, D.S., 1995: *Statistical Methods in the Atmospheric Sciences.* Academic Press, 467 pp.

World Meteorological Organization, cited 2012: Seventh International Workshop on Tropical Cyclones Keynote 1: Tropical cyclone surface wind structure and wind-pressure relationships. [Available online at http://www.wmo.int/pages/prog/arep/wwrp/tmr/otherfileformats/documents/KN1.pdf.]

Yokogawa Company, cited 2013: Company website (in Japanese). [Available online at http://www.yokogawa.com/jp-ydk/index.htm.]

INITIAL DISTRIBUTION LIST

1. Defense Technical Information Center
   Ft. Belvoir, Virginia

2. Dudley Knox Library
   Naval Postgraduate School
   Monterey, California